Doctoral theses at NTNU, 2021:117

Mengyi Zhu

Silicon purification by acid leaching and slag refining techniques

Doctoral thesis

NTNU
Norwegian University of Science and Technology
Thesis for the Degree of
Philosophiae Doctor
Faculty of Engineering
Department of Materials Science and Engineering

NTNU
Norwegian University of
Science and Technology

Mengyi Zhu

Silicon purification by acid leaching and slag refining techniques

Thesis for the Degree of Philosophiae Doctor

Trondheim, March 2021

Norwegian University of Science and Technology
Faculty of Engineering
Department of Materials Science and Engineering

NTNU
Norwegian University of
Science and Technology

NTNU
Norwegian University of Science and Technology

Thesis for the Degree of Philosophiae Doctor

Faculty of Engineering
Department of Materials Science and Engineering

ISBN 978-82-326-6057-5 (printed ver.)
ISBN 978-82-326-5949-4 (electronic ver.)
ISSN 1503-8181 (printed ver.
ISSN 2703-8084 (online ver.)

Doctoral theses at NTNU, 2021:117

Printed by NTNU Grafisk senter

Preface

This thesis is submitted to the Norwegian University of Science and Technology (NTNU), as partial fulfillment of the requirements for the degree of Philosophiae Doctor. This work has been carried out at the Department of Materials Science and Engineering in the period from August 2017 to January 2021.

This work was performed within the Research Centre for Sustainable Solar Cell Technology (FME SuSolTech, project number 257639), co-sponsored by the Norwegian Research Council and industry partners.

The thesis comprises a summary of the PhD work and seven articles published in peer-reviewed journals or conferences.

Mengyi Zhu
Trondheim, January 22, 2021

Abstract

The global energy transformation is much strengthened nowadays towards a more sustainable future. Solar energy has become the most popular and fastest-growing renewable energy resource worldwide. However, it still requires the current solar-grade silicon (SoG-Si, purity 99.9999%, 6N) production with lower cost, larger manufacturing scale and increasing sustainability to embrace the upcoming photovoltaic era.

The Elkem Solar process is a Norwegian answer to the looming challenges in the current energy-intensive SoG-Si production as an emerging transformal technology operated by REC Solar Norway in recent years. In the Elkem Solar process, the metallurgical-grade silicon (MG-Si, purity 99%, 2N) produced from submerge arc furnace is further refined to meet the restricted purity requirements of SoG-Si through a combination of a series of metallurgical refining techniques including slag refining, acid leaching, and directional solidification.

This thesis was carried out to further investigate the Elkem process by focusing on the acid leaching and slag refining techniques to gain more practical and theoretical knowledge about the alloying effect on the impurity removal process.

It was found that the alloying metals significantly affects the silicon microstructure, leaching behaviour, impurity segregation, and silicon purification efficiency. Phosphorus segregation and removal are significantly improved after alloying process with alkaline earth metals and followed by acid leaching. The novel Si-Ca-Mg ternary alloying-leaching system exhibited cleaner and more sustainable features than the two binary Si-Ca and Si-Mg systems. Purification efficiency of phosphorus and other impurities increases with increasing Ca/Mg mixing ratio but considerably decreases with fast cooling due to the suppressed impurity segregation.

Based on the principle of Gulliver-Scheil solidification and thermodynamic analysis, the effect of alloying metal concentration and metal-phosphorus affinity was quantified by establishing the phosphorus removal model. The mathematic relationship among the key process parameters such as the initial phosphorus concentration, target phosphorus concentration after purification, alloying metal concentration, and the alloying-leaching operation times are also derived. Combined with the obtained leaching results and phosphorus removal model, the averaged interaction coefficient during the solidification process of different metals (Ca, Mg, and Al) on phosphorus were fitted as, respectively -19.2, -10.8, and -1.8.

Boron removal was improved by Sn alloying and La_2O_3 addition in slag refining. A novel oxygen classification method was proposed for the structure analysis of slags containing multiple network modifiers, and further revealed the weak charge compensation effect of La cation. A thermodynamic model was derived to describe the alloying effect on impurity distribution and further highlights the positive interaction coefficient and high alloying concentration are preferred conditions for improved impurity removal.

Acknowledgements

First and foremost, I have to express my sincerest gratitude and respect to my supervisor associate professor Jafar Safarian, without whom this work would not have been possible. I am deeply impressed by his broad knowledge and keen insight to capture the hidden mechanism behind the surface. I have learned a lot from our frequent meetings and countless discussions whenever I met problems. I feel so lucky to have Jafar as my supervisor, and I would like to extend my heartfelt thanks to his sincerity, enthusiasm, caring, patience, and excellent guidance throughout my Ph.D. study and thesis writing.

I am also greatly honored to have Prof. Gabriella Tranell as my co-supervisor. It is always happy and relaxed to talk with Gabriella on various occasions, and her laughs are indeed contagious. I experienced the most challenging exam ever in my life in her famous refining course TMT4326, but it made my research much easier. In saying the courses, I would also like to express my deep respect to Prof. Leiv Kolbeinsen, who taught me another unforgettable course, MT8200 Advanced Chemical Metallurgy, but with the easiest exam in my life. It is always interesting to listen to Leiv sharing his knowledge by stories in such a gentleman way and his scientific spirit made a profound impact on everyone who attended.

My sincere and special thanks also go to Kai Tang from SINTEF Industry for his impressive insights and expertise on thermodynamics modelling and the close cooperation for this work. There is also much other fruitful cooperation outside NTNU I should acknowledge. I am grateful to Guixuan Wu and Michael Müller from Forschungszentrum Jülich for their constant support of my simulation research since my master time and the simulation cooperation from Shengying Yue at UC Santa Barbara, and also the SIMS measurements by Alexander Azarov from UiO.

I should give deep thanks my officemate Arman Hoseinpur Kermani for his countless help and discussions no matter online and offline, in and outside laboratory, staying in conference hotel or riding on bicycle.

There are also millions of thanks for the help I received from my colleagues on many issues. I would like to thank the excellent mechanical supports from Ivar Andre Ødegård, Dmitry Slizovsky, and once again Arman Hoseinpur Kermani. I publish another conclusion of my three-year doctoral research here that you guys should be the leading mechanical engineers on not only this planet but also in the milky way galaxy. I want to also thank Yingda Yu for his long-standing impressive SEM guidance from the viewpoint of scientific principles and even living philosophy, and for all kinds of his kindhearted help as always. I am also thankful to Syverin Lierhagen for the huge number of ICP-MS measurements, to Torild Krogstad, Birgitte Karlsen, Irene Bragstad, and Gagan Paudel for the teaching and help of ICP-MS sample preparation, Morten Peder Raanes for the help with EPMA analysis, Berit Vinje Kramer for the training of various equipment.

I also want to express my gratitude to Ronny Gløckner from REC Solar AS for his interests, help, and valuable advice from the industrial point of view. I also appreciate Valentina Nilsen for her measurement of some samples, and the constructive discussions with Adrian Murgau in my first year.

I would also like to thank the SiManTi group and the organization by Prof. Merete Tangstad. These three years would be much different without working with those great colleagues and friends: Jian Meng Jiao, Yan Ma, Fabian Imanasa Azof, Adamantia Lazou, Hossein Salehi, Azam Rasouli, Shokouh Haghdani, James Mwase, Dmitry Sukhomlinov, Gerrit Ralf Surup, Erlend Lunnan Bjørnstad, Mertol

Gökelma, Andrea Estragon Broggi, Are Bergin, David Dominikus Eide Brennhaugen, Didier Ngoy, Leandro Gustavo Mendes de Jesus and so on.

I also gratefully appreciate Torunn Kjeldstad from the SuSolTech Research Center and Steinar Brandslet from Gemini for the help of the public dissemination of my work.

It is also a great pleasure to thank my sincere friends who provided invaluable help and went through my times in Trondheim: Di Wan, Dong Wang, Xu Lu, Yijiang Xu, Dongdong Zhao.

Last but not the least, I am forever indebted to my parents for their endless love and unconditional support. This thesis is also heartily dedicated to my wife Lingyi Ren. This thesis would have not been possible without her continuing love and support. Finally, to my upcoming daughter, it is such a great privilege and wonderful feeling for me to be your father. May you grow up with good health and filled with joy and happiness!

List of Papers

Peer-reviewed journal papers:

1. **Mengyi Zhu**, Guixuan Wu, Alexander Azarov, Edouard Monakhov, Kai Tang, Jafar Safarian, "Effects of La_2O_3 addition into CaO-SiO_2 slag: structural evolution and impurity separation from Si-Sn alloy", submitted.

2. **Mengyi Zhu**, Sheng Ying Yue, Guixuan Wu, Kai Tang, Yijiang Xu, Jafar Safarian, "P removal from Si by Si-Ca-Al alloying-leaching refining: Effect of Al and the $CaAl_2Si_2$ phase", submitted.

3. **Mengyi Zhu**, Di Wan, Kai Tang, Jafar Safarian "Impurity removal from Si by Si-Ca-Mg ternary alloying-leaching system." *Materials & Design* 198 (2021): 109348.

4. **Mengyi Zhu**, Sheng Ying Yue, Kai Tang, Jafar Safarian,"New Insights into Silicon Purification by Alloying–Leaching Refining: A Comparative Study of Mg–Si, Ca–Si, and Ca–Mg–Si Systems." *ACS Sustainable Chemistry & Engineering* 8.42 (2020): 15953-15966.

5. **Mengyi Zhu**, Alexander Azarov, Edouard Monakhov, Kai Tang, Jafar Safarian, "Phosphorus separation from metallurgical-grade silicon by magnesium alloying and acid leaching", *Separation and Purification Technology* 240 (2020): 116614.

Conference papers:

1. **Mengyi Zhu**, Kai Tang, Jafar Safarian, "The effect of Ti and Y addition on the microstructure and leaching purification of Ca- alloyed metallurgical silicon", S*ilicon for the Chemical and Solar Industry XV (2020),* p273-284.

2. **Mengyi Zhu**, Adrian Murgau, Jafar Safarian, "Effects of magnesium-doping on silicon leaching for solar grade feedstock production", *35th EUPVSEC Conference Proceedings (2018),* p465-468.

Contributions to conferences

Oral presentations:

1. **Mengyi Zhu**, Guixuan Wu, Kai Tang, Jafar Safarian, “Effect of La_2O_3 Addition to CaO-SiO_2 Slag on B and P Removal from Sn-doped Silicon for Solar-Grade Silicon Production”, *11th International Conference on Molten Slags, Fluxes and Salts*, February 2021, Seoul (virtual), South Korea.

2. **Mengyi Zhu**, Kai Tang, Jafar Safarian, “The effect of Ti and Y addition on the microstructure and leaching purification of Ca- alloyed metallurgical silicon”, S*ilicon for the Chemical and Solar Industry XV*, June 2020, Trondheim (virtual), Norway.

3. **Mengyi Zhu**, Jafar Safarian, " Elements behavior in solidification of Mg-doped silicon and their removal in acid leaching", *Norwegian Solar Cell Conference 2019*, May 2019, Son, Norway.

4. **Mengyi Zhu**, Jafar Safarian," Hydrochloric acid leaching of Mg-doped Si for solar grade feedstock production", *Norwegian Solar Cell Conference 2018*, May 2018, Son, Norway.

Posters:

1. **Mengyi Zhu**, Adrian Murgau, Jafar Safarian, “Effects of magnesium-doping on silicon leaching for solar grade feedstock production”, 35th EUPVSEC Conference, September 2018, Brussels, Belgium.

Content

Chapter 1
Introduction

This chapter presents the research background and major challenges for the current solar-grade silicon (SoG-Si) feedstock production. It also states the motivation and scope of this research and the outline of this thesis.

1.1 Background

Energy is an indispensable condition for modern society and the foundation that supports the progress of human civilization. However, worldwide energy development still faces significant challenges, as global energy consumption has grown too quickly at the expense of exploiting of fossil energy resources on a large scale and increasingly serious global warming effect. It has been reported that the industrial activities of human beings have raised the atmospheric carbon dioxide levels from 280 parts per million to 414 parts per million in the last 150 years and results in global average temperature 0.85 ºC higher than the pre-industrial times.[1] The increasing global temperature will bring a much higher risk of catastrophic changes in the global environment, such as extreme weather and increased sea level. Thus, the international community has recognized the urgent need to limit the global warming effect and towards a carbon-neutral society in the coming decades. For instance, China has announced its national roadmap to achieve the carbon-neutrality before 2060.[2] The goal of net-zero carbon emission in the EU-wide by 2050 has been endorsed by the European Council to be set in legislation through the first European climate law[3]. In the published Norway's national Plan in 2019 by the Norwegian Ministry of Climate and Environment, the climate target of at least 40 per cent greenhouse gas emissions reduction in 2030 compared with 1990 has also been established by law.[4]

In an age of accelerating global warming and increasing international consensus for climate change management, the global energy transformation has been much strengthened to achieve sustainable growth in the future. As one of the most alternative renewable energy sources, solar energy has become the most popular and fastest-growing renewable energy resource worldwide.[5] Figure 1- 1 presents the annual addition of global solar photovoltaic (PV) capacity from 2009-2019[5]. A distinct trend can be seen that the solar PV capacity has been continuously increasing in the past decade. As of the end of 2019, the newly added solar power capacity worldwide was a record number 115 GW, accounting for 57% of total added renewable power capacity additions, and with a cumulative installed capacity of 627 GW. With this increasing speed, predictably, the terawatt-scale era of PV is coming in the next couple of years. It has also been predicted that solar energy could play a central role in the future global energy system and expected to reach a scale 30-70 terawatt by 2050.[6] Since crystalline silicon solar cell is still the dominant product in the present solar cell market, accordingly, the strong demand for solar-grade silicon (SoG-Si) is spreading globally and expanding faster than ever before.

Nevertheless, the crystalline silicon solar cell technology is still facing looming challenges and opportunities from various aspects. To better embrace the coming terawatt PV era, it requires the crystalline silicon solar cells to decrease production cost and increase the manufacturing scale continuously. It also requires SoG-Si production with more sustainable features and better incorporated into the end-of-life solar silicon recycling issue in the future.

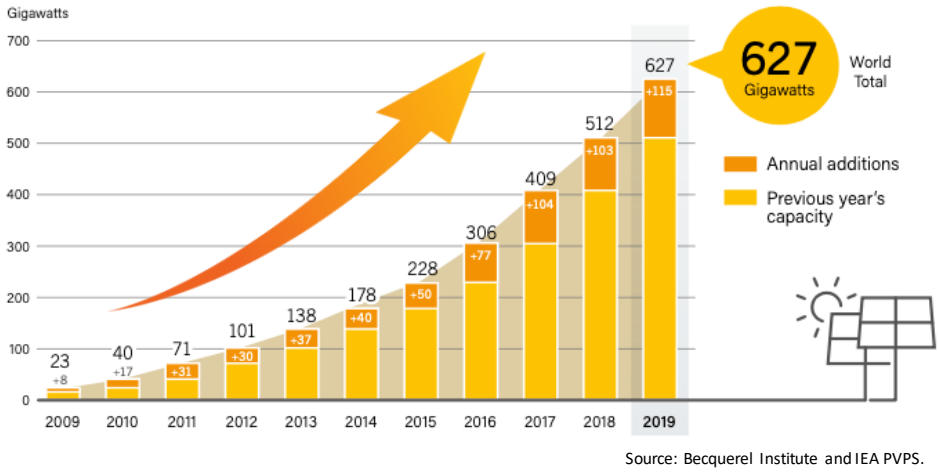

Figure 1- 1. Solar PV global capacity and annual additions, 2009-2019.[5]

1.2 Solar-grade silicon production

A crucial issue for the SoG-Si feedstock production is to supply crystalline silicon with restricted composition requirements (99.9999% purity, 6N). Nowadays, most of the SoG-Si is produced by the modified Siemens process and the fluidized bed reactor process. The Siemens process is an energy-intensive chemical vapor deposition method that involves the distillation of volatile silicon compounds and the decomposition process of the gas into silicon. The Siemens process also produces polysilicon purer than required up to electronic grade (10N to 11N purity). It is also known as very energy demanding and expensive, primarily due to the step of silicon decomposition from trichlorosilane. In this step, a large amount of energy is required to keep the rod reactor at around 1100 °C for a long time because of the slow decomposition kinetics. Compared to the Siemens process, the fluidized bed reactor process consumes much lower energy and produces polysilicon continuously. However, the energy reduction is limited, and both methods still face the potentially severe environmental issue as the chlorinated gases and silane are inflammable and may leak into the atmosphere [7]. Thus, it is therefore with great interest for the PV industry and metallurgists to develop a more sustainable and environmentally friendly process for the expanding demand on SoG-Si production. As an evolving technique for the alternate SoG-Si production, the metallurgical process has received increasing attention due to its low carbon emission and low energy consumption.[8]

As an emerging and transformational technology for alternate SoG-Si production, the Elkem Solar process, which is developed in Norway and now operated by REC Solar Norway, has significantly lower energy consumption and lower carbon footprint. The total energy consumption of the Elkem process is known significantly reduced from ~170 kWh/kg Si of modified Siemens process and 75-95 kWh/kg of fluidized bed reactor process to 30-60 kWh/kg Si, and with the equivalent carbon dioxide emission 10.8 kg CO_2/kg SoG-Si, which is only around one tenth of the other known SoG-Si production routes.[9]

The industrialized process sequence of the Elkem Solar process is shown in Figure 1- 2. It consists of several metallurgical refining techniques known as slag refining, acid leaching, directional solidification. In the slag refining process, boron is the target impurity to be removed, and the acid leaching process aims to remove another problematic impurity phosphorus. In the directional solidification process, the metallic impurities are further separated from fulfilling the restricted SoG-Si purity standard.

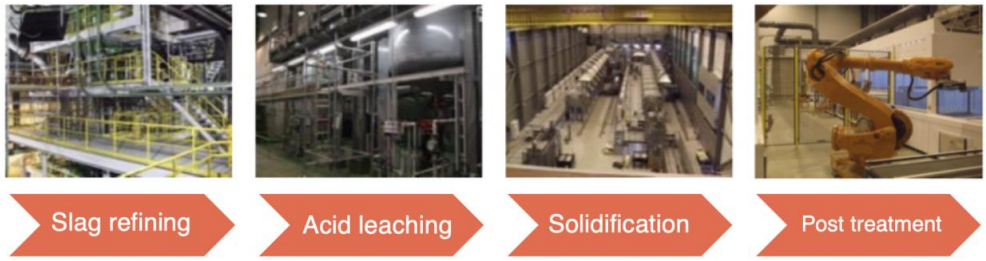

Figure 1- 2. Process sequence of the Elkem solar process for the SoG-Si feedstock production.

1.3 Motivation and scope

Driven by the formerly stated issues, this thesis was carried out to further study the Elkem process by focusing on the acid leaching and slag refining techniques. According to the results from early-stage research by the NTNU team in recent years[10–13], Mg has shown attractive features as an impurity getter for impurity removal in the acid leaching process. However, the refining mechanisms and preferred processing conditions of both alloying and leaching techniques still require further study. This work started by investigating the Si-Mg binary alloying-leaching process and was dedicated to further understanding the impurity removal mechanism towards enhanced process controllability. Thus, the following objectives were pursued:

- To experimentally investigate the Si-Mg binary alloying-leaching alloy system from the perspective of microstructure, phase reactivity, P segregation behaviour, and leaching efficiency.
- To thermodynamically understanding the alloying effect on P segregation behaviour and the relationship with key processing parameters.
- To comparatively investigate the Mg-based and Ca-based Si alloying-leaching refining process.
- To design and optimize the current alloying system and to parametrically investigate the leaching conditions and leaching kinetics.
- To experimentally and thermodynamically study the effect of other common impurities on P segregation and removal.
- To evaluate and provide necessary contributions to the study of the alloying effect on impurity distribution in slag refining.

1.4 Outline of this thesis

This thesis consists of six chapters. Chapter 1 compromises the general introduction to the research background, motivation, and scopes of this thesis. Chapter 2 summarizes the fundamental aspects of silicon purification by acid leaching and slag refining, where the literature and the previous research achievements are reviewed. Chapter 3 presents the experimental procedure and research methodology, including employed instruments for characterization and software for theoretical calculations. Chapter 4 summarizes the research work of this thesis with further recommendations. Finally, Chapter 5 presents the published or submitted manuscripts. The frame of this work can also be seen in Figure 1- 3.

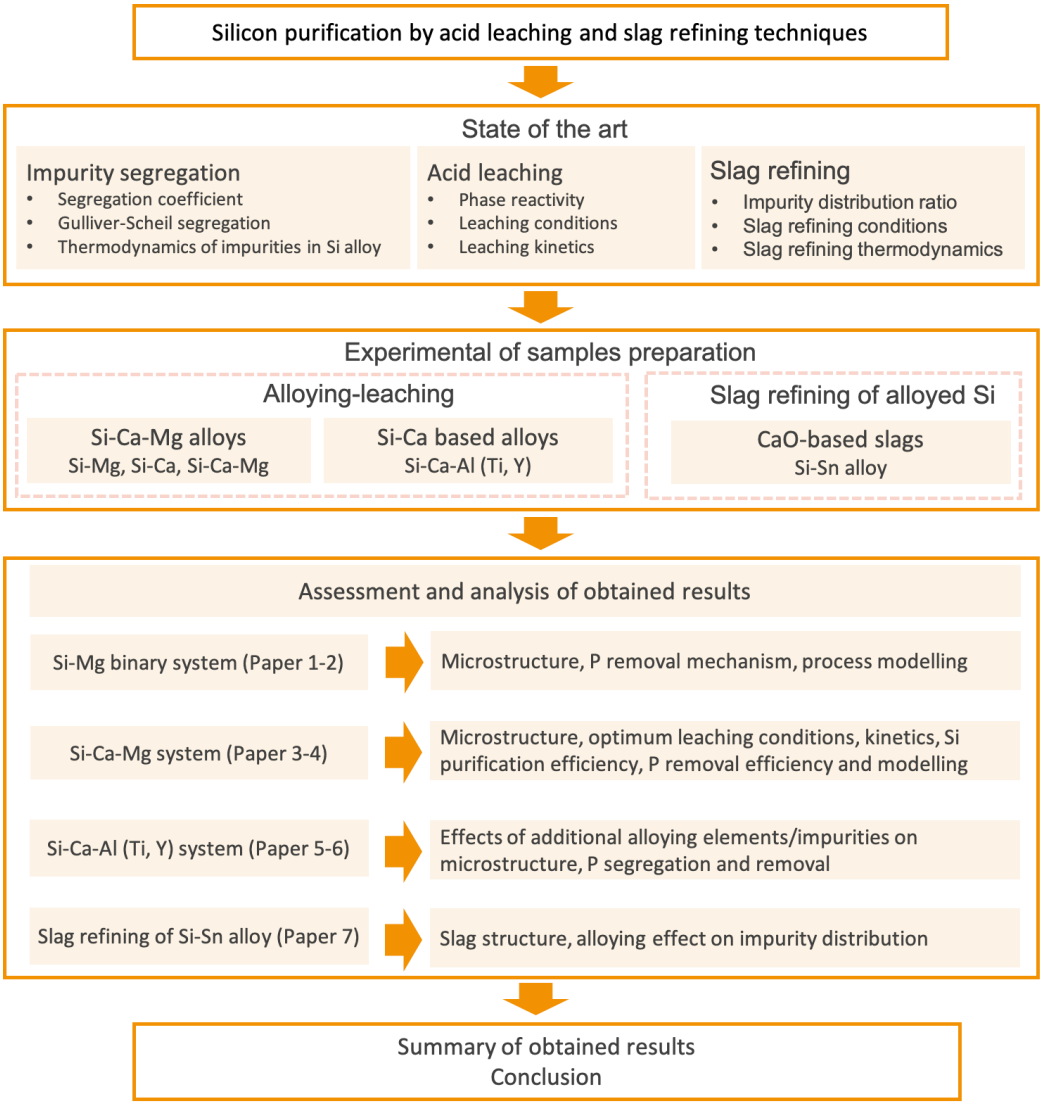

Figure 1- 3. Frame of this thesis.

Chapter 2

Metallurgical refining techniques for silicon - A literature review

The metallurgical-grade silicon (MG-Si, purity 98-99%) contains high impurity amounts. As presented in Figure 2-1, a variety of metallurgical methods have been developed and investigated to reach the purity for solar-grade silicon feedstock (SoG-Si, purity 99.9999%).

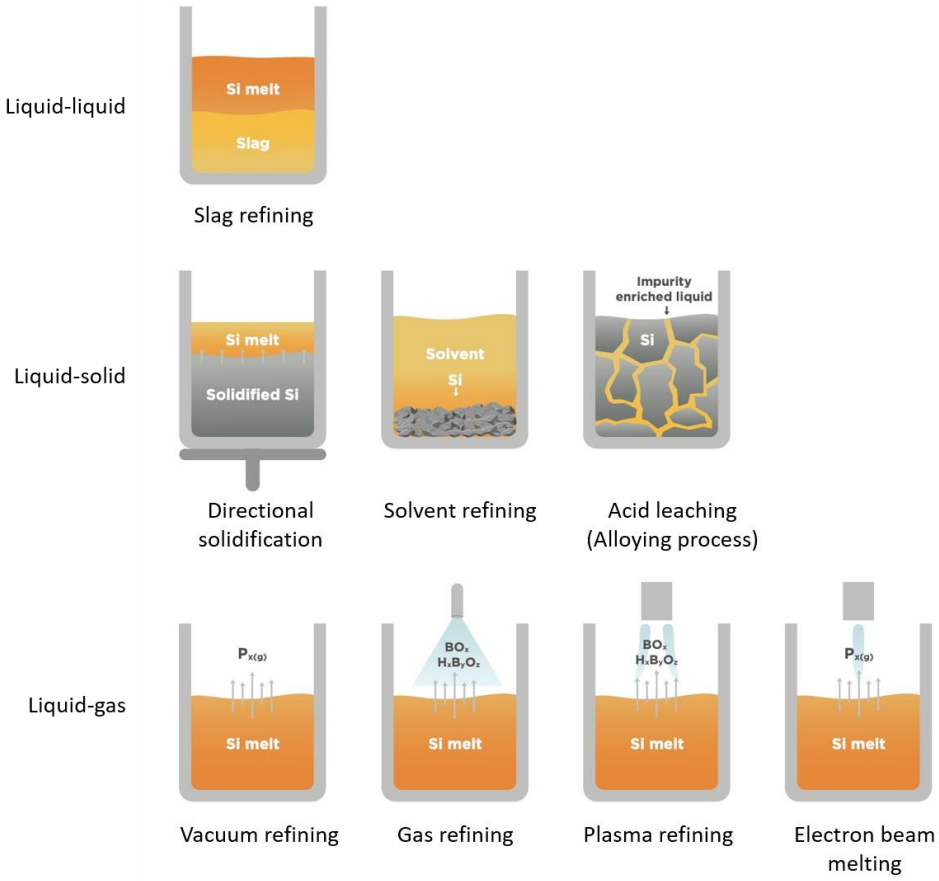

Figure 2-1. Overview of the main Si refining techniques.

The Si refining techniques can be divided into three categories of according to their different features and principles:

1) Based on impurity segregation between solid and liquid
   a) Acid leaching
   b) Solvent refining
   c) Directional solidification

2) Based on the liquid-liquid extraction
    a) Slag refining
3) Based on the volatile gas species evaporation
    a) Vacuum refining
    b) Gas refining
    c) Plasma refining
    d) Electron beam melting

In the following sections, the above metallurgical refining techniques will be reviewed and with the focus on acid leaching and slag refining as the applied methods in this research.

2.1 Acid leaching

Acid leaching is a commonly used technique for MG-Si purification due to its low cost and easy operation advantages. Depending on different purity requirements, it can be used either as the first step pre-treatment of raw materials or the main refining step. In the leaching process, impurities segregated along the Si grain boundaries, or in other word between the primary Si grains that are formed in solidification, dissolve in an acid solution, but the Si does not. Therefore, purified Si particles are obtained.

Since the acid leaching process inherently relies on the impurity segregation behaviour during the solidification of molten Si, theoretically, only impurity with low segregation coefficient is able to be removed in the acid leaching process and a theoretical limit of impurity removal degree exists. To cope with the drawbacks, alloying elements often added into Si to further promote the impurity segregation and the leachability of precipitates. Thus, according to the Si materials that acid leached, the acid leaching technique can be further classified into direct leaching of MG-Si and leaching of alloyed Si.

In general, direct leaching of MG-Si works for the removal of metallic impurities due to their strong segregation behaviour, but ineffective for the impurities with large segregation coefficient like B and P.

After alloying with reactive metals like Ca, the leaching extraction of P can be significantly improved. Thus, in the Elkem Solar process operated by REC Solar Norway AS, acid leaching is employed to refine Ca- alloyed Si that mainly targets the removal of the P impurity and large extent metallic impurities. Since the solvent technique is also based on the principle of impurity segregation, acid leaching is also a common adopted assistant procedure. For instance, in the Silicor process, acid leaching is applied for the separation of solidified Al and Si after the Si-Al solvent refining. Thus, the relevant applications for leaching solidified solvent such as Si-Al, Si-Sn, Si-Fe, Si-Cu are also included. The overview of the research/applications of the acid leaching technique is briefly presented, as shown in Figure 2-2.

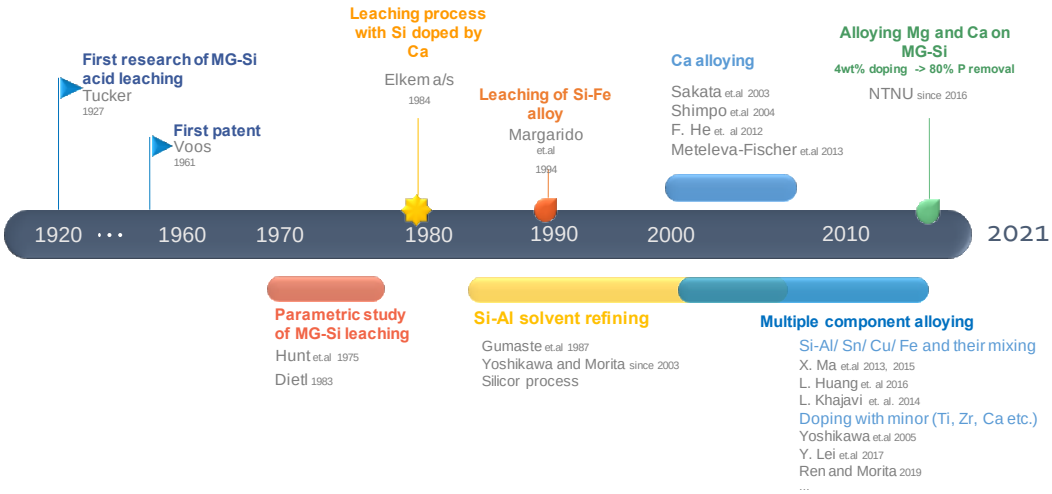

Figure 2- 2. Timeline about the application/study of acid leaching in Si refining.

2.1.1 Process principles

The principle of the acid leaching technique is based on the impurity segregation behaviour during Si solidification. As most of the impurities tend to be rejected by the solidifying Si and pushed away from the solidification front to the liquid phase, they are finally enriched along the Si grain boundaries. The impurity-containing phase could be further dissolved in an acidic solution, which is inert to Si, and the remaining is refined Si with higher purity.

The segregation coefficient for element i in silicon, k_i, is defined as the ratio of the equilibrium concentration of the element in the solid to that in the liquid phase at the solidification front:

$$k_i = C_S/C_L \qquad (2-1)$$

where C_S and C_L denote the concentration of impurity in solid and in liquid.

According to the definition, for impurity with segregation coefficient $k_i < 1$, during the solidification of molten MG-Si, the impurity tends to gather in the remaining liquid phase and the MG-Si can be refined. On the contrary, if $k_i > 1$, the impurity prefers to remain in the solid phase, and it cannot be removed from MG-Si.

The segregation coefficient for the common impurities in MG-Si are presented in Table 2-1. It can be seen that most of metallic elements such as Fe, Al, Ca, Mg, and Ti in Si are with low segregation coefficients, which indicates the possibility to be separated in large extent. However, the segregation coefficient of B ($k_B = 0.8$) and P ($k_P = 0.35$) are much higher.

Assuming no back diffusion happens into the solid phase from the solidification front, and liquid phase remains homogeneous, the distribution of an impurity during Si solidification can be described by the Scheil equation:

$$C_S = k_i C_0 (1 - f_S)^{k_i - 1} \qquad (2-2)$$

where f_S is the fraction of the melt solidified, C_S and C_0 denote the impurity concentration in solid front and in the initial melt.

Applying Equation (2-2), Figure 2- 3 is obtained and it shows the segregation extent of common impurity elements in Si as function of solid fraction. Compared to the metallic impurities, it is seen that

the segregation effect of B and P is weak. Particularly, B concentration almost remains unchanged during the whole solidification range. As shown in Figure 2- 4, the atom probe tomography reveals that B distributes sporadically and randomly in both fine and coarse MG-Si particles. Thus, in general, B separation is hardly achieved via acid leaching of MG-Si, while the separation of P requires the addition of specific alloying element to further enhance its segregation in Si. Owing to the low segregation coefficient, it can be seen that metallic impurities exhibit strong tendency to be rejected to the remaining liquid phase as their concentration in solidified Si is much lower than their initial. Consequently, the impurity concentration in the remaining liquid phase soars, especially at the final stage of solidification, and binary, ternary, or more complicated precipitates are formed, as presented in the Figure 2- 5.

Table 2- 1. Segregation coefficient of impurities in silicon [14]

Impurity	**Segregation coefficient**	**Impurity**	**Segregation coefficient**
B	0.80	Fe	6.4×10^{-6}
P	0.35	Ti	2.0×10^{-6}
C	5.0×10^{-2}	Cu	8.0×10^{-4}
Al	2.8×10^{-3}	Mg	3.2×10^{-6}
Li	1.0×10^{-2}	S	1.0×10^{-5}
Ag	1.0×10^{-6}	As	3.0×10^{-1}
Au	2.5×10^{-5}	Sb	2.3×10^{-2}
Ni	1.0×10^{-4}	Zn	1.0×10^{-5}
Ca	8.0×10^{-3}	Bi	7.0×10^{-4}
Mn	4.5×10^{-3}	Cr	1.1×10^{-5}

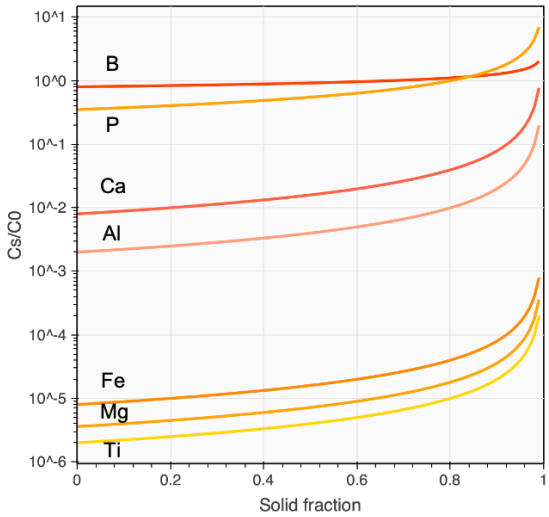

Figure 2- 3. Segregation extent of common impurity elements during Si solidification as function of solid fraction calculated using the data in Table 2-1.

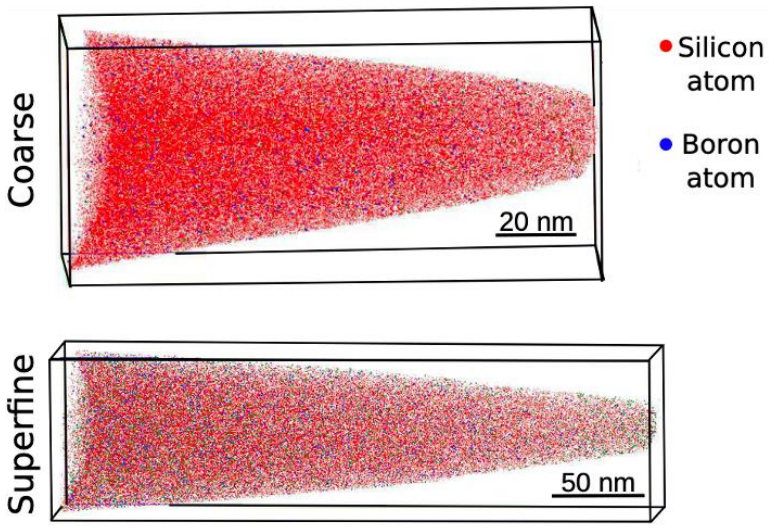

Figure 2- 4. Atom probe tomography of B and Si distribution in coarse and fine MG-Si particles.[15]

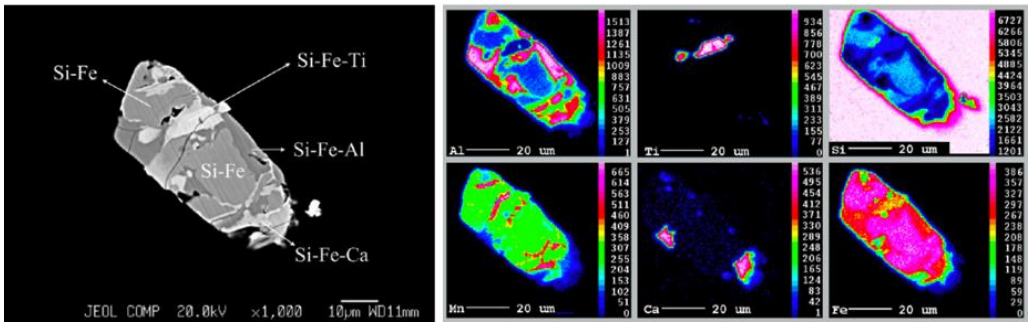

Figure 2- 5. EPMA elemental mapping results of the distribution of typical precipitated phase in MG-Si.[16]

Since the impurity enriched precipitates are generally around the Si grains, if the solidified Si is pulverized to a particle size equivalent to the size of the polycrystalline grains, a major portion of the metallic impurities will be able to be exposed to the surface. As shown in Figure 2- 6, the exposed impurity phase could be further dissolved in the leaching process by acids, and thus, the Si remains unreacted and recovered.

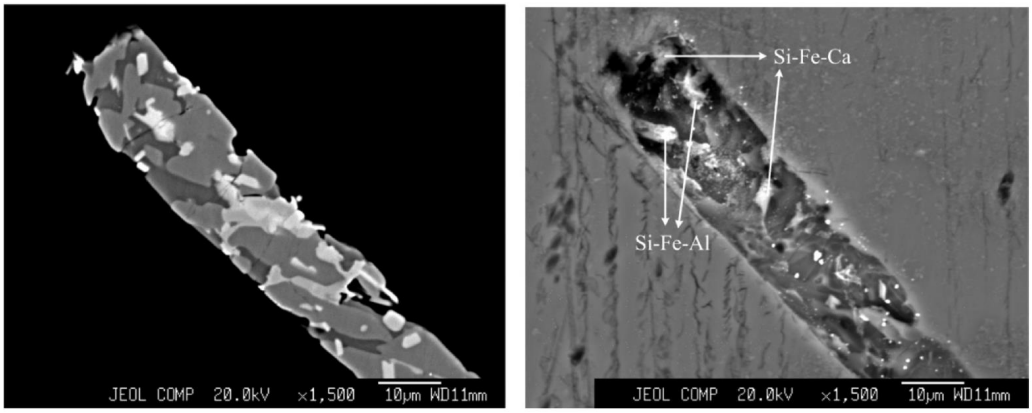

Figure 2- 6. Precipitates of MG-Si after leaching in HF.[16]

Compared with other refining techniques, acid leaching technique has the following advantages:

1. Good efficiency for impurity removal. Acid leaching is efficient for the separation of a wide number of impurities. Additionally, the addition of a refiner metal into Si further improves the segregation of impurities, especially of P, which makes the technique more practical and efficient.
2. Low energy consumption. Compared to the conventional pyrometallurgical refining process, hydrometallurgical leaching process requires much lower energy input.
3. Easy operation. The leaching process takes place at low temperature and without complicated equipment.

However, it is worth mentioning that even though the acid leaching process possesses the above advantages, the leaching treatment removes only impurities that appear as free separate phases exposed to acids. Impurities in Si solid solution or impurity phases trapped inside the silicon grains are still difficult to be separated. Additionally, the theoretically obtainable final purity is determined by the impurity segregation effect during solidification. Thus, the theoretical purification limit is determined by the solidification process and may not be reached because of incomplete leaching. From this perspective, only the leaching of MG-Si could be regarded as a typical hydrometallurgical process while the leaching of alloyed Si with a refiner metal should be considered more as a thermal metallurgical process, and the followed leaching process is only used for the final removal of the formed impurity gathering phases. Based on this fact, the terminology “alloying-leaching” is adopted in this work and refers to the Si purification process starts from alloying of MG-Si with a refiner metal, followed by solidification and acid leaching.

2.1.2 Leaching of MG-Si

The leaching procedure of MG-Si is shown in Figure 2- 7. As impurities segregate as fine precipitates during the solidification process, the solidified MG-Si is firstly crushed by a milling machine and further sieved by target particle size. After that, the pulverized MG-Si is charged into a container mixed with leaching acids. The leaching process performs under specific conditions and completes after the leaching reaction is over. Finally, the leached Si is cleaned till neutral, and the purified Si is obtained.

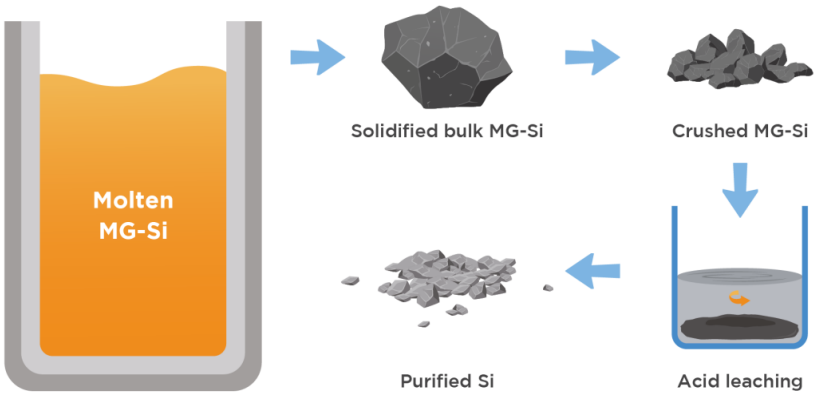

Figure 2- 7. The procedure of MG-Si acid leaching.

Acid leaching for Si purification has been studied over decades, the experimental conditions and main results for MG-Si leaching are summarized in Table 2-2. The first reported research was performed by Tucker [17] in 1927, it was pointed out that acid leaching of pulverized MG-Si is a viable purification method to purify Si with purity 93-98wt% to 99.94wt% with a successive acid treatments of aqua regia, hydrofluoric and sulphuric acids. Afterwards, a number of investigations for MG-Si leaching were conducted in order to determine the optimal hydrometallurgical condition[18–21].

Voos[22] patented an acid leaching process to purify crude Si to purity as high as 99.99%. In the claimed process, the crude MG-Si is firstly ground to fine powders passes through a screen of 0.075 mm, and then digested by finely dispersed dilute acid (HCl or H_2SO_4 or both) to form a paste. The pasty mass is then leached by acids with HF addition and finally subjected to heap leaching for at least one day or longer time.

Hunt et al.[18] found out the proper process window to remove more than 90% of the impurities of MG-Si leaching is to use silicon particles smaller than 0.05 mm at 75°C aqua regia acids for 12 hours.

In the attempt to upgrade crude Si to a solar-grade quality, Dietl [19] studied the effect of leaching conditions such as acid concentration, leaching time, temperature, and particle size of the milled MG-Si. It was found that the mixture of 2.5% HCl with 2.5 % HF is the optimal combination while increasing HF concentration abnormally led the decreases of Ca, Al impurity removal. The reason assumed to be related to the formation of some insoluble fluorides with higher HF concentration. The impurity removal efficiency was found to increase with increasing leaching temperature and decreasing particle size. The metallic impurities can be eliminated down to the order of several ppmw levels, but the removal of B and P is found ineffective.

Chu and Chu studied the effectiveness of different acid combinations for pulverized MG-Si, including HCl, aqua regia, and the mixture of H_2SO_4 and HNO_3. It was found that major portion of metallic impurities could be removed and aqua regia exhibits the highest effectiveness followed by equivolume mixture of H_2SO_4 and HNO_3, while HCl is the least, especially for the Fe removal.

HF was further found much more efficient than aqua regia from the leaching test performed by Juneja et al. [23]. In their work, 99.95 % purity Si was obtained by HF leaching at 50 °C for 4 h with a particle size from 150 μm.

Similarly, in the work by Santos et al.[20], significant improvement of Fe and Ti impurity removal was achieved by HF leaching. The reason is found due to Si-Fe and Si-Fe-Ti precipitates in solidified MG-Si are insoluble in the solution of HCl, H_2SO_4, HNO_3 or their mixtures, but can be readily dissolved

and removed by HF. However, differ with previous research [21,22], it was also found that leaching with HCl alone is possible to remove c.a. 85% of the impurities from pulverized MG-Si. The reason is assumed owing to the different types of MG-Si that contains different types of precipitates with different reactivity. After a large number of leaching trails, the optimal leaching particle size was found as 116 μm, and a two-stage leaching using 16% HCl and 2.5% HCl-2.5% HF was achieved the best purification results.

Anglezio et al.[24,25] characterized the intermetallic compounds of a MG-Si containing 0.31 wt% Fe, 0.18 wt% Al, 0.22 wt% Ca, and 0.044 wt% Ti. The impurities were found distributed in complex precipitates in MG-Si and observed as $CaSi_2$, $CaAl_2Si_2$, $CaAl_6Fe_4Si_8$, $FeSi_{2.4}$, and $TiFeSi_2$. A Si-Fe-Al-Ca quaternary phase diagram was established by Margaria et al.[26] to understand the behaviour of impurity precipitation in MG-Si solidification. Margarido et al.[27,28] determined the reactivity of different precipitates of an industrial Si alloy, in the leaching process. For example, the leaching removing ability by the hydrochloric acid can be regarded as the following sequence:

$$CaSi_2, CaAl_2Si_2 > Fe\text{-}Al\text{-}Si\text{-}Ca > Al\text{-}Fe\text{-}Si >> FeSi_2$$

However, in the aqua regia, the reactivity sequence becomes:

$$Si\text{-}Al\text{-}Ca, Si\text{-}Al\text{-}Fe\text{-}Ca > CaSi_2 >> Si\text{-}Fe, Si\text{-}Ti\text{-}Fe, Si\text{-}V\text{-}Ti, Si\text{-}Ca\text{-}Ni$$

Recently, Kim et al. investigated the leaching of pulverized MG-Si with acetic acid (CH_3COOH) addition, they found that the acid combination HNO_3+ HF+ CH_3COOH (2:1:2) at room temperature for 25 h leaching successfully purified Si to 99.99% purity with 99.92% and 99.98% removal for Fe and Al impurities. Similarly, in the research of Lu et al. [29], the addition of CH_3COOH into HCl+HF also led to better impurity removal, especially in the Fe, Mn, V, Cr, Cu, and Ti impurities.

Other than modifying the acid combination, it is also reported that impurity extraction by leaching also significantly improved by the leaching of slag treated MG-Si.[16,30–32] The main reason is owing the composition change that minor Ca diffused from slag into Si so that the secondary precipitated phases are reconstructed to more leachable phases. The further mechanism will be introduced and discussed in the following section for the alloying-leaching method.

In recent years, the metal assist chemical etching method[33,34], which is widely used for the production of porous Si and Si nanowires, is also reported with better impurity removal than conventional leaching. The method depends on the in-depth penetration of metal catalysts (e.g., Ag, Cu etc.) and in association with the cracking of Si particles, however, even though the etching of Si increases the possibility of the exposure of more impurity phases, on the contrary, the Si yield could be greatly reduced in return.

In summary, the leaching of MG-Si has been widely investigated to improve the leaching efficiency. A variety of factors play important role in the impurity extraction such as leaching temperature, leaching time, MG-Si particle size, stirring method, and acid combination. Since the metallic impurities often form fine precipitates, MG-Si is therefore required to be pulverized to expose enough impurity phase to the acid solution. In addition, as the transition metal silicide like $FeSi_{2.4}$, $TiSi_2$ are chemically inert, and cannot be attacked by a number of common acids including HCl, H_2SO_4, HNO_3, $HClO_4$, but only readily reacts with HF. Thus, high leaching efficiency could be only reached through the acid leaching with HF addition. However, the introduction of HF into Si purification unavoidably reduces the Si yield and may also increase the potential operation safety issue. However, it also worth to mention that since the principle of acid leaching is based on the impurity segregation behaviour during solidification, direct leaching of MG-Si is inherently limited for the non-metallic impurities like B and P, which are more evenly distributed in MG-Si due to their relatively low segregation upon solidification.

Table 2- 2. Summary of hydrometallurgical purification investigations on MG-Si.

Authors	Si source	Leaching agents	Particle size (µm)	Temperature & Time period	Impurities removal
Voos [22](1961)	MG-Si Si (>99.5%)	HCl, H_2SO_4, HCl+HF	<75	70-80 °C >24 h	Best purity ~99.994%
Hunt et al.[18] (1976)	MG-Si		<50	75 °C- 12 h	>90%
Dietl [19] (1983)	MG-Si Si (~99.0%) Fe (0.35-0.50%), Al (0.16-0.25%), Ca (0.05-0.27%)	HCl (2.5%) +HF (0.5-5%)	10-140	20 °C-16 h 80 °C-2 h	Fe:1800->5 ppm Al:1500->20 ppm Ca: 1450-> 4 ppm Mg: 45->0.5 ppm Ti: 250->0.2 ppm
Chu and Chu[21] (1983)	MG-Si Si (~99.5%), Fe (0.35%), Al (0.15%)	Aqua regia, HCl, H_2SO_4+HNO_3	-	96-400 h	Al: 320 ppm Fe: 350 ppm
Norman et al.[35] (1985)	MG-Si Si (~98%), Fe (0.84%), Al (0.48%), Ca (0.085%)	Stage 1:Aqua regia Stage 2: HF Stage 3: HCl	<150	Stage 1: 80 °C - 2 h Stage 2: 80 °C - 1 h Stage 3: 25 °C - 2 h	Fe: 8400-> 200 ppmw Al: 4800-> 170 ppmw Ca: 850-> 40 ppmw
Juneja et al.[23] (1986)	MG-Si Si (~98%), B (35 ppmw) Fe (1.0%), Al (0.25%), Ca (1.2%)	Aqua regia, HF	150-400	50 °C-4 h	B: 35-> 20 ppmw Fe: 10000-> 60 ppmw Al: 2500->100 ppmw Ca: 12000 -> 5 ppmw Ti: 210 -> 25 ppmw
Santos et al.[20] (1990)	MG-Si Si (~98%), Fe (0.31%), Al (0.77%), Ca (0.09%)	HNO_3, H2SO_4, HCl (16%), HF (2.5%), HCl (2.5%)+ HF (2.5%)	30-126	20,50,80 °C 2-18 h	Fe: 3100 -> 130 ppmw Al: 7700 -> 820 ppmw Ca: 900 ->24 ppmw
X. Ma et al.[36] (2009)	MG-Si Si (~99.0%), Fe (0.23%), Al (0.27%), Ca (0.058%)	HCl, HF, HNO_3	4000-5000 2000-3000 500-1000 <100	50 °C-8 h	Fe: 2340->14.6 ppmw Al: 2710->461.4 ppmw Ca: 576-> 3.6 ppmw Total: 5851-> 504.0 ppmw
Metele-va-Fischer et al.[31] (2012)	Slag treated MG-Si	HCl+HF	<100	-	P: 16 ppm (82.1% re-moval) Al: 46 ppm (94.9% removal) Ca: 132 ppm (97.9% removal)

M. Fang et al.[16] (2013)	MG-Si, Slag treated MG-Si	HCl, HF, HCl+HF (H^+: 2 mol/L)	<300	25 °C - 4 h	B: 24-> 20 ppmw P: 39-> 30 ppmw Fe: 240-> 50 ppmw Al: 753-> 65 ppmw Ca: 286->35 ppmw
M. Fang et al.[30] (2014)	Slag treated MG-Si	HCl (0.5-8 mol/L)	150-300 100-150 50-100 <50	20-80 °C 0-8 h	Fe: 96.3% removal Al: 93% removal Ca: 98.1% removal
L. Huang et al.[37] (2016)	Slag treated MG-Si	HCl (5M)	<149	25 °C-12 h	P: 23.94-> 20.73 ppmw Total: 4617.8-> 1665.9 ppmw
J. Kim et al. [38] (2015)	MG-Si Si (~99.5%), Fe (0.13%), Al (0.09%)	HNO_3+HF+ CH_3COOH	610-710	25 °C-25 h	Fe: 99.92% removal Al: 99.98% removal
H. Lai et al.[39] (2016)	MG-Si Si (~99.74%), Fe (0.14%), Al (0.04%)	HF, HF+H_2O_2,	75-154	25 °C - 90 °C 4 h	B: 8.6-> 3.0 ppmw P: 35-> 25.6 ppmw Fe: 1424-> 34.1 ppmw Al: 394-> 54.9 ppmw Ca: 39-> 5.2 ppmw Si purity: 99.74%-> 99.99%
Guan et al.[33] (2016)	MG-Si	HF+ $Cu(NO_3)_2$+H_3PO_3 HF+$Cu(NO_3)_2$+H_2O_2 both with 6-10mL ethanol	-	-	from 97.94% --> 99.5%
H. Lu et al.[29] (2017)	MG-Si Si (~99.5%), Fe (0.42%), Al (0.12%), Ca (0.028%)	HCl+HF+CH_3COOH	91	75 °C- 6 h	Fe: 4190-> 351 ppmw Al: 1230-> 375 ppmw Ca: 283-> 33 ppmw Total: 6879 -> 795 ppmw (88.44%)
H. Lu et al.[32] (2017)	MG-Si, Slag treated MG-Si	HCl (4M), HCl (4M)+HF (1M), HNO_3 (4M), HNO_3 (4M)+HF (1M), Aqua regia	250-1000, 150-250, 106-150, 75-106, <75	65 °C- (2-8) h	Fe: 4225-> 363 ppmw Al: 6223-> 435 ppmw Ca: 12291-> 112 ppmw
F. Xi et al. [34] (2018)	MG-Si Si (~99.55), Fe (0.24%), Al (0.04%), Ca (0.08%)	Stage 1: HF Stage 2: HF+$AgNO_3$ Stage 3: HF+ $AgNO_3$+H_2O_2	75-150	Stage 1: 25 °C - 2 h Stage 2: 25 °C - 1 min Stage 3: 25 °C - 2 h	Fe: 2395.0-> 22.3 ppmw Al: 418.0-> 13.5 ppmw Ca: 810.0-> 40.6 ppmw Si purity: 99.95%-> 99.99%

2.1.3 Leaching of alloyed Si

As direct leaching of MG-Si only works for the removal of metallic impurities, Si is often alloyed with a reactive metal refiner to further promote impurity segregation behaviour, especially for the improvement of P segregation. The typical procedure is presented in Figure 2- 8.

The benefits of Si alloying are distinct, firstly, the former phases transition metal impurity with poor reactivity can be reconstructed to easily leachable phase; secondly, the addition of metal refiner attracts impurity together and enhances the impurity extraction efficiency, especially for the enhanced P removal; thirdly, the precipitates in MG-Si could only sporadically distributed due to their minor amount, and thus, pulverized MG-Si is required. However, with the introduction of new alloying metal, larger precipitates could form, and the Si loss during the pulverization process is reduced.

Figure 2- 8. The procedure of MG-Si acid leaching

According to the impurity removal principle and the features of leaching process, the ideal alloying element candidate to add to silicon should follow the criteria below:

1. Strong affinity with impurities. The metal refiner is required to have strong affinity with impurities in Si, so that the segregation effect could be enhanced.
2. Limited solubility in Si. The refiner metal should have low solubility in Si otherwise new impurity would be introduced.
3. Formation of leachable phase. The addition of a refiner metal must lead to the formation of a leachable secondary phase, which can be dissolved and easily washed away in the following leaching procedure.
4. Environmentally friendly leaching process. All materials should be non-toxic, and the alloying-leaching process should not produce hazardous by-products.
5. High Si recovery. The metal refiner usually consumes Si to form silicide, the Si loss should be limited.
6. High economic effectiveness. The alloying metal candidate should be commonly used and the addition amount should not be high.

In short, the alloying-leaching approach is an efficient method that significantly improves the purification performance of MG-Si. The selection of refiner metal, solidification conditions, and leaching conditions all possibly affect the efficiency of impurity removal. The reported alloying-leaching process is summarized and listed in Table 2- 3. In the following section, the alloying-leaching approach for Si purification is discussed.

Table 2- 3. Review of alloying-leaching process for silicon purification.

Author	Si Source/Material	Alloy metal	Cooling rate	Crucible	Particle size (µm)	Acid type	Temperature (°C)	Purification degree
Schei[40] (1985)	MG-Si B (30 ppmw), P (50 ppmw), Metals (6000 ppmw)	1-3 wt% Ca	-	-	c.a. 5 cm	Stage I: HCl Stage II: HF+ oxidizing agent	-	B: 2.15-> 2.15 ppma P: 4.52-> 1.75 ppma Fe: 3600-> 17 ppmw Al: 3700-> 150 ppmw Ca: 29000-> 200 ppmw
Sakata et al.[41] (2002)	Si (~96%), Fe,Ti (~1wt%)	2-8 wt% Ca	Quenching, 4.4 K/min	Graphite	-	Aqua regia	95°C - 1h	Fe: 85-96% remval Ti: 80-93% removal
Shimpo et al.[42] (2004)	SEG-Si - 3% P alloy	5.17% Ca	4.4 K/min	Graphite	2-5 mm	Aqua regia	95°C - 1h	P: 85 --> 16.7 ppm Ca: 99.3% removal
F. He et al.[43] (2012)	MG-Si Fe (0.14%), Al (0.086%)	CaO	Casted	Graphite	100 to 120 mesh	Stage 1: HCl (4 mol/) Stage 2: aqua regia (6 mol/L) Stage 3: HF (1 mol/L)	80°C - (24h, 12h,12h for 3 cycles)	Al: 748-> 2 ppm Ti: 10 -> 8 ppm Ca: 59627 -> 427 ppm Fe: 1504 -> 4 ppm
Meteleva - Fisher et al.[44] (2012)	MG-Si Si (~98.5wt%), Fe (0.28%), Al+Ti (0.08%), B (65+-29 ppmw), P (85+- 19 ppmw)	3-10% Ca 5.17% optimal	0.01-10 K/min	Alumina	-	-	80°C - 4 h	
Meteleva-Fisher et al.[45] (2013)	MG-Si Si (~98.5wt%), Fe (0.28%), Al+Ti (0.08%), B (65+-29 ppmw), P (85+- 20 ppmw)	3-10% Ca 5.18% optimal	0.01-11 K/min	Alumina	100	20% HCl, 20% HF, 20% HCl + HF	80°C - 4 h	B: 20-50% removal by HCl P: 20-40% removal by HCl Fe: 80% removal by HF Al: 50-60% removal by HCl
Johnston and Barati[46] (2013)	doped MG-Si (P: 326 ppmw) doped MG-Si (B: 213 ppmw)	1-4 wt% Ca, 1-5 wt% Ti	4 K/min	Alumina	<1.18 mm for Ca <106 um for Ti	Stage I; diluted Aqua regia Stage II: diluted Aqua regia+ H_2SO_4	75°C - 1h	99% P was removed
H. Lai et al.[47] (2015)	MG-Si Si (~99.99%), Fe (0.14%), Al (0.04%)	5 wt% Ca	5 K/min	Alumina with lid	<160	HCl+HF (H+: 2 mol/L)	60°C - 6h	B: 9 -> 4 ppm P: 35->5 ppm Fe: 1000 -> 3 ppm Al: 300 -> 40 ppm

H. Sakiani et al. [48] (2020)	Si (6N), Fe (4N+), Ca (4N+), Si-B, Si-P	5-25wt% Ca, 5-25wt% Ca +5wt% Fe	3 K/min	Alumina with lid	-	Stage I: 10% HF + 10% HCl + 20% acetic acid Stage II: diluted aqua regia	-	B (4%) P (13.5%) removal (MG-Si) B: 1247-> 656 ppma 44.3% removal (Si-Ca-Fe) P: ~350 -> 37 ppma 88% removal (Si-Ca-Fe)
Safarian and Tranell[10] (2016)	MG-Si Fe (0.17wt%), Al (0.16wt%), Ca (0.014%), B (60 ppmw), P (27 ppmw)	0.2-4.9 wt% Mg	10 K/min	Graphite	100-300	Stage I: 15% HCl Stage II: 2.5% HCl	Stage I & II: 80°C - 3h	P: 27->7.5, 70% removal Fe: 60% removal Al: 70% removal
Espelien and Safarian[11] (2017)	MG-Si Fe (0.37wt%), Al (0.28wt%), Ca (0.017%), B (47.3 ppmw), P (16.7 ppmw)	2-5 wt% Mg	-	Graphite	1000-3150 315-1000 0-315 150-1000	10, 15% HCl	60°C - 1,3,5 h	P: 65-85% removal B: <20% removal Fe: 70% removal Al: 70-90% removal Mg: >95% removal
Espelien et al.[12] (2017)	MG-Si	2 wt% Mg	-	Graphite	315-1000	5, 10, 15, 20% HCl	22, 40, 60°C - 1,3,5 h	P: 60-70% B: <10% Fe: 68% Al: 85% Mg: 96%
Safarian and Espelien[13] (2017)	MG-Si	2 wt% Mg	10 K/min	Graphite	315-1000	5, 10, 15, 20% HCl 5, 10, 15, 20% HNO_3 5, 10, 15, 20% H_2SO_4	60°C - 3 h	P: 60-70% B: <10% Fe: 65-70% Al: 80-85% Mg: >96%
Margarido et al.[27] (1993)	Fe-Si alloy	Fe	-	-	10000-22400	22% HCl+ 40% $FeCl_3.6H_2O$	102°C	Ca: 95% Al: 55% Fe: 20%
Margarido et al.[28] (1994)	Fe-Si alloy Si: (83-83 wt%), Fe (7-12 wt%), Al (2-7 wt%), Ca (0-1.7 wt%)	7-12 wt% Fe	-	-	-	Stage I: 22% HCl Stage II: 22% HCl+ 40% $FeCl_3.6H_2O$	Stage I: 102°C- 6 h Stage II: 102°C- 18 h	-
Martins and Margarido [49] (1995)	Fe-Si alloy Si: (76-85 wt%), Fe: (7-21 wt%), Al (1-7 wt%), Ca: (0-1 wt%)	7-21 wt% Fe	-	-	10000-22400	7-22 % HCl + (0, 30,40%) $FeCl_3.6H_2O$	102°C	Ca: 90-95% Al: 50-60% Fe: 5-20%

Esfahani and Barati[50] (2011)	Fe-Si alloy B, P (0.3 wt%)	28 wt% Fe	0.5, 1.5, 3 K/ min	Mullite	600-800, 454-600, 212-454, 106-212	-	-	
Esfahani and Barati[51] (2011)	Fe-Si alloy	17 wt% Fe	0.5, 3 K/min followed by quenching at low T.	Mullite	-	9.5% HF + 20vol% acetic acid	75°C - 4 h	P: 68-> 29 ppmw (57.4%) B: 27-> 2 ppmw (92.6%) Fe: 3108->1 ppmw (100%) Total: 4723-> 53 ppmw (98.9%)
Khajavi et al.[52] (2014)	high purity Si (99.9985%) B (400-2000 ppmw)	20 wt% Fe	0.5 K/min followed by quenching	Quartz	< 37	10% HF + 20vol% acetic acid	-	B: 65-70% removal
Khajavi et al.[53] (2015)	high purity Si (99.9985%)	20 wt% Fe	0.5 K/min followed by quenching	Quartz	< 37	10% HF + 20vol% acetic acid	-	Activity coefficient of B in solid Si obtained at 1483K-1583K. B segregation coeffient decreases with decreasing teemperature.
Khajavi and Barati[54] (2017)	high purity Si (99.9985%)	20 wt% Fe	0.5 K/min + slow cooling	Quartz	< 37	10% HF + 20vol% acetic acid	-	P: 67-86% removal
L.Zong et al.[55] (2015)	Ferrosilicon Si(84wt%), Fe (9.7wt%), Al (5.4 wt%), Ca (3.5 wt%)	9.7 wt% Fe- 5.4 wt% Al- 3.5 wt% Ca	-	-	100 nm	5M HCl+ 5M HNO_3+ 0.5M HF small Ethanol to disperse particle	60°C - 2 h	Si: 84% -> 99.999% Fe: 9.7 wt% -> <0.1 wt% Al: 5.4 wt%-> <0.1 wt% Ca: 3.5 wt%-> <0.1 wt%
H. Sakiani et al.[48] (2021)	Si (6N), Fe (4N+), Ca (4N+), Si-B, Si-P	5-25 wt% Ca, 5-25wt% Ca +5wt% Fe	3 K/min	Alumina	Alumina with lid	-	-	-
Johnston and Barati[46] (2013)	doped MG-Si (B: 213 ppmw)	1-5 wt% Ti	4 K/min	Alumina	<106 um for Ti	diluted Aqua regia+ H_2SO_4	75°C - 1 h	55% B removal
H. Sakiani et al.[56] (2020)	Si (6N), Fe (5N), Ti (5N)	5-20wt% Ti, 10wt%Ti+ 5-20wt%Fe, 15wt%Ti+ 5-20wt% Fe	3 K/min, 0.5 mm/min	Alumina with lid	-	Stage I: 10% HF + 10% HCl + 20% acetic acid Stage II: diluted aqua regia	60°C	B: 80% removal (Si-Ti), 92% removal (Si-Ti-Fe) P: 75% removal (Si-Ti)

Y. Lei et al.[57] (2017)	MG-Si Si (<99.411%) B (52 ppmw)	5% Zr	1.5 K/min	Graphite	<186	HCl+HF (best) HF Aqua regia	75℃ - 2.5 h	B: 52->35 ppmw P: 51-> 12 ppmw Fe: 3567-> 20 ppmw Al: 1243-> 24 ppmw Total: 5892-> 150 ppmw (97.5%)
Y. Lei et al.[58] (2017)	MG-Si	5% Hf, Si-33wt%Al-5wt% Hf	1.5 K/min	Graphite	< 75	HCl+HF, HF, HCl+HF followed by aqua regia	75℃ - 3 h	B: 12-. 5.2 ppmw (Si-Hf) P: 52-> 21 ppmw (Si-Hf) B: 12-.0.7 ppmw, 94.2% (Si-Al-Hf) P: 52->7.2 ppmw, 86.2% (Si-Al-Hf)
Meteleva-Fisher et al.[59] (2013)	MG-Si Si (~98.5wt%), Fe (0.28%), Al+Ti (0.08%) B (65+-29 ppmw) P (85+- 19 ppmw)	2-10 wt% La, Nd	1 K/min	Alumina	-	-	-	P: 89 ppmw-> c.a. 20 ppmw
K. Tang et al.[60] (2014)	Si-B, Si-P, EG-Si	1wt% Ce	10 K/min	Graphite	-	-	-	-

2.1.3.1 Binary Si-Ca system

The Si-Ca alloying-leaching system is one of the most studied systems for Si purification studied by many researchers[31,40,42,46,47,61] . For the first time, Schei[40] reported improved P removal degree after alloying with a few percent Ca that was followed by a after a two-step acid treatment. Firstly, the initial Si-Ca alloy lumps around 5 cm in size was leached in the aqueous solution of HCl and $FeCl_3$, the lumps were found automatically disintegrated to fine particles around 2 mm, and subsequently, the particles were further purified by a second leaching step with aqueous $HF+HNO_3$ to further remove the metallic impurities such as Fe, Ti, V and so on.

By examining the microstructure of Ca alloyed Si, as shown in Figure 2- 99 by Schei, it was observed that $CaSi_2$ precipitates with network structure along the primary Si grains and also contain some other impurity phase. The inherent principle of the phase formation can be better understood from the pseudo ternary phase diagrams of the and Si-Ca-El (Figure 2- 10), which further describes the redistribution of impurities during equilibrium solidification. It is assumed that a molten Si-Ca alloy with composition at point A, Ca and small amounts of a third element El is cooled. Since the composition lies in the field of Si-rich portion, primary Si firstly precipitates. As the amount of primary Si increases, Ca and other impurities keep enriching in the liquid due to their high segregation, and the composition of the melt changes along the solidification path till the eutectic point (Eut). At Eut, the $CaSi_2$ phase starts to precipitate eutectically together with the Si phase, while followed by the precipitation of other impurities. Thus, most of impurities finally segregated together and the observed microstructure forms.

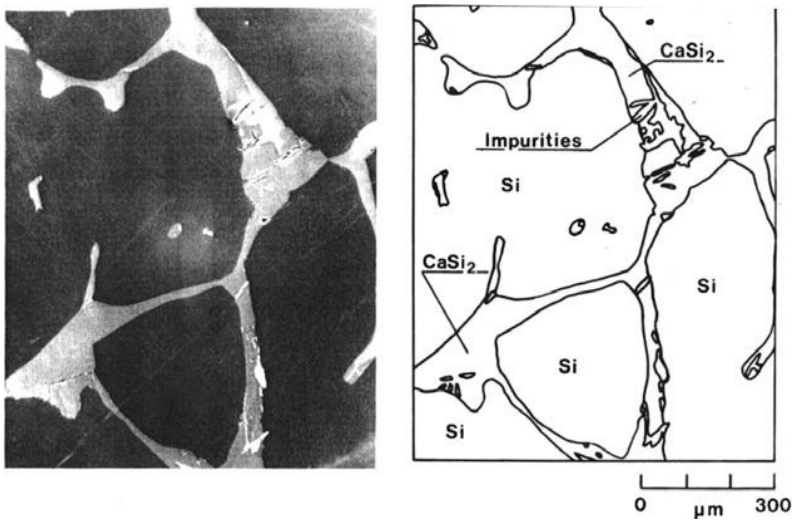

Figure 2- 9. Microstructure of Ca alloyed Si and identified phases. [40]

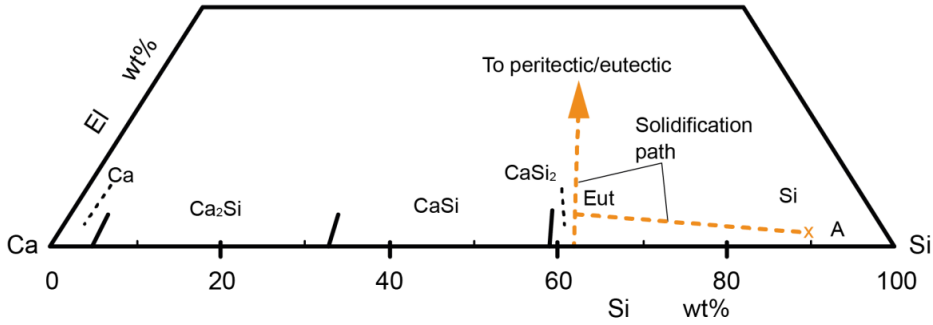

Figure 2- 10. Hypothetical ternary phase diagram Ca-Si-El, where El is an element represents impurity, e.g. Fe, Al, Ti. Reproduced from Schei [26].

In the leaching process, it is also reported by Schei that the $CaSi_2$ phase readily dissolves in HCl solution in association with a "cracking effect" due to the swelling of $CaSi_2$ and is accompany with the formation of a yellow by-product named siloxane ($Si_6H_3(OH)_3$). The reaction can be simply described by the following formula:

$$3CaSi_2 + 6HCl + 3H_2O = Si_6H_6O_{3(s)} + 3CaCl_2 + 3H_{2(g)} \quad (2-3)$$

The leaching purification results are also listed in Table 2- 4 and Table 2- 5 where significant metallic impurity removal and P removal can be seen.

Table 2- 4. Leaching results for major metallic impurities removal.[40]

Stage	Impurities, ppmw		
	Fe	Al	Ca
Before leaching	3600	3700	29000
After leaching	17	150	200

Table 2- 5. Leaching results for B and P content (ppma).[40]

Sample	Element	Before leaching	After leaching	
			Measured	Calculated
A		1.8	1.8	1.7
B		2.6	3.1	2.5
C		2.0	2.0	1.9
D	B	2.1	1.5	2.0
E		2.0	2.0	1.9
F		2.4	2.5	2.3
Mean		2.15	2.15	2.04
A		4.2	0.5	2.7
B		2.7	1.3	1.8
C		2.5	1.3	1.6
D	P	4.2	0.9	2.7
E		4.2	2.0	2.7
F		9.3	4.5	6.0
Mean		4.52	1.75	2.94

Shimpo et al. [42] studied the interaction between Ca and P in molten Si, the interaction coefficient $\varepsilon^{P}_{Ca\ in\ Si}$ was determined as -14.6($\pm$1.7) at 1723K, which indicates the strong attraction between Ca and P. Additionally, in the Si-Ca master alloy with 3wt% P addition, precipitate containing P was also

observed around some holes between $CaSi_2$ and Si phase by EPMA, while the X-ray diffraction analysis suggests most of the precipitated phosphide was Ca_3P_2 but got lost during the sample preparation with water.

In the acid leaching experiments by Shimpo et al. [42] , Si-Ca alloy granules were leached by aqua regia at 95 ℃ for 1 h. It was also found that Ca addition led to a remarkable improvement of P removal that as much as 80% of P can be removed by alloying Si with 5.17 wt% Ca.

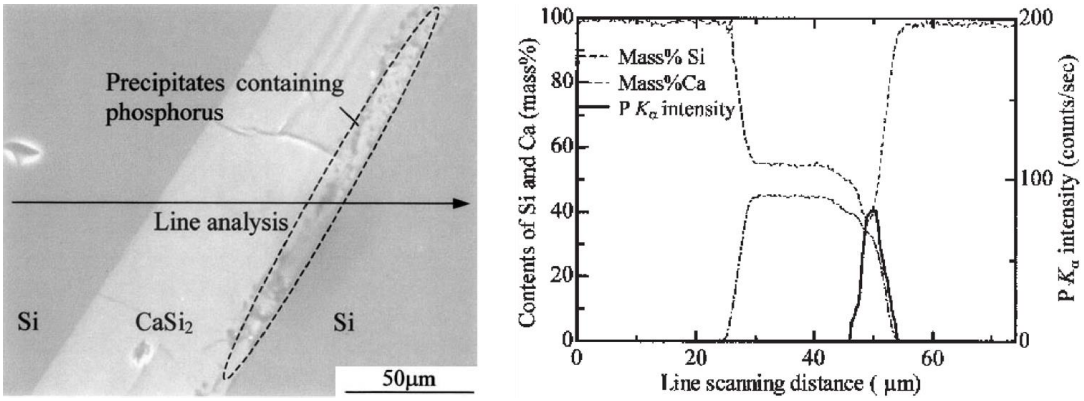

Figure 2- 11. Microstructural observation around the $CaSi_2$ precipitate (a) SEM image, (b) EPMA line analysis.

The Si-Ca alloying-leaching process was also studied by Meteleva-Fischer et al.[44,45]. In their work, 3-10 wt% Ca was doped into MG-Si contains around 85 ppmw P. Samples were melted in alumina crucible with varying cooling rate from 0.01 to 11 K/min. It was found that the cooling rate of 1 K/min is the optimal as significant amount of Ca was found lost through evaporation at a cooling rate lower than 1 K/min, but higher cooling rates limits the impurity segregation. Further leached in acid mixtures of HCl and HF, while it was found HF exhibits higher leaching efficiency. However, it was reported that with 5-6 wt% Ca addition, the P removal degree was only in the range 20-40%. It worth mentioning that the using of alumina crucible may lead to heavy Al contamination and consumes large extent of alloyed Ca element, which is harmful to the P removal efficiency.

Similarly, the application of alumina crucible as Si-Ca alloy holder were also reported by Lai et al. [47] and Johnston and Barati[46]. Nevertheless, significant P removal enhancement was still found after Ca alloying. For instance, Lai et al. reported that P content was significantly reduced from 35 ppmw to 5 ppmw after 5wt% Ca alloying followed by HCl+HF leaching. In addition to this, almost essentially complete P removal was reported by Johnston and Barati with the alloying-leaching.

Above all, the conventionally problematic P removal by direct acid leaching of MG-Si can be considerably improved after Ca addition. The formed $CaSi_2$ phase also contains other impurity phase and shows fast leaching kinetics, but, however, in the practical operation, attentions should also be paid to the Si loss caused by cracked fine particles and the treatment of solid by-product. As mentioned by Meteleva-Fischer et al.[45], the fine powder of siloxane was difficult to separate from leached Si, and may also affect the final purity control. Moreover, scientifically, the P state in Si-Ca alloy remains uncertainty, especially when its concentration is at several ppm-level.

2.1.3.2 Binary Si-Mg system

As another alkaline earth metal, Mg is also a suitable candidate for the alloying-leaching process. It is known with low segregation coefficient in Si, and with strong potential to from the stable phosphide Mg_3P_2. Recently, Mg was employed as metal refiner to enhance impurities removal from MG-Si firstly by Safarian and Tranell[10] and further studied at NTNU [12,13,62]. Remarkable improvement of P removal was achieved in association with effective removal of other metallic impurities like Al, Mn, Ca, Fe, Ti etc. by the Si-Mg alloying-leaching system.

The Si-Mg binary phase diagram is shown in Figure 2- 12, Mg_2Si is the only intermetallic and precipitates through the eutectic reaction with the eutectic point at 57.31 at% Si. Additionally, the impurity segregation process during solidification can be also described. Firstly, primary Si firstly starts to precipitate at temperature around 1400 ℃, while Mg and other impurities keep being rejected by the solidifying and growing Si into the liquid phase, and at around 930 ℃, the eutectic reaction $L \rightarrow Si+Mg_2Si$ happens, where the Mg_2Si phase finally forms along the primary Si grains.

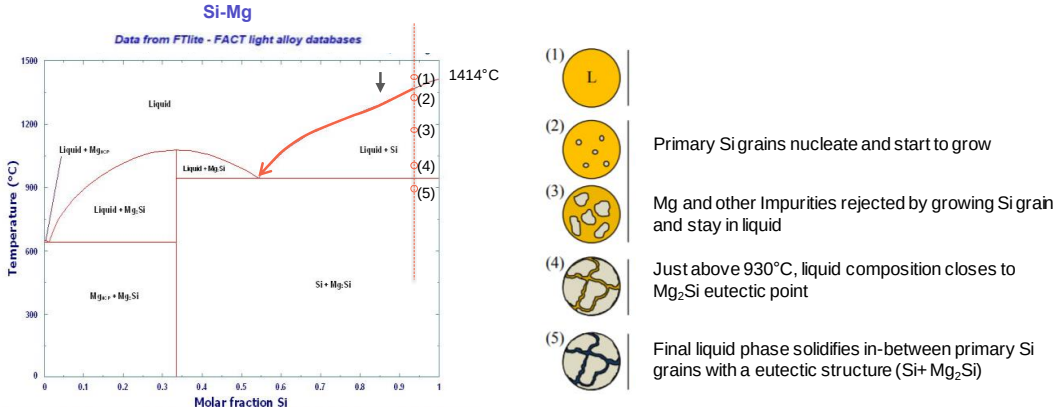

Figure 2- 12. Binary phase diagram of Si-Mg and the solidification process of Mg alloyed Si.

Figure 2- 13 shows the typical microstructure of MG-Si alloyed by Mg. It can be seen that large amount of continuous Mg_2Si phase formed between the primary Si grains through the eutectic reaction, and a series of different metallic silicides also formed and located inside the Mg_2Si phase such as Si-Fe-Al, Si-Fe-Ti, and Si-Fe-Al-Ca, which benefits their removal in the leaching process.

The leaching process of Mg alloyed Si is mainly dependent on the dissolution of Mg_2Si in acidic solution. The leaching efficiency is affected by variety of factors like acid types and concentration, leaching time, Mg alloying amount, leaching temperature, particle size and so on.

Effect of acid types and concentration on leaching efficiency was reported by Safarian and Espelien[13]. Compared to H_2SO_4 and HNO_3, HCl was found more effective especially with the concentration around 10-15%. In HCl aqueous solution, Mg_2Si reacts readily and yields the formation of silane but with no solid by-products generation. It should be also mentioned that the formed silane gas may further combust in exposure to air at the solution surface. The main reaction of Si-Mg alloy leaching is briefly written as:

$$Mg_2Si + 4HCl \rightarrow 2MgCl_2 + SiH_4(g) \qquad (2-4)$$

To study the precipitated phases removal with different leaching time, etching experiments were performed by submerging Si-Mg metallographic samples into HCl solution[10], as shown in Figure 2-14. It was observed that after etching for a short time, large amount of impurities is efficiently removed

by the dissolution especially of the Mg_2Si phase. As time goes on, the removing kinetics goes down in the deeper part of the grain boundaries. Consequently, little impurity phase remained after etching. Since Si does not react with the acid so it remains and purified.

The effect of Mg alloying concentration on purification efficiency has been also studied[10] and shown in Figure 2- 15. It is seen that the P removal degree and the removal of other metallic impurities significantly improved after Mg alloying and increases with increasing Mg addition. With around 3wt% Mg addition, almost 70% P can be effectively removed, which also indicates the strongly improved P segregation after Mg alloying. With higher Mg alloying amount, even though the amount of enriched impurities in the leachable Mg_2Si phase increases, but, however, it should be also noted that higher Mg alloying also leads to higher Si loss so that reduces the Si yield.

As a novel metal refiner, Mg has shown promising features to improve the P segregation and removal in the alloying-leaching process. Additionally, compared to the leaching of Si-Ca alloy, no solid by-product forms during the Si-Mg alloy leaching. However, as a recent studied alloying-leaching system, further investigation and knowledge are still required, especially through the thermodynamic aspects of the process.

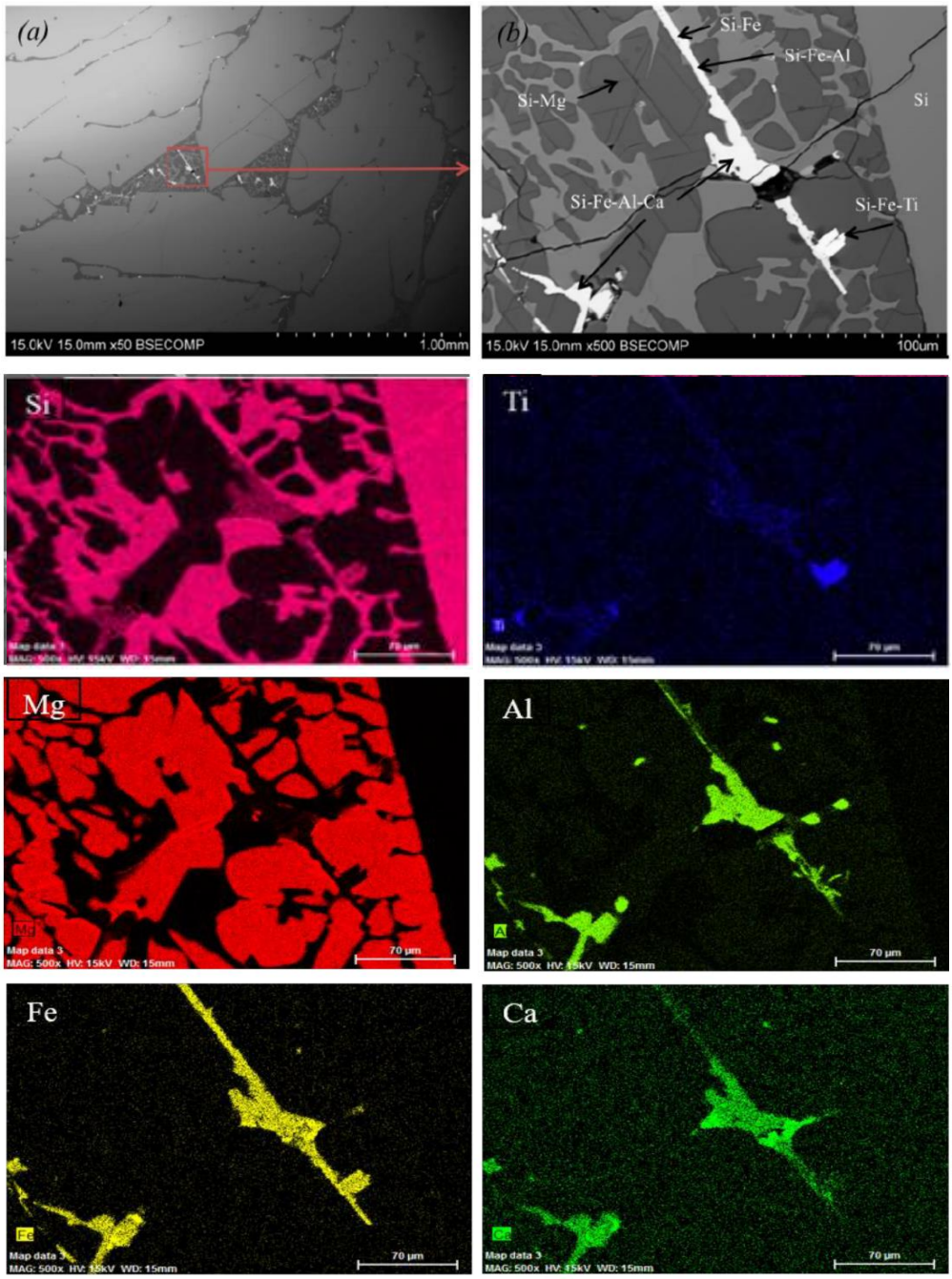

Figure 2- 13. SEM and EDS images of MG-Si doped by 5wt% Mg.

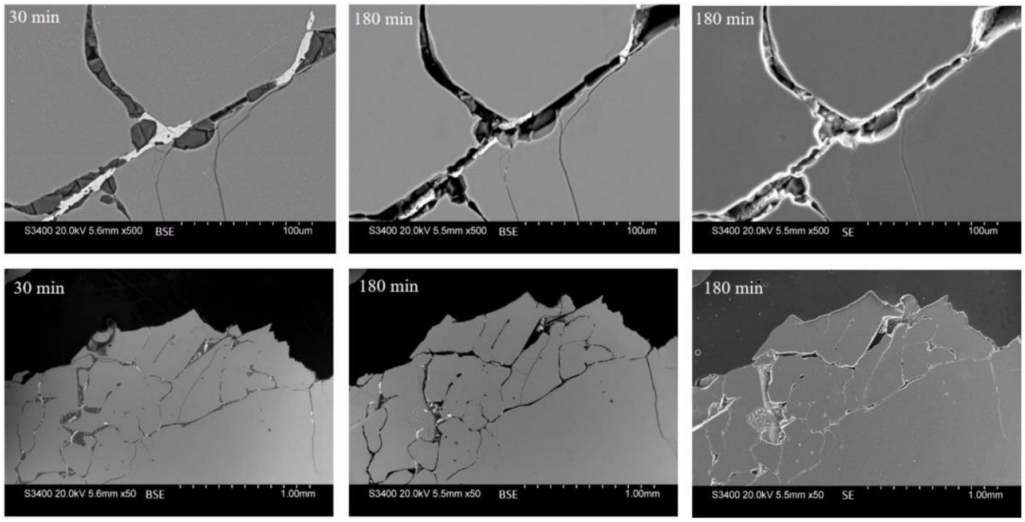

Figure 2- 14. SE and BSE images of 2.1wt% Mg metallographic sample submerged in HCl solution for different durations.[10]

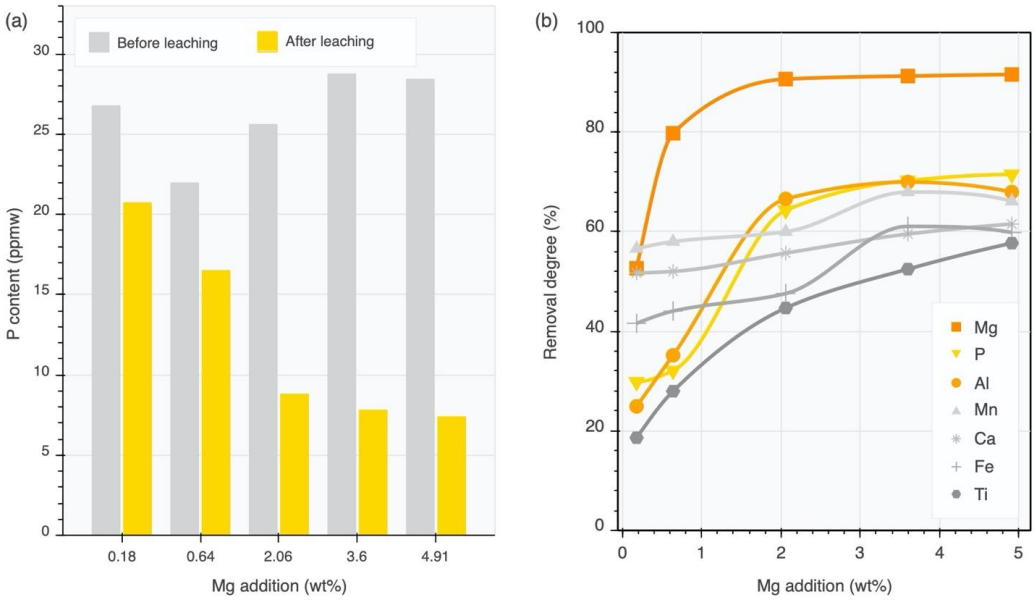

Figure 2- 15. Effect of Mg alloying concentration on impurity removal by 10%HCl solution (a) P content variation, (b) impurity removal degree. Figure reproduced from [10].

2.1.3.3 Other systems

Apart from Ca and Mg, other metals were also employed as impurity getters for the alloying-leaching process for different purposes, such as Fe, Ti, Hf, Zr, and rare earth elements.

Fe is a considerably inexpensive metal and with significantly low solid solubility in Si. Thus, it has been widely employed in both solvent refining and alloying-leaching process. Esfahani and

Barati[50,51] studied the purification of MG-Si using Fe as impurity getter, and it was found that slower cooling benefits impurity segregation, and sample quenched above eutectic temperature is significantly better than sample quenched lower than the eutectic temperature. The thermodynamics of B and P during the solidification of a Si-20wt% Fe alloy was thoroughly studied by Khajavi et al.[52–54] , while large negative interaction coefficient of B and P on Fe in solid Si were obtained in association with high B and P removal degree after leaching by a mixture of HF and acetic acid. The leaching behaviour of Si-Fe alloy was comprehensively studied by Margarido et al. [27,28,49]. They investigated the leaching process of an industrial Si-Fe alloy using HCl with $FeCl_3$ addition. The leaching efficiency was dependent on the composition of the phases and the Ca-bearing phases are soluble and with higher reactivity. The impurity removal kinetics were determined as Ca>Al>Fe. Additionally, it was found that the Si-Fe alloy cracks itself during the leaching and can be described a cracking shrinking model under the chemical reaction control[49].

Ti is known with strong affinity to B and the formation of TiB_2, thus, it is also often studied as an impurity getter in the alloying-leaching process. Johnston and Barati [46] studied the B removal from MG-Si with 1-5wt% Ti addition. After leaching with diluted aqua regia and H_2SO_4, it was found that 55% B removal achieved with 5wt% Ti addition. Recently, Sakiani et al.[56] investigated the B and P removal from Si-Ti and Si-Ti-Fe alloying systems with a two-step leaching process (10%HF+ 10%HCl+ 20% acetic acid leaching followed by leaching with diluted aqua regia). After the addition of 5-20wt% Ti, 65-75% P removal and 39-80% B removal was achieved owing to the formation of $Ti_5P_{3.16}$ and TiB_2. The Fe addition further improved B removal but shows no effects on P.

From the same group of the periodic table with Ti, Zr and Hf were also employed as impurity getter in the alloying-leaching process[57,63]. It was also reported that a significant improvement of B and P removal is achieved after leaching with HCl and HF. Additionally, improved P segregation was also reported from the application of rare earth elements use in the alloying-leaching process. However, it worth mention that the metals listed above exhibit more scientific value than practical as they are all expensive to be used in the current industrial production unless the economic recycling of the alloying elements could be established.

2.1.4 Effect of leaching conditions on Si purification

The purification of solidified Si by acid leaching can be expressed as a function of particle size, leaching temperature, leaching time and concentration and combination of leaching agents. However, results may also differ from different researchers as the type and composition of Si varies. The common selected leaching agent for Si purification are mainly acids, including sulphuric acid (H_2SO_4), hydrochloric acid (HCl), hydrofluoric acid (HF), aqua regia (HCl-HNO_3), acetic acid and so on.

2.1.4.1 Effect of leaching agent

Many researchers studied the effect of different acids and their mixtures at different temperatures and fractions of crushed Si on leaching process. For example, Santos et al. [20] found that by using only HCl (16%, 5 h, 80 °C) it is possible to remove ~ 85 % of the impurities and to obtain 99.9 % pure

Si after further leaching with HF (2.5 %, 2 h, 80°C). All the other acids and their mixtures, including aqua regia, gave results poorer than those for hydrochloric acid.

Voos[22] patented a process for treating pulverized MG-Si with aqua regia, H_2SO_4, HF, etc., to yield silicon suitable for application in microwave diodes. Hunt et al.[18] reported that over 90 % of the impurities present in MG-Si could be removed by etching MG-Si particles smaller than 500 μm size with aqua regia for 12 h at 75 °C. Leaching MG-Si with aqua regia for long periods was found to be the most effective. Dilute HCl with $FeCl_3$ addition followed by dilute HF with some oxidizing agent are used in Elkem Solar process [64].

Margarido [27,28] studied the leaching kinetics of Si-Fe alloy. The proposed that during the leaching process by HCl and $FeCl_3$ solutions, the following chemical reactions may happen:

$$\mathrm{Si(xFe, yAl, zCa)_{(s)} + (2x + 3y + 2z)HCl_{(aq)} \rightarrow Si_{(s)} + xFeCl_{2(aq)} + yAlCl_{3(aq)} + zCaCl_{2(aq)} + \frac{(2x+3y+2z)}{2}H_{2(g)}} \quad (2-5)$$

$$\mathrm{Si(xFe, yAl, zCa)_{(s)} + (2x + 3y + 2z)FeCl_{3\,(aq)} \rightarrow Si_{(s)} + x(3x + 3y + 2z) + yAlCl_{3(aq)} + zCaCl_{2(aq)} + \frac{(2x+3y+2z)}{2}H_{2(g)}} \quad (2-6)$$

Their experimental results indicated that the leaching process was dominated by the chemical reactions that large scale cracking happens on the particle surface when the Si-Fe alloy attacked by acids. As a result, more new generated micro-particles react further with the leaching agent.

Haifei et al. [29] investigated the effect of acetic acid addition on the leaching behaviour of MG-Si with a conventional mixture of HCl and HF. The leaching effect can be seen from Figure 2- 16. It was found that the extraction yield of impurities by the HCl-HF-CH_3COOH leaching increased by 7% compared to the conventional HCl-HF leaching where the total impurities drop from 6879 ppmw to 795 ppmw.

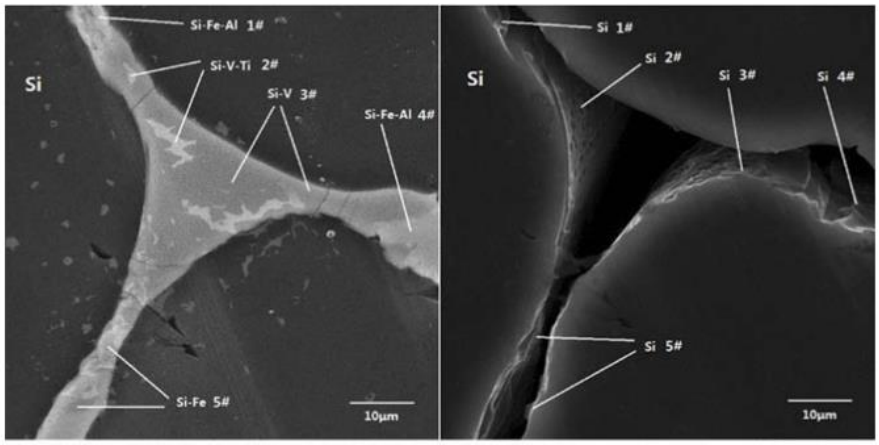

Figure 2- 16. Effect of MG-Si leaching with acids mixture of HCl-HNO_3-CH_3COOH (2:2:1), microstructure before leaching (left) after leaching (right).[29]

Even though HF has been reported to have very good purification ability for metallic impurities removal, but a portion of silicon can also dissolve during the HF leaching process. Moreover, due to its toxic nature, the requirements for the leaching equipment is highly strict. Additionally, the waste

HF acid treatment also brings challenges. Thus, compared with HCl, HF is not considered as a satisfied industrial leaching candidate.

Recently, Safarian et al.[13] investigated the effect of leaching agents on Mg doped silicon purification using HCl, H_2SO_4 and HNO_3. The best overall purification results for each type of acids can be seen from Figure 2- 17. The results showed that HCl is slightly better than the other two acids. The optimal concentration of HCl was claimed in the range 10 to 15%, while the optimal concentration for H_2SO_4 and HNO_3 is higher, respectively, 20% and 15%.

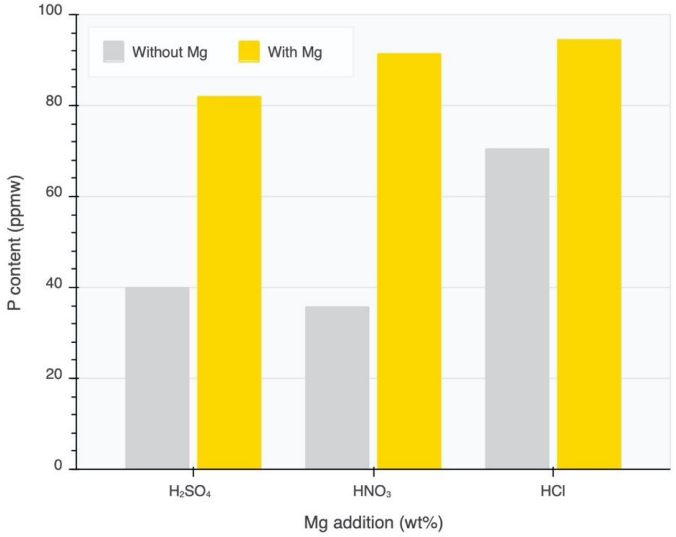

Figure 2- 17. Overall purification with the use of HCl, $H2SO_4$ and HNO_3 on Mg doped MG-Si leaching. Figure reproduced from [13].

2.1.4.2 Effect of temperature

Santos et al.[20] studied the influence of the temperature on the impurities removal from MG-Si. They found that during leaching with HCl, leaching efficiency improved significantly with increasing temperature. But with HF leaching, the influence of temperature change from 20 to 80°C is however not very significant, except for the removal of calcium.

Huang et al. [65] studied the effect of leaching temperature on a Si-Cu alloy, they also reported that with higher leaching temperature, the impurity removal facilitated. Figure 2- 18 shows the effect of temperature on the extraction yield of B and P by leaching in the range between 30°C to 70°C. It can be seen that with the increase of leaching temperature, leaching efficiency continuously increases.

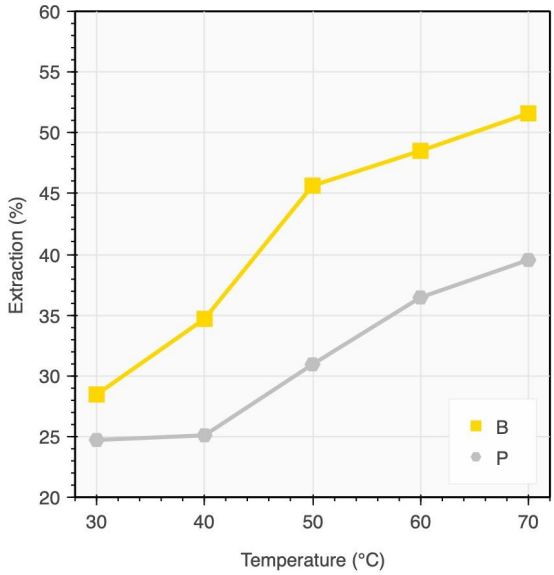

Figure 2- 18. Effect of temperature on the leaching of Si-Cu for the removal of B and P. Figure reproduced from [65].

The temperature dependency for Mg doped MG-Si leaching by HCl can be seen from Figure 2-19 according to the research by Espelien et. al[62]. The samples were leached with 15% HCl for hours and at different temperatures of 22, 40, 60, and 80°C. It is seen that the removal efficiency of nearly all impurities increases with increasing temperature

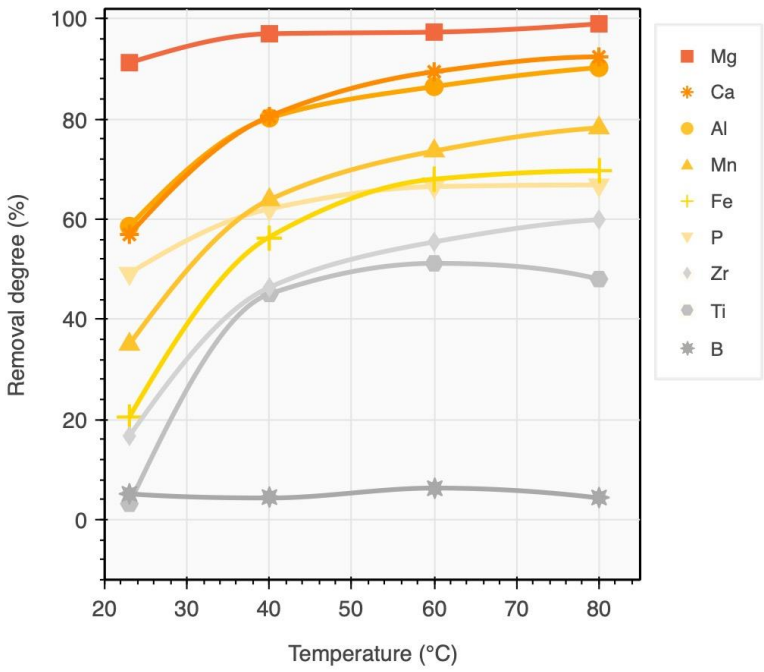

Figure 2- 19. Effect of leaching temperature, by use of 15% HCl and 5 hours leaching time. Figure reproduced from [62].

2.1.4.3 Effect of particle size

In general, it is known that with smaller particle size, more impurity phase will be exposed and leads to a higher removal efficiency. However, different results are seen in the literature about the effect of particle size on the removal of impurities through acid leaching. For instance, the effect of the particle size on the purification is illustrated in Figure 2- 20 for the cases of leaching with HCl and HF. It is found that the best results are obtained for the particle size with around 116 μm. Even taking into account the different contents of the impurities in the different fractions, the purification efficiency is lower with the finer fractions. Santos et al.[20] claimed that the reason is owing to more friable phases with higher impurities concentrated in the finely-ground particles, which are not so easily removed by the acid leaching. However, in contrast to Santos et al., Dietl [19]observed more impurity removal for smaller particles as shown in Figure 2- 21 by leaching MG-Si with aqueous solution of HCl and HF. Nevertheless, in the leaching of Si-Cu alloy with different particles, the optimal particle size was found between 74 to 106 μm for the extraction of B and P, while either bigger or smaller particle size leads to decreases of the purification efficiency, as shown in Figure 2- 22.

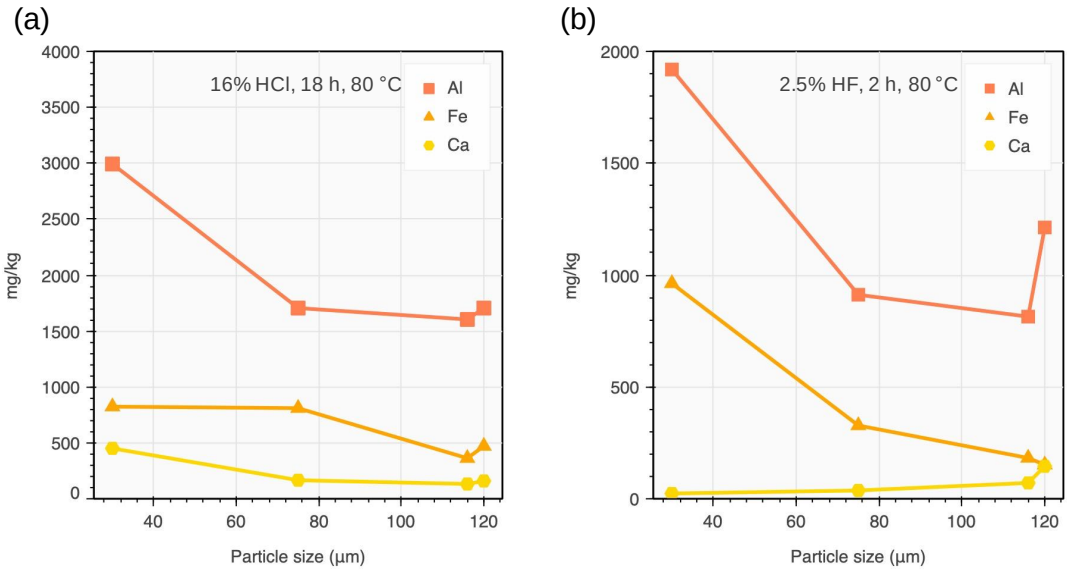

Figure 2- 20. Effect of particle size on the final concentration of major impurities after leaching with a): HC1 and b): HF. Figure reproduced from [20].

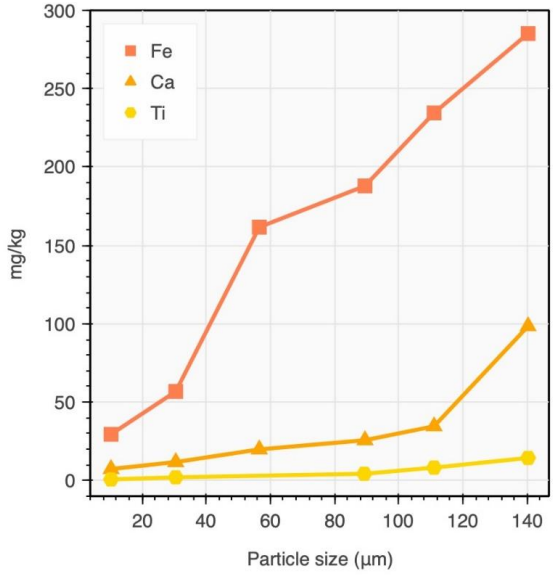

Figure 2- 21. Effect of particle size on purification of MG-Si powder by treatment with aqueous solutions of HCl and HF. Figure reproduced from [19].

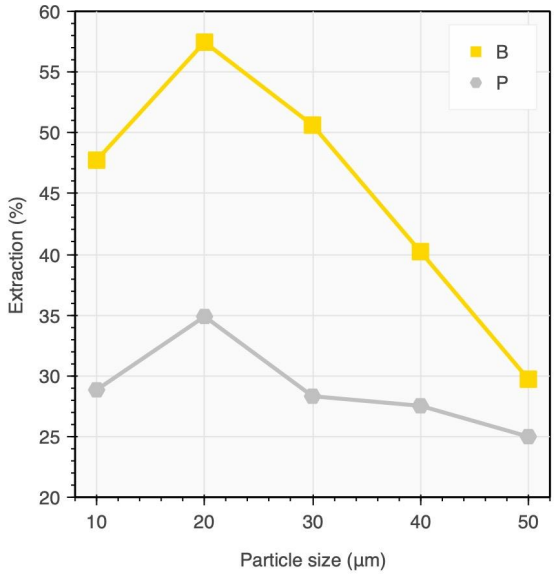

Figure 2- 22. Effect of particle size on purification of MG-Si doped by Cu powder by leaching treatment. Figure reproduced from [65].

The effect of particle size on leaching purification efficiency was also studied by Espelien and Safarian [11] for the leaching of Mg-doped MG-Si. As seen in Figure 2- 23, the results indicate that smaller particle size is more favourable for the removal of nearly all impurities. In addition, it can be also observed that the improvement of leaching efficiency narrows when the particle size is smaller than 1 mm. Thus, it is not necessary to grind particles to a size as fine as possible. Even though with finer particles lead to more exposure of the impurity phase, however, the additional milling processs may introduce other impurities into the silicon fines. On the other hand, milling to small particle size also enhances the difficulties in re-melting of the particles in subsequent procedures and higher Si loss occurs due to re-oxidation of silicon powder with high surface area. Therefore, crushing and milling of silicon to very small particles is not favourable.

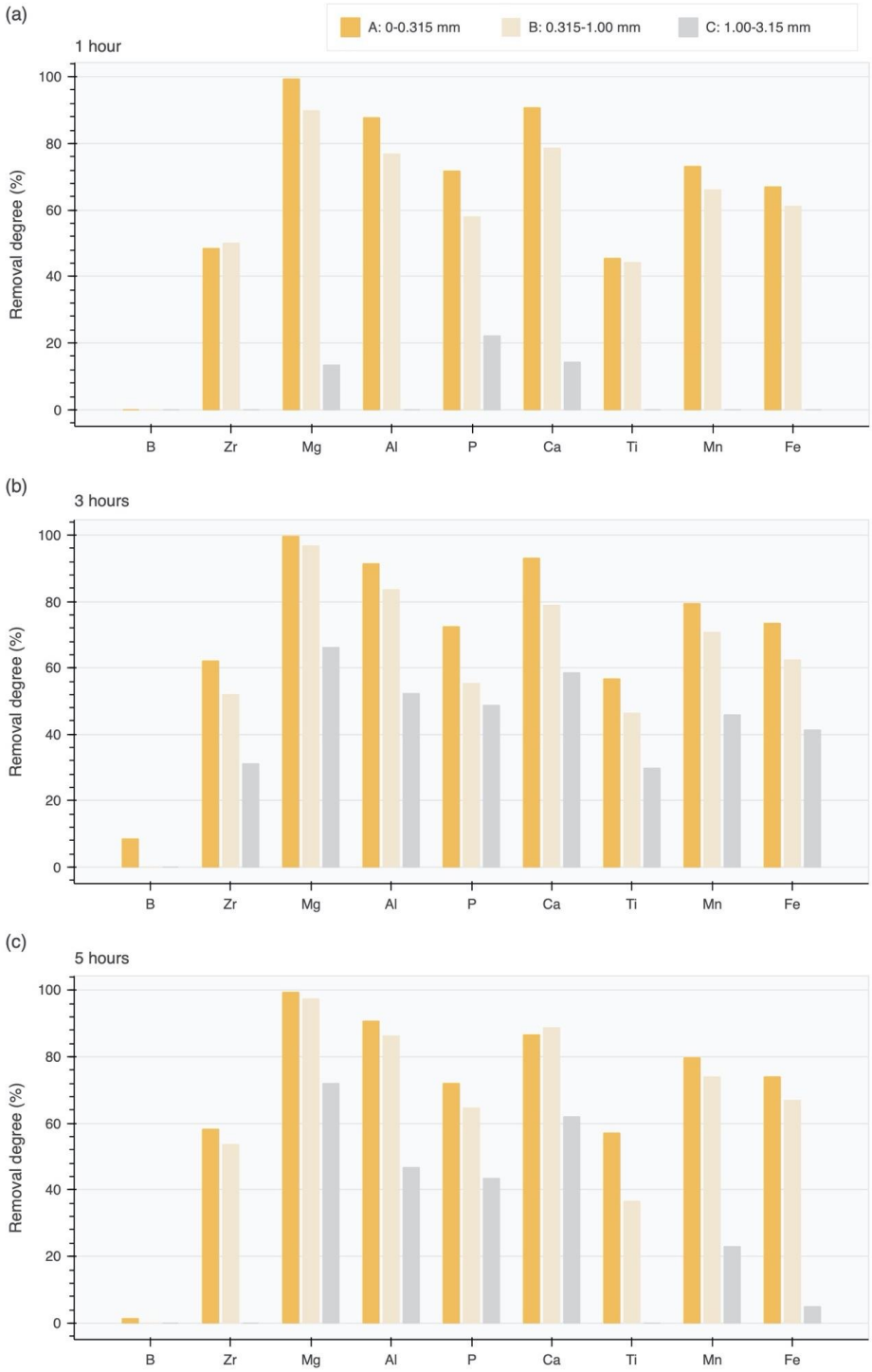

Figure 2- 23. The removal degree of impurities for 2.2 wt% Mg doped MG-Si with different particle size ranges. Figure reproduced from [11].

2.1.4.4 Effect of stirring method

In order to enhance the leaching efficiency, magnetic stirring and ultrasonic field stirring are often applied, as schematically presented in Figure 2- 24.

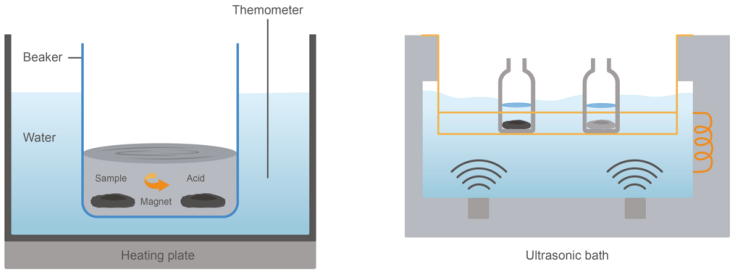

Figure 2- 24. Sketch of a setup of leaching with magnetic (left) and ultrasonic field (right).

Acid leaching under an ultrasonic field has been recently used to remove Al, Fe and Ti impurities from MG-Si by Jian et al.[66] and Ma et al.[36]. They observed that acid leaching process under an ultrasonic field is more effective than the acid leaching under magnetic stirring. It was also suggested that when an ultrasonic field is used in the acid leaching process, the mechanical interaction between the sound waves and the liquids would lead to the phenomenon of cavitation and acoustic streaming. As a result, many cavitation bubbles generated which then dramatically collapse causing high temperature, high pressure, strong shock and micro-jet in the local solution so that leads to a change of mass transfer and acceleration of the rate of dissolution of metallic impurities into the acids. This provides better chance for the impurities that are on the defects and slits under the surface of the silicon particles to react with the HCl.

2.1.5 Leaching kinetics

In this section the general kinetic models that may be proper the leaching process of silicon are shortly studied.

Jander model[67]

Jander model is known as the first three-dimensional kinetics model derived in 1920s[67]. The model was derived based on the diffusion-controlled reaction of a spherical particle from the parabolic law. The product layer substitutes the space filled by the initial reactant solid particle with no change in volume. However, Jander used a plane surface (one-dimensional, shown as Figure 2- 25) as the basis of assumption so it is strictly not correct. Even though it is empirical and contains unrealistic physics, but it has been widely used and modified.

Based on the assumptions of infinite long plane surface, and l as the thickness of the product layer, the diffusion-controlled mechanism requires:

$$\frac{dl}{dt} = \frac{k}{l} \qquad (2-7)$$

where k is a constant which effectively incorporates physical and chemical parameters and l is the thickness of the product layer. This can be integrated to yield the widely known parabolic law:

$$kt = \frac{l^2}{2} \qquad (2-8)$$

Defining α as the extent of reaction of a shrinking spherical particle, $\alpha = 1 - (\frac{r}{R})^3$, and by neglecting the surface curvature, we obtain:

$$\frac{l}{R} = 1 - (1-\alpha)^{\frac{1}{3}} \qquad (2-9)$$

Finally, the Jander model is written as:

$$\left(1 - (1-\alpha)^{\frac{1}{3}}\right)^2 = \frac{2k}{R^2}\mathrm{t} \qquad (2-10)$$

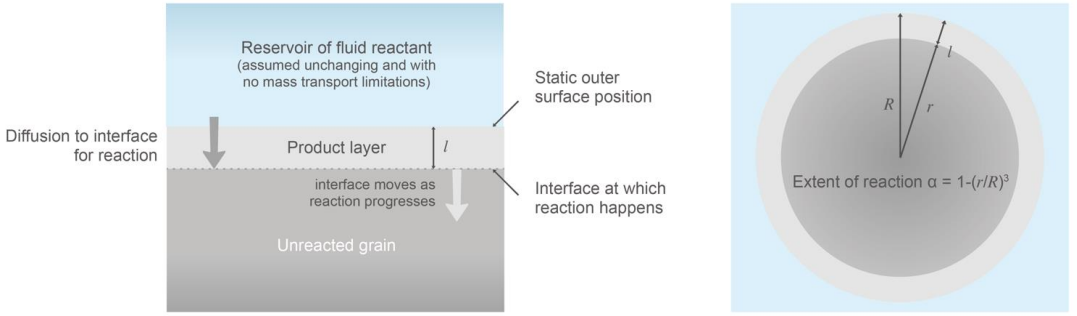

Figure 2- 25. Sketch of the assumptions applied to Jander model (left) and its definition of extent of reaction under spherical particle situation (right). Reproduced from Provis.[68][68][68][68][68][68][68][68][68][68][68][68][68][68][68][68][68][68][68][68]

Ginstling-Brounshtein model[69]

Ginstling and Brounshtein stated that the Jander model is oversimplified and holds only at low conversion values. They further introduced surface curvature into Jander model to correct the unrealistic flaw and leads to the correct description of the particle-fluid reaction assuming rate control by diffusion controlled shrinking core model for unchanged spherical particle size:

$$1 - \frac{2}{3}\alpha - (1-\alpha)^{\frac{2}{3}} = k\mathrm{t} \qquad (2-11)$$

Zhuravlev, Lesokhin and Templeman (ZLT) model[70]

The ZLT model is also a modification of the Jander model by assuming the diffusion rate constant is proportional to the remaining reactant. This yield:

$$\left((1-\alpha)^{-\frac{1}{3}} - 1\right)^2 = k\mathrm{t} \qquad (2-12)$$

Kröger and Ziegler model[71,72]

The Kröger-Ziegler model is directly modified from the original Jander model, where both are based on the assumption of a constant reaction plane surface (one-dimensional). In the Kröger-Ziegler model, the growing rate of the product layer is inversely proportional to the thickness of itself and time, and the model can be expressed as:

$$\left(1 - (1-\alpha)^{\frac{1}{3}}\right)^2 = k\ln(\mathrm{t}) \qquad (2-13)$$

Valensi-Carter model[73]

Carter improved the Jander model by considering the volume difference of the product layer with respect to that of the consumed reactant. Valensi also derived the samel model but from a different starting point, and thus, the equation is referred to the Valensi-Carter model,

1) The rate of thickening of a spherical shell of the reaction product must depend on the ratio of the outer to inner surfaces.
2) The volume of reacted and the volume of product are not equal.

$$\frac{Z-[1+(Z-1)\alpha]^{\frac{2}{3}}-(Z-1)(1-\alpha)^{\frac{2}{3}}}{Z-1}=k\mathrm{t} \qquad (2-14)$$

2.2 Slag refining

Slag refining is a widely studied technique for Si purification and plays an essential role in nearly all high temperature metallurgical processes. A typical slag refining system consists of two immiscible liquids, respectively, the molten slag phase and molten metal phase. The slag phase is generally a mixture of silicates (if SiO_2 content is significant) and absorbs the unwanted impurities from the metal phase generally based on chemical equilibrium of redox reaction. As it has been discussed before that B removal from silicon is difficult through the liquid-solid segregation process upon silicon solidification, however, slag refining is effective for the B separation from Si even at the scale of parts per million.

The experimental procedure of slag refining consists of the following steps, firstly the preparation of master slags to ensure homogenized composition, secondly, melting the mixture of master slag and Si in crucible and to reach the target refining temperature, then holds the molten slag and Si with target holding time period. Finally, the slag and Si are separated through tapping or solidification. Slag properties are essential for the Si purification as they have a decisive effect on the process control and impurity absorption. Therefore, specific requirements are needed to be fulfilled for an appropriate slag as below:

1. The slag melt should be immiscible with the molten Si (or Si-rich alloy) phase.
2. The slag should have high affinity to the key impurities like B than to Si.
3. The raw slag should have high purity so that to avoid contamination to the Si melt, particularly, the slag should contain low level of B and P.
4. An appropriate slag viscosity is required at the refining temperature range. Slag viscosity plays a vital important role since it directly determines the mass transfer of impurities and the refining kinetics. If the slag is too viscous, the mass transfer will be strongly limited and leads to insufficient impurity separation. However, if the slag viscosity is too low, it will enhance the erosion of the furnace inversely. Therefore, it is important to maintain slag viscosity in specific range to ensure good slag mobility and slag/Si interfacial contact.
5. A distinct density difference between slag and Si phase is preferred. This is because a large density difference between slag and Si facilitates separation between slag and Si through the tapping process and thus benefits the Si recovery.

2.2.1 Distribution coefficient of boron

The B distribution coefficient, which is also known as partition ratio, is widely used to evaluate the extent of B removal by slag refining, which is given by:

$$L_{\mathrm{B}} = \frac{(\%B)}{[\%B]} \qquad (2-15)$$

where $(\%B)$ and $[\%B]$ is the B concentration in slag and Si phases, respectively, typically in wt%.

If the interaction of other slag main component(s) with the dissolved B in silicon is insignificant, the mechanism of B removal can be described by the following reaction at the slag/Si interface. Regardless, the B removal reaction mechanism, the equilibrium in the system can be studied using this reaction:

$$\underline{\mathrm{B}} + \frac{3}{4}(\mathrm{SiO_2}) = (\mathrm{BO_{1.5}}) + \frac{3}{4}\underline{\mathrm{Si}} \qquad (2-16)$$

and with the equilibrium constant K given as:

$$K = \frac{\left(a_{\mathrm{Si}}^{\mathrm{Si\ melt}}\right)^{\frac{3}{4}}}{\left(a_{\mathrm{SiO_2}}^{\mathrm{slag}}\right)^{\frac{3}{4}}} \cdot \frac{a_{\mathrm{BO_{1.5}}}^{\mathrm{slag}}}{a_{\mathrm{B}}^{\mathrm{Si\ melt}}} = \frac{\left(a_{\mathrm{Si}}^{\mathrm{Si\ melt}}\right)^{\frac{3}{4}}}{\left(a_{\mathrm{SiO_2}}^{\mathrm{slag}}\right)^{\frac{3}{4}}} \cdot \frac{x_{\mathrm{BO_{1.5}}}^{\mathrm{slag}}}{x_{\mathrm{B}}^{\mathrm{Si\ melt}}} \cdot \frac{\gamma_{\mathrm{BO_{1.5}}}^{\mathrm{slag}}}{\gamma_{\mathrm{B}}^{\mathrm{Si\ melt}}} \qquad (2-17)$$

In practical, mass fraction is more convenient to use and the mole to mass conversion can be obtained by introducing the following conversion factor $k_{x\to w}$:

$$L_{\mathrm{B}} = \frac{(\%B)}{[\%B]} = \frac{x_{\mathrm{BO_{1.5}}}^{\mathrm{slag}}}{x_{\mathrm{B}}^{\mathrm{Si\ melt}}} \cdot k_{x\to w} \qquad (2-18)$$

And,

$$k_{x\to w} = \frac{x_{\mathrm{Si}} M_{\mathrm{Si}} + \sum x_{\mathrm{Me}} M_{\mathrm{Me}}}{x_{\mathrm{SiO_2}} M_{\mathrm{SiO_2}} + \sum x_{\mathrm{MeO}_x} M_{\mathrm{MeO}_x}} \qquad (2-19)$$

where the element Me and its oxide MeO_x indicate the other elements in Si and slag, and M_{Me}, M_{MeO_x} indicate their corresponding molar mass.

Rearrange the equilibrium constant, the distribution coefficient L_{B} can be expressed as:

$$L_{\mathrm{B}} = \frac{K \cdot \gamma_{\mathrm{B}}^{\mathrm{Si\ melt}} \cdot \left(a_{\mathrm{SiO_2}}^{\mathrm{slag}}\right)^{\frac{3}{4}}}{\gamma_{\mathrm{BO_{1.5}}}^{\mathrm{slag}} \cdot \left(a_{\mathrm{Si}}^{\mathrm{Si\ melt}}\right)^{\frac{3}{4}}} \cdot k_{x\to w} \qquad (2-20)$$

It is seen that B removal through slag refining is a complicated that is directly related to the slag chemistry and the silicon melt composition. Since the L_{B} value is affected by multiple factors, practically, the optimum refining condition can be obtained through modifying the parameters. However, even though the theoretical expression of L_{B} is known, it is still hard to directly calculate it due to the lack of thermodynamic data about many dilute solutions of B and $\mathrm{BO_{1.5}}$ in silicon and slag melts. Thus, the L_{B} is usually obtained through experimental work and used to evaluate the slag refining performance.

2.2.2 Factors affecting slag refining performance

The chemical equilibria of impurity partition between slag and metal phase is a complicated function of slag composition, silicon melt composition, temperature, time, and crucible materials, atmosphere and so on. Because of this, literature data often differentiate with each other. Nevertheless, this section briefly summarized the effects of the critical processing parameters.

2.2.2.1 Slag composition

By dealing with the complicated slag composition-structure-property relationship, many methods have been proposed to describe and quantify the molten slags reactivity. Slag basicity is one of the most widely used indicators to reflect the slag chemistry based on whether acidic or basic. As shown in Figure 2- 26 the classification of acidic and basic oxide depends on the structural role of the oxides in slags, while acidic oxide behaviour as network modifier and promotes the slag network polymerization and basic oxide behaviour as network modifier to depolymerize the slag network and in association with the creation of more reactive non-bridging oxygen and free oxygen. Boron oxide is known as a stable acidic oxide and therefore prefers to react with basic oxide to be stabilized as

borate. Considering the equilibrium with the oxygen partial pressure and oxygen anions, the oxidation and ionization reaction of boron can be written as:

$$\underline{\mathrm{B}} + \frac{3}{4}\mathrm{O}_2 + \frac{3}{2}\mathrm{O}^{2-} = (\mathrm{BO}_3^{3-}) \qquad (2-21)$$

where the activity of oxygen ions a_{O_2} is affected by the dissociation of the basic oxides, and the oxygen partial pressure p_{O_2} is corresponding to the activity of silica.

Based on the Equation (2-21), boron capacity is introduced to evaluate the capability of a slag to absorb boron:

$$\mathrm{C}_{\mathrm{BO}_3^{3-}} = \frac{(\%\mathrm{BO}_3^{3-})}{a_B\left(p_{O_2}\right)^{\frac{3}{4}}} = \frac{K \cdot \left(a_{O^{2-}}\right)^{\frac{3}{2}}}{\gamma_{\mathrm{BO}_3^{3-}}} \qquad (2-22)$$

It is seen that the final borate capacity expression is without the oxygen partial pressure term. This is because the slag composition can be affected by the oxygen partial pressure through the equilibrium between SiO_2 and Si. The borate capacity can be calculated if the equilibrated boron oxide mass fraction, activity of boron, and oxygen partial pressure are known. It is also seen that the defined borate capacity suggests the boron oxidation relies on the dissociated oxygen ions from basic oxides.

However, one major problem of the concept of basicity lies in dealing with the amphoteric oxide or intermediates, e.g., Al_2O_3, and differentiating the contributions from different cations. This problem is partially overcome by introducing the concept of optical basicity, which is a measure of the electron donor properties of different ions. The optical basicity of molten slag can be calculated as below:

$$\Lambda = \frac{\sum x_i n_i \Lambda_i}{\sum x_i n_i} \qquad (2-23)$$

where Λ_i is the theoretical optical basicity of pure oxide substance, x_i and n_i represent the mole fraction and the number of oxygen atoms in each oxide component. Using a normalized B distribution coefficient by dividing the oxygen partial pressure, positive relationship between B removal and optical basicity was observed by Johnston and Barati[74] and other researchers[75,76].

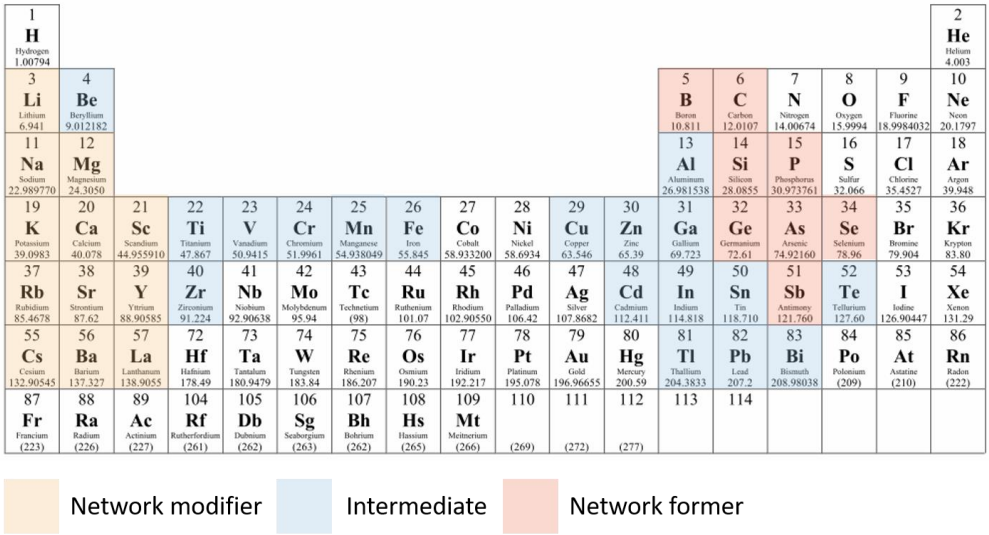

Figure 2- 26. Structural role of common oxides in silicate melt.

The composition dependence of slag refining is also known as dependent on the slag local structure changes. For instance, the thermodynamic properties variation of SiO_2 and $BO_{1.5}$ are directly affected by their local environment. As presented in Figure 2- 27, the activity coefficient of SiO_2 is strongly compositional dependent and with a distinct hierarchy that for a given SiO_2 concentration, γ_{SiO_2} increases with increasing cation field strength (Mg>Ca>Sr>Ba>Li>Na>K). The reason is that higher field strength cation leads to larger Si network distortion, which increases the tendency of the Si cation unit to escape. Additionally, as shown in Figure 2- 28, it has also been found that the activity coefficient of BO1.5 decreases with an increasing fraction of three coordinated boron in CaO-SiO_2-$BO_{1.5}$ slags with similar basicity, and a high optical basicity slag environment was found to favor the three coordinated boron.[77]

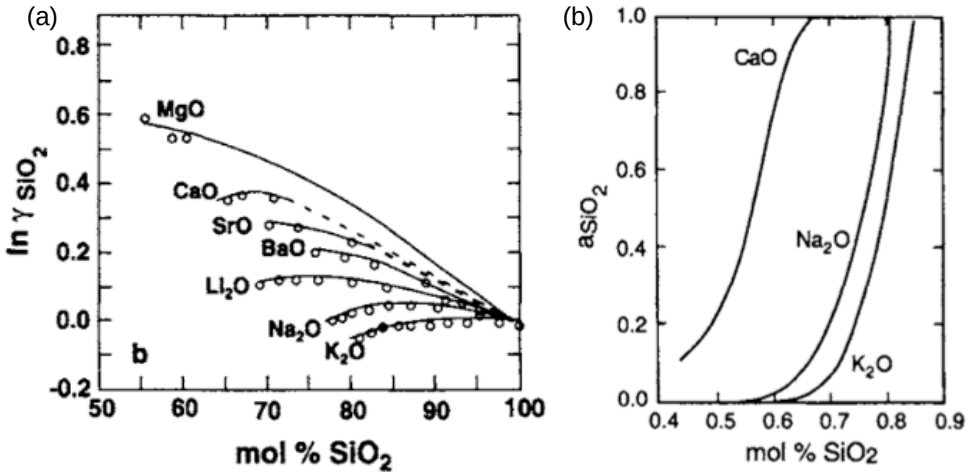

Figure 2- 27. Activity coefficient of SiO_2 in the melt at 1550°C.[78]

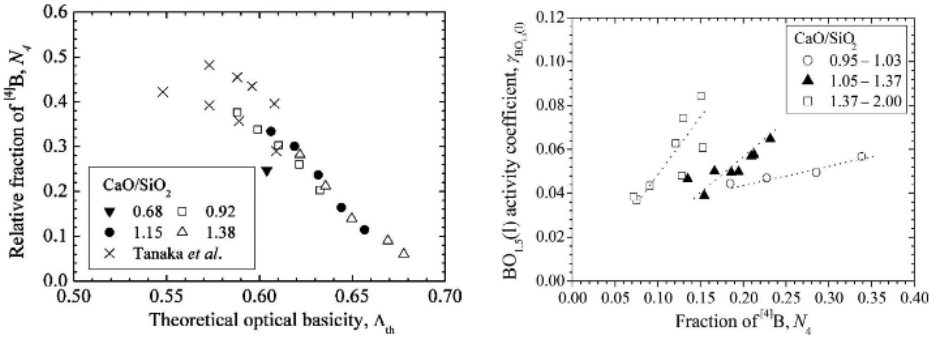

Figure 2- 28. Relationship between the boron coordination and activity coefficient of $BO_{1.5}$ with slag basicity.[77]

2.2.2.2 Si melt composition

In contrast to select suitable slag composition to reduce the activity coefficient of B_2O_3 in slag, B removal through slag refining can be promoted by increasing the activity coefficient of dissolved B in Si melt by alloying with other elements. Additionally, according to the Equation (2-20), the alloying

of Si can also reduce the Si activity which could also facilitate the B separation. A few research works have been done for the slag refining with Si alloys and shown significantly high L_B values, which will be reviewed in the next section.

2.2.2.3 Refining temperature

The operation temperature plays an important role in the slag refining process. As it directly affects the slag chemistry and the equilibrium constant *K*. Additionally, it is also known that a higher refining temperature could significantly reduce slag viscosity and facilitate the mass transfer. The effect of temperature on impurity distribution can be seen in Figure 2- 29, it can be seen that higher temperature is beneficial for the B removal. However, the equilibrium oxygen partial pressure also increases with increasing temperature, thus, higher Si loss through oxidation is also expected to happen with higher temperatures.

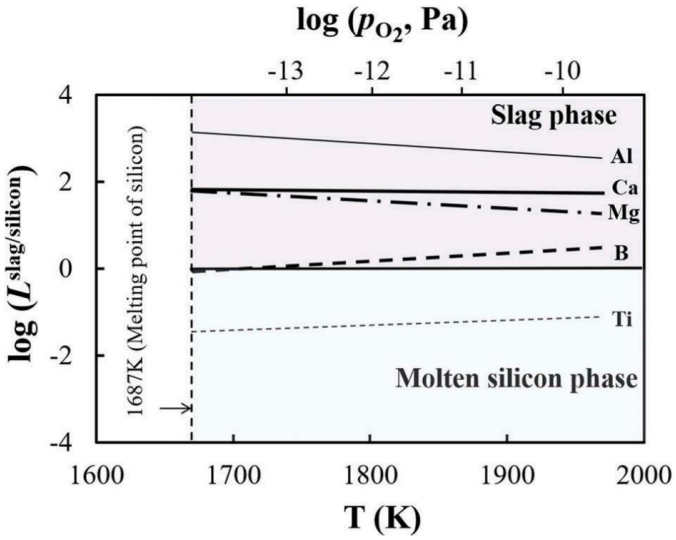

Figure 2- 29. Temperature dependence of impurity distribution ratio and equilibrium oxygen partial pressure.[79]

2.2.2.4 Mass transfer and kinetics

The kinetics aspect is also important for the slag refining especially before the chemical equilibrium reached. It has been reported that mechanical stirring could promotes the mass transfer rate to at least one order of magnitude[80]. As presented in Figure 2- 30, the mass transfer of B from Si phase to slag phase undergoes the following steps:

1. Mass transfer of the dissolved B in bulk Si to the metal phase boundary layer
2. B diffusion through the boundary layer to the reaction interface
3. B oxidation at the Si/Slag interface
4. Diffusion of the oxidized B, B_2O_3, from the interface across the slag boundary layer
5. Mass transfer of the oxidized B from the slag boundary layer to the bulk slag phase

The properties of the boundary layer are affected by multiple factors, for instances, refining temperature and composition of slag and silicon. Assuming that the melt boundary layer mass transport is the rate-limiting step, the following equation is obtained[81]:

$$\frac{[\overline{\%B}]-[\%B]_{eq}}{[\%B]_{in}-[\%B]_{eq}}=exp\left(-\frac{k_t\rho A_s}{M}\left(1+\frac{M}{M_s L_B}\right)\right) \qquad (2-24)$$

where $[\overline{\%B}]$ is the average concentration of the dissolved B in Si phase at time *t*. It is also seen that the required time to reach equilibrium is related to the initial B concentration gradient, mass transfer coefficient, interfacial area, and mass ratio of slag to silicon.

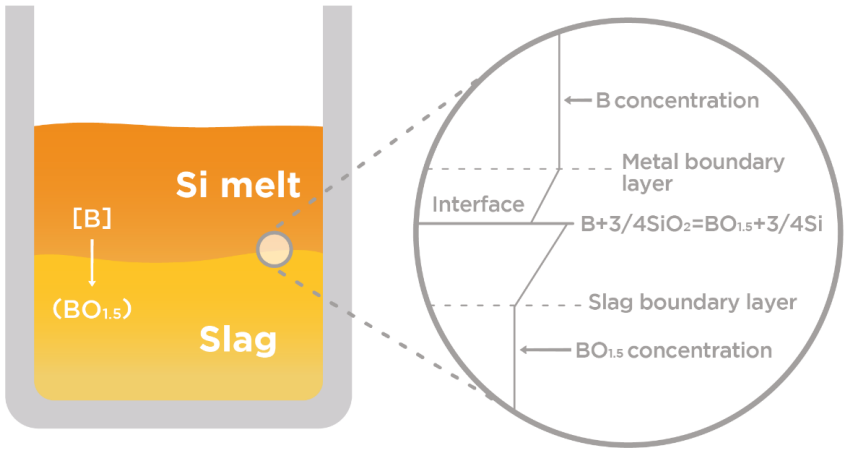

Figure 2- 30. Illustration of boron mass transfer from silicon phase to slag phase.

2.2.3 Previous works

As summarised in Table 2- 6 and Table 2- 7, many slag systems have been studied in the past two decades to investigate the effect of slag properties on B removal from Si or Si alloys. In the recent, the impurity response to various slag refining conditions has been also critically reviewed by Thomas et al.[76,82]. It has been shown that the typical L_B values ranges from 1-5 but scattered depends on different authors. In this section, the common studied slag systems are briefly reviewed below.

2.2.3.1 Binary silicate slag

As the most fundamental slag system, the binary CaO-SiO_2 slag system has been extensively studied and summarized in Figure 2- 31. Current reported slag systems are also summarized in Table 2- 6.

Suzuki et al.[83] was the first that published boron removal by slag refining with the binary calcium silicate slag, although there were many years before a lot of unpublished industrial research, i.e. at ELKEM. In their work, an initial Si contained 80 ppmw B was refined at 1450 and 1550 °C under pure Ar atmosphere or mixed with CO_2. Relatively low L_B values were reported, in the range of 0.31-1.15. The reasons are most probably due to the used low basicity slag, low refining temperature, and short refining time that caused sampling before reaching equilibrium.

Teixeira et al.[84] investigated a series of CaO-SiO_2 slags at 1550 °C using a graphite crucible and in a resistance furnace. The refining system was held for 18 h under Ar atmosphere to make sure

full equilibrium. The reported L_B values are in the range of 2-5.5, and a local minimum was reported to exist in the middle basicity range. This trend is somehow different regarding the optical basicity relationship discussed above.

Jakobsson and Tangstad [85] also investigated the B distribution between Si and CaO-SiO_2 slag system with thorough description about the experimental details. They used graphite crucible and in resistance furnace at 1600 °C for 3-18 h. With confirmed equilibrium state, the reported L_B values were found in between 2-2.5 across the entire liquid region of the CaO-SiO_2 slag system and with a linear relationship that slightly increases with increasing CaO/SiO_2 ratio. Similar trend was also reported for the MgO-SiO_2 binary system but with a slightly lower L_B[85].

The binary BaO-SiO_2 slag system was recently studied by Safarian[86]. The Si samples containing 30 ppmw B were added into graphite crucibles and fixed the slag/Si mass ratio equal to 2. Samples were held at 1500 and 1600 °C for 2 h under electromagnetic stirring. The reported L_B values increase with increasing temperature but lie in the range 0.9-1.35 and with a local minimum observed around BaO/SiO_2 ratio between 0.9-1. The thermodynamic analysis suggested B was mainly oxidized by BaO, but the lower L_B values seem to be owing to the heavy mole mass of BaO oxide dilute the B concentration in the slag phase.

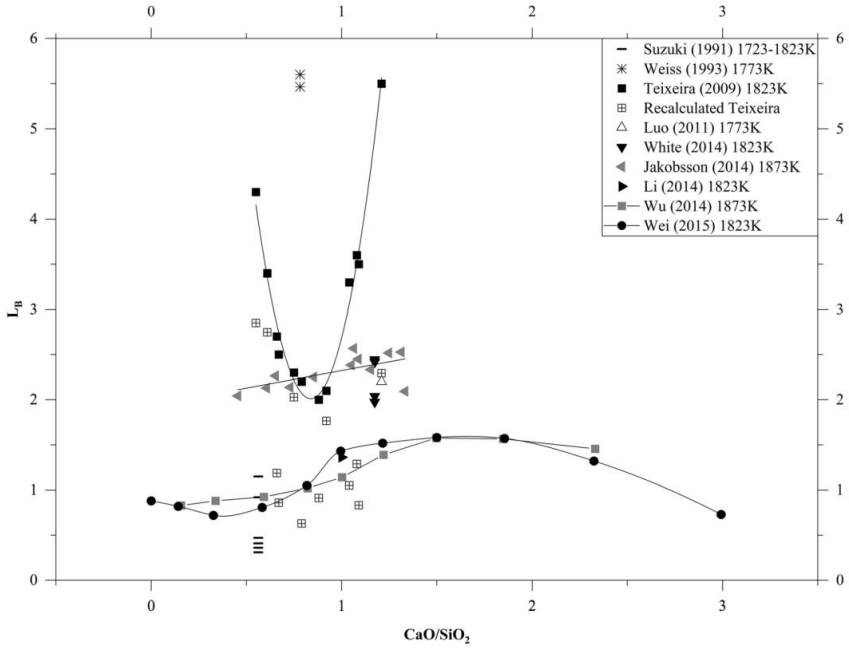

Figure 2- 31. Summarised B removal in CaO-SiO_2-based slags.[82]

Na_2O-SiO_2 slag system is also commonly studied for the B removal from Si. Safarian et al.[87] extensively studied the thermodynamics, kinetics, and mechanism of B removal through Na_2O-SiO_2 slag system. In addition to the alkaline-earth elements-based slag system, the dissolved B in Si melt was found oxidized at the interfacial area and further removed through the formation of volatile compound $Na_2B_2O_4$.

Fang et al.[88] studied the effect of refining temperature, slag composition, slag/Si mass ratio, and holding time of the Na_2O-SiO_2 slag. It was found that higher temperature promotes the B removal and

Na_2O/SiO_2 equals to 2 is the most efficient refining composition, which reached to equilibrium in 30 min at 1700 °C. Through three times slag refining operations, B was reduced from 1.8 to lower than 0.3 ppmw.

2.2.3.2 Other slag systems

As listed in Table 2- 6, there are also many other slag systems studied based on different purpose. For instance, Teixeira and Morita[89] studied the influence of CaF_2 addition into $CaO\text{-}SiO_2$ slag system, and it was found L_B values slightly increases from 1 to 2.4 with increasing CaO/SiO_2 ratio, but not dependent on the CaF_2. Safarian et al.[90] studied the ternary $CaO\text{-}Na_2O\text{-}SiO_2$ slag system and found that B removal rate is considerably higher than the binary $CaO\text{-}SiO_2$ slag because B was partially gasified through the evaporation of sodium metaborate, $Na_2B_2O_4$, while the final L_B value was between 2.4-2.6 and close to the results of $CaO\text{-}SiO_2$ binary slag. Jakobsson and Tangstad[85] investigated the B removal from the ternary $CaO\text{-}MgO\text{-}SiO_2$ and $CaO\text{-}Al_2O_3\text{-}SiO_2$ slag systems. No significant compositional dependence was observed for the $CaO\text{-}MgO\text{-}SiO_2$ slags as the L_B values varies in small range between 2-2.5, but the B removal was found to decrease with increasing Al_2O_3 addition. Johnston and Barati studied the effect of basicity and oxygen partial pressure of the quaternary $CaO\text{-}MgO\text{-}Al_2O_3\text{-}SiO_2$ slag system and found that basicity and oxygen pressure significantly affect the B removal. Recently, the addition of $CaCl_2$ in slags has been also studied[37,91], and it was proposed that B was removed by the formation of BOCl gaseous species.

2.2.3.3 Slag refining with silicon alloys

The slag refining with silicon alloys has attracted increasing attention in the recent years. It can also be regarded as a combined process of slag refining and solvent refining. A list of slag refining with silicon alloy is presented in Table 2- 7.

Ma et al.[92] studied the $CaO\text{-}SiO_2\text{-}CaF_2$ slag refining with Si-Sn alloys. It was found that the L_B values exponentially increases from 2.3 to 200 with increasing Sn concentration in the alloy. The main reason of such enhanced B removal is attributed to the increased B activity caused by Sn addition. Similarly, Li et al.[93] studied the $Na_2O\text{-}CaO\text{-}Al_2O_3\text{-}SiO_2$ slag refining with Si-Cu alloy and also reported with enhanced L_B values. The effect of slag composition was also studied and with a maximum of L_B and L_P observed by changing SiO_2/Al_2O_3 ratio, which further highlighted the counterbalancing effect between basicity and oxygen potential. In the recent, the slag refining of silicon alloys was also comprehensively reviewed by Thomas el al.[76]. In their work, the L_B values was normalized by oxygen partial pressure, and defined as D_B:

$$D_B = \frac{L_B}{(p_{O_2})^{\frac{3}{4}}} \qquad (2-25)$$

The D_B value is similar to boron capacity, which evaluates the boron removal ability of given slags. As shown in Figure 2- 32, even the reported values differ from study by study, a high D_B value can be reached through the Sn and Cu addition.

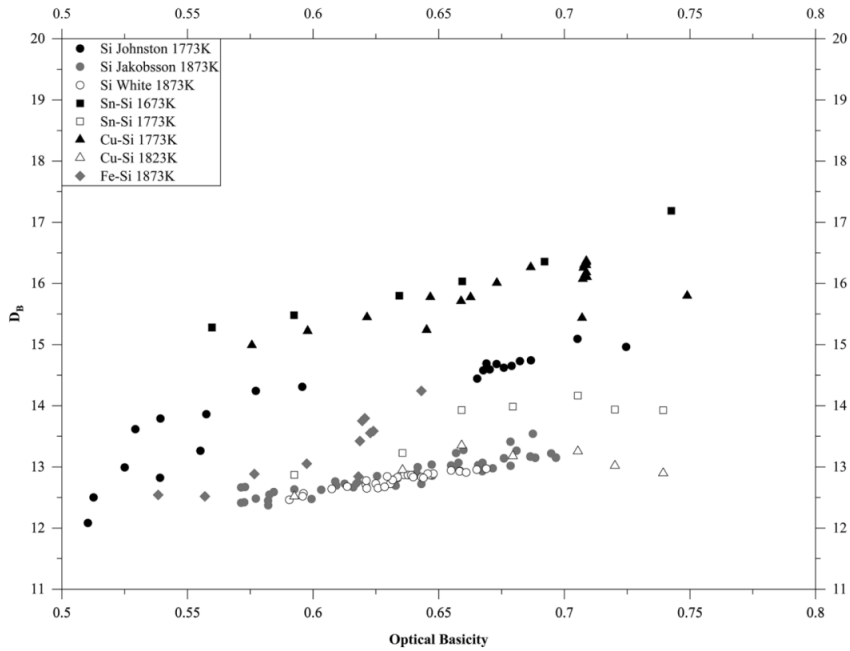

Figure 2- 32. Calculated D_B values from the slag refining oof silicon alloys.[76]

Table 2- 6. Review list of literature for slag refining with crude silicon.

Author	Furnace type	Slag system	Composition range	Crucible type	Gas phase	Si scale	Slag/ Si mass ratio	Tempera-ture (°C)	Holding time (h)	L_B
Suzuki and Sano [83](1991)	Resistance	$CaO-SiO_2$	36% CaO-64% SiO2	Graphite	Ar, CO, $Ar+CO_2$	10 g	1	1450-1550	2	0.31-1.15
Weiss and Schwerdtfeger[94] (1994)	Resistance	$CaO-SiO_2$	43wt% CaO-55% SiO_2 (2% B_2O_3)	Quartz	Ar	2 g	2.5	1500	4, 6.5	5.5
Fujiwara et al.[95] (2005)	Induction + mechanical stirring	$CaO-SiO_2$	35wt% CaO - 65% SiO_2	Alumina	Ar	2-3.5 g		1600	-	NG
Teixeira et al.[84] (2009)	Resistance	$CaO-SiO_2$	CaO/SiO_2=0.5-1.21	Graphite	Ar	3 g	2.2	1550	18	2-5.5
D. Luo et al.[96] (2011)	Induction 200kW - 3000 Hz	$CaO-SiO_2$	CaO/SiO_2=1.21	Quartz	Ar	3 kg	0.1	1550-1600	0.5-2	2.2
Z. Ding et al.[97] (2012)	Induction	$CaO-SiO_2$	45% CaO	Graphite	Ar	-	-	1550	-	1.02
Nishimoto et al.[98](2012)	Resistance	$CaO-SiO_2$	CaO/SiO_2=1.22	Graphite	Ar	1.6, 3, 3.2	1.25-2.5	1550	3	2.16
J. White et al.[80] (2014)	Resistance + mechanical stirring	$CaO-SiO_2$	54wt% CaO-46% SiO_2	Graphite		40 g	1	1550	0.17	1.98, 2.45
K. Wei et al.[99] (2015)	Induction	$CaO-SiO_2$	Optical basicity: 0.4-0.8	Graphite	Ar	-	-	1550	0.5-3	0.7-1.6
Jakobsson and Tangstad[100] (2015)	Resistance	$CaO-SiO_2$	36-54wt% CaO	Graphite	Ar	15 g	1	1600	0.6-18	2.13-2.52

Jakobsson and Tangstad[100] (2015)	Resistance	$MgO-SiO_2$	34-41wt% MgO	Graphite	Ar	5, 15 g	1	1600	0.6-18	1.92-2.41
Safarian[86] (2019)	Induction	$BaO-SiO_2$	45-60wt% BaO 40-55% SiO_2	Graphite	Ar	-	-	1500-1600	2	0.9-1.35
Suzuki and Sano[83] (1991)	Resistance	$CaO-MgO-SiO_2$	10%MgO, CaO/SiO_2=0.4-1	Graphite	CO	10 g	1	1450	2	1-1.6
J. White et al.[101] (2013)	Resistance	$CaO-MgO-SiO_2$	Not given	Graphite	CO (0.6, 0.8, 1 atm)	3 g	3.3	1600	48	2.3-3.45
J. White et al.[102] (2013)	Resistance	$CaO-MgO-SiO_2$	NG	Graphite	Ar+CO, $CO+N_2$	3 g	3.3	1600	48	1.3-3.4
Jakobsson and Tangstad[100] (2015)	Resistance	$CaO-MgO-SiO_2$	8-48wt% CaO, 6-31% MgO, 45-65% SiO_2	Graphite	Ar	15 g	1	1600	0.6-18	1.84-2.52
Suzuki and Sano[83] (1991)	Resistance	$CaO-BaO-SiO_2$	10%BaO, CaO/SiO_2=0.6-1.2	Graphite	CO	10 g	1	1450	2	1.5-2
Safarian[86] (2019)	Induction	$CaO-BaO-SiO_2$	0-10wt% BaO, 36-40% CaO, 53-59% SiO_2	Graphite	Ar	-	-	1500-1600	2	1.9-2.2
Suzuki and Sano[83] (1991)	Resistance	$CaO-SiO_2-CaF_2$	30% CaF_2, CaO/SiO_2=0.8-4.2	Graphite	CO	10 g	1	1450	2	1-1.7
Teixeira and Morita[89] (2009)	Resistance	$CaO-SiO_2-CaF_2$	25%CaF_2 CaO/SiO_2=0.3-3, 40% CaF_2 CaO/SiO_2=1-5	Graphite	Ar	3 g	2.2	1550	18	1-2.4
J. Cai et al.[89] (2011)	Induction	$CaO-SiO_2-CaF_2$	10wt% CaF_2 CaO/SiO_2=1.0-4.0	Graphite	Ar	-	3	1600, 1500-1700	1	2.86-4.61
H. Cheng et al.[103] (2018)	Induction	$CaO-SiO_2-CaF_2$	55wt% CaO, 30% SiO_2, 15% CaF_2	Graphite	Ambient air	140 g	2.2	1550	2	NG
H. Cheng et al.[104] (2019)	Induction	$CaO-SiO_2-CaF_2$	10-30wt% CaF_2	Graphite	Ambient air	140 g	1-3	1600	0.25-0.5	1.2-1.8

Suzuki and Sano[83] (1991)	Resistance	CaO-MgO-SiO_2-CaF_2	10% MgO, CaO/SiO_2=1-1.4	Graphite	CO	10 g	1	1450	2	1-1.4
Suzuki and Sano[83] (1991)	Resistance	CaO-BaO-SiO_2-CaF_2	10%BaO, CaO/SiO_2=1.2-1.4	Graphite	CO	10 g	1	1450	2	1.2-6
Z. Ding et al.[97] (2012)	Induction	CaO-SiO_2-LiF	LiF=0-40wt% CaO/SiO_2=0.8	Graphite	Ar	-	0.5-5	1550		1.0-2.77
Y. Li et al.[105] (2014)	Induction	CaO-SiO_2-LiF	20wt% LiF, CaO/SiO_2=1	Graphite	Ar	NG	1	1550	0.25-3	1.8
Wang et al.[106] (2016)	Induction	CaO-ZnO-SiO_2	0-30wt% Zn, CaO/SiO_2=1	Graphite	Ar	30 g	1	1550	1	1.8-3.04
H. Lai et al.[107] (2016)	Induction	Li_2O-SiO_2	16-75wt% Li_2O	Graphite	Ambient air	20 g	0.5-3	1700	0.17-0.5	NG
Y. Li et al.[105] (2014)	Induction	Li_2O-CaO-SiO_2	20wt% Li_2O, CaO/SiO_2=1	Graphite	Ar	NG	1	1550	0.25-3	1.4
H. Lai et al.[107] (2016)	Induction	Li_2O-SiO_2-CaF_2	15-67.5wt%Li_2O, 23-75%SiO_2, 10% CaF_2	Graphite	Ambient air	20 g	1	1700	0.17-1	
Z. Ding et al.[97] (2012)	Induction	Li_2O-CaO-SiO_2	Li_2O=0-40wt% CaO/SiO_2=0.8	Graphite	Ar	-	0.5-5	1550	0.5-4	1.0-2.0
J. Wu et al.[108] (2012)	Induction	Li_2O-CaO-SiO_2	Li_2O=2.5-20wt%	Graphite	Ar	-	0.5-4	1600	2	0.82-1.56
Safarian et al.[87] (2013)	Induction	Na_2O-SiO_2	20-50wt% Na_2O	Graphite	Ar	15 g	2	1500, 1550	0.25-0.75	0.3-1
M. Fang et al.[88] (2014)	Induction	Na_2O-SiO_2	Na_2O/SiO_2=0-4	Graphite	Ambient air	NG	0.5-2.5	1550-1750	0.5	NG
Y. Li et al.[109] (2018)	Induction	Na_2O-SiO_2	40wt%Na_2O-60%SiO_2	Graphite	NG	NG	0.5-1.5	1600	0.17-1	NG
Teixeira and Morita[89] (2009)	Resistance	Na_2O-CaO-SiO_2	Na_2O=0, 7, 10wt% CaO/SiO_2=1.21	Graphite	Ar	3 g	2.2	1550	1	1.6-2.3
L. Zhang et al.[110] (2013)	Induction	Na_2O-CaO-SiO_2	10wt% Na_2O, CaO/SiO_2=0.35-1.21	Graphite, Quartz	Ar	NG	0.2	1500	1	2.12-5.81
Safarian et al.[90] (2015)	Induction	Na_2O-CaO-SiO_2	5wt% Na_2O, 47.5%CaO, 47.5%SiO_2	Graphite	Ar	30 g	1-3	1600	0.17-2	2.4, 2.6
Y. Li et al.[105] (2014)	Induction	K_2CO_3-CaO-SiO_2	20wt% K_2CO_3, CaO/SiO_2=1	Graphite	Ar	NG	1	1550	0.25-3	1.9

J. Wu et al.[111] (2016)	Induction	K_2CO_3-CaO-SiO_2	5-25wt% K_2O, CaO/SiO_2=1	Graphite	Ar	40 g	1	1550	0.5-5	1.17-2.08
Jakobsson and Tangstad[112] (2018)	Resistance	CaO-Al_2O_3-SiO_2	36-50wt%CaO, 10-40% Al_2O_3, 11-40% SiO_2	Graphite	Ar	15 g	1	1600	6-9	1.33-2.08
J. Li[113] (2014)	Induction	CaO-Al_2O_3-SiO_2-CaF_2	10-40wt% CaO, 10-15% Al_2O_3, 45-70% SiO_2, 5% CaF_2	Graphite	Ambient air	NG	0.4-1	1800	0.5-2	1.0-2.2
Johnston et al.[114] (2010)	Resistance	BaO-Al_2O_3-SiO_2	25-45wt% BaO, 20% Al_2O_3, 35-5% SiO_2	Alumina	Ar	5.5 g	1.4	1500	2	0.1-0.5
Jakobsson and Tangstad[112] (2018)	Resistance	MgO-Al_2O_3-SiO_2	23wt% MgO, 48% SiO_2, 28%Al_2O_3	Graphite	Ar	15 g	1	1600	6-9	1.8
Johnston et al.[114] (2010)	Resistance	CaO-MgO-Al_2O_3-SiO_2	I. 35wt% Al_2O_3, 3% MgO, 15-55% CaO, 7-48% SiO_2 II. 42wt% CaO, 10% MgO, 15-45% Al_2O_3, 3-33% SiO_2	I. Alumina, II. MgO	Ar	5.5 g	1.4	1500	2	I. 0.9-1.8 II. 1-2
C. Yin et al.[115] (2011)	Induction	Na_2O-CaO-Al_2O_3-SiO_2	55wt% Na_2O, 42-45% SiO_2, 0-2% Al_2O_3	Graphite	NG	10 kg	0.1-0.5	1600-1750	0-4h	NG
Y. Wang et al.[116] (2014)	Resistance	CaO-SiO_2-$CaCl_2$	-	Graphite	Ar	5 g	2	1450	12	0.23-2.4

Table 2- 7. Review list of literature for slag refining with silicon alloy.

Author	Furnace type	Slag system	Alloy composition	Crucible type	Gas phase	Si Scale	Slag/ Si mass ratio	Temperature (°C)	Holding time (h)	L_B
Ma et al.[92]	Induction	CaO-SiO_2-24 mol%CaF_2	0-82.4 mol% Sn	Graphite	Ar	3 g	3	1400	18	2.3-200
J. Li et al.[117]	Resistance	70wt% Na_2SiO_2-5% CaO- 25% SiO_2	0-50 mol% Sn	Graphite	Ar	10 g	1-2	1450	0.5-3	NG
Al-khazraji et al.[118]	Resistance	10wt% $CaCl_2$, CaO/SiO_2=0.5-2	25wt% Sn	Graphite	Ar	NG	1,2	1500	0-1	NG
Li et. al[119]	Resistance	Na_2O-CaO-Al_2O_3-SiO_2	70 wt% Cu	Alumina	Ar	1 g	10	1500	0.17	0.7-46.8
Huang et al.[120]	Induction	CaO-SiO_2-$CaCl_2$	30-70wt% Cu	Graphite	Ambient air	50 g	1	1550	0.5	NG
Jakobsson[121]	Resistance	CaO-SiO_2	0-50wt% Fe	Graphite	Ar	15 g	1	1600	6	2.6-3
Krystad et. al[122]	Resistance	CaO-SiO_2	0-85wt% Fe	Graphite	Ar	4 g	0.57	1600	0-3	2.4-6
Hosseinpour et al.[123]	Resistance	CaO-Al_2O_3-SiO_2	20wt% Fe	Alumina	Ar	5 g	1	1600	0-8	0.8-11.4
Hosseinpour et al.[124]	Resistance	CaO-Al_2O_3-SiO_2	20wt% Fe	Alumina	Ar	5 g	1	1600	0-8	L_P: 0-0.11

2.3 Other refining techniques

2.3.1 Solvent refining

Solvent refining is a widely studied MG-Si purification technique that is done via alloying Si with another component to enable the solvation and followed by the re-solidification of Si from the molten alloy. Like the acid leaching technique, the basic principle of solvent refining is also to adjust the impurity segregation behaviour via alloying elements addition during Si solidification. To clarify here the main difference between the alloying leaching refining and the solvent refining, it is emphasized that in the leaching refining there is no other main metallic by-product, while in the solvent refining there is a main metallic by-product that can be later utilized or potentially recycled into the process. Moreover, as shown in Figure 2- 33, a unique marker and advantage of the solvent refining process is the low-temperature operation due to the addition of large amount alloying element. During the cooling process, primary Si is firstly precipitated and the impurities keep enriching in the remaining liquid phase that is becoming high with the solvent metal content. Subsequently, the purified Si obtained can be cleaned up via acidic solutions.

Si-Al melt is the most studied solvent refining system since 1950s as firstly reported by Obinata and Komatsu[125]. The segregation behaviour of P in the Si-Al melt was investigated by Yoshikawa and Morita[126]. It was found that P segregation coefficient decreases with decreasing temperature, such as 0.12 (1373 K), 0.085 (1273 K), 0.061 (1173 K). It was also reported that with Ti addition into the Si-Al melt, B can be effectively removed due to the formation of TiB_2 precipitates. As an example of the commercialized solvent refining process, the Silicor process produces SoG-Si through Si-Al solvent refining, followed by further HCl acid leaching of the precipitated Si flakes. The leaching by-product $AlCl_3$ is recycled commercially for wastewater treatment facilities, and the SoG-Si is obtained after remelting and solidification of the remained Si flakes to further remove the trace amount Al. In addition to Si-Al melt, a variety of other solvent refining systems were also developed recently with good purification performance such as Si-Sn, Si-Fe, Si-Cu, and so on. Moreover, other minor alloying elements addition (like Ti, Zr, Hf etc.) were also been studied mainly for the improvement of B removal. Additionally, the solvation of Si melt at low temperature also makes solvent refining compatible to other separation techniques for instances, combined with directional solidification, electromagnetic solidification, and super gravity separation and so on. According to the similar principle between solvent refining and the acid leaching process (in primary Si grains precipitation), the literatures about solvent refining were also summarised in Table 2- 8.

However, even though the solvent refining technique has exhibited promising features like low-temperature operation and effective impurity removal, as the SoG-Si market becomes intensely price-sensitive in these years, the required large amount of alloying metal addition is challenging to bring lower cost and higher Si yield. Moreover, the solvation of Si also requires restricted purity tolerance of the alloying metal, which should be another important issue to be considered.

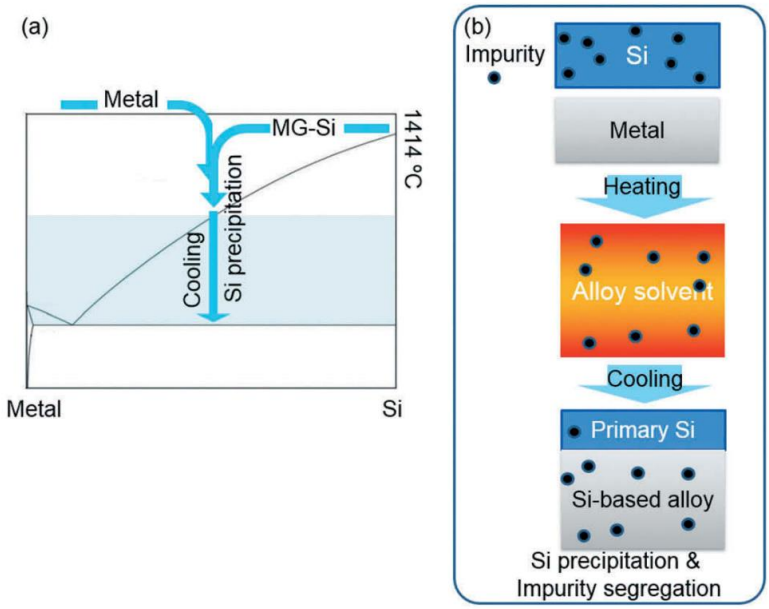

Figure 2- 33. Schematic diagram of the solvent refining process.[127]

Table 2- 8. Review list of literature for solvent refining.

Author	Si Source/Material	Refiner element	Main Equipment/ mixing method	Cooling rate	Crucible	Acid type	Tempera-ture (°C)	Purification degree
Obinata and Komattsu[125] (1954)	-	Al	-	-	-	-	-	P: 120-> 20 ppmw (83.3%)
Gumaste et al.[128] (1987)	MG-Si: B (6 ppm), P (45 ppm), Fe (890 ppm)	65% Al	-	20, 40, 60 K/h	-	HCl	48h	B: 6->6 ppm P: 45->15 ppm (98.6%) Fe: 890->15 ppm Ti: 230-> 2ppm
Yoshikawa and Morita[129] (2003)	Si-Al alloy, Al-P pellet	50-80% Al	SiC resistance furance 1173-1373K - 12 h	Quenched after equilibrium		-	-	P: 95-99% removal
Yoshikawa and Morita[130] (2005)	Si (11N), Al-B foils	44.8, 55.3 at% Al	1273-1473 K - 24 h induction furnace	40 K/cm	Alumina	-	-	B: 90% removal
Yoshikawa and Morita[131] (2005)	Si-Al alloy	55.3, 64.6 at% Al	1223 K - 10 min induction furnace	0.25-1 mm/min	Graphite	Aqua regia+H_2SO_4	-	B: 36 or 56 -> c.a. 1 ppmw P: 19 or 36 -> c.a. 1 ppmw B, P > 98% removal
Yoshikawa et al.[132] (2005)	Si-55at% Al B (100 ppma), Ti or Al-Ti alloy	55 at%Al + 82-933 ppma Ti	induction furnace (50kHz)	5-10 K/min	Graphite	Aqua regia+H_2SO_4	-	B: 170-> 1.1 ppma
X. Gu et al.[133] (2011)	MG-SI (99wt%), Al (99wt%)	60,65,70wt% Al	800-1250 C - 2-10 h Resistance furance	0.5 K/min	Quartz	Stage I: HCl Stage II: HF + HNO_3 + CH_3COOH	-	B: 8-> 1.55 ppmw (80.6%) P: 13->0.41 ppmw (96.8%)
H. Lei et al.[134] (2013)	MG-Si, Refined Si-Sn re-alloyed with Al	88wt% Sn 56wt% Al	1773 K - 1 h Reheated at 673 K - 0.5 h for gravity separation	3 K/min	Alumina	Stage I: aqua regia Stage II: HF	70°C - 6 h	B: 12.1 -> 3.3-> 0.28 ppmw P: 242.6-> 44.5-> 0.46 ppmw (MG-Si-> Si-Sn -> Si-Al)
B. Ban et al.[135] (2015)	SoG-Si, Al (99.96wt%), Si-P Final P: 1000 ppmw	60, 70, 80wt% Al	1473K - 3 h stirred twice by quartz rod resistance furance	0.556 mK/s (0.033 K/min)	Alumina	diluted HCl	-	P: 1000-> 7-476 ppmw
Y. Li et al.[136] (2015)	MG-Si, industrial grade Al Final P: 25.4-30.2	60, 70, 80wt% Al	1323K - 3 h stirred by quartz rod resistance furance	0.55-32 mK/s (0.033-1.9 K/min)	Alumina	diluted HCl	-	P 27.8-> 4.5-26 ppmw
B. Ban et al.[137] (2016)	SoG-Si, Al (99.96wt%), Si-P Final P: 890 ppma	60, 70, 80wt% Al	1473K - 3 h stirred by quartz rod resistance furnace	0.556 mK/s (0.033 K/min)	Alumina	diluted HCl+ HNO_3	-	P:890-> 6-24 ppma

B. Ban et al.[138] (2016)	SoG-Si, Al (99.96wt%), Si-B Final B: 300 ppma	70wt% Al + 0-575 ppma Ti	1323K - 3 h resistance furance	50mK/S (3 K/min)	Alumina	diluted HCl+ HNO_3	-	B: 300-> 12-232 ppma
L. Sun et al.[139] (2017)	MG-Si, Al Final B: 7 ppma Final P: 23 ppma	30 at% Al	Melting: 1773 K - 1 h induction furnace Directional solidification: 1373-1574 K	0.05 mm/min	Graphite	-	-	P: 85-95% removal
Y. Li et al.[140] (2019)	Resistance furnace	63.8 wt% Al+Zn	1273K - 10 min Cooled to 873K SiC resistance furance	1 K/min, 10-20 K/min, 200-400 K/min	Alumina	Stage I: 6 mol/L HCl Stage II: aqua regia Stage III: HF-H_2O (vol: 1:17)	Stage I: 25°C - 64 h Stage II: 60°C - 3 h Stage III: 60°C - 3 h	B: 71.6-90.5% removal
Y. Lei et al.[63] (2016)	Si (99.9999%), Al (99.999%), Si-1wt%B, Si-10wt% Hf Final B: 153 ppm	45-64at% Al + 205-1024 ppm Hf	1473K - 0.5 h	4.5-7.6 K/min	Graphite	Aqua regia + H_2SO_4	6 h	B: 153-> 4.6 ppm
Y. Lei et al.[141] (2015)	Si (99.9999%), Al (99.999%), Si-1wt% B, Si-1wt% Zr Final B: 153 ppm	55 at%Al+ 0-1057 ppm Zr, 55at%Al + 1019 ppmw Ti	1473K - 0.5 h induction furnace (20kHz)	1.6-20.6 K/min	Graphite	Aqua regia + H_2SO_4	-	B: 153-> 4.3 ppm
Y. Lei et al.[142] (2016)	Al-46wt% Si	45-64at% Al + <2037 ppm Ti	1473K - 0.5 h induction furnace (20kHz)	0.55 mm/min	Graphite	Aqua regia + H_2SO_4	70°C - 6 h	B: 153-> 1.2 ppma (0.46 ppmw)
J. Li et al.[143] (2013)	MG-Si (99wt%, B:14.8. ppmw), Al (99wt%), Sn (99.99wt%)	38,58,68 at% Al+ 0,10,30 at% Sn	900-1100C - 0.5 h Induction furance	1,3,10 K/min	Alumina	Stage I: 6 mol/L HCl Stage II: aqua regia Stage III: HF-H_2O (vol: 1:17)	Stage I: 25°C - 64 h Stage II: 60°C - 2 h Stage III: 60°C - 2 h	B: 14.8 (in MG-Si) -> (3.8, 5.1, 8.6) ppmw (after leaching)
Y. Li et al.[144] (2014)	MG-Si (B: 14.8 ppmw), Al (99.9% pure, B: 24 ppmw), Sn (99.99% pure)	Al-Sn	1000-1100C - 2 h Induction furance	3 K/min	Alumina	Stage I: 6 mol/L HCl Stage II: aqua regia Stage III: HF-H_2O (vol: 1:17)	Stage I: 25°C - 64 h Stage II: 60°C - 3 h Stage III: 60°C - 3 h	Si-Al system: B: 22.9-82.6% removal Si-Al-Sn system: B: 40.5-73.6% removal

T. Tang et al.[145] (2016)	MG-Si (99.5wt%), Al (99.9wt%), Sn (99.9wt%)	44-68wt% Al + 0-24 wt% Sn	1273 K - 2 h Resistance furance	5 K/min	Alumina	5 mol/L HCl + 5 mol/L HNO_3	60°C - 3 h	P: 65-80% removal, Fe: c.a. 100% removal Ca: 80-90% removal
L. Hu et al.[146] (2013)	MG-Si B (10.3 ppmw), P (108.5 ppmw), Fe (925 ppmw), Al (926 ppmw)	88wt% Sn + 4 wt% Ca	1773 K - 2 h Remelted with gravity separation	3 K/min	Alumina	20wt% Aqua regia + 5wt% HF	60°C - 6 h	B: 10.3 (in MG-Si)-> 3.12 ppmw (69.7%) P: 108.5 -> 28.9 ppmw (73.4%) Fe: -> 1.97 ppmw (99.8%) Ca: -> 0.98 ppmw (97.2%)
X. Ma et al.[147] (2015)	MG-Si B (33 ppmw), P (37 ppmw), Fe (2600 ppmw), Al (790 ppmw)	40 mol% Sn	1628 K - 0.5 h	4 K/min	Graphite	HCl	3 h	B: 33 (in MG-Si)->13.5 ppmw (59.1%) P: 37(in MG-Si)-> 10.3 ppmw (72.2%)
Y. Ren et al.[148] (2018)	Si (6N), Sn (99.9%)	50 at% Sn	Liquidus temperature - 1 h SiC resistance furance	0.01-0.1 mm/min	Graphite	concentrated HCl	-	-
Y. Ren et al.[149] (2019)	Si (6N), Si-1wt% Zr, Si-1wt%B	50, 60 at% Sn	Liquidus temperature - 1 h SiC resistance furance	0.01-0.1 mm/min	Graphite	HCl+HF (concen-trated, 1:1 volume ratio)	-	B: 20-70% removal (20-80at% Sn)
J. Li et al.[150] (2017)	MG-Si B (25 ppmw), P (43 ppmw)	75 wt% Ga	1573K - 2 h	1 K/min	Alumina	Stage I: Aqua regia Stage II: HF	-	B: 83.28% removal P: 14.84% removal
Juneja et al.[23] (1986)	MG-Si Si (~98%), B (35 ppmw) Fe (1.0%), Al (0.25%), Ca (1.2%)	60 wt% Cu	Induction furnace	-	Silica, Gaphite	Aqua regia, HF	-	B: 35-> 200 ppm Al: 2500 -> 27 ppm Mg: 110 -> 9 ppm Ti: 210 -> 5 ppm Ca: 12000 -> 5 ppm Fe: 10000 -> 60 ppm
Visnovec et al.[151] (2012)	MG-Si Fe (0.23%), Al (0.26%)	50%Cu	-	1 K/min. 0.5 K/min	-	10% HNO_3, 5% HCl+ 7% HNO_3	25°C - 1620 min	impurities: 5277->225 ppm
M. Fang et al.[152] (2013)	MG-Si Fe (0.15%), Al (0.26%), Ca (0.05%)	50 wt% Cu	1773K - 1 h	10, 50, 100 mm/h	Graphite	-	-	B: 35-45% removal P: 20-60% removal Fe, Al, Ca: >95% removal

L. Huang et al.[153] (2016)	MG-Si: B (2.94 ppmw), P (13.51 ppmw), Cu: B (3.86 ppmw), P (15.17 ppmw)	30,50,70wt% Cu	1823K - 2 h Resistance furance	5, 10, 20 K/min	Al_2O_3 coated by Si_3N_4	Stage I: 2M HNO_3 Stage II: 2M HNO_3 + 1 M HF Stage III: 1M HNO_3	Stage I: 70°C - 5 h Stage II: 70°C - 2 h Stage III: 70°C - 1 h	Fe: 968.6-> 4.12 ppmw (99.6%, 30wt% Cu) 697.1-> 2.75 (99.6% 50wt%Cu) 545.6-> 1.44 (99.75 70wt% Cu)
L. Huang et al.[65] (2016)	MG-Si: B (3.12 ppmw), P (17.14 ppmw) Final Si-Cu: B: 2.67 ppmw P: 12.34 ppmw	50 wt% Cu	1823K - 2 h Resistance furance	5 K/min	-	Stage I: 2 M HCl/ HNO_3/aqua regia Stage II: 2 M HNO_3+ trace HF Stage III: 1 M HNO_3	70°C - 5h	B: 2.67 ppm --> 58.7% removal P: 12.34 ppm -->42.2% removal
L. Huang et al.[154] (2018)	Si-Cu: B: 27 ppmw, P: 1622 ppmw Fe: 2705 ppmw, Al: 1788 ppmw Initial: Si-Cu-3wt% P	50 wt% Cu + 0-5 wt% Ca	1823K - 3 h Resistance furance	10 K/min	Graphite	Stage I: 2 M HCl/ HNO_3/aqua regia Stage II: 2 M HNO_3+ trace HF Stage III: 1 M HNO_3	70°C - 5h	P: 82% removal
L. Huang et al.[155] (2017)	MG-Si: B (15 ppmw), P (27 ppmw) Fe (2476 ppmw), Al (1363 ppmw)	45-49 wt% Cu + 1-5 wt% Ti	1823K - 3 h Resistance furance	6 K/min	Graphite	Stage I: 2 M HCl/ HNO_3/aqua regia Stage II: 2 M HNO_3+ trace HF Stage III: 1 M HNO_3	Stage I: 70°C - 12 h Stage II: 70°C - 6 h Stage III: 70°C - 6 h	B: 624-> 94 ppmw, 85% removal 24-85%
Y. Ren et al.[156] (2020)	Si-1wt% Zr, Si-1wt%B	25-50 at% Cu + 305-1525 ppmw Zr	Si-1wt% Zr, Si-1wt%B	0.01, 0.02, 0.04 mm/min	Graphite	HNO_3+ H_2SO_4 + HCl	-	B: 80-> 5.3-53.7 ppmw (highest 93.4%)
Y. Ren et al.[157] (2020)	Si-1wt% Zr, Si-1wt%B	50 at% Cu +200-3000 Zr ppma	1258-1345K - 12h Resistance furance	3.33 K/min	Graphite	-	-	-

Morito et al.[158] (2012)	MG-Si: Si (~99%), Fe (0.32%), Al (0.05%)	60 mol% Na	1173K, 24 h	-	BN	-	-	B: 9.1-> 120 ppmw P: 73-> 3.4 ppmw Fe: 3200-> 1.5 ppmw Al: 510-> 6 ppmw Ca: 96-> 1.7 ppmw
Morito et al.[159] (2013)	MG-Si: Si (~99%), Fe (0.32%), Al (0.05%)	60 mol% Na	1173K, 24 h	-	MgO	-	-	B: 9.1-> 0.3 ppmw P: 73-> 35 ppmw Fe: 3200-> 17 ppmw Al: 510-> 6.9 ppmw Ca: 96-> 24 ppmw

2.3.2 Directional solidification

Directional solidification is another impurity segregation-based technique that highly efficient for the removal of metallic impurities in Si. Just as its name implies, it is performed during Si solidification with temperature gradient along a direction (usually from bottom to top), so that Si solidifies from one side to another side directionally and impurities are pushed and accumulated in the remaining liquid phase. Owing to the significantly low segregation coefficient of most of metallic impurities, the SoG-Si purity requirements could be fulfilled by repeating the directional solidification process.

However, even though vast majority of metallic impurities could be removed by directional solidification, it is still inefficient for the removal of B and P as their segregation coefficients are high and close to 1.

2.3.3 Vacuum refining

Vacuum refining is an effective technique for the removal of volatile impurities in MG-Si (P, Zn, Mg, Ca, etc.). The fundamental principle of vacuum refining is based on the vapor pressure differences of the impurities at high temperatures compared to silicon. As can be seen in Figure 2- 34, a number of elements exhibit higher vapor pressure than Si in a wide temperature range, thus, the removal of such elements becomes possible. The vacuum refining efficiency of monoatomic evaporation of impurity *i* in dilute Si solution could be evaluated through the criterion[160]:

$$\alpha = \frac{\gamma_i^0 p_i^0}{p_{Si}^0}\left(\frac{M_{Si}}{M_i}\right)^{\frac{1}{2}} \qquad (2-26)$$

where p_i^0 and p_{Si}^0 are the vapor pressure of impurity *i* and pure Si at given temperature, M_i and M_{Si} are the atomic mass of impurity *i* and pure Si, γ_i^0 is the Henrian activity coefficient of the impurity *i*. When $\alpha > 1$, it indicates that the impurity *i* can be completely removed from Si through evaporation, on the contrary, when $\alpha < 1$, it indicates that impurity cannot be removed from Si as the evaporation rate of Si becomes greater than the targeted impurity *i*. Additionally, if the value of α closes to 1, it indicates the evaporation rate of the two species are similar and the separation efficiency becomes limited.

Practically, P is the main impurity that is removed by vacuum refining due to its higher vapor pressure than Si. The performance of vacuum refining is also affected by multiple factors such as the refining temperature, applied pressure, and the chemical composition of Si melt.

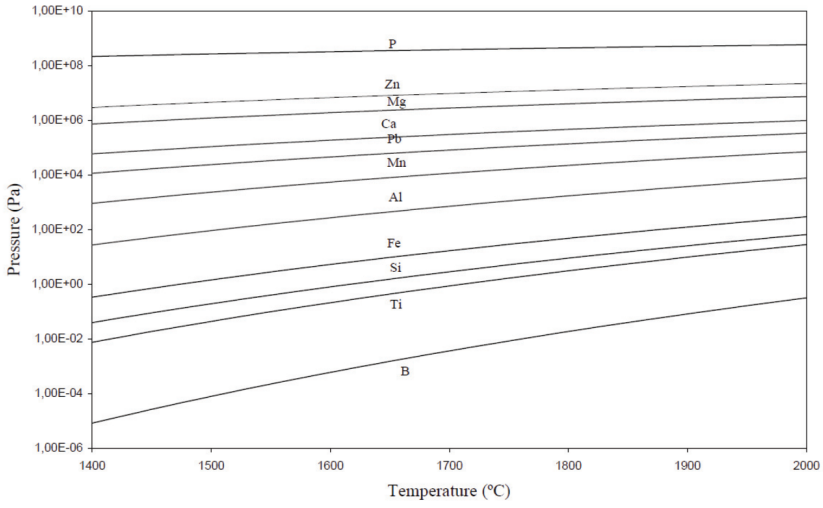

Figure 2- 34. Standard vapour pressure changes of pure substances against temperature.[161]

2.3.4 Gas refining

Gas refining is an efficient technique to remove B impurity in Si by blowing reactive gas (i.e. O_2, H_2, Cl_2, H_2O, CO_2 etc.) into Si melt. During the refining process, B is oxidized as gaseous products like BO, B_2O, BO_2, B_2O_2, HBO, HBO_2, BH_2 etc., which are volatile and spontaneously removed from the melt. Additionally, the melt would be stirred by purged gas or other techniques so that the process of impurity reaction and desorption could be further accelerated.

The oxidant gas can be blown into the melt through a lance or nozzle on the top of the melt surface or plugged in the bottom. The purification efficiency is also affected by the blowing gas types, flow rate, refining temperature, and time period. In principle, gas refining is a non-equilibrium process (as vacuum refining), thus, B concentration in Si could be infinitely reduced, however, it is also worth noting that parts of Si could be also oxidized as SiO gas or SiO_2 and so some Si loss occurs.

2.3.5 Plasma refining

Plasma refining is a technique using plasma-activated reacting gas to convert B in Si melt to volatile compounds, like the gas refining, however, at higher temperatures and significantly different technology. The formation of plasma flame requires ultra-high temperature and leads to the ionization of the oxidizing gas like O_2, H_2, H_2O to O, H, OH, O^+, OH^+, etc. in plasma flame so that to dramatically enhance their chemical reactivity. Accordingly, like gas refining, B in Si melt could be effectively converted into volatile species like HBO, HBO_2, BO, B_2O, BO_2, and so on.

The advantage of plasma refining is that the ultra-high temperature and chemical reactivity of ionized refining gas significantly benefits B removal in a short time. However, the plasma refining currently still requires expensive equipment and only suitable for small scale Si refining.

2.3.6 Electron beam melting

Electron beam melting is a technique to remove volatile impurities such as P, Al, and Ca from molten silicon heated by electron beam radiation. This technique also takes advantage of vacuum refining as the pressure can be pumped to less than 10^{-4} Pa[162]. Additionally, the formation of localized molten pool results in a convective, which further promotes the P evaporation.[163]

Due to the low vapor pressure of B, the electron beam melting technique is not suitable for B removal. Therefore, it can be coupled with the plasma refining, known as the NEDO melt-purification process[164]. Even though unique heating characteristics benefits in a short heating time of the radiated area, however, it still needs further investigation related to the feasibility on larger production scale.

Chapter 3

Research methodology

Both the experimental and theoretical methods that were applied in this thesis are described in this chapter.

3.1 Experimental

The used materials for making silicon alloys with the refiner metals are described. Moreover, the applied leaching and slag refining techniques to treat typical high Si alloys are presented.

3.1.1 Raw materials

The two types of Si sources were used in this work, respectively, commercial MG-Si (99.5% purity) and ultra-high purity Si produced from the fluidized bed reactor process (FBR-Si). Two batches of MG-Si were used (Batch 1 for paper 1-2 and Batch 2 for paper 3-7). Their measured compositions are listed in Table 3- 1. The FBR-Si was used to minimize the influence of other minor impurities in MG-Si and attain a lower P impurity concentration at several ppmw levels. The MG-Si and FBR-Si mixing ratio was fixed as 40% MG-Si and 60% FBR-Si for all the alloys.

High purity Mg-rod (99.8% purity, Alfa Aesar), and granular Ca (99% purity, Sigma Aldrich) were employed as the alloying metal sources. Considering the higher volatility of Mg at high temperature, it was doped into Si after melting, while Ca granulates were directly charged with Si before heating. For the preparation of other alloying system, the used alloying metals are reagent grade Al, Ti, Y, Sn with confirmed low B and P content.

Table 3- 1. Measured composition of MG-Si used in this study.

Sample	B	P	Mg	Ca	Al	Fe	Ti	Mn
Batch 1	46.2	15.8	9.6	266.7	2548.0	3167.5	299.8	70.4
Batch 2	42.5	14.8	10.7	331.7	1859.7	2723.9	218.2	23.2

Graphite and alumina crucibles were used for the alloy making. The used high-density isotropic graphite crucibles (cylindrical shape with inner diameter: 70 mm, outer diameter: 85 cm, height: 150 mm) were supplied by Svenska Tanso AB. The graphite crucible was manufactured through hot static pressing with a density 1.77 g/cm^3. The documented thermal conductivity is 116 W/m^{-1}·K^{-1} and with also other good mechanic properties such as tensile strength 25.5 MPa, compressive strength 78.4 MPa, and elasticity 9.8 GPa. In the experiments, the graphite crucible was mainly used for the Si-Ca-Mg alloys preparation and master slag preparation.

The used Alsint alumina crucible (cylindrical shape with inner diameter: 26 mm, outer diameter: 30 mm, height: 40 mm) was supplied by CoorsTek, Inc. with a. purity 99.7%, density 3.98 g/cm^3, and gas tight level permeability. Around 12-gram materials were charged in the experiments making Ca-based Si-Ca-Al (Ti, Y) alloys.

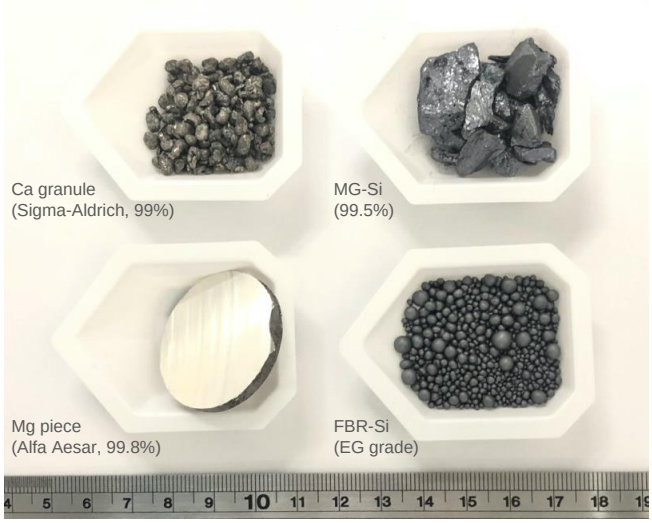

Figure 3- 1. Raw materials used for the Si-Ca-Mg alloys preparation.

3.1.2 High-temperature furnace and its operation

The induction furnace operates with manual heating control and a maximum heating temperature of up to 2000 °C. The vacuum limit inside the furnace chamber reaches lower than 1.3×10^{-5} bar. A swing handle is installed to support the casting operation that pours the melt into a water-cooled copper mold.

During the experiments, a high-density isotropic graphite crucible was placed inside the induction coil and covered by carbon wool and mica roll. A type-C thermocouple was inserted into alumina tube and further placed in the graphite crucible through a graphite tube as protection for the temperature control. Before heating, the furnace was evacuated to 10^{-1} mbar and refilled to 1 bar with continuous high purity Ar flow (+99.999% purity) three times. Crucibles were later on heated to 1500 °C and held for target time period to make sure the sample is completely melted and homogenized by the electromagnetic force induced stirring. The generated off-gas leaves the chamber through gas outlet with the continuously purged high purity Ar flow. After melting, samples were cooled down in the crucible or directly casted into the water-cooled copper mold.

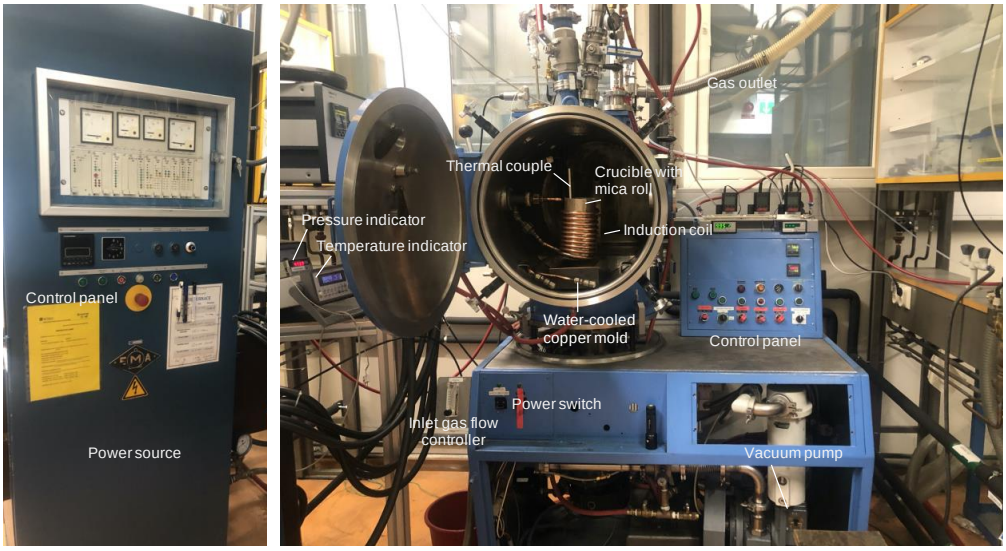

Figure 3- 2. Setup of the induction furnace and its affiliated parts.

3.1.3 Acid leaching procedure

As shown in Figure 3- 3, the obtained Si bulk alloys were firstly crushed to lumps using a hammer. All materials were handled using sealed plastic bags and nitrile gloves to prevent contamination. The crushed Si alloys were further milled in a ring mill to the target particle sizes (0.2-1 mm for Si-Ca-Mg alloys, 0.6-1 mm for Si-Ca-Al (Ti,Y) and Si-Sn alloys) using Retsch Vibratory Disc Mill RS200 with the tungsten carbide sets. Before milling, the FBR-Si was first crushed by the tungsten carbide sets three times to avoid unexpected contamination.

An ultrasonic bath and hot plate with magnetic stirring were employed for the acid leaching experiments. In the ultrasonic leaching, 1-2 g Si alloy particles were charged into perfluoroalkoxy alkane (PFA) bottles and further filled by 10 mL acid solution. By using the magnetic stirring leaching, the sample 20-40 g Si alloy particles were charged into beaker and with 100-200 mL acid solution addition. The stirring speed was fixed at 200 rpm for all leaching trials. The leaching temperature of the two devices was manually calibrated by the same mercurial thermometer. The leached samples were then washed three times by deionized water and ethanol.

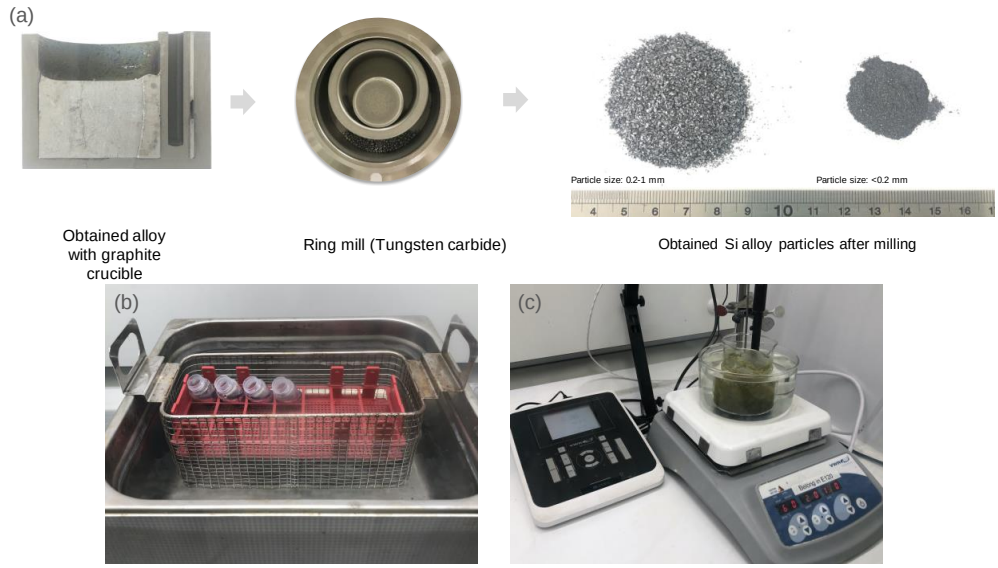

Figure 3- 3. Procedure of acid leaching and used equipment. (a) milling process, (b) ultrasonic bath, (c) hot plate with magnetic stirring.

3.1.4 Slag refining procedure

As shown in Figure 3- 4, the slag refining experiments were performed using the mixture of Si-10wt% Sn alloy and different master slags. The Si-Sn alloy was obtained through the melt-casting procedure as introduced above by mixing MG-Si and high-purity Sn in a dense graphite crucible.

The CaO-SiO_2 master slag was obtained by mixing the reagent grade CaO powder (99.9% purity, Sigma-Aldrich) and ultra-high purity SiO_2 fines from The Quartz Corp with an equimolar ratio in a graphite crucible that followed by the same melt-casting approach in the induction furnace as well. The master slags were also milled by the tungsten carbide ring mill to fine powders and then re-melted with 2wt% and 10wt% reagent grade La_2O_3 powder (99.9 pct purity, Sigma-Aldrich) addition. All the obtained materials were milled to fine powders for homogenization before using in slag refining experiments.

In the slag refining trials, 20 g Si-10 wt% Sn powders and 20 g slag powders were mixed into the dense graphite crucible and further placed inside the induction furnace chamber. The refining temperature was measured by a type C thermocouple and fixed at 1600±20 °C for 1 h in association with the electromagnetic stirring, and then cooled down to the room temperature. After experiments, samples were cut longitudinally for further metallographic analysis and ultrasonic acid leaching experiments.

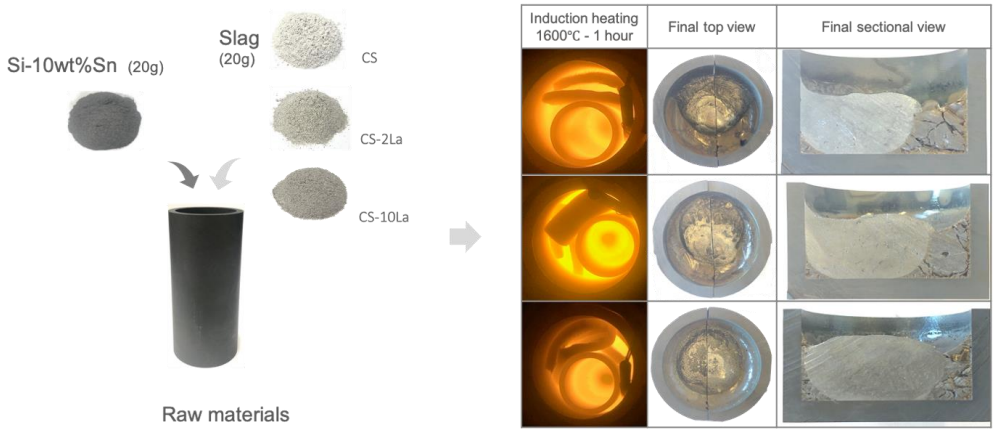

Figure 3- 4. Experimental procedure of slag refining and obtained samples.

3.2 Analysis and test methods

The applied materials characterization methods in the present research are shortly described as follows.

3.2.1 Inductively Coupled Plasma Mass Spectrometry (ICP-MS)

ICP-MS is a type of mass spectrometry for elemental analysis and capable for detection of most of the elements in periodic table with high precision and sensitivity at the level of parts per billion. Samples are introduced in liquid and further decomposed to its constituent elements and transformed into ions by the ionization source named inductively coupled plasma, which generates ultra-high temperature of approximately 8000 °C. The generated ions are then introduced to the mass spectrometer for measurement with extremely high sensitivity and up to 70 elements can be determined simultaneously in a single sample analysis.

In the presented work, high-resolution ICP-MS (Agilent 8800) was employed to measure the impurities content to ensure a low detection limit. The workflow of ICP-MS sample preparation mainly consists of the following three steps: Firstly, weighing sample with target amount (30 to 60 mg) using high-precision balance and clean PFA bottles. Secondly, digestion of weighted samples through specific acids combination (1.5 mL HNO_3 (69%) + 0.5 mL HF (40%)). Thirdly, further dilution of the digested solution using ultrapure water to around 200 mL and then filled in specific clean tube for ICP-MS analysis.

In order to obtain accurate and reliable results with impurity content at ppmw levels, both the sample preparation and measurement follow restrict and standardized rules for all samples in the lab. Every Si sample was measured at least two parallels for average and the NIST 57b Si powder sample was used as the reference material. In the digestion procedure, electronic grade acid mixture of HF and HNO_3 were employed and carefully added by droplets into clean PFA bottles. The PFA bottles are only used for Si sample digestion and cleaned by ultra-pure deionized water at least three times before and after use. The digestion of Si samples lasts at least 6 hours to make sure all Si particles fully dissolved, and no remaining solids or precipitations could be observed by naked eyes. The digested solution was further carefully diluted by ultrapure deionized water for ICP-MS measurement.

3.2.2 Scanning Electron Microscopy (SEM)

SEM is commonly used in materials science and engineering for the micro-scale topography observation and often coupled with energy dispersive x-ray spectroscopy (EDS) to detect chemical composition on the sample surface. As the name suggests, the SEM produces images by scanning the sample surface with a focused electron beam in a vacuum chamber as schematically illustrated in Figure 3-5. The electrons interplay with sample surface and results in the excitation of different signals for detection such as secondary electrons, backscattered electrons, and characteristic X-rays. Characteristics X-ray for EDS analysis can be collected from points or areas of the sample (depending on the size of the phases) and the technique was used to identify approximate chemical compositions of the co-existing samples in this study.

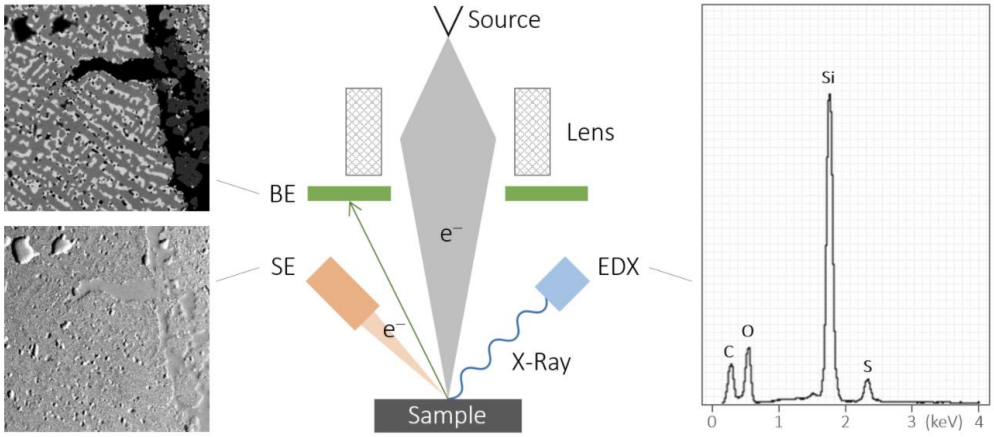

Figure 3- 5. Sketch of the working principles of SEM and EDS.[165]

In this work, the microstructure of obtained Si alloys was investigated by field-emission scanning electron microscopy (LVFSEM, Zeiss Supra 55VP) with installed energy-dispersive X-ray spectrometers (EDX). Before the observation, samples were mounted in EpoFix cold-setting resin and further ground and polished using Struers automatic grinder and polisher (RotoPol-31). Carbon coating was also applied to improve the electrical conductivity of the samples surfaces (to prevent electron charging over the surface in SEM) using SEM Turbo Coater (AGB7230).

3.2.3 Electron Probe Micro-Analyzer (EPMA)

EPMA is a microbeam instrument used for non-destructive elemental analysis of micron-sized volumes on sample surface. It fundamentally shares the same principle as SEM but with advanced capability for quantitative chemical analysis by wavelength-dispersive spectroscopy (WDS).

In this work, JXA-8500F was used for the high-resolution elemental mapping and the precipitate composition was measured through the WDS. The acceleration voltage was set as 15 kV with a probe current 9.9×10^{-9} A. The advantage of WDS in EPMA compared to EDS is the more accurate chemical composition measurement and also the possibility to analyze more fine phases, i.e. about one micron and larger.

3.2.4 Secondary Ion Mass Spectrometry (SIMS)

SIMS is a surface destructive technique to analyze the composition of solid materials by sputtering primary ions over the sample surface. The ejected secondary ions are further collected and measured by mass spectrometer which provides in-depth distribution analysis of trace elements with a detection limit down to ppb level.

In this work, 2D elemental distributions were measured by SIMS using CAMECA IMS 7f microanalyzer. The measurements were performed in the imaging mode using 15 keV Cs^+ ions as the primary beam for Si-Mg sample and 10 keV O^{2+} for Si-Sn sample. The primary beam rastered over an area of 500×500 μm^2. A typical scanning result is presented in Figure 3-6.

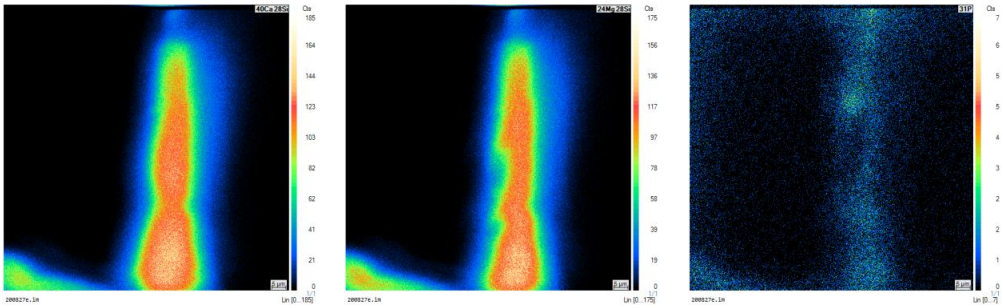

Ca+Si Mg+Si P

Figure 3- 6. Typical example of SIMS elemental mapping results shown by a studied Si-Ca-Mg alloy (sample CM1-Casted in paper 4) with presented signals of Ca+Si, Mg+Si, and P.

3.2.5 Electron Backscatter Diffraction (EBSD)

EBSD is a microstructural-crystallographic characterization technique used to perform quantitative microstructural analysis, grain size and orientation analysis. In this work, the crystallographic properties were also measured using NORDIF system. The EBSD scan was conducted in a Quanta 650 scanning electron microscope (SEM, ThermoFisher Scientific Inc.) operated at an accelerating voltage of 20 kV, an aperture of 100 μm and a spot size of4.0. The working distance was about 20 mm for the 70° pre-tilt specimen, and the dynamic focus in the SEM was adopted to improve the focal distance over a relatively large probe area of about 1.2 × 1.2 mm^2. A typical EBSD mapping results can be seen in Figure 3-7.

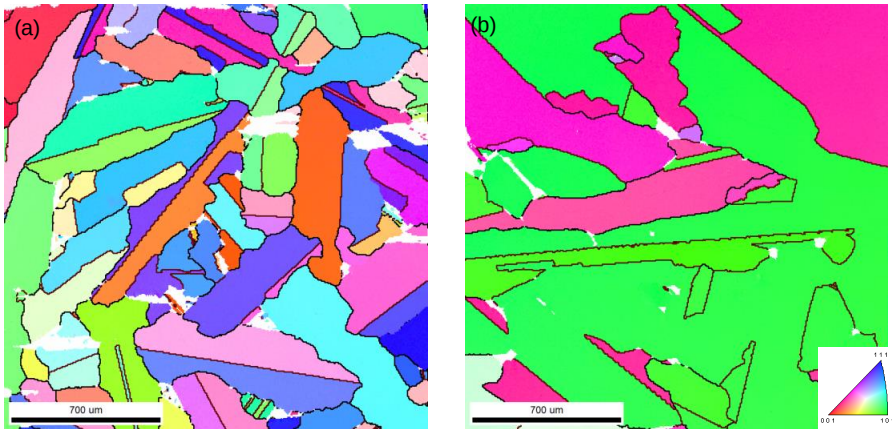

Figure 3- 7. Typical EBSD crystallographic mapping results shown by studied Si-Ca-Mg alloys (a) sample CM1 in paper 4, (b) sample CM1-Casted in paper 4, where the colored regions indicate Si phase and the white regions are precipitates. The color-coded according to the legend in the bottom-right corner. The lines presented indicate grain boundaries of Si.

3.2.6 Particle size distribution test

The particle size distribution of studied Si materials was measured by laser scattering particle size distribution analyzer Horiba Partica LA-960. The measured particle size ranges between 10 nm to 5 mm. Si particles were dispersed in deionized water and their sizes measured by the laser scattering technique. The refractive index value of pure Si is adopted for analyzing Si-rich alloy samples as an approximation since the real value should be reasonably close to the adopted value. The particle size measured by laser scattering is usually larger than the sieving particle size, as it is the diameter of a sphere with the particle's equivalent volume and the sieving particle size is the minimum diameter passing through the sieve aperture.

3.3 Computational methods

3.3.1 FactSage software

FactSage^{TM} is a thermochemical software and thermodynamic database developed through decades-long cooperation between Thermfact/CRCT (Montreal, Canada) and GTT-Technologies (Aachen, Germany). Based on the advanced Gibbs Energy minimization routine, FactSage provides the calculation for multiphase, multicomponent materials under a large range of constraints. The FactPS, FTlite, FToxid database in association with the SINTEF database developed by Kai Tang et al.[166] were used for the relevant calculations in this work.

3.3.2 Molecular dynamics simulation

Molecular dynamics (MD) simulation is a computational simulation approach that deals with atoms and/or molecules movements using basic physics laws and the empirical force field to describe the interaction between them. It overcomes the shortcomings of high-temperature experiments and facilitates the study of molten slags at atomistic scale.

In this work, LAMMPS (Large-scale Atomic/Molecular Massively Parallel Simulator)[167] was employed for the MD simulations of slag properties. LAMMPS is an open source code developed by Sandia National Laboratories and has been widely used in MD simulations. It models an ensemble of particles in a liquid, solid, or gaseous state, and atomic, polymeric, biological, metallic, granular, and coarse-grained systems using a variety of force fields and boundary conditions. In the most general sense, LAMMPS integrates Newton's equations of motion for collections of atoms, molecules, or macroscopic particles, from a few up to millions or billions, that interact via short- or long-range forces with a variety of initial and boundary conditions.

Chapter 4

Conclusions and future work

4.1 Conclusions

The work performed in this thesis focused on the experimental and theoretical investigation of the alloying effect on the phosphorus removal from silicon by acid leaching and on the boron removal by slag refining with silicon alloys. Based on a large amount of published literature in this area and the preliminary research at the NTNU research team, a number of Si alloy systems were studied and documented in this thesis, such as the Si-Mg, Si-Ca, Si-Ca-Mg, Si-Ca-Al, and Si-Sn systems. The research conducted in this thesis also serves as a stepping-stone towards more sustainable production of SoG-Si feedstock from the metallurgical route. The conclusions of each research part are summarized below:

Silicon purification by Si-Mg alloying-leaching system:

Mg alloying has a significant effect on the microstructure of MG-Si by forming various impurity-bearing phases embedded inside the Mg_2Si eutectic precipitates. Phosphorus segregation is also enhanced and validated by SIMS elemental mapping. Results of acid leaching experiments indicated that Mg is an efficient impurity getter, especially for P removal. Leaching efficiency is slightly dependent on acid concentration, and 10% HCl was found as the optimum. In a two-times Mg alloying-leaching process, P concentration was reduced from 15.1 ppmw to 0.2 ppmw. Based on Gulliver-Scheil solidification, further thermodynamics analysis revealed that P removal by the alloying-leaching process could be described by a two-parameter analytical model for arbitrary binary Si alloy system where alloy concentration and the first order interaction coefficient between the alloying element to P play a dominant effect. Combined with the obtained leaching results and P removal model, the interaction coefficient ε_{Mg}^{P} was estimated as -10.8 and further confirmed the P affinity of Mg. A process window model was also proposed by establishing the mathematical relationships among initial P concentration, target P concentration after purification, alloying metal concentration, and the alloying-leaching operation times.

Silicon purification by Si-Ca-Mg alloying-leaching system:

The novel Si-Ca-Mg ternary alloying-leaching system exhibits a cleaner leaching process due to the formation of the ternary precipitate $Ca_7Mg_{7.5\pm\delta}Si_{14}$. The leaching of the Si-Ca-Mg alloy avoids the disadvantages of viscous byproducts formation in the Si-Ca system and sparks in the Si-Mg systems. In the comparative study of the Mg, Ca, and Mg–Ca additions on the alloying-leaching process, the Si-Ca system has the highest impurity removal efficiency, fastest leaching kinetics, but lowest Si recovery due to the strongest cracking effect; the Si-Mg alloy system achieved the highest Si recovery but with the lowest leaching kinetics and impurity removal efficiency. The Si-Ca-Mg alloy system introduces a more sustainable feature with good leaching kinetics, high impurity removal, high Si recovery, and no additional solid byproducts formation. The leaching kinetics of Si-Mg and Si-Ca-Mg alloys was found to follow a modified Kröger-Ziegler model based on the cracking-shrinking principle.

In the parametric study of the novel Si-Ca-Mg ternary alloys with varying Ca/Mg mixing

ratio and solidification conditions, $Ca_7Mg_{7.5\pm\delta}Si_{14}$ was found as the main phase in all studied Si-Ca-Mg alloys, while the Mg_2Si phase appears in high-Mg sample and the $CaSi_2$ phase appears in high-Ca sample. Purification efficiency of P and other impurities increase with increasing Ca/Mg mixing ratio but considerably decreases with fast cooling due to the suppressed impurity segregation. HCl is found as the most economical leaching agents among the studied combinations. Finer particle size promotes higher leaching efficiency, but the increment narrows with increasing Ca/Mg ratio. The P removal model for the ternary Si-Ca-Mg system was developed and was found in good agreement with the leaching results.

Silicon purification by Si-Ca-Al (Ti, Y) alloying-leaching system:

P removal degree was found to increase with increasing Ca/Al mixing ratio and increasing total alloying amount (Ca+Al), while the addition of Ti and Y only slightly improves B removal. Alumina crucible was therefore not recommended for Ca-based Si alloy preparation as it will react with Ca to contaminate the alloy and reduce the final P removal degree to a large extent. Through the established P removal model for the Si-Ca-Al refining system, the average interaction coefficients between P and Ca, Al are fitted as $\varepsilon_{Ca}^{P} = -19.2$ and $\varepsilon_{Al}^{P} = -1.8$, which further confirms Ca concentration in the liquid phase is the essential driving force for P segregation. The possible formation of P solid solution was verified by first-principle simulations, and further revealed that $CaAl_2Si_2$ exhibits higher P solubility than $CaSi_2$ phase, which explains the reason of the high P concentration observed in $CaAl_2Si_2$.

Silicon purification by CaO-(La_2O_3)-SiO_2 slag refining of Si-Sn alloy:

Both La_2O_3 addition in slag and Sn addition in silicon improved B removal by slag refining. The L_B values readily increased from 2.93 in binary CaO-SiO_2 slag system to 3.33 and 3.65 with 2 wt% and 10 wt% La_2O_3 addition. Slag treatment also improved the B and P removal in the following acid leaching process. A novel defined oxygen classification method was proposed to distinguish the different behaviour of Ca and La in slags. It was found that La^{3+} plays the role of a typical network modifier with a coordination number of around 6.5. It mainly appeared in the depolymerized region and connected with NBO which requires the co-appearance of Ca for charge compensation. The proposed method is also suitable for the analysis of other slag systems containing multiple network modifiers. A thermodynamic model was derived to describe the alloying effect on impurity distribution in the slag refining. It was found that the slag refining performance affected by multiple factors, respectively, the concentration of alloying element, activity coefficient of Si, the valence of the impurity, and the interaction coefficient of the alloying element to the target impurity, where the positive interaction coefficient and high alloying concentration are preferred for improved impurity removal.

4.2 Future work

There are still several aspects and open questions concerning the silicon purification by acid leaching and slag refining need further investigation.

- Since the small-scale laboratory work of the novel Si-Ca-Mg alloys has shown attractive features, thus, larger-scale verification would be necessary for the potential industrial application. Further investigations are also required on the optimum solidification conditions of the Si-Ca-Mg alloys.
- Combination of CaO-MgO-SiO_2 slag refining and Si-Ca-Mg alloying-leaching would be necessary to be investigated.

- It would be necessary to investigate if the sparks issue of the leaching of Si-Mg binary alloys could be reduced or eliminated under other special leaching methods or conditions.
- Phosphate solid solution can be formed in Ca_2SiO_4 with high solubility. Therefore, it may be worth to investigate the possibility of multi-phase slag refining by introducing the solid Ca_2SiO_4 phase in a proper way to further improve phosphorus removal. Similar principle may also apply for enhanced boron removal by slag refining, which also needs further investigation.
- Despite the disordering nature, the measured structure of quenched glassy slag at room temperature still differs from its molten state. Thus, current experimental investigations of boron behaviour in slags remain with unavoidable uncertainties since boron coordination is also sensitive to temperature. Therefore, more high-temperature experimental measurements and computational simulations would be necessary to further understand the local structural environment of boron in molten slags. It is also worth further understanding how the different boron coordination affects its structural role and thermodynamic properties in molten slag.

Reference

[1] European Comission, Causes of climate change | Climate Action, (2018). https://ec.europa.eu/clima/change/causes_en (accessed January 19, 2021).

[2] S. Mallapay, How China could be carbon neutral by mid-century, Nature. 586 (2020) 482–483. doi:10.7748/eldc.9.1.6.s6.

[3] 2050 long-term strategy | Climate Action, (n.d.). https://ec.europa.eu/clima/policies/strategies/2050_en (accessed January 2, 2021).

[4] N. Ministry of Climate, Norway's National Plan, 2019.

[5] Renewables 2020 Global Status Report, Paris, 2020. https://www.ren21.net/reports/global-status-report/ (accessed November 15, 2020).

[6] N.M. Haegel, H. Atwater, T. Barnes, C. Breyer, A. Burrell, Y.-M. Chiang, S. De Wolf, B. Dimmler, D. Feldman, S. Glunz, J.C. Goldschmidt, D. Hochschild, R. Inzunza, I. Kaizuka, B. Kroposki, S. Kurtz, S. Leu, R. Margolis, K. Matsubara, A. Metz, W.K. Metzger, M. Morjaria, S. Niki, S. Nowak, I.M. Peters, S. Philipps, T. Reindl, A. Richter, D. Rose, K. Sakurai, R. Schlatmann, M. Shikano, W. Sinke, R. Sinton, B.J. Stanbery, M. Topic, W. Tumas, Y. Ueda, J. van de Lagemaat, P. Verlinden, M. Vetter, E. Warren, M. Werner, M. Yamaguchi, A.W. Bett, Terawatt-scale photovoltaics: Transform global energy, Science (80-.). 364 (2019) 836–838. doi:10.1126/science.aaw1845.

[7] S. Pizzini, Towards solar grade silicon: Challenges and benefits for low cost photovoltaics, Sol. Energy Mater. Sol. Cells. 94 (2010) 1528–1533. doi:10.1016/J.SOLMAT.2010.01.016.

[8] J. Safarian, M. Tangstad, Processes for Upgrading Metallurgical Grade Silicon to Solar Grade Silicon, Energy Procedia. 20 (2012) 88–97. doi:10.1016/J.EGYPRO.2012.03.011.

[9] A. Murgau, J. Safarian, Solar silicon production through metallurgical route and REC solar advancements, in: Silicon Chem. Sol. Ind. XIV, Svolvær, Norway, 2018: pp. 183–192.

[10] J. Safarian, T. Gabriella, Silicon purification through magnesium addition and acid leaching, in: 32 Eur. PV Conf. Exhib., 2016: pp. 1011–1015.

[11] S. Espelien, J. Safarian, Effect of acid leaching conditions on impurity removal from silicon doped by magnesium, AIMS Energy. 5 (2017) 636–651. doi:10.3934/energy.2017.4.636.

[12] S. Espelien, G. Tranell, J. Safarian, Effect of magnesium addition on removal of impurities from silicon by hydrometallurgical treatment, in: Energy Technol. 2017, Springer, 2017: pp. 355–366. doi:https://doi.org/10.1007/978-3-319-52192-3_35.

[13] J. Safarian, S. Espelien, Hydrometallurgical purification of Maganesium-doped silicon by different acids, in: 33 Eur. Photovolt. Sol. Energy Conf. Exhib., 2017: pp. 480–482.

[14] R.H. Hopkins, A. Rohatgi, Impurity effects in silicon for high efficiency solar cells, J. Cryst. Growth. 75 (1986) 67–79. doi:10.1016/0022-0248(86)90226-5.

[15] E. Kewes, Silicon Grinding and Fine Particles- Generation and Behavior of Metallurgical-Grade Silicon Fine Particles during Grinding for the Silicones Industry, University of Lyon, 2015.

[16] M. Fang, C. Lu, L. Huang, H. Lai, J. Chen, J. Li, W. Ma, P. Xing, X. Luo, Effect of calcium-based slag treatment on hydrometallurgical purification of metallurgical-grade silicon, Ind. Eng. Chem. Res. 53 (2014) 972–979. doi:10.1021/ie403047m.

[17] N.P. Tucker, Preparation of high purity silicon, J. Iron Steel Ind. 15 (1927) 412–414.

[18] L.P. Hunt, V.D. Dosaj, J.R. McCormick, L.D. Crossman, Production of solar-grade silicon from purified metallurgical silicon, in: 12th IEEE Photovolt. Spec. Conf., 1976: pp. 125–129.
[19] J. Dietl, Hydrometallurgical purification of metallurgical-grade silicon, Sol. Cells. 10 (1983) 145–154. doi:10.1016/0379-6787(83)90015-7.
[20] I.C. Santos, A.P. Goncalves, C.S. Santos, M. Almeida, M.H. Afonso, M.J. Cruz, Purification of Metallurgical Grade Silicon by Acid Leaching, Hydrometallurgy. 23 (1990) 237–246. doi:10.4028/www.scientific.net/AMR.418-420.1590.
[21] T.L. Chu, S.S. Chu, Partial Purification of Metallurgical Silicon by Acid Extraction, J. Electrochem. Soc. 130 (1983) 455. doi:10.1149/1.2119730.
[22] W. Voos, Production of pure silicon, 2972521, 1961.
[23] J.M. Juneja, T.K. Mukherjee, A study of the purification of metallurgical grade silicon, Hydrometallurgy. 16 (1986) 69–75. doi:10.1016/0304-386X(86)90052-6.
[24] J.C. Anglézio, C. Servant, F. Dubrous, Characterization of metallurgical grade silicon, J. Mater. Res. 5 (1990) 1894–1899. doi:10.1557/JMR.1990.1894.
[25] J.C. Anglezio, C. Servant, I. Ansara, Contribution to the experimental and thermodynamic assessment of the Al-Ca-Fe-Si system-I. Al-Ca-Fe, Al-Ca-Si, Al-Fe-Si and Ca-Fe-Si systems, Calphad. 18 (1994) 273–309. doi:10.1016/0364-5916(94)90034-5.
[26] T. Margaria, J. Anglezio, C. Servant, Intermetallic compounds in metallurgical silicon, in: Proc. 6th Int. Ferroalloys Congr., Cape Town, 1992: pp. 209–214. https://www.pyro.co.za/InfaconVI/1209-Margaria.pdf.
[27] F. Margarido, J.P. Martins, M.O. Figueiredo, M.H. Bastos, Kinetics of acid leaching refining of an industrial Fe-Si alloy, Hydrometallurgy. 34 (1993) 1–11. doi:10.1016/0304-386X(93)90077-Q.
[28] F. Margarido, M.H. Bastos, M.O. Figueiredo, J.P. Martins, The structural effect on the kinetics of acid leaching refining of Fe-Si alloys, Mater. Chem. Phys. 38 (1994) 342–347. doi:10.1016/0254-0584(94)90211-9.
[29] H. Lu, K. Wei, W. Ma, K. Xie, J. Wu, Y. Lei, Y. Dai, Effect of acetic acid on the leaching behavior of impurities in metallurgical grade silicon, Sep. Sci. Technol. 52 (2017) 1257–1264. doi:10.1080/01496395.2017.1282964.
[30] M. Fang, C.H. Lu, L.Q. Huang, H.X. Lai, J. Chen, J.T. Li, W.H. Ma, P.F. Xing, X.T. Luo, Separation of Metal Impurities from Metallurgical Grade Silicon via CaO-SiO2-CaF2 Slag Treatment Followed by Leaching with Hydrochloric Acid, Sep. Sci. Technol. 49 (2014) 2261–2270. doi:10.1080/01496395.2014.919323.
[31] Y. V. Meteleva-Fischer, Y. Yang, R. Boom, B. Kraaijveld, H. Kuntzel, Slag treatment followed by acid leaching as a route to solar-grade silicon, Jom. 64 (2012) 957–967. doi:10.1007/s11837-012-0383-4.
[32] H. Lu, K. Wei, W. Ma, K. Xie, J. Wu, Y. Lei, The Effect of Secondary Refining on the Removal of Phosphorus from Metallurgical-Grade Silicon by Acid Leaching, Metall. Mater. Trans. B Process Metall. Mater. Process. Sci. 48 (2017) 2768–2780. doi:10.1007/s11663-017-1042-5.
[33] B. Guan, Y. Sun, X. Li, J. Wang, S. Chen, S. Schweizer, Y. Wang, R.B. Wehrspohn, Conversion of Bulk Metallurgical Silicon into Photocatalytic Nanoparticles by Copper-Assisted Chemical Etching, ACS Sustain. Chem. Eng. 4 (2016) 6590–6599. doi:10.1021/acssuschemeng.6b01481.
[34] F. Xi, S. Li, W. Ma, Z. Ding, Y. Lei, Z. Chen, K. Wei, K. Xie, J. Wu, Removal of impurities from metallurgical grade silicon with metal assisted chemical leaching, Hydrometallurgy. 178 (2018) 250–255. doi:10.1016/j.hydromet.2018.05.013.

[35] C.E. Norman, E.M. Absi, R.E. Thomas, SOLAR-GRADE SILICON SUBSTRATES BY A POWDER-TO-RIBBON PROCESS., Can. J. Phys. 63 (1984) 859–862. doi:10.1139/p85-139.
[36] X. Ma, J. Zhang, T. Wang, T. Li, Hydrometallurgical purification of metallurgical grade silicon, Rare Met. 28 (2009) 221–225. doi:10.1007/s12598-009-0043-1.
[37] L. Huang, H. Lai, C. Lu, M. Fang, W. Ma, P. Xing, X. Luo, J. Li, Evaporation Behavior of Phosphorus from Metallurgical Grade Silicon via Calcium-Based Slag Treatment and Hydrochloric Acid Leaching, J. Electron. Mater. 45 (2016) 541–552. doi:10.1007/s11664-015-4146-1.
[38] J. Kim, J. No, S. Choi, J. Lee, B. Jang, Effects of a new acid mixture on extraction of the main impurities from metallurgical grade silicon, Hydrometallurgy. 157 (2015) 234–238. doi:10.1016/j.hydromet.2015.08.011.
[39] H. Lai, L. Huang, C. Gan, P. Xing, J. Li, X. Luo, Enhanced acid leaching of metallurgical grade silicon in hydrofluoric acid containing hydrogen peroxide as oxidizing agent, Hydrometallurgy. 164 (2016) 103–110. doi:10.1016/j.hydromet.2016.06.003.
[40] A. Schei, High Purity Silicon Production, in: Int. Semin. Refin. Alloy. Liq. Alum. Ferro-Alloys, Trondheim, Norway, 1985.
[41] T. Sakata, T. Miki, K. Morita, Removal of iron and titanium in poly-crystalline silicon by acid leaching, 2002. doi:10.2320/jinstmet1952.66.5_459.
[42] T. Shimpo, T. Yoshikawa, K. Morita, Thermodynamic study of the effect of calcium on removal of phosphorus from silicon by acid leaching treatment, Metall. Mater. Trans. B. 35 (2004) 277–284. doi:10.1007/s11663-004-0029-1.
[43] F. He, S. Zheng, C. Chen, The effect of calcium oxide addition on the removal of metal impurities from metallurgical-grade silicon by acid leaching, Metall. Mater. Trans. B Process Metall. Mater. Process. Sci. 43 (2012) 1011–1018. doi:10.1007/s11663-012-9681-z.
[44] Y. V. Meteleva-Fischer, Y. Yang, R. Boom, B. Kraaijveld, H. Kuntzel, Microstructure of metallurgical grade silicon during alloying refining with calcium, Intermetallics. 25 (2012) 9–17. doi:10.1016/j.intermet.2012.02.009.
[45] Y. V. Meteleva-Fischer, Y. Yang, R. Boom, B. Kraaijveld, H. Kuntzel, Microstructure of metallurgical grade silicon and its acid leaching behaviour by alloying with calcium, Trans. Institutions Min. Metall. Sect. C Miner. Process. Extr. Metall. 122 (2013) 229–237. doi:10.1179/0371955313Z.00000000068.
[46] M.D. Johnston, M. Barati, Calcium and titanium as impurity getter metals in purification of silicon, Sep. Purif. Technol. 107 (2013) 129–134. doi:10.1016/j.seppur.2013.01.028.
[47] H. Lai, L. Huang, C. Lu, M. Fang, W. Ma, P. Xing, J. Li, X. Luo, Leaching behavior of impurities in Ca-alloyed metallurgical grade silicon, Hydrometallurgy. 156 (2015) 173–181. doi:10.1016/j.hydromet.2015.06.012.
[48] H. Sakiani, S.H. Tabaian, J. Chen, Influence of interactions between alumina crucible and Si-Ca-Fe melt on B and P removal from silicon, Sep. Purif. Technol. 255 (2021) 117743. doi:10.1016/j.seppur.2020.117743.
[49] J.P. Martins, F. Margarido, The cracking shrinking model for solid-fluid reactions, Mater. Chem. Phys. 44 (1996) 156–169. doi:10.1016/0254-0584(95)01670-P.
[50] S. Esfahani, M. Barati, Purification of metallurgical silicon using iron as an impurity getter part I: Growth and separation of Si, Met. Mater. Int. 17 (2011) 823–829. doi:10.1007/s12540-011-1021-3.

[51] S. Esfahani, M. Barati, Purification of metallurgical silicon using iron as impurity getter, part II: Extent of silicon purification, Met. Mater. Int. 17 (2011) 1009–1015. doi:10.1007/s12540-011-6020-x.
[52] L.T. Khajavi, K. Morita, T. Yoshikawa, M. Barati, Removal of Boron from Silicon by Solvent Refining Using Ferrosilicon Alloys, Metall. Mater. Trans. B Process Metall. Mater. Process. Sci. 46 (2014) 615–620. doi:10.1007/s11663-014-0236-3.
[53] L.T. Khajavi, K. Morita, T. Yoshikawa, M. Barati, Thermodynamics of boron distribution in solvent refining of silicon using ferrosilicon alloys, J. Alloys Compd. 619 (2015) 634–638. doi:10.1016/j.jallcom.2014.09.062.
[54] L. Tafaghodi Khajavi, M. Barati, Thermodynamics of Phosphorus in Solvent Refining of Silicon Using Ferrosilicon Alloys, Metall. Mater. Trans. B Process Metall. Mater. Process. Sci. 48 (2017) 268–275. doi:10.1007/s11663-016-0804-9.
[55] L. Zong, B. Zhu, Z. Lu, Y. Tan, Y. Jin, N. Liu, Y. Hu, S. Gu, J. Zhu, Y. Cui, Nanopurification of silicon from 84% to 99.999% purity with a simple and scalable process, Proc. Natl. Acad. Sci. 112 (2015) 13473–13477. doi:10.1073/pnas.1513012112.
[56] H. Sakiani, S.H. Tabaian, J. Chen, J. Li, B. Ban, Investigating boron and phosphorus removal from silicon by Si-Ti and Si-Ti-Fe alloying systems, Sep. Purif. Technol. 250 (2020) 117227. doi:10.1016/j.seppur.2020.117227.
[57] Y. Lei, W. Ma, G. Lv, K. Wei, S. Li, K. Morita, Purification of metallurgical-grade silicon using zirconium as an impurity getter, Sep. Purif. Technol. 173 (2017) 364–371. doi:10.1016/j.seppur.2016.09.051.
[58] Y. Lei, W. Ma, X. Ma, J. Wu, K. Wei, S. Li, K. Morita, Leaching behaviors of impurities in metallurgical-grade silicon with hafnium addition, Hydrometallurgy. 169 (2017) 433–439.
[59] Y. Meteleva-Fischer, Y. Yang, R. Boom, B. Kraaijveld, H. Kuntzel, Alloying Refining of Metallurgical Grade Silicon with Rare Earth Elements, in: EPD Congr. 2013, John Wiley & Sons, Inc., Hoboken, NJ, USA, 2013: pp. 201–209. doi:10.1002/9781118658468.ch23.
[60] K. Tang, O.M. Løvvik, J. Safarian, X. Ma, M. Tangstad, Removal of Phosphorus in Metallurgical Silicon by Rare Earth Elements, Metall. Mater. Trans. E. 1 (2014) 257–262. doi:10.1007/s40553-014-0025-6.
[61] Y. V. Meteleva-Fischer, Y. Yang, R. Boom, B. Kraaijveld, H. Kuntzel, Microstructure of metallurgical grade silicon during alloying refining with calcium, Intermetallics. 25 (2012) 9–17. doi:10.1016/j.intermet.2012.02.009.
[62] S. Espelien, G. Tranell, J. Safarian, Effect of Magnesium Addition on Removal of Impurities from Silicon by Hydrometallurgical Treatment, in: Springer, Cham, 2017: pp. 355–365. doi:10.1007/978-3-319-52192-3_35.
[63] Y. Lei, W. Ma, L. Sun, J. Wu, Y. Dai, K. Morita, Removal of B from Si by Hf addition during Al–Si solvent refining process, Sci. Technol. Adv. Mater. 17 (2016) 12–19. doi:10.1080/14686996.2016.1140303.
[64] S. Anders, J.K. Tuset, H. Tveit, Production of high silicon alloys, Trondheim, Norway, 1998.
[65] L. Huang, H. Lai, C. Lu, M. Fang, W. Ma, P. Xing, J. Li, X. Luo, Enhancement in extraction of boron and phosphorus from metallurgical grade silicon by copper alloying and aqua regia leaching, Hydrometallurgy. 161 (2016) 14–21. doi:10.1016/j.hydromet.2016.01.013.
[66] Z. Jian, L. Tingju, M. Xiaodong, L. Dawei, L. Ning, L. Dehua, Optimization of the acid leaching process by using an ultrasonic field for metallurgical grade silicon, J. Semicond. 30 (2009) 053002. doi:10.1088/1674-4926/30/5/053002.

[67] W. Jander, Reaktionen im festen Zustande bei höheren Temperaturen. Säureplatzwechsel bei einigen Wolframaten und Molybdaten, Zeitschrift Für Anorg. Und Allg. Chemie. 190 (1930) 397–406. doi:10.1002/zaac.19301900139.
[68] J.L. Provis, On the use of the Jander equation in cement hydration modelling, RILEM Tech. Lett. 1 (2016) 62. doi:10.21809/rilemtechlett.2016.13.
[69] A. Ginstling, BI Brounshtein, Concerning the diffusion kinetics of reactions in spherical particles, J. Appl. Chem. USSR. 23 (1950) 1327–1338.
[70] C.F. Dickinson, G.R. Heal, Solid-liquid diffusion controlled rate equations, Thermochim. Acta. 340–341 (1999) 89–103. doi:10.1016/s0040-6031(99)00256-7.
[71] C. Kröger, G. Ziegler, Über die Geschwindigkeiten der zur Glasschmelze führenden Reaktionen. II, Glas. Berichte. 26 (1953) 346–353.
[72] C. Kröger, G. Ziegler, Über die Geschwindigkeiten der zur Glasschmelze führenden Reaktionen. III, Glas. Berichte. 27 (1954) 199–212.
[73] R.E. Carter, Kinetic model for solid-state reactions, J. Chem. Phys. 34 (1961) 2010–2015. doi:10.1063/1.1731812.
[74] M.D. Johnston, M. Barati, Effect of slag basicity and oxygen potential on the distribution of boron and phosphorus between slag and silicon, J. Non. Cryst. Solids. 357 (2011) 970–975. doi:10.1016/j.jnoncrysol.2010.10.033.
[75] E.J. Jung, B.M. Moon, S.H. Seok, D.J. Min, The mechanism of boron removal in the CaO-SiO2-Al2O3 slag system for SoG-Si, Energy. 66 (2014) 35–40. doi:10.1016/j.energy.2013.08.010.
[76] S. Thomas, M. Barati, K. Morita, A Review of Slag Refining of Silicon Alloys, Jom. 73 (2021) 282–292. doi:10.1007/s11837-020-04474-0.
[77] M. Sakamoto, Y. Yanaba, H. Yamamura, K. Morita, Relationship between Structure and Thermodynamic Properties in the CaO–SiO2–BO1.5 Slag System, ISIJ Int. 53 (2013) 1143–1151. doi:10.2355/isijinternational.53.1143.
[78] B.O. Mysen, P. Richet, Silicate Glasses and Melts, Elsevier, 2005.
[79] X. Lu, T. Miki, O. Takeda, H. Zhu, T. Nagasaka, Thermodynamic criteria of the end-of-life silicon wafers refining for closing the recycling loop of photovoltaic panels, Sci. Technol. Adv. Mater. 20 (2019) 813–825. doi:10.1080/14686996.2019.1641429.
[80] J.F. White, D. Sichen, Mass transfer in slag refining of silicon with mechanical stirring: Transient interfacial phenomena, Metall. Mater. Trans. B Process Metall. Mater. Process. Sci. 45 (2014) 96–105. doi:10.1007/s11663-013-0010-y.
[81] T.A. Engh, Principles of Metal Refining, Oxford science publications, 2002.
[82] S. Thomas, L. Huang, M. Barati, A Review of Slag Refining of Crude Silicon, Jom. 73 (2021) 260–281. doi:10.1007/s11837-020-04470-4.
[83] K. Suzuki, N. Sano, Thermodynamics for removal of boron from metallurgical silicon by flux treatment, 10th Eur. Photovolt. Sol. Energy Conf. (1991) 273–275. doi:10.1007/978-94-011-3622-8_68.
[84] L.A.V. Teixeira, Y. Tokuda, T. Yoko, K. Morita, Behavior and State of Boron in CaO–SiO2 Slags during Refining of Solar Grade Silicon, ISIJ Int. 49 (2009) 777–782. doi:10.2355/isijinternational.49.777.
[85] L.K. Jakobsson, M. Tangstad, Distribution of Boron Between Silicon and CaO-MgO-Al2O3-SiO2 Slags, Metall. Mater. Trans. B Process Metall. Mater. Process. Sci. 45 (2014) 1644–1655. doi:10.1007/s11663-014-0088-x.
[86] J. Safarian, Thermochemical Aspects of Boron and Phosphorus Distribution Between Silicon and BaO-SiO2 and CaO-BaO-SiO2 lags, Silicon. 11 (2019) 437–451. doi:10.1007/s12633-018-9919-8.
[87] J. Safarian, G. Tranell, M. Tangstad, Thermodynamic and kinetic behavior of B and Na through the contact of B-doped silicon with Na2O-SiO2 slags, Metall. Mater.

Trans. B Process Metall. Mater. Process. Sci. 44 (2013) 571–583. doi:10.1007/s11663-013-9823-y.
[88] M. Fang, C. Lu, L. Huang, H. Lai, J. Chen, X. Yang, J. Li, W. Ma, P. Xing, X. Luo, Multiple slag operation on boron removal from metallurgical-grade silicon using Na2O-SiO2 slags, Ind. Eng. Chem. Res. 53 (2014) 12054–12062. doi:10.1021/ie404427c.
[89] L.A.V. Teixeira, K. Morita, Removal of Boron from Molten Silicon Using CaO-SiO2 Based Slags, ISIJ Int. 49 (2009) 783–787. doi:10.2355/isijinternational.49.783.
[90] J. Safarian, G. Tranell, M. Tangstad, Boron Removal from Silicon by CaO-Na2O-SiO2 Ternary Slag, Metall. Mater. Trans. E. 2 (2015) 109–118. doi:10.1007/s40553-015-0048-7.
[91] Y. Wang, K. Morita, Evaporation removal of boron in molten silicon using reactive fluxes, Miner. Met. Mater. Ser. (2017) 367–375. doi:10.1007/978-3-319-52192-3_36.
[92] X. Ma, T. Yoshikawa, K. Morita, Removal of boron from silicon-tin solvent by slag treatment, Metall. Mater. Trans. B Process Metall. Mater. Process. Sci. 44 (2013) 528–533. doi:10.1007/s11663-013-9812-1.
[93] M.X. Li, Boron and Phosphorus Removal from Si-Cu Alloy Using CaO-SiO2-Na2O-Al2O3 Slag, 2014. https://tspace.library.utoronto.ca/bitstream/1807/68208/1/Li_Mark_Xiang_201411_PhD_thesis.pdf (accessed September 9, 2018).
[94] T. Weiss, K. Schwerdtfeger, Chemical equilibria between silicon and slag melts, Metall. Mater. Trans. B. 25 (1994) 497–504. doi:10.1007/BF02650071.
[95] H. Fujiwara, R. Otsuka, K. Wada, T. Fukuyama, Silicon purifying method, slag for purifying silicon and purified silicon, 2005. doi:10.1107/S1600536811050525/zj2038sup1.cif.
[96] D.W. Luo, N. Liu, Y.P. Lu, G.L. Zhang, T.J. Li, Removal of boron from metallurgical grade silicon by electromagnetic induction slag melting, Trans. Nonferrous Met. Soc. China (English Ed. 21 (2011) 1178–1184. doi:10.1016/S1003-6326(11)60840-6.
[97] Z. Ding, W. Ma, K. Wei, J. Wu, Y. Zhou, K. Xie, Boron removal from metallurgical-grade silicon using lithium containing slag, J. Non. Cryst. Solids. 358 (2012) 2708–2712. doi:10.1016/j.jnoncrysol.2012.06.031.
[98] H. Nishimoto, Y. Kang, T. Yoshikawa, K. Morita, The rate of boron removal from molten silicon by CaO-SiO2 slag and Cl2 treatment, High Temp. Mater. Process. 31 (2012) 471–477. doi:10.1515/htmp-2012-0083.
[99] K.X. Wei, H.F. Lu, W.H. Ma, Y.L. Li, Z. Ding, J.J. Wu, Y.N. Dai, Boron removal from metallurgical-grade silicon by CaO–SiO2 slag refining, Rare Met. 34 (2015) 522–526. doi:10.1007/s12598-015-0496-3.
[100] L.K. Jakobsson, M. Tangstad, Thermodynamic Activities and Distributions of Calcium and Magnesium Between Silicon and CaO-MgO-SiO2 Slags at 1873 K (1600 °C), Metall. Mater. Trans. B Process Metall. Mater. Process. Sci. 46 (2015) 595–605. doi:10.1007/s11663-014-0268-8.
[101] J.F. White, C. Allertz, S. Du, The thermodynamics of boron extraction from liquid silicon using SiO2 -CaO-MgO slag treatment, Int. J. Mater. Res. 104 (2013) 229–234. doi:10.3139/146.110867.
[102] J.F. White, C. Allertz, D. Sichen, Boron partitioning between SiO2 -CaO-MgO slags and liquid silicon at controlled nitrogen potential, Int. J. Mater. Res. 104 (2013) 650–656. doi:10.3139/146.110913.
[103] H. Cheng, S. Zheng, C. Chen, The behavior of Ca and its compounds in Si during the slag refining with CaO-SiO2-CaF2 system under air atmosphere, Sep. Purif. Technol. 201 (2018) 60–70. doi:10.1016/j.seppur.2018.02.052.

[104] H. Cheng, S. Zheng, C. Chen, Evaluation of Factors on Removing Boron from Silicon by Slag Refining Under Atmospheric Conditions, JOM. 71 (2019) 2120–2127. doi:10.1007/s11837-019-03450-7.
[105] Y. Li, J. Wu, W. Ma, Kinetics of Boron Removal from Metallurgical Grade Silicon using a Slag Refining Technique Based on CaO-SiO2 Binary System, Sep. Sci. Technol. 49 (2014) 1946–1952. doi:10.1080/01496395.2014.904877.
[106] F. Wang, J. Wu, W. Ma, M. Xu, Y. Lei, B. Yang, Removal of impurities from metallurgical grade silicon by addition of ZnO to calcium silicate slag, Sep. Purif. Technol. 170 (2016) 248–255. doi:10.1016/j.seppur.2016.06.060.
[107] H. Lai, L. Huang, C. Lu, M. Fang, W. Ma, P. Xing, J. Li, X. Luo, Reaction Mechanism and Kinetics of Boron Removal from Metallurgical-Grade Silicon Based on Li2O-SiO2 Slags, JOM. 68 (2016) 2371–2380. doi:10.1007/s11837-015-1656-5.
[108] J. Wu, W. Ma, B. Jia, B. Yang, D. Liu, Y. Dai, Boron removal from metallurgical grade silicon using a CaO-Li2O-SiO 2 molten slag refining technique, J. Non. Cryst. Solids. 358 (2012) 3079–3083. doi:10.1016/j.jnoncrysol.2012.09.004.
[109] P. Li, K. Wang, M. Fang, L. Zhang, D. Jiang, J. Li, Y. Tan, Boron removal from silicon by slag refining using Na $_2$ O-SiO $_2$ in industrial applications, Sep. Sci. Technol. 53 (2018) 2144–2149. doi:10.1080/01496395.2017.1405035.
[110] L. Zhang, Y. Tan, F.M. Xu, J.Y. Li, H.Y. Wang, Z. Gu, Removal of Boron from Molten Silicon using Na2O-CaO-SiO2 Slags, Sep. Sci. Technol. 48 (2013) 1140–1144. doi:10.1080/01496395.2012.714438.
[111] J. Wu, F. Wang, W. Ma, Y. Lei, B. Yang, Thermodynamics and Kinetics of Boron Removal from Metallurgical Grade Silicon by Addition of High Basic Potassium Carbonate to Calcium Silicate Slag, Metall. Mater. Trans. B Process Metall. Mater. Process. Sci. 47 (2016) 1796–1803. doi:10.1007/s11663-016-0615-z.
[112] L.K. Jakobsson, M. Tangstad, Thermodynamics of Boron Removal from Silicon Using CaO-MgO-Al2O3-SiO2 Slags, Metall. Mater. Trans. B Process Metall. Mater. Process. Sci. 49 (2018) 1699–1708. doi:10.1007/s11663-018-1250-7.
[113] J. Li, L. Zhang, Y. Tan, D. Jiang, D. Wang, Y. Li, Research of boron removal from polysilicon using CaO-Al2O 3-SiO2-CaF2 slags, Vacuum. 103 (2014) 33–37. doi:10.1016/j.vacuum.2013.12.002.
[114] M.D. Johnston, M. Barati, Distribution of impurity elements in slagsilicon equilibria for oxidative refining of metallurgical silicon for solar cell applications, Sol. Energy Mater. Sol. Cells. 94 (2010) 2085–2090. doi:10.1016/j.solmat.2010.06.025.
[115] C. Yin, B. Hu, X. Huang, Boron removal from molten silicon using sodium-based slags, J. Semicond. 32 (2011) 092003. doi:10.1088/1674-4926/32/9/092003.
[116] Y. Wang, X. Ma, K. Morita, Evaporation removal of boron from metallurgical-grade silicon using CaO-CaCl 2 -SiO 2 slag, Metall. Mater. Trans. B Process Metall. Mater. Process. Sci. 45 (2014) 334–337. doi:10.1007/s11663-014-0031-1.
[117] J. Li, P. Cao, P. Ni, Y. Li, Y. Tan, Enhanced boron removal from metallurgical grade silicon by the slag refining method with the addition of tin, Sep. Sci. Technol. 51 (2016) 1–6. doi:10.1080/01496395.2016.1165702.
[118] R. Al-khazraji, Y. Li, L. Zhang, Boron separation from Si–Sn alloy by slag treatment, Int. J. Miner. Metall. Mater. 25 (2018) 1439–1446. doi:10.1007/s12613-018-1698-0.
[119] M. Li, T. Utigard, M. Barati, Removal of boron and phosphorus from silicon using CaO-SiO 2-Na2O-Al2O3 flux, in: Metall. Mater. Trans. B Process Metall. Mater. Process. Sci., Springer, 2014: pp. 221–228. doi:10.1007/s11663-013-0011-x.
[120] L. Huang, H. Lai, C. Gan, H. Xiong, P. Xing, X. Luo, Separation of boron and phosphorus from Cu-alloyed metallurgical grade silicon by CaO–SiO2–CaCl2 slag

treatment, Sep. Purif. Technol. 170 (2016) 408–416. doi:10.1016/j.seppur.2016.07.004.
[121] L.K. Jakobsson, Distribution of boron between silicon and CaO2, MgO-SiO2, CaO-MgO-SiO2 and CaO-Al2O3-SiO2 slags at 1600 ° C, Norwegian University of Science and Technology, 2013.
[122] E. Krystad, L.K. Jakobsson, K. Tang, G. Tranell, Thermodynamic Behavior and Mass Transfer Kinetics of Boron Between Ferrosilicon and CaO-SiO2 Slag, Metall. Mater. Trans. B Process Metall. Mater. Process. Sci. 48 (2017) 2574–2582. doi:10.1007/s11663-017-1015-8.
[123] A. Hosseinpour, L. Tafaghodi Khajavi, Thermodynamics of boron removal in slag refining of Fe-Si alloy, J. Alloys Compd. 768 (2018) 545–552. doi:10.1016/j.jallcom.2018.07.246.
[124] A. Hosseinpour, L. Tafaghodi Khajavi, Phosphorus Removal from Si-Fe Alloy Using SiO2-Al2O3-CaO Slag, Metall. Mater. Trans. B Process Metall. Mater. Process. Sci. 50 (2019) 1773–1781. doi:10.1007/s11663-019-01586-0.
[125] I. Obinata, N. Komatsu, A study on purification of metallurgical grade silicon by Si-Al alloy, Sci. Rep. RITU 9. 9 (1957) 118.
[126] T. Yoshikawa, K. Morita, Removal of phosphorus by the solidification refining with Si-Al melts, Sci. Technol. Adv. Mater. 4 (2003) 531–537. doi:10.1016/j.stam.2003.12.007.
[127] Y. Li, L. Zhang, Application of Si-Based Solvents to the Purification of Metallurgical Grade-Silicon, Sep. Purif. Rev. (2019) 1–24. doi:10.1080/15422119.2019.1623253.
[128] J.L. Gumaste, B.C. Mohanty, R.K. Galgali, U. Syamaprasad, B.B. Nayak, S.K. Singh, P.K. Jena, Solvent refining of metallurgical grade silicon, Sol. Energy Mater. 16 (1987) 289–296. doi:10.1016/0165-1633(87)90077-3.
[129] T. Yoshikawa, K. Morita, Removal of phosphorus by the solidification refining with Si-Al melts, Sci. Technol. Adv. Mater. 4 (2003) 531–537. doi:10.1016/j.stam.2003.12.007.
[130] T. Yoshikawa, K. Morita, Removal of B from Si by solidification refining with Si-Al melts, Metall. Mater. Trans. B Process Metall. Mater. Process. Sci. 36 (2005) 731–736. doi:10.1007/s11663-005-0076-2.
[131] T. Yoshikawa, K. Morita, Refining of Si by the solidification of Si-Al melt with electromagnetic force, ISIJ Int. 45 (2005) 967–971. doi:10.2355/isijinternational.45.967.
[132] T. Yoshikawa, K. Arimura, K. Morita, Boron removal by Titanium addition in solidification refining of silicon with Si-Al melt, Metall. Mater. Trans. B Process Metall. Mater. Process. Sci. 36 (2005) 837–842. doi:10.1007/s11663-005-0085-1.
[133] X. Gu, X. Yu, D. Yang, Low-cost solar grade silicon purification process with Al-Si system using a powder metallurgy technique, Sep. Purif. Technol. 77 (2011) 33–39. doi:10.1016/j.seppur.2010.11.016.
[134] L. Hu, Z. Wang, X. Gong, Z. Guo, H. Zhang, Impurities removal from metallurgical-grade silicon by combined Sn-Si and Al-Si refining processes, Metall. Mater. Trans. B Process Metall. Mater. Process. Sci. 44 (2013) 828–836. doi:10.1007/s11663-013-9850-8.
[135] B. Ban, X. Bai, J. Li, Y. Li, J. Chen, S. Dai, The Mechanism of P Removal by Solvent Refining in Al-Si-P System, Metall. Mater. Trans. B Process Metall. Mater. Process. Sci. 46 (2015) 2430–2437. doi:10.1007/s11663-015-0449-0.
[136] Y. Li, B. Ban, J. Li, T. Zhang, X. Bai, J. Chen, S. Dai, Effect of Cooling Rate on Phosphorus Removal During Al-Si Solvent Refining, Metall. Mater. Trans. B Process Metall. Mater. Process. Sci. 46 (2015) 542–544. doi:10.1007/s11663-015-0291-4.

[137] B. Ban, X. Bai, J. Li, J. Chen, S. Dai, Effect of kinetics on P removal by Al-Si solvent refining at low solidification temperature, J. Alloys Compd. 685 (2016) 604–609. doi:10.1016/j.jallcom.2016.05.312.
[138] B. Ban, J. Li, X. Bai, Q. He, J. Chen, S. Dai, Mechanism of B removal by solvent refining of silicon in Al-Si melt with Ti addition, J. Alloys Compd. 672 (2016) 489–496. doi:10.1016/j.jallcom.2016.02.198.
[139] L. Sun, Z. Wang, H. Chen, D. Wang, G. Qian, Removal of Phosphorus in Silicon by the Formation of CaAl2Si2 Phase at the Solidification Interface, Metall. Mater. Trans. B Process Metall. Mater. Process. Sci. 48 (2017) 420–428. doi:10.1007/s11663-016-0848-x.
[140] Y. Li, Y. Tan, J. Li, K. Morita, Si purity control and separation from Si–Al alloy melt with Zn addition, J. Alloys Compd. 611 (2014) 267–272. doi:10.1016/J.JALLCOM.2014.05.138.
[141] Y. Lei, W. Ma, L. Sun, Y. Dai, K. Morita, B Removal by Zr Addition in Electromagnetic Solidification Refinement of Si with Si-Al Melt, Metall. Mater. Trans. B Process Metall. Mater. Process. Sci. 47 (2016) 27–31. doi:10.1007/s11663-015-0506-8.
[142] Y. Lei, L. Sun, W. Ma, K. Wei, K. Morita, Enhancing B removal from Si with small amounts of Ti in electromagnetic solidification refining with Al-Si alloy, J. Alloys Compd. 666 (2016) 406–411. doi:10.1016/j.jallcom.2016.01.127.
[143] J. Li, Y. Liu, Y. Tan, Y. Li, L. Zhang, S. Wu, P. Jia, Effect of tin addition on primary silicon recovery in Si–Al melt during solidification refining of silicon, J. Cryst. Growth. 371 (2013) 1–6. doi:10.1016/J.JCRYSGRO.2012.12.098.
[144] Y. Li, Y. Tan, J. Li, Q. Xu, Y. Liu, Effect of Sn content on microstructure and boron distribution in Si-Al alloy, J. Alloys Compd. 583 (2014) 85–90. doi:10.1016/j.jallcom.2013.08.145.
[145] T. Tang, H. Lai, Z. Sheng, C. Gan, P. Xing, X. Luo, Effect of tin addition on the distribution of phosphorus and metallic impurities in Si–Al alloys, J. Cryst. Growth. 453 (2016) 13–19. doi:10.1016/j.jcrysgro.2016.07.036.
[146] L. Hu, Z. Wang, X. Gong, Z. Guo, H. Zhang, Purification of metallurgical-grade silicon by Sn-Si refining system with calcium addition, Sep. Purif. Technol. 118 (2013) 699–703. doi:10.1016/j.seppur.2013.08.013.
[147] X. Ma, Y. Lei, T. Yoshikawa, B. Zhao, K. Morita, Effect of solidification conditions on the silicon growth and refining using Si–Sn melt, J. Cryst. Growth. 430 (2015) 98–102. doi:10.1016/J.JCRYSGRO.2015.08.001.
[148] Y. Ren, H. Wang, K. Morita, Growth control and enrichment of Si crystals from Si-Sn melt by directional solidification, Vacuum. 158 (2018) 86–92. doi:10.1016/j.vacuum.2018.09.044.
[149] Y. Ren, H. Wang, K. Morita, Effect of Zr addition on B-removal behaviour during solidification purification of Si with Si–Sn solvent, Vacuum. 167 (2019) 319–328. doi:10.1016/j.vacuum.2019.06.029.
[150] J. Li, B. Ban, Y. Li, X. Bai, T. Zhang, J. Chen, Removal of Impurities from Metallurgical Grade Silicon During Ga-Si Solvent Refining, Silicon. 9 (2017) 77–83. doi:10.1007/s12633-014-9269-0.
[151] K. Visnovec, C. Variawa, T. Utigard, A. Mitrašinović, Elimination of impurities from the surface of silicon using hydrochloric and nitric acid, Mater. Sci. Semicond. Process. 16 (2013) 106–110. doi:10.1016/J.MSSP.2012.06.009.
[152] M. Fang, C.H. Lu, H.X. Lai, L.Q. Huang, J. Chen, W.H. Ma, Z.L. Sheng, J.N. Shen, J.T. Li, X.T. Luo, Effect of solidification rate on representative impurities distribution

in Si-Cu alloy, Mater. Sci. Technol. (United Kingdom). 29 (2013) 861–867. doi:10.1179/1743284713Y.0000000212.
[153] L. Huang, H. Lai, C. Lu, C. Gan, M. Fang, P. Xing, J. Li, X. Luo, Segregation behavior of iron in metallurgical grade silicon during Si-Cu solvent refining, Vacuum. 129 (2016) 38–44. doi:10.1016/J.VACUUM.2016.04.013.
[154] L. Huang, A. Danaei, S. Thomas, P. Xing, J. Li, X. Luo, M. Barati, Solvent extraction of phosphorus from Si-Cu refining system with calcium addition, Sep. Purif. Technol. 204 (2018) 205–212. doi:10.1016/J.SEPPUR.2018.04.087.
[155] L. Huang, J. Chen, A. Danaei, S. Thomas, L. Huang, X. Luo, M. Barati, Effect of Ti addition to Cu-Si alloy on the boron distribution in various phases, J. Alloys Compd. 734 (2018) 235–242. doi:10.1016/j.jallcom.2017.10.279.
[156] Y. Ren, K. Morita, Low-Temperature Process for the Fabrication of Low-Boron Content Bulk Si from Si–Cu Solution with Zr Addition, ACS Sustain. Chem. Eng. (2020). doi:10.1021/acssuschemeng.0c01785.
[157] Y. Ren, S. Ueda, K. Morita, Formation Mechanism of ZrB2 in a Si-Cu Melt and Its Potential Application for Refining Si and Recycling Si Waste, ACS Sustain. Chem. Eng. 7 (2019) 20107–20113. doi:10.1021/acssuschemeng.9b05986.
[158] H. Morito, T. Karahashi, M. Uchikoshi, M. Isshiki, H. Yamane, Low-Temperature Purification of Silicon by Dissolution and Solution Growth in Sodium Solvent, Silicon. 4 (2012) 121–125. doi:10.1007/s12633-011-9105-8.
[159] H. Morito, M. Uchikoshi, H. Yamane, Boron removal by dissolution and recrystallization of silicon in a sodium-silicon solution, Sep. Purif. Technol. 118 (2013) 723–726. doi:10.1016/j.seppur.2013.08.022.
[160] J. Safarian, G. Tranell, M. Tangstad, Upgrading metallurgical grade silicon to solar grade silicon, Energy Procedia. 20 (2012) 88–97. doi:10.1016/j.egypro.2012.03.011.
[161] J. Safarian, M. Tangstad, Vacuum refining of molten silicon, Metall. Mater. Trans. B Process Metall. Mater. Process. Sci. 43 (2012) 1427–1445. doi:10.1007/s11663-012-9728-1.
[162] C. Gan, S. Wen, Y. Liu, W. Wen, P. Dou, J. Su, X. Luo, Preparation of Si-SiOx nanoparticles from volatile residue produced by refining of silicon, Waste Manag. 84 (2019) 373–382. doi:10.1016/j.wasman.2018.11.032.
[163] H. Sasaki, Y. Kobashi, T. Nagai, M. Maeda, Application of electron beam melting to the removal of phosphorus from silicon: Toward production of solar-grade silicon by metallurgical processes, Adv. Mater. Sci. Eng. 2013 (2013). doi:10.1155/2013/857196.
[164] N. Yuge, M. Abe, K. Hanazawa, H. Baba, N. Nakamura, Y. Kato, Y. Sakaguchi, S. Hiwasa, F. Aratani, Purification of metallurgical-grade silicon up to solar grade, Prog. Photovoltaics Res. Appl. 9 (2001) 203–209. doi:10.1002/pip.372.
[165] SEM-EDX-Analyse Bauteile & Werkstoffe | RJL Micro & Analytic, (n.d.). https://www.rjl-microanalytic.de/en/analysenservice-mit-iso-17025-akkreditierung/sem-edx-analytik-von-strukturen-und-werkstoffen/ (accessed January 22, 2021).
[166] K. Tang, E.J. Øvrelid, G. Tranell, M. Tangstad, A Thermochemical Database for the Solar Cell Silicon Materials, Mater. Trans. 50 (2009) 1978–1984. doi:10.2320/matertrans.M2009110.
[167] S. Plimpton, Fast Parallel Algorithms for Short-Range Molecular Dynamics, J. Comput. Phys. 117 (1995) 1–19. doi:10.1006/jcph.1995.1039.

Chapter 5
Published and submitted publications

Paper 1

EFFECTS OF MAGNESIUM-DOPING ON SILICON LEACHING FOR SOLAR GRADE FEEDSTOCK PRODUCTION

Mengyi Zhu[1], Adrian Murgau[2], Jafar Safarian[1]
[1] Department of Materials Science and Engineering, Norwegian University of Science and Technology (NTNU), Trondheim, Norway
[2] R&D Director, REC Solar Norway, Kristiansand, Norway

ABSTRACT: The rapid growth of photovoltaic industry has led to large demands of solar grade silicon (SoG-Si) feedstock production in recent years. Acid leaching as a low-cost and important part of the only available commercial process by the metallurgical route of SoG-Si feedstock production, has accordingly received significant attention. In this work, pure Mg_2Si is doped into a commercial metallurgical grade silicon (MG-Si) in molten state, solidified under controlled conditions, and leached by 10% HCl. The effect of Mg doping on the removal of impurities in leaching is studied at different conditions, at 60 ˚C and 80˚C for different leaching durations from 5 minutes up to 1 hour. The results indicate high temperature and long leaching time are in favor of impurities removal. The eutectic Mg_2Si phase which contains the silicides of the impurities in association such as Al, Fe, Ca, Ti on the grain boundaries is leached. This causes the purification of silicon and it is shown that P and metallic impurities can be removed in large extents.

Keywords: Silicon, Magnesium, Phosphorus, Impurity, Acid leaching

1 INTRODUCTION

The development of cheaper processes for high purity solar grade silicon feedstock has become worldwide imperative demands and attrached significant attentions from both photovaltic industry and academia in recent years. Among the proposed alternative metallurgical purification methods, acid leaching is usually considered as one of the most promising candidates for the metallurgical grade silicon (MG-Si) refining due to its low-temperature operation feature and the ability to remove large amounts of impurities.

The main principle of acid leaching is based on the low segregation coeffiicent of the impurities in silicon, representative values of some selected impurites are listed below as Table I. It can be clearly seen that the segregation coefficient of most of metallic impurities such as Fe, Al, Ti etc. are between 10^{-3} and 10^{-6}. As a result, these impurities tend to segregate together as precipitate phase which can be leached away treated by acids while silicon is fairly noble. However it is also worth noting that the segregation coefficients of B and P are much higher compared to other impurites. This unqiue feature makes them, in principle, difficult to remove by MG-Si acid leaching process.

Table I: Representative segregation coefficient values of impurities at Si melting point[1]

Impurity	Segregation coefficient	Impurity	Segregation coefficient
B	8.0×10^{-1}	Ti	2.0×10^{-6}
P	3.5×10^{-1}	Zn	1.0×10^{-5}
Fe	6.4×10^{-6}	Mn	4.5×10^{-3}
Al	2.8×10^{-3}	Cu	4.0×10^{-4}

The research about acid leaching for silicon refining has been actively studied over decades. The first acid leaching of pulverized MG-Si was pointed out nearly hundred years ago in the pioneering work of Tucker in 1927[2]. After many years, Voos[3] obtained a patent in 1961 about a leaching process for pulverized MG-Si with different leaching agent. In addition Hunt et al.[4] later removed successfully more than 90% impurities from MG-Si by aqua regia leaching. In the 1980s, Dietl[5] systematically studied the optimal leaching purification conditions using a mixture of HF and HCl. Furthermore, Elkem A/S demonstrated higher leaching efficiency can be achieved after an alloying process of MG-Si with the association of precipitated $CaSi_2$ phase. Based on this method, leaching of alloyed MG-Si received increasing attention in the past few decades. Many additive refiner metals (or impurity getters) have been reported such as Ca[6]-[9], Fe[10],[11], Zr[12], Hf[13] and so on. As the most studied alloying elements, Ca is considered to have a strong affinity to impurities like P and some metallic impurities, it also have high reactivity with leaching acids. For example, according to the research of Shimpo et al [7], as much as 80% P can be removed by alloying 5.17% Ca. Based on the recent research conducted at NTNU in Norway[14]-[17], Mg also shows promising potential as the impurity getter for MG-Si doping due to the similar alkali earth element properties and high leaching efficiency.

In this work, the leaching of Mg doped MG-Si and original MG-Si were compared. Effects of leaching time and temperature on different impurities removal of Mg-doped Si was also studied in order to gain deeper understanding about the leaching mechanisms.

2 EXPERIMENTAL

2.1 Raw material and MG-Si doping

A commercial MG-Si was used in present study. The raw MG-Si was mixed in graphite crucible with certain amount of pure Mg_2Si was heated up to 1500 °C to form a Si-4.5wt% Mg melt in an induction furnace. After the Si-Mg alloy was fully melted and reach equilibrium, the melt was then slowly cooled down with an average cooling rate of 10 °C/min inside the induction furnace. The Si-Mg alloy obtained was then crushed and sieved to different particle sizes, and particles with 0.2-2.15 mm were further used. The same particle size for MG-Si was also used.

The chemical composition of raw MG-Si and obtained Mg-doped Si alloy were analyzed by high-resolution

Inductively Coupled Plasma-Mass Spectroscopy (ICP-MS) before acid leaching, results are shown as Table II.

Table II: Composition of MG-Si and Mg doped MG-Si by ICP-MS analysis.

Impurity	MG-Si	Alloyed MG-Si
B	46.2	42.4
P	15.8	15.6
Mg	9.6	44879.4
Ca	266.7	282.0
Ti	299.8	204.0
Fe	3167.5	2281.0
Al	2548.0	1744.0
Mn	70.4	53.9
Zr	10.7	7.0

2.2 Leaching and impurities analysis

The Mg doped MG-Si and raw MG-Si were leached by 10% HCl at the temperature of 60°C and 80°C within 1 hour. Totally 4 samples were made to understand the effects of different process parameters. All the leaching trials were performed in an ultrasonic bath. The samples after leaching were washed by distilled water and ethanol and then dried at 80°C.

Samples after leaching were also analyzed by ICP-MS for the impurities determination. Ultra-fine particles were separated and removed by a 50 microns sieve after drying in order to reduce the interference of metallic impurities.

3 RESULTS AND DISCUSSION

3.1 Effects of Mg doping on Si microstructure

The leaching effect of with and without Mg doping on Si microstructure was studied by SEM shown as Figure 1.

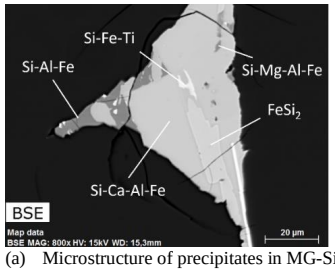

(a) Microstructure of precipitates in MG-Si

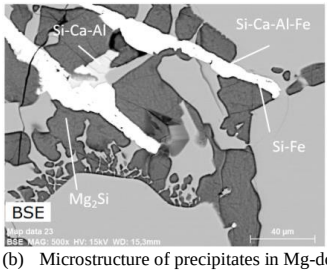

(b) Microstructure of precipitates in Mg-doped Si

Figure 1: SEM images of (a) MG-Si and (b) Mg-doped MG-Si.

It can be seen that the observed main phases in MG-Si are $FeSi_2$, Si-Fe-Ti, Si-Ca-Al-Fe, Si-Mg-Al-Fe, respectively. All these phases are Fe-bearing silicides and known as poor leachability. However, with the addition of Mg into MG-Si, it was found that the eutectic Mg_2Si becomes the dominant precipitated phase. The Fe-bearing silicides were embedded inside the Mg_2Si phase. It is known that Mg_2Si has a high reactivity with mineral acids. Thus, when the dominant Mg_2Si phase removed by acids during leaching, the poorly leachable Fe-bearing phases could be carried away at the same time. This feature offers an opportunity to enhance the leaching efficiency.

3.2 Effects of leaching time

The effects of leaching time on different impurities in Mg alloyed Si at 80 ˚C is shown as Figure 2. It can be seen that with the increasing of leaching time, the concentration of nearly all the impurities are decreased except B. More than a half of metallic impurities like Fe, Al, Mn, Ti were effectively removed after 1 hour leaching. It is also worth noting that the P removal is beyond 90%, which is problematical to be removed by conventional acid leaching of raw MG-Si. This result may suggest the formation of some complex magnesium phosphide compounds in the precipitate phase. The reason of no B removal during acid leaching might due to the high segregation coefficient of B in Si, which makes majority of B stay inside the Si grain and locked by the dislocations.

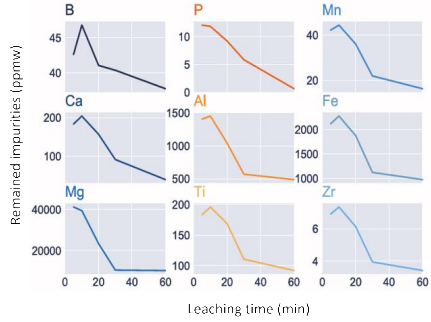

Figure 2: Time dependence of impurity concentration of Mg-doped Si during 10% HCl acid leaching at 80℃ in ultrasonic bath.

In addition, it can be observed that the removal of impurities can be divided into two stages; a fast removal stage in the first 30min, which indicates a chemical reaction control mechanism followed by a slow removal stage after 30 min, which is believed to be a diffusion controlled stage.

Detailed comparison of leaching performance of MG-Si and Mg-doped Si can be seen from Figure 3 in the following section.

3.2 Impurities after leaching

The remained impurity concentration of 4 different leaching conditions are shown as Figure 3, detailed data can be seen from Appendix Table I. It is clear that after Mg-doping, the remained concentrations of most impurities distinctly reduced. It is also worth noting that a

great number of Mg impurity remained for Mg doped MG-Si leaching. This might be the reason that some amount of Mg_2Si precipitates close to Si grain boundaries were not completely removed within 1 hour leaching. In addition, it can be seen that for the conventional problematic P removal in MG-Si leaching, Mg-doping exhibits a promising potential to significantly remove P impurity amount as high as more than 90%.

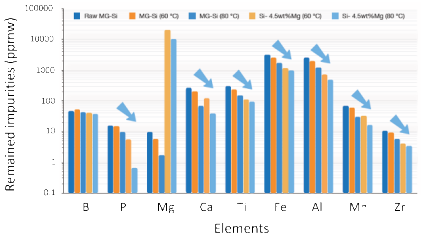

Figure 3: Remained impurities concentration after 1h leaching. The five bars from left to right respectively denotes the concentration of raw MG-Si, MG-Si after leaching at 60℃, MG-Si after leaching at 80℃, Mg-doped Si after leaching at 60℃, and Mg-doped Si after leaching at 80℃. The X-axis presents different impurity elements, while the Y-axis presents impurity level from 0.1 to 100000 ppmw.

The impurity removal degree is also calculated in order to compare the purification ability under different conditions. The results can be seen as Figure 4, detailed data seen from Appendix Table I. The calculation of specific impurity *i* based on ICP-MS analysis shown as:

$$Re\ \ v\ al\ deg\ e\ \ \mathbf{m}\frac{c_i - c_f}{c_i} \times 100\%\ \boldsymbol{e}$$

where c_i and c_f denotes the initial impurity concentration and final concentration.

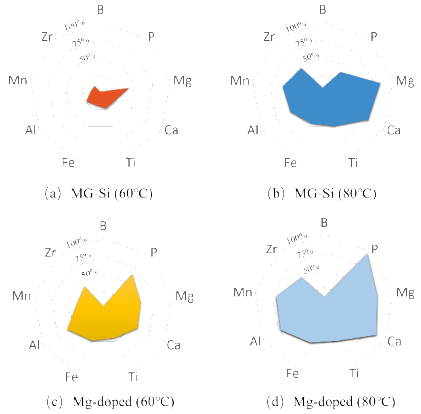

Figure 4: Remained impurities concentration of MG-Si and Mg-doped Si samples after 1h acid leaching by 10% HCl at different temperature in ultrasonic bath.

Owing to the Mg addition, more impurities are removed with the assistance of highly acid reactive Mg_2Si during leaching as well as the P removal. Additionally, higher temperature is in favor of impurity removal by enhancing the reaction kinetics. Therefore, a simple leaching efficiency order can be obtained as MG-Si (60℃)< MG-Si (80℃) <Mg-doped Si (60℃) <Mg-doped Si (80℃) from Figure 4, where the leaching of Mg-doped Si at 80℃ shows the highest impurities removal degree in present work.

4 CONCLUSIONS

A commercial MG-Si was doped with 4.5 wt% Mg and leached by 10% HCl with different leaching temperature. The leaching behaviour of different impurities were studied and the following conclusions have been obtained:

(1) Longer time and higher temperature benefits the impurities removal. A faster chemical control impurity removal stage and a slow diffusion control impurity removal stage were observed.

(2) Mg doping of silicon effectively improved the leaching efficiency for metallic impurities as well as the P removal due to the precipitated acid reactive Mg_2Si eutectic phase.

5 ACKNOWLEDGEMENT

This work was performed at NTNU within the Research Centre for Sustainable Solar Cell Technology (FME SuSolTech, project number 257639), co-sponsored by the Norwegian Research Council and industry partners.

6 REFERENCE

[1] K. Morita, and M. Takahiro. “Thermodynamics of solar-grade-silicon refining. ” *Intermetallics*, vol. 11, pp. 1111-1117, 2003.

[2] N. P. Tucker, “Preparation of high purity silicon” *J. Iron Steel Ind.*, vol. 15, pp. 412–414, 1927.

[3] W. Voos, “Production of pure silicon” *U.S. Patent*, 2972521, 1961.

[4] L. P. Hunt, V. D. Dosaj, J. R. McCormick, and L. D. Crossman, “Production of solar-grade silicon from purified metallurgical silicon” in *12th IEEE Photovoltaic Specialists Conference*, 1976, pp. 125–129.

[5] J. Dietl, “Hydrometallurgical purification of metallurgical-grade silicon” *Sol. Cells*, vol. 10, no. 2, pp. 145–154, 1983.

[6] Y. V Meteleva-fischer, Y. Yang, R. Boom, B. Kraaijveld, and H. Kuntzel, “Intermetallics Microstructure of metallurgical grade silicon during alloying re fi ning with calcium” *Meta*, vol. 25, pp. 9–17, 2012.

[7] T. Shimpo, T. Yoshikawa, and K. Morita, “Thermodynamic study of the effect of calcium on removal of phosphorus from silicon by acid leaching treatment” *Metall. Mater. Trans. B*, vol. 35, no. April, pp. 277–284, 2004.

[8] M. D. Johnston and M. Barati, “Calcium and titanium as impurity getter metals in purification of silicon” *Sep. Purif. Technol.*, vol. 107, pp. 129–134, 2013.

[9] H. Lai *et al.*, “Leaching behavior of impurities in Ca-alloyed metallurgical grade silicon” *Hydrometallurgy*, vol. 156, pp. 173–181, 2015.

[10] F. Margarido, J. P. Martins, M. O. Figueiredo, and M. H. Bastos, “Kinetics of acid leaching refining of an

industrial Fe-Si alloy," *Hydrometallurgy*, vol. 34, no. 1, pp. 1–11, 1993.
[11] F. Margarido, M. H. Bastos, M. O. Figueiredo, and J. P. Martins, "The structural effect on the kinetics of acid leaching refining of Fe-Si alloys" *Mater. Chem. Phys.*, vol. 38, no. 4, pp. 342–347, 1994.
[12] Y. Lei, W. Ma, G. Lv, K. Wei, S. Li, and K. Morita, "Purification of metallurgical-grade silicon using zirconium as an impurity getter" *Sep. Purif. Technol.*, vol. 173, pp. 364–371, 2017.
[13] Y. Lei *et al.*, "Leaching behaviors of impurities in metallurgical-grade silicon with hafnium addition" *Hydrometallurgy*, vol. 169, pp. 433–439, 2017.
[14] J. Safarian and T. Gabriella, "Silicon purification through magnesium addition and acid leaching" in *32 European PV conference and Exhibition*, 2016, no. 7491, pp. 1011–1015.
[15] S. Espelien and J. Safarian, "Effect of acid leaching conditions on impurity removal from silicon doped by magnesium" *AIMS Energy*, vol. 5, no. 4, pp. 636–651, 2017.
[16] J. Safarian and S. Espelien, "Hydrometallurgical purification of Maganesium-doped silicon by difference acids" in *33 European Photovoltaic Solar Energy Conference and Exhibition*, 2017, pp. 480–482.
[17] S. Espelien, G. Tranell, and J. Safarian, "Effect of magnesium addition on removal of impurities from silicon by hydrometallurgical treatment" in *Energy Technology 2017*, Springer, 2017, pp. 355–366.

7 APPENDIX

Remained impurities content measured by ICP-MS and the calculated removal degree of each sample are listed in this appendix as Appendix Table I.

Appendix Table I: Leaching performance of 4 samples. The above line shows impurities content in unit ppmw while below indicates removal degree (%).

	MG-Si (60℃)	MG-Si (80℃)	Mg-doped (60℃)	Mg-doped (80℃)
B	52.5 (-13.6%)	42.5 (7.9%)	41 (3.3%)	37.7 (11.0%)
P	15.3 (3.2%)	9.6 (39.0%)	5.6 (64.1%)	0.7 (95.8%)
Mg	5.7 (40.6%)	1.7 (82.6%)	20609.0 (54.1%)	10344.8 (76.9%)
Ca	206.7 (22.5%)	69.4 (74.0%)	122.8 (56.5%)	39.5 (86.0%)
Ti	231.9 (22.6%)	152.8 (49.0%)	112.8 (44.7%)	92.1 (54.8%)
Fe	2602.6 (17.8%)	1730.5 (45.4%)	1173.2 (48.6%)	973.8 (57.2%)
Al	1975.0 (22.5%)	1215.5 (52.3%)	710.0 (58.3%)	487.8 (72.0%)
Mn	60.8 (13.6%)	30.1 (57.3%)	33.3 (38.2%)	16.3 (69.8%)
Zr	9.3 (13.1%)	5.7 (46.4%)	4.1 (41.4%)	3.4 (51.0%)

Paper 2

Separation and Purification Technology 240 (2020) 116614

Contents lists available at ScienceDirect

Separation and Purification Technology

journal homepage: www.elsevier.com/locate/seppur

Phosphorus separation from metallurgical-grade silicon by magnesium alloying and acid leaching

Mengyi Zhu[a], Alexander Azarov[b], Eduard Monakhov[b], Kai Tang[c], Jafar Safarian[a,*]

[a] Department of Materials Science and Engineering, Norwegian University of Science and Technology (NTNU), Trondheim, Norway
[b] Centre for Materials Science and Nanotechnology, Department of Physics, University of Oslo, P.O. Box 1048 Blindern, N-0316 Oslo, Norway
[c] SINTEF Materials and Chemistry, N-7465 Trondheim, Norway

ARTICLE INFO

Keywords:
Metallurgical grade silicon
Purification
Acid leaching
Phosphorus
Impurities

ABSTRACT

In this paper, the separation of phosphorus from metallurgical-grade silicon was investigated based on an Mg alloying and HCl leaching approach. Experimental results show that P concentration was reduced from initial 15.1 ppmw to 0.2 ppmw with also large extent removal of metallic impurities by two times Mg alloying-leaching purification. The mechanism of enhanced P separation is clarified owing to the strong affinity between Mg and P, which is validated by SIMS elemental mapping. A two-parameter analytical model was developed to predict the P removal degree based on the variables of alloying metal concentration and interaction coefficient between alloying metal and P. The model is validated with experimental results and the interaction coefficient $\varepsilon^{P}_{Mg\ in\ Si}$ was obtained as −10.8. This approach can be applied to model the removal of impurity which follows Gulliver-Scheil solidification from other binary alloying systems. Furthermore, in order to study the effect of applied alloying-leaching operation times, a model was proposed which establishes the mathematical relationships among key processing variables like initial and target P concentrations, the amount of the alloying metal, and the process operation times.

1. Introduction

The rapid growth of the photovoltaic industry worldwide has given rise to large demands of solar grade silicon (SoG-Si, purity 99.9999%) feedstock production. The metallurgical route for SoG-Si production has, therefore, become an emerging technology due to its large production capacity, low-cost, and environment-friendly features [1,2]. However, the main challenge of the metallurgical route for SoG-Si production is the removal of large concentration of impurities from the raw material metallurgical grade silicon (MG-Si, 99% Si), especially the removal B and P, which are the major important impurities for the solar cells. In the commercialized Elkem Solar metallurgical process operated by REC Solar Norway, MG-Si is purified through the combination of slag refining, acid leaching, and directional solidification [2]. As one of the crucial steps, the task of acid leaching is aiming at removing large extent metallic impurities, and, more importantly, to reduce the P concentration down to 0.1–0.3 ppmw to meet the restricted high-purity requirement of SoG-Si.

The research of silicon purification by acid leaching has been carried out over decades in respect of determining optimum leaching conditions [3–7], precipitated phase reactivity [8–10], and leaching kinetics [11,12]. However, it is generally accepted that only parts of P and metallic impurities can be removed due to the weak segregation and low chemical reactivity of the Fe-bearing precipitates. In order to further improve the impurity removal efficiency, new method has emerged to purify Si by means of introducing new alloying element to modify the impurity segregation behavior during solidification. One typical example is the widely known solvent refining [13,14], which mainly relies on a large amount of alloying metal addition like Al [15–24], Sn [24–28], Cu [29–31], and Fe [32] and so on. In this way, low operation temperature can be achieved for lower process energy consumption, but the large amount of the alloying metal addition causes high cost of the process. Unlike solvent refining, the addition of only small amount of more reactive alloying elements into Si melt brings more economic benefits and also reaches high impurity removal degree. Schei et al. [33] investigated the effect of Ca addition on impurities removal and found that the impurities embedded inside a leachable $CaSi_2$ phase. Shimpo et al. [34] investigated the thermodynamic interaction between Ca and P, and confirmed Ca has a strong affinity to P in molten Si. Other researchers also reported high P removal degree after Ca alloying [35–39], but the difficulty of separating viscous byproduct siloxene still remains challenging [1]. Alternative

* Corresponding author.
E-mail address: Jafar.Safarian@ntnu.no (J. Safarian).

https://doi.org/10.1016/j.seppur.2020.116614
Received 17 October 2019; Received in revised form 7 January 2020; Accepted 21 January 2020
Available online 25 January 2020

Table 1
Composition of starting materials before acid leaching (in ppmw).

	S1 MG-Si	S2 Si-2.2 wt% Mg	S3 Si-5.5 wt% Mg	S4 Si-1.8 wt% Mg	S5 Si-3.8w%Mg	Re-alloyed S3 4 wt%Mg
B	46.2	44.9	44.3	19.5	18.9	44.0
P	15.8	12.2	15.1	4.4	3.9	3.4
Mg	9.6	19424.9	54804.5	17908.9	37774.8	41251.5
Ca	266.7	252.2	267.0	73.3	97.9	26.8
Al	2548.0	259.8	1717.8	610.2	618.8	207.4
Fe	3167.5	1619.3	2154.0	948.1	966.4	1014.8
Ti	299.8	138.4	190.4	67.8	66.4	74.0
Mn	70.4	34.6	49.8	16.8	17.8	18.2
Zr	10.7	5.5	7.2	2.7	2.7	4.1
Si	Balance	Balance	Balance	Balance	Balance	Balance

alloying elements such as Ti [35], Hf [40], Zr [41], have been also studied for different purposes and with their own features, but they are not feasible to be used in practice due to the high prices of these metals and the difficulties in their further removal for solar silicon production.

In this work, a comprehensive study of novel Mg alloyed MG-Si acid leaching was conducted according to the attractive features exhibited by the Mg alloying in our recent research works [42–44]. Various parameters such as acid concentration, leaching time, and Mg addition amount are studied to validate the applicability of Mg alloying on impurities removal. Moreover, two theoretical models were proposed to better understand the P removal via the Si alloying-leaching process.

2. Materials and methods

2.1. Materials

A commercial MG-Si was selected as the starting material, the detailed composition can be seen in Table 1. High purity (99.8%, Alfa Aesar) Mg rod with low P concentration was cut into pieces used for MG-Si alloying. Analytical grade reagents hydrochloric acid (HCl) was supplied by VWR International. The concentrated HCl aqueous solution was diluted by deionized water to obtain different concentration for leaching trials.

2.2. Silicon alloying by Mg and leaching

The alloying and leaching process of MG-Si purification can be seen in Fig. 1. MG-Si lumps were first carefully put into a graphite crucible with ultra-high purity. The crucible was then placed in an induction furnace. Before heating, the furnace chamber was evacuated to high vacuum and then re-filled by pure Argon gas to 1 atm followed by continuous Ar flow. MG-Si lumps were subsequently heated up to 1500 °C as molten state. Specific amount of Mg piece was then added into the melt for targeting alloy composition. After Mg addition, the molten alloy was slowly cooled down and solidified under the same condition inside the furnace chamber. It is worth noting that even though P has a high vapor pressure, but the P loss caused by evaporation can be ignored due to the ultra-low activity and short melting time.[45,46] The obtained Si-Mg alloy was then crushed and sieved to specific particle size (0.2–1 mm) for the following acid leaching. The chemical compositions of MG-Si and Mg-doped samples were measured by high-resolution Inductively Coupled Plasma-Mass Spectroscopy (ICP-MS, Thermo Scientific Element 2, US) are listed in Table 1.

Table 2
Detailed conditions of performed leaching trials.

ID	Si source	HCl Concentration	Leaching Time (h)	Leaching Temperature (°C)	Leaching method
L1	S1	10%	3	60	M
L2	S2	5%	5	60	M
L3		10%	5	60	M
L4		15%	5	60	M
L5		20%	5	60	M
L6	S3	10%	0.5	60	M
L7			1	60	M
L8			2	60	M
L9			3	60	M
L10	Re-	10%	0.5	60	M
L11	alloyed		1	60	M
L12	S3		2	60	M
L13			3	60	M
L14	S2	10%	3	60	U
L15	S3	10%	3	60	U
L16	S4	10%	3	60	U
L17	S5	10%	3	60	U

A number of leaching trials were designed for different research purposes as shown in Table 2. Herein, the leaching trials and conditions are determined based on our preliminary work [42–44]. For the magnetic-stirrer leaching (M), 100 g fine particle sample was placed in a 500 mL Pyrex beaker with 250 mL 10% HCl preheated at 60 °C on hotplate. A total leaching period up to 3 h was performed using a magnetic stirring condition with 200 rpm. For the ultrasonic leaching trials (U), 2 g sample with 10 mL 10%HCl was mixed in perfluoroalkoxy alkane (PFA) bottle and then put into ultrasonic bath with the same temperature as the magnetic-stirrer leaching. After leaching, the remaining particles were washed by distilled water and dried. Ultra-fine particles were sieved by a 100 μm sieve before analysis in order to reduce the interference of undissolved metallic impurities.

2.3. Characterization

The MG-Si material and produced Si-Mg alloys were analyzed by a Secondary Electron Microscope (SEM, Hitachi SU6600, Japan) with Energy Dispersive X-ray Spectrometry (EDS) detector to study the microstructure variation. The chemical composition of all the samples after leaching was measured by the high-resolution ICP-MS. A magnetic sector Secondary Ion Mass Spectrometry (SIMS) instrument (CAMECA IMS 7f) was employed to analyze the P distribution in Mg alloyed samples. The SIMS measurements were performed in the imaging mode using 15 keV Cs^+ ions as a primary beam rastered over the area of 500 × 500 μm^2. The beam current was kept at 1nA during the measurements.

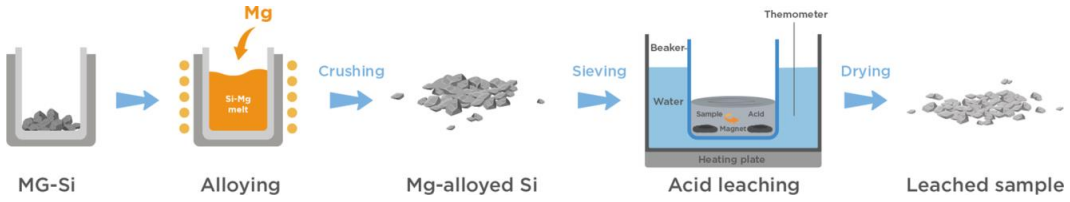

Fig. 1. Schematic of the Mg alloying and acid leaching process.

3. Results

3.1. Microstructure

Before acid leaching, the microstructure of sample S1, S2, S3, and Re-alloyed S3 was analyzed by SEM and shown in Fig. 2. A number of precipitated phases are observed, and the chemical composition was further analyzed by EDS.

In Fig. 2(a and b) of the raw MG-Si sample Si, the identified precipitates are mainly as Fe-bearing silicide, respectively, $CaAl_6Fe_4Si_8$, Al_3FeSi_2, $TiFeSi_2$, and $FeSi_{2.4}$.

The effect of Mg alloying on the microstructure of MG-Si can be observed in Fig. 2(c–f). A large amount of eutectic Mg_2Si phase can be distinctly observed in both of the Mg-alloyed samples. In sample S3, there is also some eutectic silicon phase observed in Mg_2Si, while in the sample S2 much less eutectic silicon was found. In addition, the Fe-bearing silicide phases were found embedded inside the Mg_2Si phase. Meanwhile, the $TiFeSi_2$ phase was also found in the Mg_2Si phase rather than in the $CaAl_6Fe_4Si_8$ phase as in MG-Si. The $CaAl_2Si_2$ phase was found in the Mg-alloyed samples as well.

For the leached and re-alloyed S3 sample, it can be seen from Fig. 2(g–h) that the eutectic Mg_2Si is still the main precipitate, but the content of the other impurities is much lower than that in sample S3. It can be also seen that Ca-bearing phase barely exists, and only a very

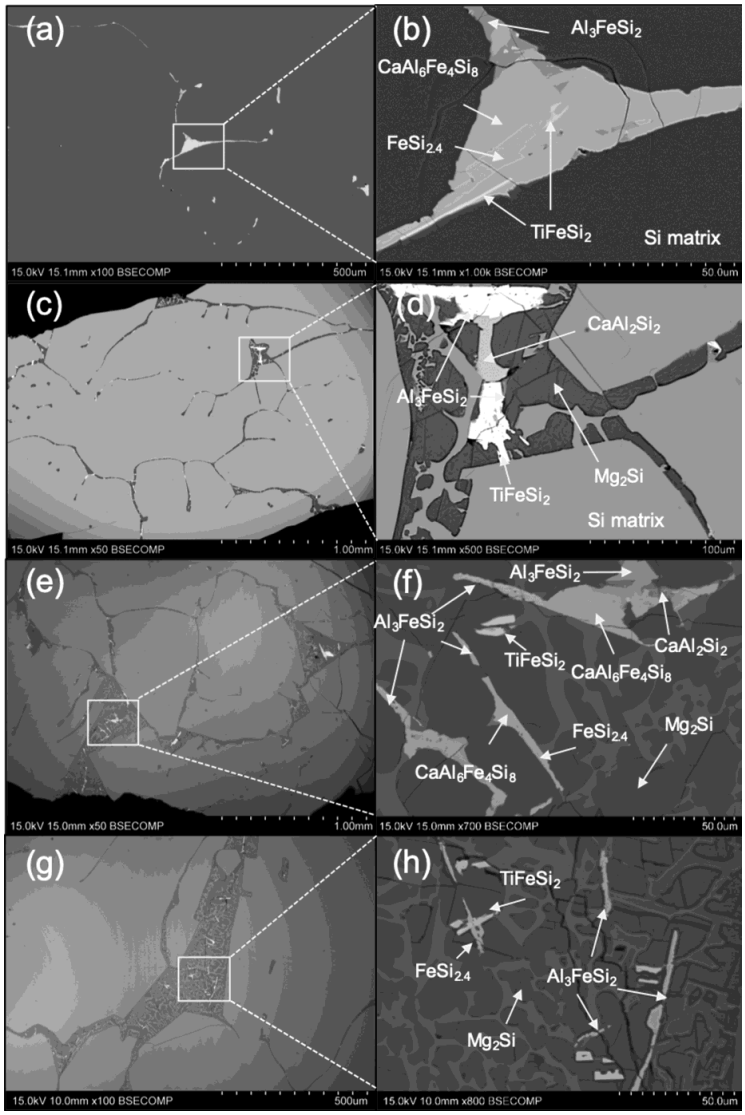

Fig. 2. Microstructure of precipitated phases in samples: (a–b) S1 (MG-Si); (c–d) S2 (Si-2.2 wt%Mg); (e–f) S3 (Si-5.5 wt%Mg), and (g–h) leached and re-alloyed S3.

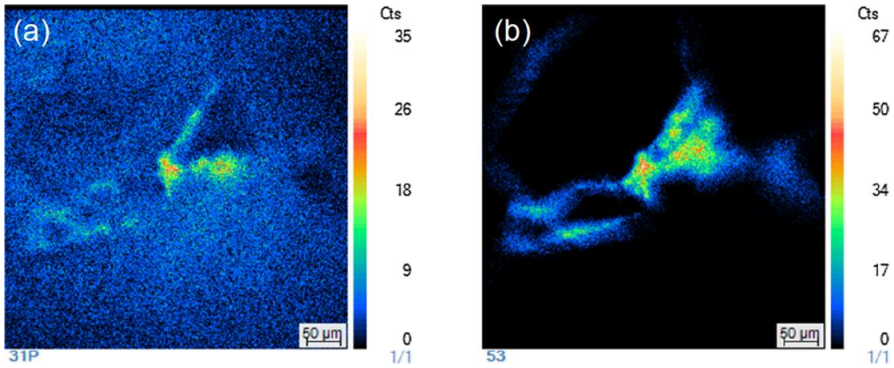

Fig. 3. SIMS mapping of (a) P distribution signal and (b) Mg + Si signal of sample S2 (Si-2.2 wt%Mg).

small amount of Al-bearing was found. The main impurity phases embedded inside Mg_2Si were determined as $TiFeSi_2$ and $FeSi_{2.4}$.

3.2. Phosphorus distribution

In order to detect the P distribution in Si-Mg alloy system, SIMS mapping analysis was performed as normal EDS analysis results for very low concentrations at ppm level are not reliable. The mapping images in Fig. 3 show a distinct enrichment of P signal in the Mg-alloyed Si sample S2. Moreover, the P signal is found partially overlapped with the signal of "Mg + Si" and close to the Mg_2Si/Si interface, which confirms the attraction of Mg to P and the enhanced P segregation in the Mg-alloyed Si subsequently.

3.3. Phase sensitivity to acid

A metallographic sample of S2 was leached three times in 10% HCl solution at 60 °C within total time period 0.2 h, 0.5 h, and 1 h to study the precipitated phase sensitivity to the acid solution. The microstructure evolution at each leaching trial was captured by SEM and the results are shown in Fig. 4.

It can be seen in Fig. 4 that the removal of the precipitated phase increases visibly with increasing leaching time. After 0.2 h leaching, most of the $CaAl_2Si_2$ phase was leached away and some of the $CaAl_6Fe_4Si_8$ phase was also removed in the short period. In addition, most of the Mg_2Si phase was dissolved into to aqueous acid solution and a distinct cracking effect was observed as well. After 0.5 h leaching, more of the Al_3FeSi_2 and $FeSi_{2.4}$ phases were dissolved. After 1 h leaching, a majority of precipitated phases were significantly removed except the insoluble $TiFeSi_2$ phase. A reactivity sequence of precipitates in Mg-alloyed MG-Si is subsequently obtained according to the metallographic sample leaching results:

$$CaAl_2Si_2,\ CaAl_6Fe_4Si_8 \ > \ Mg_2Si \gg Al_3FeSi_2,\ FeSi_{2.4} \ > \ TiFeSi_2$$

3.4. Variation of acid concentration

The impurity removal efficiency is expected to depend on the acid leaching conditions. As shown in Fig. 5, by plotting the leaching results as a function of acid concentration, a well-defined maximum can be observed at around 10% HCl that neither higher concentration nor lower HCl concentration improves the impurity removal degree. Here the removal degree of the impurities is calculated as:

$$Impurity\ \ removal\ \ degree = \frac{C_{Initial} - C_{Purified}}{C_{Initial}} \times 100\% \quad (1)$$

where $C_{Initial}$ and $C_{Purified}$ are the overall impurity concentration of samples before and after leaching in weight percent, respectively.

Since all the leaching trials were performed within the same time period, the different results thus indicate the difference of reaction kinetics with respect to different acid concentrations. More details are discussed in Section 4.1.

3.5. Re-alloying and re-leaching

Two sets of acid leaching trials (L6-L9 and L10-L13) were performed under constant conditions (60 °C, 10%HCl, magnetic stirring) to compare the effect of alloying-leaching times on impurities removal. The sample of the first leaching set is Mg-alloyed MG-Si sample S3. In the second leaching set, the sample is from the former 3 h leached S3 sample and re-alloyed by 4 wt% Mg once again. Samples used for ICP-MS measurement were subsequently taken at different leaching time of 0.5 h, 1 h, 2 h, and 3 h, respectively. Results can be seen in Fig. 6.

In the first leaching set (L6-L9), it is obvious that the concentration of the metallic impurities (Mg, Ca, Al, Fe, Ti, Mn, Zr) are decreases with increasing leaching time, especially in the first 1 h of acid leaching. P amount is also effectively reduced from 15.1 ppmw to 5.4 ppmw within 1 h leaching and further reduced to 5.1 ppmw after the first 3 h acid leaching for the sample S3. The exception is the removal of B, which has a high segregation coefficient ($k_B = 0.8$ [47]) in Si, and is generally considered to be not removed by the leaching method.

In the second leaching set of the Mg re-alloyed sample (L10-L13), a similar trend was observed again that most impurities were removed as the leaching process continues. More importantly, the concentration of impurities significantly reduced compares to the first leaching set. Furthermore, it was detected that P concentration after leaching successfully reduced to 0.2 ppmw, which meets the restricted requirements of the SoG-Si standard (P < 0.3 ppmw). Hence, the Mg alloying and re-alloying method exhibits a promising potential for the practical applications of MG-Si purification.

In order to further compare the leaching performance of the different alloying-leaching methods, the purification degree is calculated as below:

$$Purification\ \ degree = \frac{C_{MG-Si} - C_{Purified}}{C_{MG-Si}} \times 100\% \quad (2)$$

where the C_{MG-Si} and $C_{Purified}$ are impurity concentration of raw material MG-Si and after purification in weight percent.

The purification degree of studied three samples can be seen in Fig. 7. It can be observed that the purification efficiency follows the trend: direct MG-Si leaching < 1-time Mg alloying-leaching < 2-time Mg alloying. For sample S1, direct leaching of MG-Si, only limited P

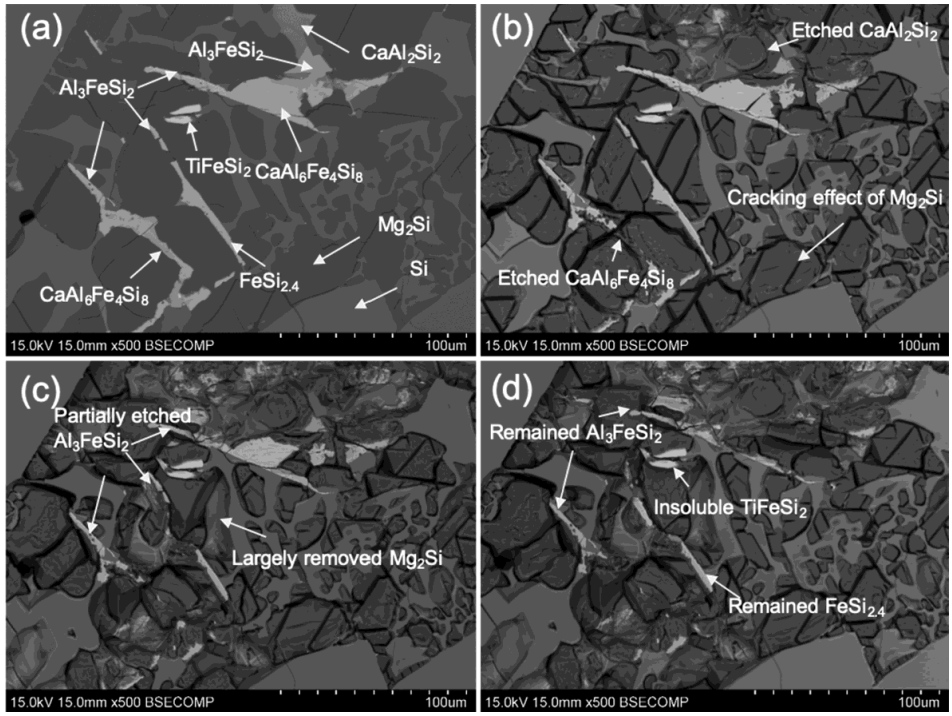

Fig. 4. Microstructure of sample S2 before leaching (a), and after acid leaching at 60 °C at (b) 0.2 h; (c) 0.5 h; (d) 1 h times by 10% HCl.

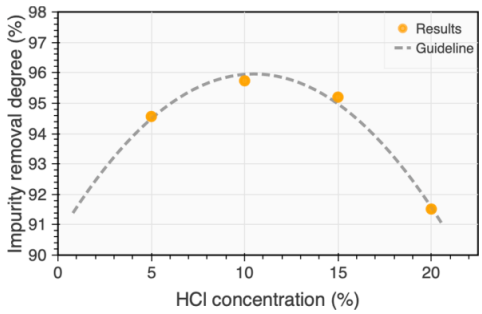

Fig. 5. Relationship between HCl concentration and the overall impurity removal degree from leaching trials L2-L5.

purification is achieved. The P purification degree is significantly improved from 31.1% to 69.5% after Mg alloying, and especially for the leached and re-alloyed S3 sample, nearly complete P removal is achieved. Moreover, for the purification of metallic impurities such as Ca, Al, Fe, Ti, Mn, and Zr, distinguished improvement can be observed as well by the re-alloying method.

4. Discussion

4.1. Mechanism of impurities removal

Based on the microscopic examinations and the leaching behavior of the phases, the mechanism of impurity removal for both MG-Si and Mg-doped Si samples by acid leaching can be explained as schematically illustrated in Fig. 8.

In MG-Si, it is known that the precipitates are mainly Fe-bearing silicide phases with poor leaching ability. In addition, these Fe-bearing silicides dispersed unevenly and usually with fine microstructure at the grain boundaries. When the leaching process starts, only a portion of these particles can be exposed to acid, and only small parts of them can be dissolved due to the limited reactivity, which is depending on process characteristics. Consequently, impurity removal efficiency is limited.

In the MG-Si with Mg alloying sample, the dominant precipitate becomes Mg_2Si, and it is widely spread at the grain boundaries, or in other words, as a secondary phase between the primary silicon grains. Meanwhile, many other insoluble phases, e.g., Fe-bearing silicide, are found embedded inside the Mg_2Si precipitate matrix. Subsequently, when the acid leaching process starts, the highly reactive Mg_2Si phase is dissolved into the acid solution. At the same time, the poorly leachable silicide, which is embedded in Mg_2Si precipitates, could also be carried away physically. In addition, the observed cracking effect due to the intensive exothermic reaction between Mg_2Si and aqueous HCl solution is also favorable to promote the kinetics of further impurity removal. Consequently, after sufficient leaching time, impurities can be effectively removed.

4.2. Effect of acid concentration

Although the entire acid leaching process of Mg-alloyed Si is a heterogeneous solid-state reaction, the governed reaction is expected to be the decomposition of Mg_2Si due to its principal amount. However, since a distinct maximum of impurity removal degree was observed, it

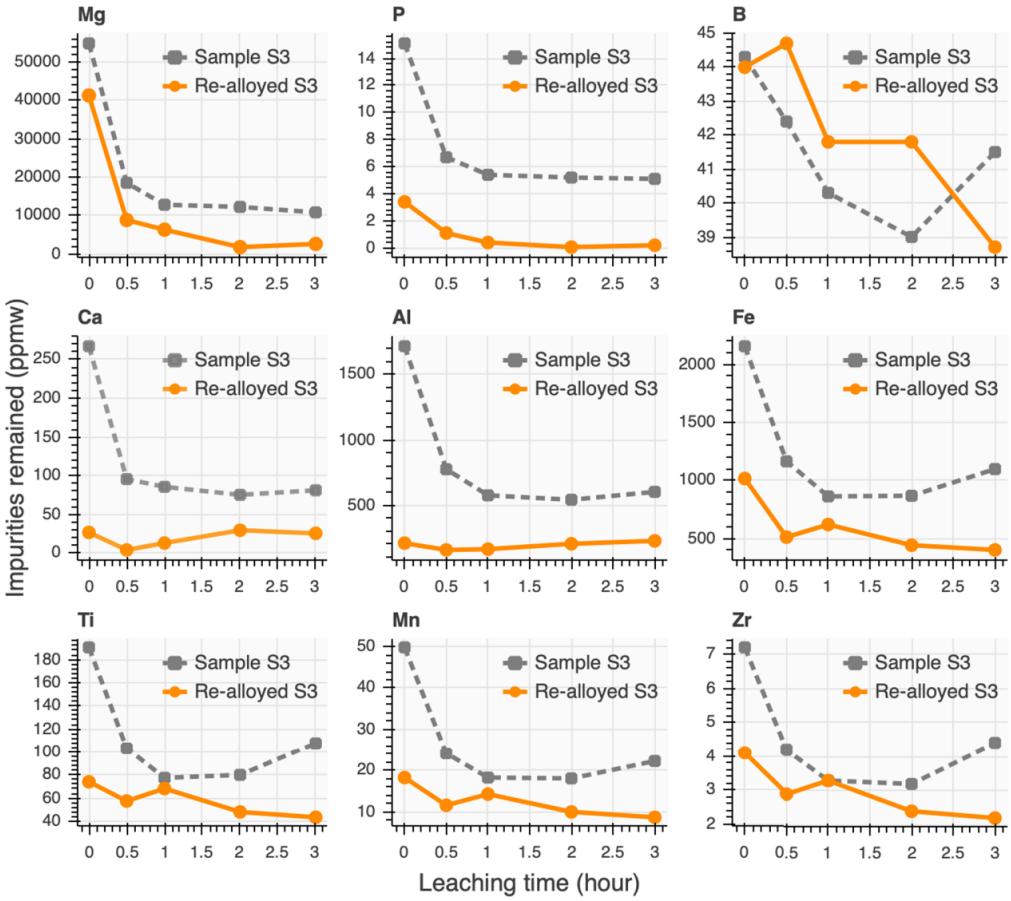

Fig. 6. Remained impurities concentration in leaching samples as a function of leaching time. Symbols show the measured concentrations of the leached samples S3 (L6-L9) and S3-leached sample that was re-alloyed by Mg and re-leached (L10-L13).

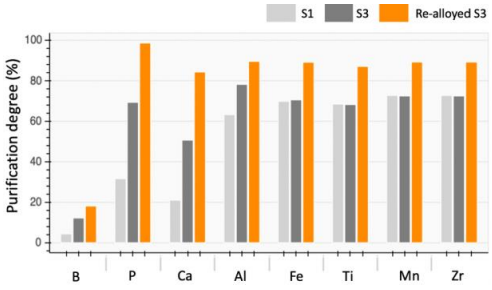

Fig. 7. Acid leaching purification efficiency comparison of sample S1 (MG-Si), S3 (Si-5.5 wt% Mg), and Re-alloyed S3.

implies that different factors govern the leaching process.

From the viewpoint of reaction kinetic factors, high concentration HCl solution is usually with high surface tension, which may suppress the chemical reaction located at micro pores. Consequently, with very high HCl concentration, the impurity removal degree in a given time decreased. On the other hand, from the viewpoint of the chemical reaction itself, the Mg_2Si decomposition in aqueous HCl is controlled by more complicated steps rather than HCl in the anhydrous condition which can be simply considered as [48]

$$Mg_2Si(s) + HCl(aq.) \rightarrow MgCl_2(aq.) + SiH_4(g) \quad (3)$$

The detailed reaction mechanism of Mg_2Si decomposition in aqueous HCl has been comprehensively investigated by Schwarz et al. [49]. It was found that the total reaction can be separated into several steps. Firstly, a primary hydrolysis reaction takes place and leads to the formation of an intermediate hydrolysis product dihydroxymagenesiosilane ($(HOMg)_2SiH_2$),

$$Mg_2Si + 2H_2O \xrightarrow{HCl} \begin{bmatrix} HO-Mg \\ HO-Mg \end{bmatrix} \diagup\!\diagdown SiH_2 \quad (4)$$

This intermediate is then further acidic hydrolyzed by breaking the two Mg-Si bonds and form silane gas:

$$\begin{bmatrix} HO-Mg \\ HO-Mg \end{bmatrix} \diagup\!\diagdown SiH_2 + 4HCl \rightarrow 2MgCl_2 + SiH_4 + 2H_2O \quad (5)$$

And also may result in the formation of some hydrogen gas:

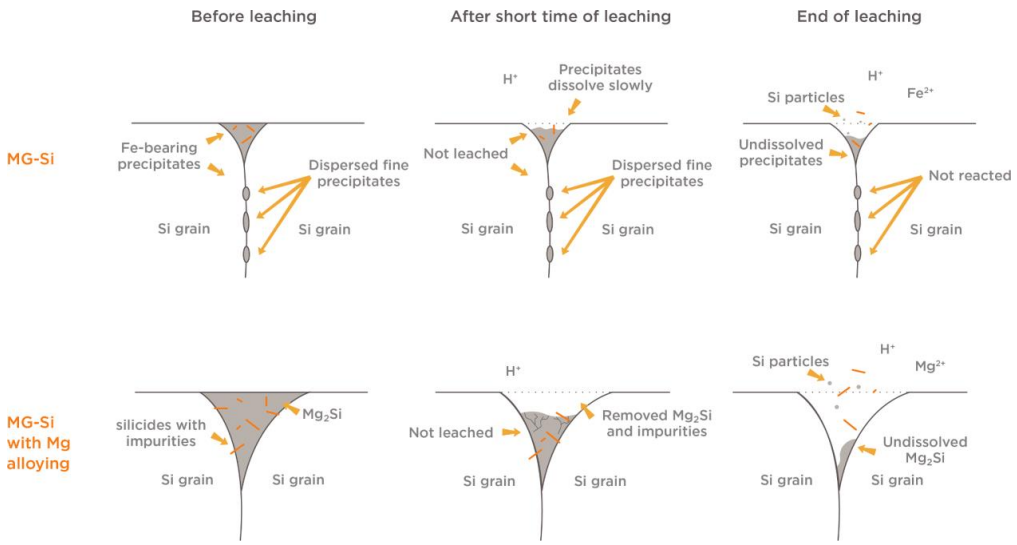

Fig. 8. Sketch of the impurity removal mechanism of MG-Si and Mg alloyed Si during acid leaching.

$$\begin{bmatrix}\mathrm{HO-Mg}\\ \mathrm{HO-Mg}\end{bmatrix}\!\!\diagup\!\!\mathrm{SiH_2}\!\!\diagdown + 2\mathrm{H_2O} + 4\mathrm{HCl} \rightarrow 2\mathrm{MgCl_2} + 4\mathrm{H_2} + \mathrm{SiO_2} \quad (6)$$

It can be seen that the total reaction of Mg_2Si decomposition is governed by both hydrolysis and reactive HCl acid interaction. On one hand, the primary hydrolysis reaction rate is determined by the amount of available H_2O in solution, which decreases with increasing HCl concentration. The total leaching efficiency is therefore limited under concentrated HCl condition. On the other hand, if the concentration of reactive HCl molecules becomes too low, the subsequent reactions will be suppressed as well and result in a lower leaching efficiency accordingly. While at the concentration of HCl around 10%, the optimum condition of the process is achieved, the acid leaching results thus exhibit a well-defined maximum observed in Fig. 5.

4.3. Enhancement of phosphorus segregation

In Section 3.2, it was confirmed by the SIMS mapping that the P segregation is evidently enhanced in the Si-Mg alloy system. Hence, the possible reasons for Mg alloying effects on P segregation enhancement are discussed below, respectively, from the liquidus variation based physical perspective and elements interactionbased chemical perspective.

- Physical perspective

P segregation coefficient in Si is defined as the ratio of P concentration in the solid phase and in the liquid phase during solidification, which is equivalent to the ratio of solidus line and liquidus line and can be calculated as:

$$k_P^{Si} = \frac{X_{Solidus,Si-P}}{X_{Liquidus,Si-P}} \quad (7)$$

where $X_{Solidus,Si-P}$ and $X_{Liquidus,Si-P}$ represent the molar concentrations of P in solid state and in liquid state of Si, respectively. The P segregation coefficient k_P^{Si} is well-known to be $k_P^{Si} = 0.35$ [47] for low P-containing Si-P alloys.

If one assumes there is no significant variation on the solidus line of P in Si after Mg addition (the interaction between Mg and P is ignored in solidified primary silicon due to the low concentration), and the very low concentration of P in Si-Mg alloys has no effect on the liquidus curve, the segregation coefficient of P in Si-Mg system then only relies on the change of liquidus line from Si-P system to Si-Mg system. Therefore, Eq. (7) can be written for the dilute solutions of P in Si-Mg-P system as:

$$k_P^{Si-Mg} = \frac{X_{Solidus,Si-P}}{X_{Liquidus,Si-Mg}} = \frac{X_{Solidus,Si-P}}{X_{Liquidus,Si-P}}\frac{X_{Liquidus,Si-P}}{X_{Liquidus,Si-Mg}} = k_P^{Si}\frac{X_{Liquidus,Si-P}}{X_{Liquidus,Si-Mg}} \quad (8)$$

where $X_{Liquidus,Si-Mg}$ represents the liquidus composition of Si-Mg system, and the term $\frac{X_{Liquidus,Si-P}}{X_{Liquidus,Si-Mg}}$ is regarded as the correction factor of k_P^{Si}. If $\frac{X_{Liquidus,Si-P}}{X_{Liquidus,Si-Mg}} < 1$, then the actual segregation coefficient of P is subsequently reduced from the theoretical 0.35 in Eq. (7).

The liquidus of binary Si-P and Si-Mg systems are plotted and compared at the Si-rich portion shown in Fig. 9. The Si-Mg liquidus line is obtained from the former work of Safarian et al.[50], and the Si-P liquidus is calculated by the same method based on the data in the Si-rich portion [51,52].

It can be seen from Fig. 9 that for a given temperature, the Si-Mg liquidus appears in the right side of Si-P liquidus. In other word, $X_{Liquidus,Si-P}$ is smaller than $X_{Liquidus,Si-Mg}$ at a given temperature, so we have $\frac{X_{Liquidus,Si-P}}{X_{Liquidus,Si-Mg}} < 1$. Therefore, the segregation coefficient of P is assumed to be reduced accordingly with the Mg alloying. However, it has to be noted that the liquidus variation assumption only works when Mg concentration is low because only in such case the interaction between Mg and P in Si melt can be ignored.

- Chemical perspective

From the chemical perspective, the segregation coefficient of P in Mg-alloyed Si can be obtained from the chemical potential equilibrium between the solid and liquid as the following equation:

$$\mu_{P\ \text{in}\ Si(s)} = \mu_{P\ \text{in}\ Si-Mg(l)} \quad (9)$$

where $\mu_{P\ \text{in}\ Si(s)}$ and $\mu_{P\ \text{in}\ Si-Mg(l)}$ are the chemical potential of P in primary solid Si front and in the liquid front.

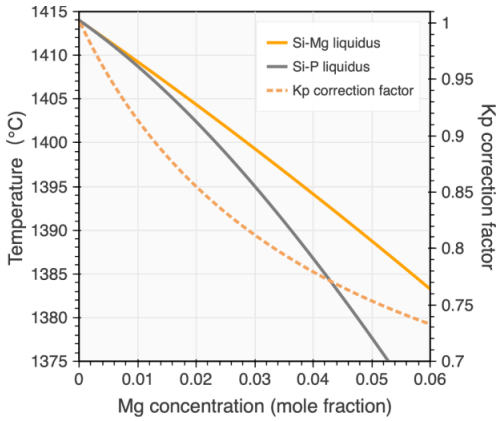

Fig. 9. Liquidus of Si-P and Si-Mg systems in the Si-rich portion and the correction factor changes.

Therefore,

$$RT\ln a_{\mathrm{P\ in\ Si}(s)} = RT\ln a_{\mathrm{P\ in\ Si-Mg}(l)} \tag{10}$$

where $a_{\mathrm{P\ in\ Si}(s)}$ and $a_{\mathrm{P\ in\ Si-Mg}(l)}$ are the activity of P in primary solid Si front and in the liquid front.

Based on the above equilibrium condition, it then gives

$$X_{\mathrm{P\ in\ Si}(s)}\gamma^0_{\mathrm{P\ in\ Si}(s)} = X_{\mathrm{P\ in\ Si-Mg}(l)}\gamma_{\mathrm{P\ in\ Si-Mg}(l)} \tag{11}$$

The segregation coefficient is then can be calculated as:

$$k_{\mathrm{P}}^{\mathrm{Si-Mg}} = \frac{X_{\mathrm{P\ in\ Si}(s)}}{X_{\mathrm{P\ in\ Si-Mg}(l)}} = \frac{\gamma_{\mathrm{P\ in\ Si-Mg}(l)}}{\gamma^0_{\mathrm{P\ in\ Si}(s)}} = \frac{\gamma^0_{\mathrm{P\ in\ Si}(l)}}{\gamma^0_{\mathrm{P\ in\ Si}(s)}}\frac{\gamma_{\mathrm{P\ in\ Si-Mg}(l)}}{\gamma^0_{\mathrm{P\ in\ Si}(l)}} = k_{\mathrm{P}}^{\mathrm{Si}}\frac{\gamma_{\mathrm{P\ in\ Si-Mg}(l)}}{\gamma^0_{\mathrm{P\ in\ Si}(l)}} \tag{12}$$

where $\gamma^0_{\mathrm{P\ in\ Si}(s)}$ and $\gamma^0_{\mathrm{P\ in\ Si}(l)}$ represent the activity coefficient of P in solid and liquid Si, $\gamma_{\mathrm{P\ in\ Si-Mg}(l)}$ represents the activity coefficient of P in Si-Mg melt. The above equation is obtained based on the fact that the two solid and liquid phases are at equilibrium and necessarily the chemical potential, or the chemical activity, of P in the two phases are equal. In principle, the activity coefficient of P in Si-Mg-P melt can be expressed as:

$$\ln\gamma_{\mathrm{P\ in\ Si-Mg}(l)} = \ln\gamma^0_{\mathrm{P\ in\ Si}(l)} + \varepsilon^{\mathrm{P}}_{\mathrm{P\ in\ Si}}X_{\mathrm{P\ in\ Si}(l)} + \varepsilon^{\mathrm{P}}_{\mathrm{Mgin\ Si}}X_{\mathrm{Mg\ in\ Si}(l)} \tag{13}$$

where $\varepsilon^{\mathrm{P}}_{\mathrm{Mg\ in\ Si}}$ represents the interaction coefficient of Mg and P in Si melt on each other. Parameter$\varepsilon^{\mathrm{P}}_{\mathrm{P\ in\ Si}}$is the self-interaction coefficient of P, and the term $\varepsilon^{\mathrm{P}}_{\mathrm{P\ in\ Si}}X_{\mathrm{P\ in\ Si}(l)}$ can be ignored due to the ultra-low P concentration at ppmw level in the melt. Therefore, we have:

$$\ln\frac{\gamma_{\mathrm{P\ in\ Si-Mg}(l)}}{\gamma^0_{\mathrm{P\ in\ Si}(l)}} = \varepsilon^{\mathrm{P}}_{\mathrm{Mg\ in\ Si}}X_{\mathrm{Mg\ in\ Si}(l)} \tag{14}$$

Combining the above Eqs. (12) and (14), $k_{\mathrm{P}}^{\mathrm{Si-Mg}}$ can be rewritten as:

$$k_{\mathrm{P}}^{\mathrm{Si-Mg}} = k_{\mathrm{P}}^{\mathrm{Si}}\exp(\varepsilon^{\mathrm{P}}_{\mathrm{Mg\ in\ Si}}X_{\mathrm{Mg\ in\ Si}(l)}) \tag{15}$$

Since $X_{\mathrm{Mg\ in\ Si}(l)}$ is always larger than 0 in Si-Mg alloy system, and the sign of term $\varepsilon^{\mathrm{P}}_{\mathrm{Mg\ in\ Si}}$ is negative due to the widely known strong attraction of alkaline-earth element to P to form stable phosphide [53–55], it is expected that the segregation coefficient of P continuously decreases with increasing Mg addition into Si. The value of $\varepsilon^{\mathrm{P}}_{\mathrm{Mg\ in\ Si}}$ is later estimated to be as negative as −10.8 in present work in Section 4.4 and it confirms this explanation. Indeed, the enhancement of P segregation is thought due to the interaction and formation of some stable P-bearing clusters in the melt, suggested by the following two paths:

$$2\mathrm{P} + 1.5\mathrm{Mg_2Si} \rightarrow \mathrm{Mg_3P_2} + 1.5\mathrm{Si} \tag{16}$$

$$2\mathrm{SiP} + \mathrm{Mg_2Si} \rightarrow \mathrm{MgSiP_2} + \mathrm{Si} \tag{17}$$

Although P is known favorable to segregate at several specific sites in pure Si [56], it is expected that Mg addition attracts more P into the Mg_2Si precipitates, which are further easily removed in acid leaching and yielding higher P removal degree. The chemical interaction between Mg and P is considered the main reason for the successful P removal. Moreover, this interaction governs the P segregation enhancement during the whole solidification temperature-composition range.

4.4. Phosphorus removal modeling for Mg-doped silicon

The modeling method applied here refers to the methodology employed by Shimpo et al.[34]. The assumptions are made here as follows:

A1. The behavior of solute element during growth of primary silicon grains from the Mg-alloyed Si melts follows the Gulliver-Scheil equation, the diffusion of solute in solid Si can be ignored and the remaining liquid alloy is homogeneous.
A2. The secondary precipitates (eutectic phases) are completely removed in acid leaching step. Thus, the value of P content that is measured by ICP-MS after leaching is equivalent to the P in primary Si (solid solution) before the eutectic reaction starts.
A3. Thermodynamic properties of ultra-low P concentration at ppmw level are independent of temperature. Thus, the interaction parameter $\varepsilon^{\mathrm{P}}_{\mathrm{Mg\ in\ Si}}$ remains constant during the whole solidification range.

As illustrated in Fig. 10, the above assumptions yield P redistribution during solidification in solidified primary silicon grains and in the remained melt. It is seen that for a given initial P concentration $X^{initial}_{\mathrm{P\ in\ Si}(l)}$, the segregation starts from the beginning of primary Si grains formation and ends up to the beginning of the eutectic reaction. In addition, the concentration of P in solidified Si grains increases as the solid fraction increases. The trend becomes more rapidly at the final stage that is close to the eutectic point. The dotted lines plotted in the eutectic region are theoretically and experimentally approved concentration profile trend assuming no eutectic reaction (low P-containing Si-P melt solidification).

The theoretical P removal degree for the ternary system is defined here as Eq. (18):

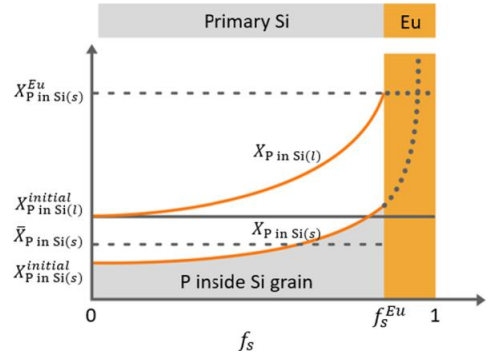

Fig. 10. Sketch of concentration profile of P in solidified primary silicon and the corresponding average P concentration in the remained melt and solidified eutectic portion.

$$\eta = \left(\frac{X_{\mathrm{P\ in\ Si}(l)}^{initial} - \bar{X}_{\mathrm{P\ in\ Si(s)}}}{X_{\mathrm{P\ in\ Si}(l)}^{initial}} \right) \times 100\% \tag{18}$$

where $X_{\mathrm{P\ in\ Si}(l)}^{initial}$ is the initial P concentration before the acid leaching, and $\bar{X}_{\mathrm{P\ in\ Si(s)}}$ is the average concentration of P segregated inside primary Si grain, and from mathematical point of view it is the shaded grey area under the $X_{\mathrm{P\ in\ Si}(s)}^{initial}$ curve in Fig. 10. The following mass balance is further applied to determine the value of $\bar{X}_{\mathrm{P\ in\ Si}(s)}$,

$$\bar{X}_{\mathrm{P\ in\ Si}(s)} f_s^{Eu} = \int_0^{f_s^{Eu}} X_{\mathrm{P\ in\ Si}(s)} df_s \tag{19}$$

where f_s is the solid fraction of primary Si, f_s^{Eu} is the primary Si solid fraction at the starting point of eutectic reaction, and $X_{\mathrm{P\ in\ Si}(s)}$ is the concentration of P at solid front which can be calculated as:

$$X_{\mathrm{P\ in\ Si}(s)} = k_P^{\mathrm{Si-Mg}} X_{\mathrm{P\ in\ Si}(l)}^{initial} (1 - f_s)^{k_P^{\mathrm{Si-Mg}} - 1} \tag{20}$$

By rearranging and integrating Eq. (20), the following relationship can be derived:

$$\bar{X}_{\mathrm{P\ in\ Si(s)}} = \frac{X_{\mathrm{P\ in\ Si}(l)}^{initial}}{f_s^{Eu}} (1 - (1 - f_s^{Eu})^{k_P^{\mathrm{Si-Mg}}}) \tag{21}$$

Hence, combing Eqs. (18) and (21), we obtain:

$$\eta = \left(1 - \frac{1 - \frac{X_{\mathrm{P\ in\ Si}(l)}^{Eu}}{X_{\mathrm{P\ in\ Si}(l)}^{initial}} (1 - f_s^{Eu})}{f_s^{Eu}} \right) \times 100\% \tag{22}$$

The term $\frac{X_{\mathrm{P\ in\ Si}(l)}^{Eu}}{X_{\mathrm{P\ in\ Si}(l)}^{initial}}$ can be further obtained from Gulliver-Scheil equation that:

$$(1 - f_s) dX_{\mathrm{P}(l)} = (X_{\mathrm{P\ in\ Si}(l)} - X_{\mathrm{P\ in\ Si}(s)}) df_s \tag{23}$$

Considering the relationship $X_{\mathrm{P\ in\ Si}(s)} = k_P^{\mathrm{Si-Mg}} X_{\mathrm{P\ in\ Si}(l)}$, it yields:

$$\frac{dX_{\mathrm{P}(l)}}{X_{\mathrm{P}(l)}} = \frac{1 - k_P^{\mathrm{Si-Mg}}}{(1 - f_s)} df_s \tag{24}$$

Integrating Eq. (24) from solidification start point to the eutectic solidification starting point gives:

$$\ln \frac{X_{\mathrm{P\ in\ Si}(l)}^{Eu}}{X_{\mathrm{P\ in\ Si}(l)}^{initial}} = \int_0^{f_s^{Eu}} \frac{1 - k_P^{\mathrm{Si-Mg}}}{1 - f_s} df_s \tag{25}$$

Since the relationship between segregation coefficient and f_s has been derived by Eq. (20), and the segregation coefficient of Mg in Si is very low, so that we can approximate $k_{\mathrm{Mg}}^{\mathrm{Si}} \approx 0$, for the liquid concentration $X_{\mathrm{Mg\ in\ Si}(l)}$, it can be calculated as:

$$X_{\mathrm{Mg\ in\ Si}(l)} = \frac{X_{\mathrm{Mg\ in\ Si}(l)}^{initial}}{(1 - f_s)} \tag{26}$$

Combining Eqs. (15) and (26) we obtain:

$$k_P^{\mathrm{Si-Mg}} = k_P^{\mathrm{Si}} \exp\left(\frac{\varepsilon_{\mathrm{Mg\ in\ Si}}^{\mathrm{P}} X_{\mathrm{Mg\ in\ Si}(l)}^{initial}}{(1 - f_s)} \right) \tag{27}$$

And therefore, we can re-write Eq. (25) as:

$$\ln \frac{X_{\mathrm{P}(l)}^{Eu}}{X_{\mathrm{P\ in\ Si}(l)}^{initial}} = \int_0^{f_s^{Eu}} \frac{1 - k_P^{\mathrm{Si}} \exp\left(\frac{\varepsilon_{\mathrm{Mg\ in\ Si}}^{\mathrm{P}} X_{\mathrm{Mg\ in\ Si}(l)}^{initial}}{(1 - f_s)} \right)}{1 - f_s} df_s \tag{28}$$

Thus, integrating Eq. (28) over the whole primary Si solidification range gives the result:

$$\frac{X_{\mathrm{P}(l)}^{Eu}}{X_{\mathrm{P\ in\ Si}(l)}^{initial}} = \frac{\exp\left[k_P^{\mathrm{Si}} \left(E_i\left(\frac{\varepsilon_{\mathrm{Mg\ in\ Si}}^{\mathrm{P}} X_{\mathrm{Mg\ in\ Si}(l)}^{initial}}{(1 - f_s^{Eu})} \right) - E_i(\varepsilon_{\mathrm{Mg\ in\ Si}}^{\mathrm{P}} X_{\mathrm{Mg\ in\ Si}(l)}^{initial}) \right) \right]}{1 - f_s} \tag{29}$$

where the $E_i(x)$ function is defined as the integral $E_i(x) = \int_{-\infty}^{x} \frac{e^t dt}{t}$. Hence, a formula of the theoretical P removal degree from a P-containing Si-Mg melt is obtained as:

$$\eta = \left(1 - \frac{1 - \frac{\exp\left(k_P^{\mathrm{Si}} E_i\left(\frac{\varepsilon_{\mathrm{Mg\ in\ Si}}^{\mathrm{P}} X_{\mathrm{Mg\ in\ Si}(l)}^{initial}}{1 - f_s^{Eu}} \right) \right)}{\exp(k_P^{\mathrm{Si}} E_i(\varepsilon_{\mathrm{Mg\ in\ Si}}^{\mathrm{P}} X_{\mathrm{Mg\ in\ Si}(l)}^{initial}))}}{f_s^{Eu}} \right) \times 100\% \tag{30}$$

Considering the solid fraction at eutectic temperature can be written as:

$$f_s^{Eu} = 1 - \frac{X_{\mathrm{Mg\ in\ Si}(l)}^{initial}}{0.4629} \tag{31}$$

where 0.4629 is the mole composition of Mg at Si-Mg eutectic point [57].

Combing Eqs. (30) and (31), a final P removal degree model for the dilute P solutions of Si-Mg-P alloys can be obtained:

$$\eta = \frac{0.4629 \frac{\exp(0.35 E_i(0.4629 \varepsilon_{\mathrm{Mg\ in\ Si}}^{\mathrm{P}}))}{\exp(0.35 E_i(X_{\mathrm{Mg\ in\ Si}(l)}^{initial} \varepsilon_{\mathrm{Mg\ in\ Si}}^{\mathrm{P}}))} - X_{\mathrm{Mg\ in\ Si}(l)}^{initial}}{0.4629 - X_{\mathrm{Mg\ in\ Si}(l)}^{initial}} \times 100\% \tag{32}$$

The obtained model here reveals clearly that there are only two independent variables that control the final P removal degree: the initial Mg content $X_{\mathrm{Mg\ in\ Si}(l)}^{initial}$, and the interaction coefficient $\varepsilon_{\mathrm{Mg\ in\ Si}}^{\mathrm{P}}$. Thus, for this two-parameter dependent relationship, if one variable is known, the other can be determined based on experimental results. In the present work, the Mg-P interaction coefficient $\varepsilon_{\mathrm{Mg\ in\ Si}}^{\mathrm{P}}$ is determined by fitting the experimental results from the leaching set (L14-L17) where the ultrasonic condition applied. This is because the acoustic cavitation effects [58] and more dispersed fine particles [59] make the ultrasonic leaching generally more efficient than magnetic stirring leaching. Thus, a near complete removal of the eutectic secondary precipitates can be achieved to better meet the assumption A2.

The plotted η against the amount of added Mg in Fig. 11 shows that the proposed P removal model tends to give predictions, which are in good agreement with existing results. Furthermore, $\varepsilon_{\mathrm{Mg\ in\ Si}}^{\mathrm{P}}$ is fitted to be −10.8. This negative value also confirms the strong chemical attraction of Mg to P in Si melt as discussed before in Section 4.3. Moreover, by employing Eq. (15), the relationship between Mg addition and P segregation coefficient variation can be further determined as Eq. (33) and it is shown in Fig. 12. Seeing that the segregation coefficient of P continuously decreases with Mg addition, the Mg addition is therefore expected to enhance the P removal in the applied process.

$$k_P^{\mathrm{Si-Mg}} = 0.35 \exp(-10.8 X_{\mathrm{Mg\ in\ Si}(l)}) \tag{33}$$

It is worth to note that the obtained P removal model here can be extended to more general scenarios for the leaching of other alloying systems in which silicon is doped by metal Me to obtain Si-Me alloy system in the Si-rich port. Hence, a more general model concentrates on the theoretical analysis of P removal degree by acid leaching of an arbitrary binary Si-Me eutectic alloy system can be written as:

$$\eta = \frac{X^{eu} \varphi(\varepsilon_{\mathrm{Me\ in\ Si}}^{\mathrm{P}}, X^{initial}) - X^{initial}}{X^{eu} - X^{initial}} \times 100\% \tag{34}$$

where $X^{initial}$ and X^{eu} are the alloying metal concentrations at initial and at the eutectic point. It is worth noting that for a specific alloy system, the X^{eu} is a constant. $\varepsilon_{\mathrm{Me\ in\ Si}}^{\mathrm{P}}$ indicates the Me-P interaction

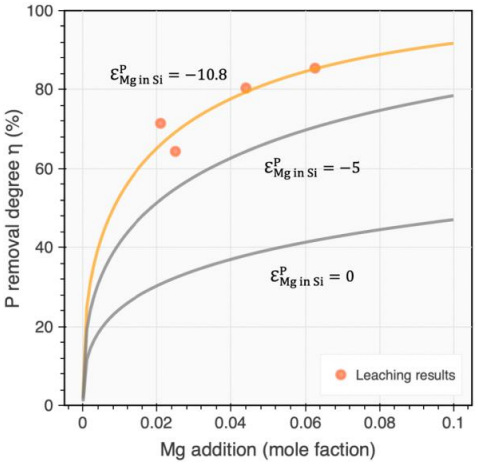

Fig. 11. Interaction parameter fitting results based on experimental results of leaching trials (L14-L17) and comparison of the estimated P removal degree as a function of Mg addition.

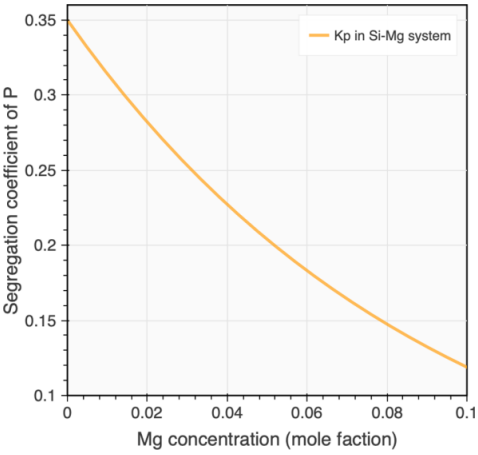

Fig. 12. Effect of Mg alloying concentration on the segregation coefficient of P in Si-Mg-P system.

coefficient, and the $\varphi(\varepsilon^{P}_{Me\ in\ Si}, X^{initial})$ is further defined as:

$$\varphi(\varepsilon^{P}_{Me\ in\ Si}, X^{initial}) = \frac{\exp(0.35E_i(\varepsilon^{P}_{Me\ in\ Si}X^{eu}))}{\exp(0.35E_i(\varepsilon^{P}_{Me\ in\ Si}X^{initial}))} \tag{35}$$

The above model also shows that P segregation in Si-Me binary system follows a two-parameter dependent relationship, further to say, the purification process is mainly controlled by interaction coefficient and the alloying concentration. Based on the present theoretical and experimental work, if one wants to achieve high P removal by the alloying method, the following strategies can be applied: (1) increase the alloying element amount, (2) adopt the alloying element with more negative interaction parameter value to P or bigger solid fraction at eutectic point, and (3) repeat the alloying-leaching process multiple times.

4.5. Effect of process operation times

In Section 3.5, it was observed that after a two-time Mg alloying-leaching process, P concentration could be further removed and meet the purity requirement of SoG-Si. For an arbitrary Si-Me system, if the averaged P segregation coefficient $\bar{k}_P^{Si-Me}$ during solidification is known, the relationship between P concentration before and after the first time alloying-leaching purification process can be directly obtained by rearranging Eq. (21) as:

$$\frac{\bar{X}_{P\ in\ Si(s)}}{X^{initial}_{P\ in\ Si(l)}} = \frac{(1-(1-f_S^{Eu})\bar{k}_P^{Si-Me})}{f_S^{Eu}} \tag{36}$$

Considering the relation $f_S^{Eu} = 1 - f_L^{Eu}$, it yields:

$$\frac{\bar{X}_{P\ in\ Si(s)}}{X^{initial}_{P\ in\ Si(l)}} = \frac{1-f_L^{Eu}\bar{k}_P^{Si-Me}}{1-f_L^{Eu}} \tag{37}$$

So that,

$$\eta = \left(\frac{X^{initial}_{P\ in\ Si(l)} - \bar{X}_{P\ in\ Si(s)}}{X^{initial}_{P\ in\ Si(l)}}\right) \times 100\% = \frac{f_L^{Eu}\bar{k}_P^{Si-Me} - f_L^{Eu}}{1-f_L^{Eu}} \times 100\% \tag{38}$$

Thus, by considering the effect of multiple operation times into Eq. (38), the final P concentration after conducting the alloying-leaching process for n times can be written as:

$$\frac{\bar{X}^n_{P\ in\ Si(s)}}{X^{initial}_{P\ in\ Si(l)}} = \left(\frac{1-f_L^{Eu}\bar{k}_P^{Si-Me}}{1-f_L^{Eu}}\right)^n \tag{39}$$

where $\bar{X}^n_{P\ in\ Si(s)}$ is the final P concentration in Si after n times alloying-leaching process.

The above model offers another method to calculate the P removal degree and to calculate required process operation times based on the averaged P segregation coefficient $\bar{k}_P^{Si-Me}$ and liquid fraction at eutectic point f_L^{Eu}. Here, the $\bar{k}_P^{Si-Me}$ can be calculated as Eq. (40), by integrating the k_P^{Si-Me} from the initial alloying metal concentration to the eutectic temperature and divided by the composition range.

$$\bar{k}_P^{Si-Me} = \frac{k_P^{Si}\int_{X^{initial}_{Me\ in\ Si(l)}}^{X^{Eu}_{Me\ in\ Si(l)}} \exp(\varepsilon^{P}_{Me\ in\ Si}X_{Me\ in\ Si(l)})dX_{Me\ in\ Si(l)}}{(X^{Eu}_{Me\ in\ Si(l)} - X^{initial}_{Me\ in\ Si(l)})} \tag{40}$$

After solving Eq. (40), we have:

$$\bar{k}_P^{Si-Me} = \frac{k_P^{Si}\exp(\varepsilon^{P}_{Me\ in\ Si}X_{Me\ in\ Si(l)})}{\varepsilon^{P}_{Me\ in\ Si}(X^{Eu}_{Me\ in\ Si(l)} - X^{initial}_{Me\ in\ Si(l)})} \tag{41}$$

In present work, the averaged P segregation coefficient is calculated as:

$$\bar{k}_P^{Si-Me} = \frac{k_P^{Si}\exp(-10.8X_{Me\ in\ Si(l)})}{-10.8(X^{Eu}_{Me\ in\ Si(l)} - X^{initial}_{Me\ in\ Si(l)})} \tag{42}$$

If one assumes $\bar{X}^n_{P\ in\ Si(s)} = 0.3$, 0.5, and 1.0 ppmw are the target P purification level, the relationship among Mg alloying concentration, initial P concentration, and the process operation times can be subsequently obtained, as shown in Fig. 13.

It is seen in Fig. 13 that the required purification process times can be adjusted based on by varying the initial P concentration and Mg alloying concentration. For the most often scenarios, MG-Si can be purified to a target purification level by 1-time or 2-time Mg alloying-leaching process. With more restrict purification reequipments (lowering the target P concentration), this process window gets narrower. Higher process operation time ($n > 2$) is then required with small Mg addition and high initial P concentration.

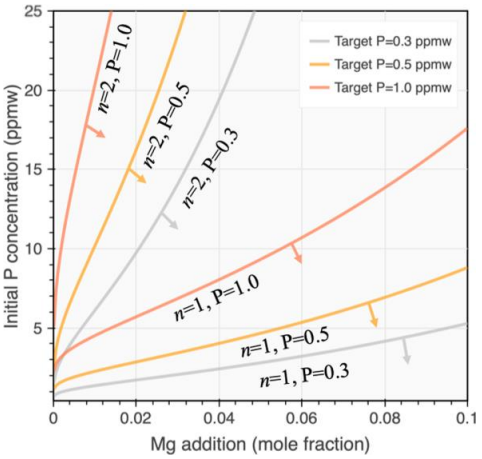

Fig. 13. A chart for the Mg alloying - acid leaching process; the initial P concentration before leaching (vertical axis), the target P concentration (on the curves), and the required Mg amount (horizontal axis) and the required operation times n (on the curves). Regions below the curve indicates the P concentration can be purified to the target level no more than n times.

5. Conclusions

In the present work, MG-Si purification by a combined process of Mg-alloying followed by HCl acid leaching was comprehensively investigated. The main conclusions can be summarized as:

(1) After Mg alloying, impurity-bearing phases were observed embedded inside the Mg_2Si eutectic precipitates and further removed to a large extent after acid leaching. The leaching efficiency of Mg alloyed MG-Si depends on acid concentration with an optimum as 10% HCl.
(2) A two times Mg alloying-leaching process was found able to effectively reduce P concentration from 15.1 ppmw to 0.2 ppmw, which meets the requirement of SoG-Si feedstock production.
(3) Enhancement of P segregation after Mg alloying was confirmed by SIMS mapping and thermodynamic analysis. The interaction coefficient $\varepsilon^{P}_{Mg\ in\ Si}$ was estimated to be −10.8.
(4) A theoretical model was developed for the P segregation of arbitrary low P-containing Si-Me-P alloy systems subjected to acid leaching process. The Si purification degree is dependent on the alloying metal concentration and the interaction coefficient between alloying metal Me to P.
(5) A process model was proposed by establishing the mathematical relationships among initial P concentration, target P concentration after purification, the amount of the alloying metal addition, and alloying-leaching operation times.

CRediT authorship contribution statement

Mengyi Zhu: Investigation, Validation, Visualization, Writing - original draft. **Alexander Azarov:** Investigation. **Eduard Monakhov:** Investigation. **Kai Tang:** Conceptualization. **Jafar Safarian:** Conceptualization, Methodology, Supervision, Project administration, Writing - review & editing.

Declaration of Competing Interest

The authors declare that they have no known competing financial interests or personal relationships that could have appeared to influence the work reported in this paper.

Acknowledgements

This work was performed at NTNU within the Research Centre for Sustainable Solar Cell Technology (FME SuSolTech, project number 257639), co-sponsored by the Norwegian Research Council and industry partners.

Appendix A. Supplementary material

Supplementary data to this article can be found online at https://doi.org/10.1016/j.seppur.2020.116614.

References

[1] A. Murgau, J. Safarian, Solar silicon production through metallurgical route and REC solar advancements, in: Silicon Chem. Sol. Ind. XIV, Svolvær, Norway, 2018, pp. 183–192.
[2] J. Safarian, M. Tangstad, Processes for upgrading metallurgical grade silicon to solar grade silicon, Energy Procedia 20 (2012) 88–97, https://doi.org/10.1016/J.EGYPRO.2012.03.011.
[3] N.P. Tucker, Preparation of high purity silicon, J. Iron Steel Ind. 15 (1927) 412–414.
[4] L.P. Hunt, V.D. Dosaj, J.R. McCormick, L.D. Crossman, Production of solar-grade silicon from purified metallurgical silicon, in: 12th IEEE Photovolt. Spec. Conf., 1976, pp. 125–129.
[5] J. Dietl, Hydrometallurgical purification of metallurgical-grade silicon, Sol. Cells 10 (1983) 145–154, https://doi.org/10.1016/0379-6787(83)90015-7.
[6] I.C. Santos, A.P. Goncalves, C.S. Santos, M. Almeida, M.H. Afonso, M.J. Cruz, Purification of metallurgical grade silicon by acid leaching, Hydrometallurgy 23 (1990) 237–246, https://doi.org/10.4028/www.scientific.net/AMR.418-420.1590.
[7] T.L. Chu, S.S. Chu, Partial purification of metallurgical silicon by acid extraction, J. Electrochem. Soc. 130 (1983) 455, https://doi.org/10.1149/1.2119730.
[8] J.C. Anglézio, C. Servant, F. Dubrous, Characterization of metallurgical grade silicon, J. Mater. Res. 5 (1990) 1894–1899, https://doi.org/10.1557/JMR.1990.1894.
[9] J.C. Anglezio, C. Servant, I. Ansara, Contribution to the experimental and thermodynamic assessment of the Al-Ca-Fe-Si system-I. Al-Ca-Fe, Al-Ca-Si, Al-Fe-Si and Ca-Fe-Si systems, Calphad 18 (1994) 273–309, https://doi.org/10.1016/0364-5916(94)90034-5.
[10] T. Margaria, J. Anglezio, C. Servant, Inlcrmetallic compounds in metallurgical silicon, in: Proc. 6th Int. Ferroalloys Congr., Cape Town, 1992, pp. 209–214.
[11] F. Margarido, J.P. Martins, M.O. Figueiredo, M.H. Bastos, Kinetics of acid leaching refining of an industrial Fe-Si alloy, Hydrometallurgy 34 (1993) 1–11, https://doi.org/10.1016/0304-386X(93)90077-Q.
[12] F. Margarido, M.H. Bastos, M.O. Figueiredo, J.P. Martins, The structural effect on the kinetics of acid leaching refining of Fe-Si alloys, Mater. Chem. Phys. 38 (1994) 342–347, https://doi.org/10.1016/0254-0584(94)90211-9.
[13] T. Yoshikawa, K. Morita, An evolving method for solar-grade silicon production: solvent refining, JOM 64 (2012) 946–951, https://doi.org/10.1007/s11837-012-0371-8.
[14] Y. Li, L. Zhang, Application of Si-based solvents to the purification of metallurgical grade-silicon, Sep. Purif. Rev. (2019) 1–24, https://doi.org/10.1080/15422119.2019.1623253.
[15] J.C. Jie, Q.C. Zou, J.L. Sun, Y.P. Lu, T.M. Wang, T.J. Li, Separation mechanism of the primary Si phase from the hypereutectic Al-Si alloy using a rotating magnetic field during solidification, Acta Mater. 72 (2014) 57–66, https://doi.org/10.1016/j.actamat.2014.03.031.
[16] T. Yoshikawa, K. Morita, Refining of silicon during its solidification from a Si–Al melt, J. Cryst. Growth. 311 (2009) 776–779, https://doi.org/10.1016/J.JCRYSGRO.2008.09.095.
[17] T. Yoshikawa, K. Morita, Refining of Si by the solidification of Si-Al melt with electromagnetic force, ISIJ Int. 45 (2005) 967–971, https://doi.org/10.2355/isijinternational.45.967.
[18] T. Yoshikawa, K. Morita, Removal of phosphorus by the solidification refining with Si-Al melts, Sci. Technol. Adv. Mater. 4 (2003) 531–537, https://doi.org/10.1016/j.stam.2003.12.007.
[19] Y. Li, Y. Tan, J. Li, K. Morita, Si purity control and separation from Si–Al alloy melt with Zn addition, J. Alloys Compd. 611 (2014) 267–272, https://doi.org/10.1016/J.JALLCOM.2014.05.138.
[20] T. Yoshikawa, K. Morita, An evolving method for solar-grade silicon production: solvent refining, n.d. doi: 10.1007/s11837-012-0371-8.
[21] Y. Lei, W. Ma, L. Sun, J. Wu, Y. Dai, K. Morita, Removal of B from Si by Hf addition during Al–Si solvent refining process, Sci. Technol. Adv. Mater. 17 (2016) 12–19, https://doi.org/10.1080/14686996.2016.1140303.
[22] Y. Li, B. Ban, J. Li, T. Zhang, X. Bai, J. Chen, S. Dai, Effect of cooling rate on phosphorus removal during Al-Si solvent refining, Metall. Mater. Trans. B 46 (2015) 542–544, https://doi.org/10.1007/s11663-015-0291-4.
[23] W. Yu, W. Ma, G. Lv, Y. Ren, Y. Dai, K. Morita, Low-cost process for silicon purification with bubble adsorption in Al-Si melt, Metall. Mater. Trans. B 45 (2014) 1573–1578, https://doi.org/10.1007/s11663-014-0050-y.
[24] J. Li, Y. Liu, Y. Tan, Y. Li, L. Zhang, S. Wu, P. Jia, Effect of tin addition on primary

silicon recovery in Si–Al melt during solidification refining of silicon, J. Cryst. Growth 371 (2013) 1–6, https://doi.org/10.1016/J.JCRYSGRO.2012.12.098.
[25] L. Hu, Z. Wang, X. Gong, Z. Guo, H. Zhang, Purification of metallurgical-grade silicon by Sn–Si refining system with calcium addition, Sep. Purif. Technol. 118 (2013) 699–703, https://doi.org/10.1016/J.SEPPUR.2013.08.013.
[26] X. Ma, T. Yoshikawa, K. Morita, Si growth by directional solidification of Si–Sn alloys to produce solar-grade Si, J. Cryst. Growth 377 (2013) 192–196, https://doi.org/10.1016/J.JCRYSGRO.2013.05.024.
[27] X. Ma, Y. Lei, T. Yoshikawa, B. Zhao, K. Morita, Effect of solidification conditions on the silicon growth and refining using Si–Sn melt, J. Cryst. Growth 430 (2015) 98–102, https://doi.org/10.1016/J.JCRYSGRO.2015.08.001.
[28] L. Zhang, Y. Ma, Y. Li, Preparing crystalline silicon from Si-Sn solvent by zone melting directional solidification method, Mater. Sci. Semicond. Process. 71 (2017) 12–19, https://doi.org/10.1016/J.MSSP.2017.06.044.
[29] K. Visnovec, C. Variawa, T. Utigard, A. Mitrašinović, Elimination of impurities from the surface of silicon using hydrochloric and nitric acid, Mater. Sci. Semicond. Process. 16 (2013) 106–110, https://doi.org/10.1016/j.mssp.2012.06.009.
[30] L. Huang, H. Lai, C. Lu, M. Fang, W. Ma, P. Xing, J. Li, X. Luo, Enhancement in extraction of boron and phosphorus from metallurgical grade silicon by copper alloying and aqua regia leaching, Hydrometallurgy 161 (2016) 14–21, https://doi.org/10.1016/j.hydromet.2016.01.013.
[31] L. Huang, A. Danaei, S. Thomas, P. Xing, J. Li, X. Luo, M. Barati, Solvent extraction of phosphorus from Si-Cu refining system with calcium addition, Sep. Purif. Technol. 204 (2018) 205–212, https://doi.org/10.1016/J.SEPPUR.2018.04.087.
[32] L.T. Khajavi, K. Morita, T. Yoshikawa, M. Barati, Removal of boron from silicon by solvent refining using ferrosilicon alloys, Metall. Mater. Trans. B. 46 (2015) 615–620, https://doi.org/10.1007/s11663-014-0236-3.
[33] A. Schei, High purity silicon production, in: Int. Semin. Refin. Alloy. Liq. Alum. Ferro-Alloys, Trondheim, Norway, 1985.
[34] T. Shimpo, T. Yoshikawa, K. Morita, Thermodynamic study of the effect of calcium on removal of phosphorus from silicon by acid leaching treatment, Metall. Mater. Trans. B 35 (2004) 277–284, https://doi.org/10.1007/s11663-004-0029-1.
[35] M.D. Johnston, M. Barati, Calcium and titanium as impurity getter metals in purification of silicon, Sep. Purif. Technol. 107 (2013) 129–134, https://doi.org/10.1016/j.seppur.2013.01.028.
[36] Y.V. Meteleva-Fischer, Y. Yang, R. Boom, B. Kraaijveld, H. Kuntzel, Slag treatment followed by acid leaching as a route to solar-grade silicon, Jom 64 (2012) 957–967, https://doi.org/10.1007/s11837-012-0383-4.
[37] Y.V. Meteleva-Fischer, Y. Yang, R. Boom, B. Kraaijveld, H. Kuntzel, Microstructure of metallurgical grade silicon during alloying refining with calcium, Intermetallics 25 (2012) 9–17, https://doi.org/10.1016/j.intermet.2012.02.009.
[38] Y.V. Meteleva-Fischer, Y. Yang, R. Boom, B. Kraaijveld, H. Kuntzel, Microstructure of metallurgical grade silicon and its acid leaching behaviour by alloying with calcium, Miner. Process. Extr. Metall. 122 (2013) 229–237, https://doi.org/10.1179/0371955313Z.00000000068.
[39] M. Fang, C. Lu, L. Huang, H. Lai, J. Chen, J. Li, W. Ma, P. Xing, X. Luo, Effect of calcium-based slag treatment on hydrometallurgical purification of metallurgical-grade silicon, Ind. Eng. Chem. Res. 53 (2014) 972–979, https://doi.org/10.1021/ie403047m.
[40] Y. Lei, W. Ma, X. Ma, J. Wu, K. Wei, S. Li, K. Morita, Leaching behaviors of impurities in metallurgical-grade silicon with hafnium addition, Hydrometallurgy 169 (2017) 433–439.
[41] Y. Lei, W. Ma, G. Lv, K. Wei, S. Li, K. Morita, Purification of metallurgical-grade silicon using zirconium as an impurity getter, Sep. Purif. Technol. 173 (2017) 364–371, https://doi.org/10.1016/j.seppur.2016.09.051.
[42] S. Espelien, G. Tranell, J. Safarian, Effect of magnesium addition on removal of impurities from silicon by hydrometallurgical treatment, in: Energy Technol. 2017, Springer, 2017, pp. 355–366.
[43] J. Safarian, S. Espelien, Hydrometallurgical purification of maganesium-doped silicon by difference acids, in: 33 Eur. Photovolt. Sol. Energy Conf. Exhib., 2017, pp. 480–482.
[44] M. Zhu, A. Murgau, J. Safarian, Effects of magnesium-doping on silicon leaching for solar grade feedstock production, in: 35th EU PVSEC 2018 Proc., 2018, pp. 465–468. doi: 10.4229/35thEUPVSEC20182018-2AV.1.3.
[45] J. Safarian, M. Tangstad, Vacuum refining of molten silicon, Metall. Mater. Trans. B Process Metall. Mater. Process. Sci. 43 (2012) 1427–1445, https://doi.org/10.1007/s11663-012-9728-1.
[46] A. Hoseinpur, K. Tang, J. Safarian, Kinetic study of vacuum evaporation of elements from ternary melts; case of dilute solution of P in Si-Al melts, Sep. Purif. Technol. 235 (2020), https://doi.org/10.1016/j.seppur.2019.116284.
[47] K. Morita, T. Miki, Thermodynamics of solar-grade-silicon refining, Intermetallics 11 (2003) 1111–1117, https://doi.org/10.1016/S0966-9795(03)00148-1.
[48] F. Fehér, W. Tromm, Die Darstellung von Silanen aus Magnesiumsilicid und Hydrazoniumchlorid in wasserfreiem Hydrazin, Zeitschrift Für Anorg. Und Allg. Chemie. 282 (1955) 29–40, https://doi.org/10.1002/zaac.19552820107.
[49] R. Schwarz, E. Konrad, Über den Reaktionsmechanismus der Silan-Bildung aus Magnesiumsilicid (I.), Berichte Der Dtsch, Chem. Gesellschaft (A B Ser.) 55 (1922) 3242–3252, https://doi.org/10.1002/cber.19220550938.
[50] J. Safarian, L. Kolbeinsen, M. Tangstad, Liquidus of Silicon Binary Systems, Metall. Mater. Trans. B 42 (2011) 852–874, https://doi.org/10.1007/s11663-011-9507-4.
[51] S. Liang, R. Schmid-Fetzer, Modeling of Thermodynamic Properties and Phase Equilibria of the Si-P System, J. Phase Equilibria Diffus. 35 (2014) 24–35, https://doi.org/10.1007/s11669-013-0269-3.
[52] J. Safarian, M. Tangstad, Phase diagram study of the Si-P system in Si-rich region, J. Mater. Res. 26 (2011) 1494–1503, https://doi.org/10.1557/jmr.2011.130.
[53] M.E. Schlesinger, The thermodynamic properties of phosphorus and solid binary phosphides, Chem. Rev. 102 (2002) 4267–4302, https://doi.org/10.1021/cr000039m.
[54] A.I. Zaitsev, N.V. Korolyov, B.M. Mogutnov, Thermodynamic properties of {xCa + (1–x)P}, J. Chem. Thermodyn. 23 (1991) 11–23, https://doi.org/10.1016/S0021-9614(05)80053-9.
[55] Z.V. Dobrokhotova, A.I. Zaitsev, M.A. Zemchenko, A.D. Litvina, B.M. Mogutnov, S.N. Yaschenko, Thermodynamic properties of calcium and barium phosphides, J. Therm. Anal. 38 (1992) 1113–1122, https://doi.org/10.1007/BF01979173.
[56] D. Zhao, Y. Li, Revealing the factors influencing grain boundary segregation of P, As in Si: Insights from first-principles, Acta Mater. 168 (2019) 52–62, https://doi.org/10.1016/J.ACTAMAT.2019.02.014.
[57] S. Liang, P. Wang, R. Schmid-Fetzer, Inherently consistent temperature function for interaction parameters demonstrated for the Mg-Si assessment, Calphad Comput. Coupling Phase Diagrams Thermochem. 54 (2016) 82–96, https://doi.org/10.1016/j.calphad.2016.06.003.
[58] X. Ma, J. Zhang, T. Wang, T. Li, Hydrometallurgical purification of metallurgical grade silicon, Rare Met. 28 (2009) 221–225, https://doi.org/10.1007/s12598-009-0043-1.
[59] S. Liu, K. Huang, H. Zhu, Removal of Fe, B and P impurities by enhanced separation technique from silicon-rich powder of the multi-wire sawing slurry, Chem. Eng. J. 299 (2016) 276–281, https://doi.org/10.1016/J.CEJ.2016.04.081.

Paper 3

ACS Sustainable Chemistry & Engineering

pubs.acs.org/journal/ascecg

Research Article

New Insights into Silicon Purification by Alloying–Leaching Refining: A Comparative Study of Mg–Si, Ca–Si, and Ca–Mg–Si Systems

Mengyi Zhu,* Sheng Ying Yue,* Kai Tang, and Jafar Safarian

Cite This: *ACS Sustainable Chem. Eng.* 2020, 8, 15953–15966

Read Online

ACCESS | Metrics & More | Article Recommendations

ABSTRACT: In the present work, a comparative study of the silicon alloying–leaching purification process was carried out on the recently developed Mg–Si system, the Ca–Si system, and the novel ternary Ca–Mg–Si system. Insights were provided into the integrated process from aspects of thermodynamic assessment, microstructural analysis, experimental observation, computational simulation, and analytical modeling. The main silicide precipitates of the three Mg–Si, Ca–Si, and Ca–Mg–Si alloys studied were determined as Mg_2Si, $CaSi_2$, and ternary $Ca_7Mg_{7.5\pm\delta}Si_{14}$, respectively. Other metallic impurities were found to form complex silicides embedded inside the main precipitate, where P also segregated and precipitated according to the interaction with the alloying elements. All of the impurities were further carried away with the removal of the main precipitates through the subsequent leaching process. It was found that the ternary Ca–Mg–Si alloy exhibits a cleaner leaching process due to the unique crystal structure of $Ca_7Mg_{7.5\pm\delta}Si_{14}$. A novel cracking–shrinking principle-based kinetics model was developed to further describe the impurity removal process. The segregation behavior of P was also modeled through a thermodynamic approach and Ca was found to have stronger P affinity compared to Mg. It was finally concluded that the novel Ca–Mg–Si ternary alloy system exhibited better performance overall as compared to the other two binary alloys.

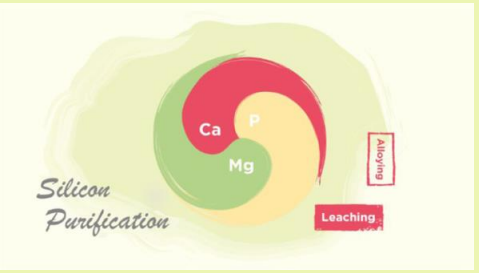

KEYWORDS: *metallurgical-grade silicon, impurities, silicide, purification, acid leaching, kinetics*

INTRODUCTION

The contribution of solar energy to the world's total energy supply has grown significantly in the past two decades. With the rapid photovoltaic market growth and installation of Si-based solar modules worldwide, it has become increasingly critical to develop an environmentally friendly approach for solar-grade silicon (SoG-Si) production.[1] Owing to the low energy consumption and low carbon footprint features, the emerging metallurgical route of SoG-Si production has received increasing attention.[1−3] As one of the recent successfully commercialized processes, the Elkem Solar process, which is operated by REC Solar Norway, is known to purify crude metallurgical-grade Si (MG-Si) through the combination of a series of metallurgical methods of slag refining, acid leaching, and direction solidification. The goal of acid leaching among these methods is to separate nonmetallic impurity P, which is one of the essential impurities in MG-Si needed to meet the strict SoG-Si impurity requirement, and also to remove the majority of metallic impurities at the same time.

The principle of acid leaching is mainly based on the digestion of segregated impurities from silicon grains during Si solidification. Impurities with lower segregation coefficients will precipitate more in the last formed solid phases (precipitates) in solidification due to their strong tendency to stay in the liquid phase. By exposing the solidified silicon to the acid solution, impurities located at grain boundaries of precipitates between the primary silicon grains can be carried away, and pure Si can be obtained. Considerable research has been performed to study the impurity extraction from MG-Si by acid leaching.[4−12] It has been found that most of the metallic impurities can be effectively extracted by adjusting a variety of processing parameters like leaching temperature, time, acid combination, and particle size, but the effective P extraction by direct leaching of MG-Si still remains a challenge. Even though it has been theoretically and experimentally confirmed that P tends to segregate along Si grain boundaries,[13] its segregation coefficient (k_p = 0.35) is still

Received: July 31, 2020
Revised: September 22, 2020
Published: October 13, 2020

Table 1. Impurity Concentrations (ppmw) of the Produced Ca- and Mg-Doped Silicon Alloys

sample	P	Mg	Ca	Al	Fe	Ti	Mn
Mg−Si	5.39	47 022.93	125.10	785.54	1213.10	85.93	23.17
Ca−Mg−Si	5.76	24 549.51	20 847.08	919.85	1264.52	108.04	27.81
Ca−Si	4.64	7.17	35 807.49	845.79	1191.27	94.35	23.49

relatively high compared to metallic impurities, which is usually less than 10^{-3}. To further improve the extraction efficiency of P and other impurities, considerable attention has been paid to redistribute impurities by adding alloying elements as impurity getters such as calcium (Ca),[14−18] magnesium (Mg),[19−23] titanium (Ti),[17] aluminum (Al),[24−29] copper (Cu),[30−33] tin (Sn),[34,35] iron (Fe),[36−38] and nickel (Ni).[39] The widely known solvent refining usually involves alloying by Al, Sn, Cu, and Fe with a large amount of metal addition (around or more than 50 wt %). The low-temperature operation and high impurity removal degree features make the solvent-refining process promising. However, the industrialization process is hampered by the concerns of the potentially high production cost and low Si productivity caused by the need for large metal addition. From this perspective, small alloying metal addition has a better cost-effective feature, but this requires a distinctly strong impurity-gathering ability of the alloying elements.

Alkaline-earth metals are known for their strong affinity to P. Thus, metals in this group are of increasing interest for P removal from MG-Si. Anders[14] doped Ca into MG-Si and found that pure Si can be obtained after acid leaching. Shimpo et al.[15] measured the interaction coefficient of Ca and P in the Ca−Si−P system and observed the formation of Ca_3P_2 along the Si grain boundary. It was also reported that efficient P removal could be achieved by altering the Ca alloying concentration, cooling rate, and leaching conditions.[16−18] Mg is a relatively new alloying impurity getter proposed by the NTNU team in recent years,[19−23] and more knowledge about Mg is needed, in particular for comparison with the Ca−Si alloying−leaching system. In addition, according to the Zintl−Klemm concept,[40] the mixing of Ca and Mg in Si may show a pronounced variation of the electronic structure compared to the binary silicide as a result of unbalanced valence electron transfer. It is believed that the segregation behavior of the impurities and also the leaching process of the Ca−Mg−Si ternary alloying system may differ for both Ca−Si and Mg−Si binary alloying systems. Hence, it is essential to study Si purification by Ca and Mg alloying together.

In this work, a comparative study of Ca−Si, Mg−Si, and Ca−Mg−Si systems is carried out experimentally and theoretically to provide essential insights into MG-Si purification for the whole integrated process including aspects of thermodynamic assessment, alloy microstructure and impurity distribution, acid leaching experiments, kinetics modeling, and purification efficiency evaluation.

METHODOLOGY

Experimental Procedure. The Si sources used in this work are commercial MG-Si (99.5% purity, P: 15 ppmw) and mixed with commercial impurity-free Si produced from the fluidized bed reactor process (FBR-Si) to minimize the influence of other minor impurities in the present study and attain a lower P impurity concentration at several ppmw levels. The MG-Si and FBR-Si mixing ratio was fixed as 40% MG-Si and 60% FBR-Si for all of the alloys. A high-purity Mg rod (99.8% purity, Alfa Aesar) and granular Ca (99% purity, Sigma-Aldrich) were employed as the alloying metal sources, and the initial charging composition of the alloys is 5.2 wt % Mg, 4.2 wt % Ca, and 2.2 wt % Ca−2.6 wt % Mg. Considering the higher volatility of Mg at high temperatures, it was doped into Si after melting, while Ca granulates were directly charged with Si before heating. Thus, about 400 g of Si and Ca granules were first put in a high-density isotropic graphite crucible (inner diameter: 70 mm, height: 150 mm). The crucible was further heated in an induction furnace under a high-purity Ar flow (99.9999% purity) with the chamber pressure maintained at around 1030−1050 mbar. After the samples were fully melted at around 1500 °C, metallic Mg pieces were doped into the molten alloy to form the target Ca−Mg−Si and Mg−Si alloys. The molten alloys were then homogenized through induction stirring for 10 min and cooled down to room temperature. The cooling rate was kept at 20−30 °C/min as faster cooling may suppress impurity segregation, and slower cooling may lead to higher evaporation loss of the volatile alkaline-earth alloying metals. The final composition of obtained bulk alloys is listed in Table 1.

The obtained bulk alloys were crushed by a ring mill (Retsch Vibratory Disc Mill RS200, tungsten carbide sets) into fine particles within the specific particle size range from 0.2 to 1 mm before leaching. Acid leaching was performed by mixing 20 g of particles with 120 mL of reagent-grade 10% HCl (VMR International) in a beaker on a magnetic stirring hot plate, the stirring speed was fixed at 200 rpm, and the leaching temperature was fixed at 60 °C throughout the whole leaching period. Samples were taken at specific leaching times (5, 10, 20, 60, and 180 min). After 3 h leaching, samples were further cleaned by deionized water and ethanol.

The microstructure of the obtained alloys was studied by an electron probe micro-analyzer (EPMA, JXA-8500F) and the precipitate composition was measured by wavelength-dispersive spectroscopy (WDS). The impurity contents were measured by high-resolution inductively coupled plasma mass spectrometry (ICP-MS, Agilent 8800). The particle size distribution (PSD) was measured by a Horiba LA-960 instrument with the laser diffraction method. The refractive index value of pure Si is adopted for the analyzed Si-rich alloy samples as an approximation since the real value remains unknown but should reasonably be close to the value of pure Si. The particle size measurement range of the instrument is 10 nm to 5 mm. It is also worth noting that the particle size measured by laser diffraction is usually larger than the sieving particle size, as it is the diameter of a sphere with the particle's equivalent volume and the sieving particle size is the minimum diameter passing through the sieve aperture.

Computational Methods. The structural and electronic properties of the main precipitate compounds studied, Mg_2Si, $CaSi_2$, and $Ca_7Mg_{7.5\pm\delta}Si_{14}$, are investigated based on density functional theory (DFT) calculations. The crystal structures were fully optimized with the DFT simulation employing the Vienna ab initio simulation package (VASP).[41,42] The projector-augmented wave (PAW) method[43,44] for the pseudopotential, and generalized gradient approximation (GGA) with the Perdew−Burke−Ernzerhof (PBE) exchange−correlation functional are adopted.[45] The van der Waals (vdW)-corrected

https://dx.doi.org/10.1021/acssuschemeng.0c05564
ACS Sustainable Chem. Eng. 2020, 8, 15953−15966

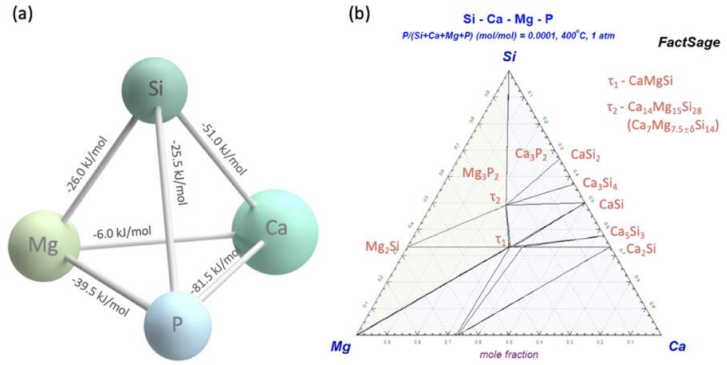

Figure 1. (a) Heat of mixing among the key elements pair in the Si−Ca−Mg−P alloy system shown with the relative atomic radius difference. (b) Modified isothermal section phase diagram of the Si−Ca−Mg−P system with 100 ppm P calculated by Factsage, where the left side shadowed region denotes Mg_3P_2 precipitation and the right-side shadowed region denotes Ca_3P_2 precipitation.

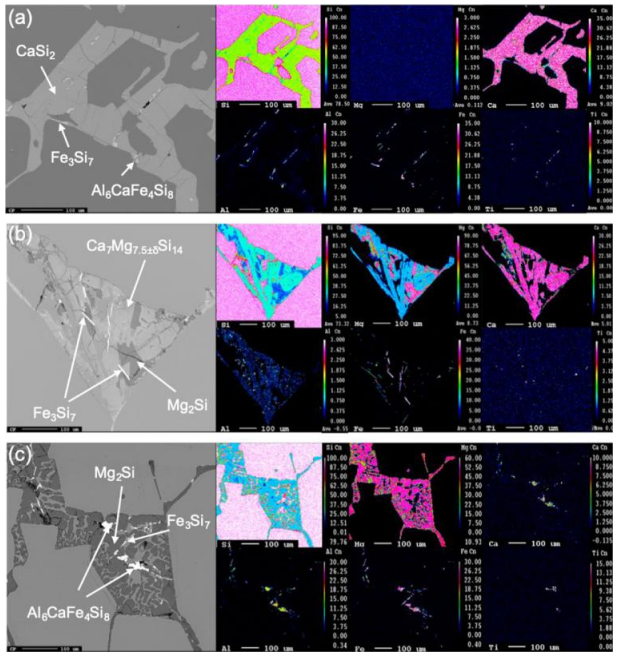

Figure 2. EPMA elemental mapping of the Ca−Si, Ca−Mg−Si, and Mg−Si alloying systems.

optB86b-vdW functional[46,47] was used throughout all of the calculations. The energy cutoff of the plane wave for the pseudopotential was 520 eV for all crystals. The γ-centered k meshes 6 × 6 × 2 were taken for $Ca_7Mg_{7.5\pm\delta}Si_{14}$. The k mesh density and the energy cutoff of augmented plane waves were checked to ensure convergence. The Hellmann−Feynman force tolerance 0.0001 eV/Å was used in all of the optimizations for structures. For the DFT calculations of $Ca_7Mg_{7.5\pm\delta}Si_{14}$, the virtual crystal approximation (VCA) method[48] was adopted employing VASP.

RESULTS AND DISCUSSION

Assessment of the Si−Ca−Mg−P System. Alkaline-earth metals are known for their strong potential to form stable phosphides as M_3P_2, where M denotes a metal.[49] Hints of the strong P affinity of Ca and Mg can also be obtained from the mixing enthalpy calculation via the Miedema model,[50] which

https://dx.doi.org/10.1021/acssuschemeng.0c05564
ACS Sustainable Chem. Eng. 2020, 8, 15953−15966

Table 2. Measured Composition of Major Impurities in Alloyed MG-Si by WDS

		composition (atom %)					
sample	phase	Si	Mg	Ca	Al	Fe	Ti
Ca−Si	$CaSi_2$	65.91	0.01	33.81	0.24	0.02	0.00
	$CaAl_2Si_2$	40.03	0.30	19.79	39.74	0.13	0.01
	$Al_6CaFe_4Si_8$	43.83	0.09	6.93	28.99	20.14	0.02
	Fe_3Si_7	69.01	0.44	0.77	0.70	29.09	0.00
	$TiFeSi_2$	50.66	0.00	1.43	1.25	23.83	22.83
Ca−Mg−Si	$Ca_7Mg_{7.5\pm\delta}Si_{14}$	48.15	26.52	24.13	1.16	0.03	0.00
	Mg_2Si	34.61	65.05	0.17	0.11	0.06	0.00
	Fe_3Si_7	69.94	0.74	0.50	0.47	28.35	0.00
	$TiFeSi_2$	50.78	4.83	1.90	0.42	22.09	19.97
Mg−Si	Mg_2Si	34.51	65.21	0.01	0.23	0.03	0.00
	$Al_6CaFe_4Si_8$	42.78	3.18	5.25	29.04	19.74	0.01
	Fe_3Si_7	70.87	1.18	0.41	0.46	27.09	0.00
	$TiFeSi_2$	50.82	0.93	0.21	1.25	23.91	22.89

provides a semiempirical thermodynamic insight into the cohesion state of atoms. As the calculated results presented in Figure 1a show, the Ca−P and Mg−P pair interactions have the most negative values in the Ca−Si−P and Mg−Si−P subsystems, respectively, which implies the effectiveness of enhanced P extraction employing Ca and Mg as impurity getters. In addition, the negative values of the Ca−Mg−Si subsystems also indicate the formation of the ternary intermetallic of the Ca−Mg−Si alloy system.

To further reassess the phase equilibria of the Ca−Mg−Si−P system, a quaternary phase diagram was constructed using the commercial software Factsage using a reassessed database, as shown in Figure 1b. In the Si-rich corner, P is predicted to exist in the form of Ca_3P_2 and Mg_3P_2, mainly depending on the alloying concentration. In the Mg−Si alloy system, it is seen that only one intermetallic exists in the binary Mg−Si system, where Mg and Si form a eutectic Mg_2Si phase at 57.31 atom % Si. The eutectic temperature is 930 °C, and the Mg_2Si phase melts at temperatures above 1085 °C. The Ca−Si system becomes much more complicated when five Ca-based silicides exist, which also indicates the strong interaction between Ca and Si with each other in the melt and during solidification. In the Si-rich portion, $CaSi_2$ is the only available binary compound in the alloying−leaching approach that is known to form at 1023 °C with a eutectic point at 69.4 atom % Si. Two ternary compounds (τ_1 and τ_2) exist in the Ca−Mg−Si system, according to the study by Gröbner et al.[51] The exact stoichiometry remains controversial for the τ_2 phase as several stoichiometries ($Ca_7Mg_6Si_{14}$,[51,52] $Ca_7Mg_{7.5\pm\delta}Si_{14}$,[53] and $Ca_7Mg_{7.25}Si_{14}$[54]) have been used. Nesper et al.[53] obtained the stoichiometry of $Ca_7Mg_{7.6}Si_{14}$ from single-crystal diffraction measurements, but their simulation yields a composition of $Ca_7Mg_{7.25}Si_{14}$. Thus, the correct stoichiometry is adopted as $Ca_7Mg_{7.5\pm\delta}Si_{14}$, where δ is a measure of insecurity from the X-ray refinement. In our work, the WDS-EPMA measurement also suggests a stoichiometry of $Ca_7Mg_{7.6}Si_{14}$, but both the compositions $Ca_7Mg_6Si_{14}$ and $Ca_7Mg_{7.25}Si_{14}$ lead to a stable crystal structure from DFT calculations. Thus, the stoichiometry of the τ_2 phase presented in our work is still recommended as $Ca_7Mg_{7.5\pm\delta}Si_{14}$.

Microstructure and Impurity Redistribution. Microstructural analysis is crucial for understanding the impurity distribution during the solidification of a silicon alloy. EPMA elemental mapping was conducted for the microstructure of the studied Mg−Si, Ca−Si, and Ca−Mg−Si alloys; the results are presented in Figure 2.

The microstructure of the utilized raw MG-Si has been studied in the authors' previous work,[21−23] where only fine and dispersed Fe-bearing phases were observed in the silicon grains. However, in the alloyed MG-Si, the main precipitates were found to be strongly dependent on the alloying metals and with a thickness of around 100−200 μm after furnace cooling. The detailed compositions of the observed phases are given in Table 2. In the Ca−Si sample, the dominant precipitate phase is observed to be $CaSi_2$, with a small amount of other diversely distributed phases, such as $Al_6CaFe_4Si_8$ and Fe_3Si_7 (known as high-temperature $FeSi_2$, also called $FeSi_{2.4}$ or α-leboite),[55] as well as surrounded by some minor quantity of $CaAl_2Si_2$. Ti impurity was found to only form the ternary $TiFeSi_2$ phase, and no binary $TiSi_2$ phase was observed due to the larger amount of Fe impurity. In the Mg−Si sample, Mg_2Si is found as the main precipitate, and with a typical eutectic morphology, while other Fe-bearing phases like $Al_6CaFe_4Si_8$, Fe_3Si_7, and $TiFeSi_2$ were found embedded inside.

In the Ca−Mg−Si sample, the $Ca_7Mg_{7.5\pm\delta}Si_{14}$ ternary phase was observed as the main precipitate, and a small amount of the Mg_2Si phase was also found to coexist in the sample due to a slight Mg excess. It is also worth noting that the Al impurity found is more like to stay as a solid solution in the $Ca_7Mg_{7.5\pm\delta}Si_{14}$ phase (~1 atom %) rather than forming specific precipitates like the $CaAl_2Si_2$ and $Al_6CaFe_4Si_8$ phases in Ca−Si and Mg−Si alloys. It is also seen that Fe_3Si_7 and $FeTiSi_2$ were found to be the common phases among the Mg−Si, Ca−Si, and Ca−Mg−Si alloys, which may imply the partial substitution effect of transition metals during the solidification of Si.

The evolution of impurity redistribution was further determined by equilibrium computation by Factsage using a reassessed database shown in Figure 3. Since the temperature effect caused by the recalescence of the small amount of precipitates can be ignored, the impurity solidification sequence can be subsequently examined as well. It is seen that the primary Si is always the first nucleate phase, followed by a series of eutectic reactions that take place in the temperature range between 800 and 1000 °C, while the remaining liquid phase percentage is around 10%. The calculated main precipitates ($CaSi_2$, $Ca_7Mg_{7.5\pm\delta}Si_{14}$, Mg_2Si) in each sample also show good consistency with the EPMA results, and P suggested as the form of Ca_3P_2 and Mg_3P_2, which is dependent on the doping metal concentration. However, since their amounts are too little to detect, this cannot be confirmed by the EPMA results in this work. The Fe-bearing phases are calculated as the first

https://dx.doi.org/10.1021/acssuschemeng.0c05564
ACS Sustainable Chem. Eng. 2020, 8, 15953−15966

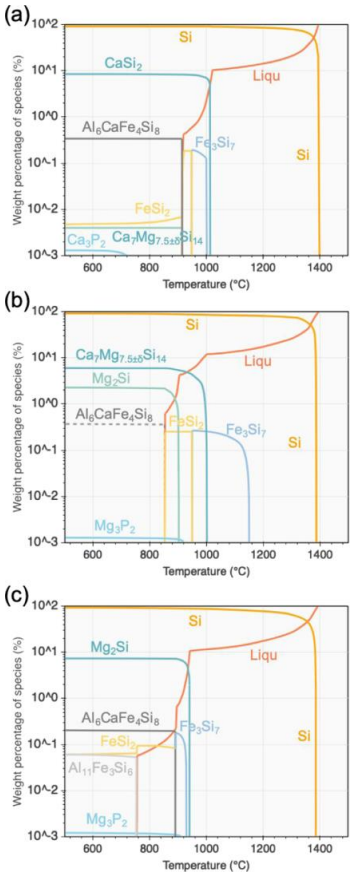

Figure 3. Calculated precipitated phase fraction and solidification sequence with the composition of studied alloys (a) Ca−Si, (b) Ca−Mg−Si, and (c) Mg−Si.

precipitated phases of minor impurity, and undergo a solid transition from the high-temperature phase Fe_3Si_7 to the low-temperature phase $FeSi_2$ via the equilibrium

$$Fe_3Si_7 \rightarrow 3FeSi_2 + Si \quad (1)$$

Since no $FeSi_2$ phase is detected in our work, it may indicate that the decomposition kinetics is slow. Al-bearing phases are suggested to form at the end of solidification. The $CaAl_2Si_2$ phase observed in the Ca−Si alloy sample is not presented in Figure 3a, which may be owing to the following reaction[56]

$$9CaAl_2Si_2 + 4Fe_3Si_7 \rightarrow 3Al_6CaFe_4Si_8 + 6CaSi_2 + 10Si \quad (2)$$

The above reactions may also explain why the observed $CaAl_2Si_2$, $Al_6CaFe_4Si_8$, and the Fe_3Si_7 phases in the Ca−Si alloy sample are often located close to each other. Nevertheless, $Al_6CaFe_4Si_8$ precipitation was not found in the Ca−Mg−Si sample; instead, Al was found as a solid solution in the $Ca_7Mg_{7.5\pm\delta}Si_{14}$ phase. Thus, the calculated precipitation of the quaternary phase in Figure 3b is marked as a dashed line.

Leaching Phenomena and Mechanism. In the initial leaching stage of all of the studied alloys, heterogeneous exothermic reactions took place rapidly along with the formation of a large number of gas bubbles. Different leaching phenomena were observed in the studied alloys, as shown in Figure 4. In the leaching of the Ca−Si sample, a yellow-green color byproduct named siloxene was formed, which is foamy and floating over the surface. Consequently, foaming bubbles were observed on top of the solution as shown in Figure 4a. In the leaching of the Mg−Si sample, intensive sparks were observed above the solution surface. Obvious minor residue (fine solid particles) can be seen in Figure 4b. Unlike the leaching of Ca−Si and Mg−Si samples, neither viscous siloxane nor intensive sparks were observed in the leaching of the Ca−Mg−Si sample, shown in Figure 4c, which makes the leaching of the Ca−Mg−Si system a cleaner process.

Leaching Mechanism. To further understand the leaching mechanism, the crystal structure and electronic characteristics of the main precipitates were investigated. The perspective views on crystal structures, Brillouin zone shape, and the band structure of $CaSi_2$, $Ca_7Mg_{7.5\pm\delta}Si_{14}$, and Mg_2Si along [001] are presented in Figure 5a−f, respectively. The differences between the three compounds are also listed in Table 3.

The formation of the foamy siloxene and massive amounts of hydrogen is the main feature of $CaSi_2$ leaching. The total leaching reaction corresponds to

$$(CaSi_2)_n + 2n\mathrm{HCl} + xnH_2O \rightarrow (Si_2H_{2-x}(OH)_x)_n + n\mathrm{CaCl}_2 + xnH_2\,(g) \qquad (0 \le x \le 2) \quad (3)$$

where the parameter x indicates the hydrolysis degree during the leaching process and usually equals to 1.[57] As the crystal structure of $CaSi_2$ presented in Figure 5a shows, the Ca^{2+} cations formed a planar layer and were sandwiched between the

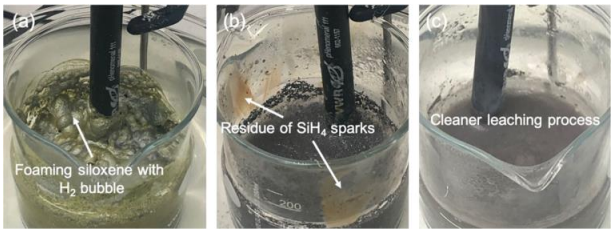

Figure 4. Top view of the solution surface after 10 min HCl leaching at 60 °C (a) Ca−Si, (b) Mg−Si, and (c) Ca−Mg−Si.

https://dx.doi.org/10.1021/acssuschemeng.0c05564
ACS Sustainable Chem. Eng. 2020, 8, 15953−15966

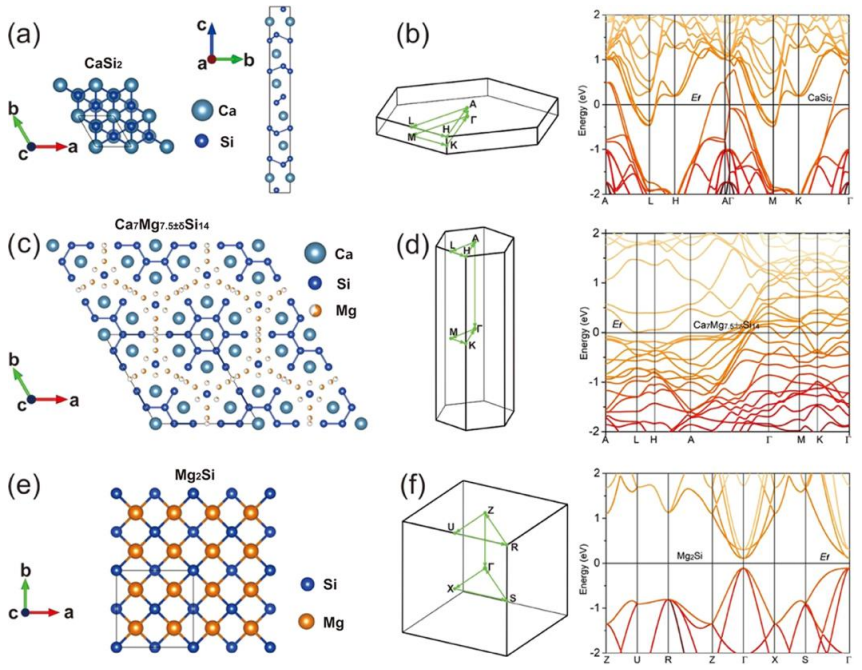

Figure 5. Crystal structure, Brillouin zone shape, and band structure of the main precipitates at the Si-rich portion in the Ca−Mg−Si system obtained by DFT calculations.

Table 3. Crystal Structure Information of the Main Precipitates of Si-rich Ca−Si, Mg−Si, and Ca−Mg−Si Alloys

compound	crystal system	space group	electrical classification
$CaSi_2$	trigonal	$R\bar{3}m$ (No.166)	metallic
Mg_2Si	cubic	$Fm\bar{3}m$ (No. 255)	semiconducting
$Ca_7Mg_{7.5\pm\delta}Si_{14}$	hexagonal	$P6/mmm$ (No.191)	metallic

corrugated Si double-anion layer. As a result, the Ca^{2+} cation layer will be replaced by the −OH and −H ions in a HCl aqueous solution, while the Si−Si bond remains unchanged. Subsequently, the siloxene forms with an intense visible luminescence, which is owing to its unique band structure.[58] The formed siloxene is water-soluble but leads to a more viscous solution and increases the difficulty of the post-cleaning procedure.

The leaching of Mg_2Si in a HCl aqueous solution is known to yield silane gas, which further combusts on exposure to air at the surface. The main reaction of Mg−Si alloy leaching is briefly written as

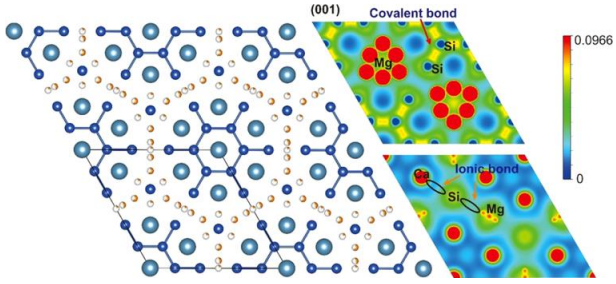

Figure 6. Charge density in the space of $Ca_7Mg_{7.5\pm\delta}Si_{14}$. The specific two-dimensional (2D)-slice projections are chosen to present the covalent and ionic bonds in $Ca_7Mg_{7.5\pm\delta}Si_{14}$. The color bar indicates the intensity of the electron charge density. The high and low values represent the positive and negative charges in space, respectively.

https://dx.doi.org/10.1021/acssuschemeng.0c05564
ACS Sustainable Chem. Eng. 2020, 8, 15953−15966

$$Mg_2Si + 4HCl \rightarrow 2MgCl_2 + SiH_4(g) \quad (4)$$

As a half-silicide, Mg_2Si has a face-centered anti-CaF_2-type structure, as shown in Figure 5e, where the Mg−Si bond shows a mixed ionic and covalent nature.[59] The silane formation is thus proposed to be related to the violent breakage of the Mg−Si bonds of the isolated Si^{4-} by an acidic hydrolysis reaction. The reaction kinetics has been found to be dependent on the acid concentration in our previous work.[23] Moreover, the yield of silane gas is reported to increase with increasing temperature and acid concentration in a dilute HCl aqueous solution.[60]

The leaching mechanism of $Ca_7Mg_{7.5\pm\delta}Si_{14}$ has barely been studied so far. To the best of the authors' knowledge, only Nesper et al.[53] reported that it reacts with mineral acids with the formation of silane gas and amorphous Si. According to the experimental observations in our work, a massive gas bubble formed but with much fewer sparks compared to the leaching of the Mg−Si alloy system, and there is also no siloxene formation. Apparently, this unusual leaching behavior of $Ca_7Mg_{7.5\pm\delta}Si_{14}$ is attributed to its unique crystal structure.[53] As shown in Figure 5c, $Ca_7Mg_{7.5\pm\delta}Si_{14}$ has a highly anisotropic hexagonal crystal structure. Two types of Si atoms can be found in the unit cell: the Si_{12} planar ring type with a Ca atom in between and the isolated Si type that is coordinated by Mg atoms. The band structure obtained by DFT calculations also suggests that it is a metallic compound. Since hydrogen evolution in an acidic solution is a common phenomenon for a number of metallic silicides,[61] it is also reasonable that the generated massive gas is hydrogen. To further characterize the electronic bonding structures of $Ca_7Mg_{7.5\pm\delta}Si_{14}$, we present the atomic bonding styles via the spatial charge density in Figure 6, which is based on the jellium electron gas model. The bonding behavior of $Ca_7Mg_{7.5\pm\delta}Si_{14}$ is also strongly anisotropic with the mixing of covalent, ionic bonding features. It is also seen that in the Si_{12} planar ring, Si has a smaller charge than the isolated Si surrounded by Mg. Thus, the stoichiometry of $Ca_7Mg_{7.5\pm\delta}Si_{14}$ can also be written as $(Ca_7Mg_{7.5\pm\delta})[Si_{12}](Si_2)$.

According to the above discussion, the leaching reaction of $Ca_7Mg_{7.5\pm\delta}Si_{14}$ is, therefore, suggested to be

$$Ca_7Mg_{7.5\pm\delta}Si_{14} + (29 + 2\delta)HCl \rightarrow 7CaCl_2 + (7.5 \pm \delta)MgCl_2 + xSiH_4(g) + (14.5 - 2x)H_2(g) + (14 - x)Si \quad (0 \le x \le 7.25) \quad (5)$$

where x is close to the side of more H_2 formation and supposed to be 2 according to the stoichiometry $(Ca_7Mg_{7.5})[Si_{12}](Si_2)$.

Cracking Effect and Si Recovery. As shown in Figure 7a−c, the particle size of all studied samples decreases considerably after leaching, especially for the leaching of Ca−Si and Ca−Mg−Si samples, such that after shrinkage the size is almost half of the original size. It is apparent that strong cracking effects occurred during leaching and seem to be closely related to the Ca concentration. By directly comparing the particle size distribution after leaching, as shown in Figure 7d, it is found that the cracking effect follows the trend Mg−Si sample < Ca−Mg−Si sample < Ca−Si sample. As a result of the cracking, the particles are more open, and accordingly, more surface is exposed to the acid solution so that it significantly accelerates the reaction progression.

Another parameter strongly related to the cracking effect is Si recovery, which is also crucial for the purification process evaluation. Its value was measured by comparing the sample weight before and after leaching, shown in Figure 8. A distinct

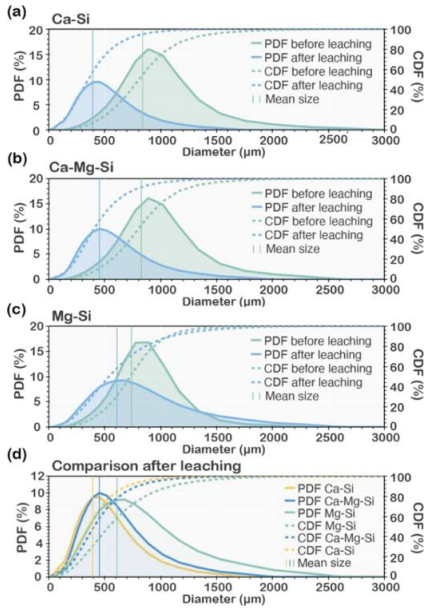

Figure 7. Particle size distribution of Si alloys before and after leaching (PDF is the probability density function, CDF is the cumulative density function): (a) Ca−Si, (b) Mg−Si, (c) Ca−Mg−Si, and (d) comparison of particle size distribution after leaching.

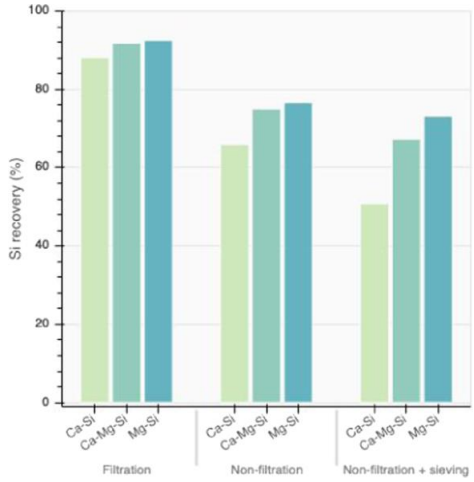

Figure 8. Comparison of Si recovery in the Ca−Si, Ca−Mg−Si, and Mg−Si systems under conditions of filtration, nonfiltration, and 0.2 mm mesh sieving after nonfiltration.

trend can be seen where the filtration method shows the highest Si recovery systematically, followed by nonfiltration (direct pouring of the solution after leaching). The nonfiltration process

https://dx.doi.org/10.1021/acssuschemeng.0c05564
ACS Sustainable Chem. Eng. 2020, 8, 15953−15966

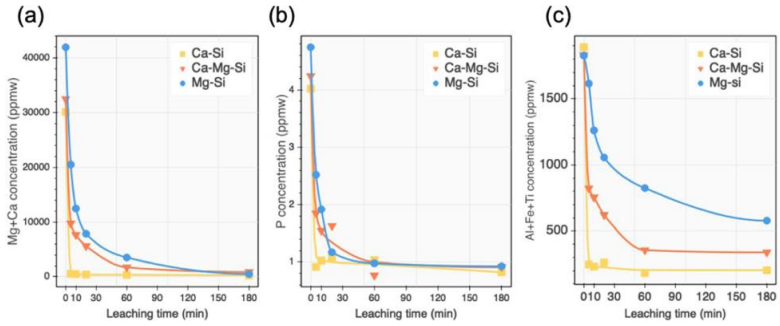

Figure 9. Effect of leaching time on the remaining impurity (a) removal of Mg + Ca, (b) removal of P, and (c) removal of Al + Fe + Ti.

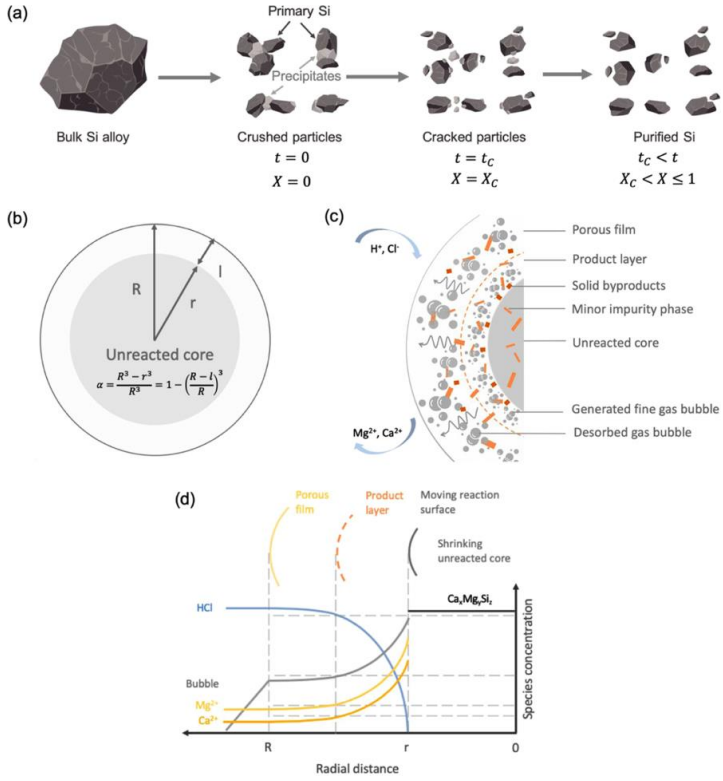

Figure 10. Illustration of the proposed cracking−shrinking model (a) representation of the entire impurity extraction process of the main stages, (b) representation of the extent of impurity conversion during the shrinking stage as a spherical particle, (c) sketch of the leaching mechanism with heterogeneous byproducts and a shrinking unreacted core, and (d) concentration profile with different radial distances.

with additional sieving obtains the least recovery, which further removes insoluble fine particles that are concentrated on the impurities. For the leached samples, the Si recovery rate exhibits the sequence Mg−Si sample > Ca−Mg−Si sample > Ca−Si sample, especially when the fine particles with a diameter smaller than 0.2 mm are sieved out. This is attributed to the increase in particle cracking with increasing Ca content, as shown in Figure 7. Consequently, the generated ultrafine particles were easily lost due to the buoyancy and hydrodynamic thrust in the post-cleaning and washing process, and most of them were sieved out after drying. Thus, the lowest recovery of Si was observed in the

https://dx.doi.org/10.1021/acssuschemeng.0c05564
ACS Sustainable Chem. Eng. 2020, 8, 15953−15966

Ca−Si system, and only 50.8% purified Si was obtained from the Ca−Si alloy after sieving out the fine particles.

Leaching Kinetics. The results of the concentration measurements of the remaining impurities in the three leached alloys at different times are shown in Figure 9. It can be distinctly seen that the Ca−Si leaching displays the fastest kinetics, where most of the impurities were removed in around 10 min. Meanwhile, for the leaching of Ca−Mg−Si and Mg−Si alloys, even though for both of them the P removal shows similar efficiency, in general, impurity removal kinetics in the Ca−Mg−Si alloys is faster than that in the Mg−Si alloys, especially for the removal kinetics of Al, Fe, and Ti impurities. In fact, leaching kinetics is mainly affected by the properties of the main precipitated silicide. As shown in Figure 2, although the size of the main precipitates is similar, significant morphology differences can be observed in the Mg−Si sample. The complex two-phase eutectic pattern may impede the acid attack and suppress the cracking effect during leaching.

As one of the most important factors that affect the kinetics, the cracking of particles has been widely reported in the literature for several Si-rich alloys, such as the Fe−Si,[38,62] Ca−Si,[63] and Cu−Si[30] systems. Margarido et al.[38,64] proposed a cracking−shrinking model to describe the kinetics of Fe−Si leaching. It was also found that this model works for the leaching of the slag-treated Ca−Si alloy system as well. In the aqua regia leaching of Cu−Si briquettes by Huang et al.,[30] a modified shrinking mechanism controlled by both interfacial transfer and product layer diffusion was observed after cracking. However, in the present work, neither the mentioned models nor other commonly used and reviewed models[65] can be adopted to fit our leaching results. Thus, a novel cracking−shrinking model was developed to describe the leaching behavior of Mg−Si and Ca−Mg−Si alloys.

Modeling Assumptions. To simplify the problem, the purification process is assumed to take place in two separate stages, a leaching−cracking stage and a leaching−shrinking stage, as shown in Figure 10a. The total impurity conversion during the leaching−cracking stage is summarized as X_c. The time period of the leaching−cracking stage is set as t_c, which mainly depends on the alloy composition. More details are described below.

- Leaching−cracking stage: at $t = 0$, acid leaching starts with a total impurity conversion $X = 0$, precipitates start to be attacked by chemicals, while the microcracks keep propagating; it is worth noting that when the cracking finishes at $t = t_c$, the leaching−shrinking stage starts with the conversion $X = X_c$.
- Leaching−shrinking stage: from $t \geq t_c$, to the end of leaching, the core shrinking stage follows the kinetic model. The total impurity conversion at this stage varies as $X_c < X \leq 1$, while the impurity conversion in the shrinking stage is specifically denoted as α, which can be seen in Figure 10b, and is described later in Modeling Approach.

Figure 10c illustrates the heterogeneous reaction that occurs during the leaching−shrinking stage. A large number of gas bubbles form at the reaction surface, and particularly in the early shrinking stage. It is assumed that a product layer is formed due to the massive outspreading bubbles and also some solid byproducts. Therefore, the diffusion of acidic species is significantly limited. Meanwhile, the growing bubble also forms a bubble−liquid film, which also inhibits the diffusion process. Consequently, the concentration gradient is formed, as can be seen from Figure 10d.

Modeling Approach. In the shrinking stage, impurity conversion is defined as

$$\alpha = \frac{X - X_C}{1 - X_C} \tag{6}$$

where X is the measured impurity removal degree and α is the fraction conversion during shrinking. Considering a layer of the leachable phase around the Si grain particle (Figure 10b), the geometric relationship of the impurity removal degree can be written as

$$\alpha = \frac{R^3 - r^3}{R^3} = 1 - \left(\frac{r}{R}\right)^3 = 1 - \left(\frac{R - l}{R}\right)^3 \tag{7}$$

where R and r indicate the initial radius and unreacted radius of particles in the shrinking stage, respectively, and l indicates the thickness of the reacted eutectic phase in radial dimensions, which is a reacted shell.

Rearranging eq 7, we obtain

$$\left(\frac{R - l}{R}\right)^3 = 1 - \alpha \tag{8}$$

$$l = R[1 - (1 - \alpha)^{1/3}] \tag{9}$$

As described before, the massive erupted gas bubble actively suppresses the diffusion and reveals time-dependent characteristics. Several fluid−solid kinetic models were tested, and it was found that the product layer assumption of the Kröger−Ziegler model[65−67] fits our case. In this case, the growth rate of the product layer is inversely proportional to its thickness and time, which can be expressed as

$$\frac{dl}{dt} = \frac{k}{lt} \tag{10}$$

where k is a constant that incorporates physical and chemical parameters. However, it is known that the Kröger−Ziegler model is directly modified from the original Jander model,[68,69] where both are based on the assumption of a constant reaction surface. Nevertheless, for a shrinking particle in our case, the surface curvature should be considered since the reaction area is not constant anymore and keeps decreasing.[69−71] Thus, in the current model, the approach of the Ginstling−Brounshtein model[69−71] is introduced to describe the shrinking of spherical particles under spherical coordinates

$$\frac{dl}{dt} = \left(\frac{R}{l(R - l)}\right)\frac{k}{6t} \tag{11}$$

Integrating eq 11 by considering the boundary conditions gives

$$\int_0^l \frac{l(R - l)}{6R} dl = \int_{t_c}^t k\frac{1}{t} dt \tag{12}$$

It yields

$$l^2\left(\frac{2l}{R} - 3\right) = k \ln\left(\frac{t}{t_c}\right) \tag{13}$$

Combining eqs 9 and 13, we then obtain the following shrinking shell model equation

https://dx.doi.org/10.1021/acssuschemeng.0c05564
ACS Sustainable Chem. Eng. 2020, 8, 15953−15966

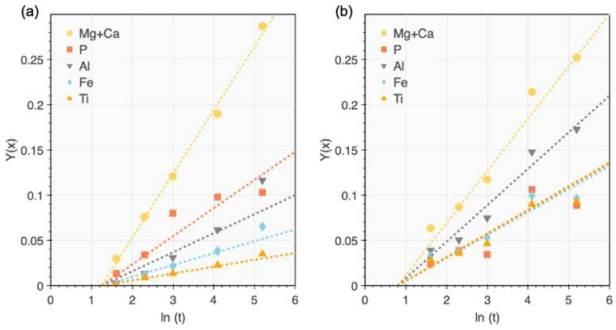

Figure 11. Application of the present cracking−shrinking shell model to the leaching of impurities with 10% HCl at 60 °C under magnetic stirring of (a) Mg−Si and (b) Ca−Mg−Si alloys.

Table 4. Obtained Fitting Parameters of Impurity Elimination from Mg−Si and Ca−Mg−Si Alloys by Leaching

	Mg−Si					Ca−Mg−Si				
impurity	ln (t_c) (min)	X_c	ξ	K_C (min^{-1})	K_S	ln (t_c) (min)	X_c	ξ	K_C (min^{-1})	K_S
Mg + Ca	1.25	0.1	1.0	0.029	0.071	0.8	0.2	1.0	0.246	0.058
P			0.8	0.023	0.031			0.6	0.147	0.026
Al			0.1	0.003	0.021			0.6	0.147	0.040
Fe			0.05	0.001	0.013			0.6	0.147	0.025
Ti			0.05	0.001	0.008			0.6	0.147	0.026

$$1 - \frac{2}{3}\alpha - (1-\alpha)^{2/3} = \frac{2k}{R^2}\ln\left(\frac{t}{t_c}\right) \qquad (t \geq t_c) \tag{14}$$

Finally, after introducing the cracking term and let $K_S = \frac{2k}{R^2}$ The model becomes

$$1 - \frac{2}{3}\left(\frac{X - X_C}{1 - X_C}\right) - \left(1 - \left(\frac{X - X_C}{1 - X_C}\right)\right)^{2/3} = K_S \ln\left(\frac{t}{t_c}\right) \qquad (t \geq t_c) \tag{15}$$

Since the conversion rate for different impurities is different, the value of X_C for each impurity should be different. For instance, the conversion of Ca and Mg was observed to be the most rapid, but the conversion of Fe and Ti was much slower. Herein, a term $\xi_i \in [0, 1]$ is introduced to evaluate the impurity i removal extent in connection with the Ca and Mg silicide conversions. Therefore, $\xi_{Mg+Ca} = 1$ is defined as the benchmark. Subsequently, the total conversion of impurities in the cracking stage can be expressed as $X_{i,c} = \xi_i X_c^{Mg+Ca}$. Hence, a more general expression of the derived kinetics model is rewritten as

$$1 - \frac{2}{3}\left(\frac{X_i - \xi_i X_c^{Mg+Ca}}{1 - \xi_i X_c^{Mg+Ca}}\right) - \left(1 - \left(\frac{X_i - \xi_i X_c^{Mg+Ca}}{1 - \xi_i X_c^{Mg+Ca}}\right)\right)^{2/3} = K_S \ln\left(\frac{t}{t_c}\right) \qquad (t \geq t_c) \tag{16}$$

It can be seen that when $t = t_c$, we have $X_i = X_{i,C} = \xi_i X_c^{Mg+Ca}$; subsequently, the term $\frac{X_i - \xi_i X_c^{Mg+Ca}}{1 - \xi_i X_c^{Mg+Ca}}$ becomes zero. If the cracking effect can be ignored as $X_c^{Mg+Ca} = 0$, the left-hand side equation is then reduced to the Ginstling−Brounshtein model. Thus, the developed model merges the features of the Ginstling−Brounshtein model and the Kröger−Ziegler model. In addition, some drawbacks in the original Kröger−Ziegler model are overcome in the present modification. For instance, the original mathematic singularity issue of the term $\ln(t)$ no longer exists. The sign paradox between $0 < t < 1$ and $1 < t$ is also avoided. Furthermore, the effect integration constant is also ruled out through definite integration in eq 12. Nevertheless, the cost of this modification is that the total rate constant is split into two parts: the cracking stage rate constant K_C and the shrinking stage rate constant K_S. As a result, the two rate constants should be considered together to compare the overall kinetics of different impurities or of different materials.

Model Evaluation. Based on the developed model above, a series of calculations were carried out to evaluate it. It is also worth noting that special modification should be applied to P prior to the calculations because of its relatively high segregation coefficient, which makes a part of P remain in Si grains and theoretically is not involved in the conversion process. Thus, the modified P conversion is expressed as

$$X_P = \frac{\eta N_{bulk} - N_t}{\eta N_{bulk}} \tag{17}$$

where N_{bulk} is the measured P concentration in bulk material and N_t is the measured P concentration at leaching time t. η is the percentage of P that segregated outside Si; ηN_{bulk} also indicates the effective concentration of P that takes part in the leaching process.

In the calculation, η is set as 0.85 approximately for both alloys based on the P segregation model in the Si alloy.[23] Since the error range is quite narrow for η, the impact on the calculation accuracy can be ignored. As shown in Figure 11, by fitting the experimental data of Mg−Si and Mg−Ca−Si alloys, a linear relationship is observed by setting $Y(X_i) = 1 - \frac{2}{3}\left(\frac{X_i - \xi_i X_c^{Mg+Ca}}{1 - \xi_i X_c^{Mg+Ca}}\right) - \left(1 - \left(\frac{X_i - \xi_i X_c^{Mg+Ca}}{1 - \xi_i X_c^{Mg+Ca}}\right)\right)^{2/3}$, and all origins from the same starting time, which is the cracking time. The

https://dx.doi.org/10.1021/acssuschemeng.0c05564
ACS Sustainable Chem. Eng. 2020, 8, 15953−15966

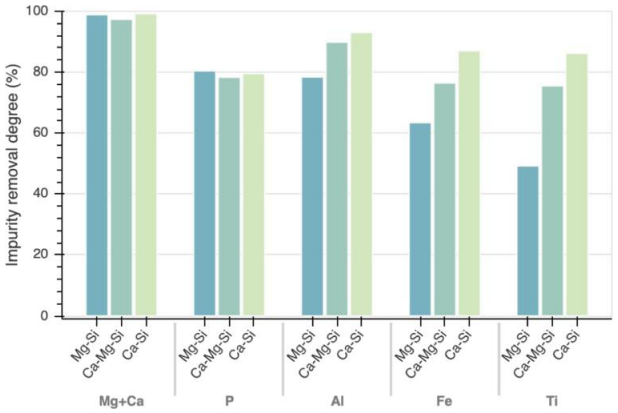

Figure 12. Comparison of impurity removal degree of the Mg−Si, Ca−Si, and Ca−Mg−Si alloying systems after 3 h acid leaching by 10% HCl at 60 °C under magnetic stirring.

fitting parameters are listed in Table 4, where K_C is calculated by $K_{i,C} = \frac{\varepsilon_i Y_c^{Mg+Ca}}{t_c}$. It can be seen from Table 4 that t_c in Mg−Si is longer than that in the Ca−Mg−Si alloy accompanied by a minor value of X_C, which reflects a more intense cracking effect for the leaching of the Ca−Mg−Si alloy.

Impurity Removal. *Overall Impurity Removal Degree.* The impurity removal degree is calculated as

$$\text{removal degree } (\%) = \frac{C_{\text{initial}} - C_{\text{final}}}{C_{\text{initial}}} \times 100 \tag{18}$$

where C_{initial} and C_{final} represent the impurity concentrations of leaching particles before and after leaching, respectively.

Ca and Mg can be nearly completely removed from all of the alloys by leaching as shown in Figure 12, while for the removal of other metallic impurities like Al, Fe, and Ti, the following order is determined: Ca−Si sample > Ca−Mg−Si sample > Mg−Si sample. The P removal degree of the investigated systems is similar and close to 80% under the applied leaching conditions. Thus, it is considered that the P removal of the three studied alloys is at an equivalent level since the differences are insignificant to distinguish, and it is necessary to consider a certain level of uncertainty when dealing with trace amounts of impurity. However, it is worth noting that this equivalent P removal degree is reached by different Ca and Mg alloying amounts. By comparing the required alloying concentration for the equivalent P removal, as presented in Figure 13, it can be seen that more Mg addition is required than Ca based on both molar and weight percentage. Consequently, with a fixed total alloying amount, the P removal efficiency from high to low should follow the trend Ca addition > Ca−Mg addition > Mg addition. Further theoretical comparison of the efficiency of alloying elements is described in the following section through thermodynamic calculations.

P Segregation Coefficient. Impurity elements are subject to solid/liquid segregation during the Si alloy solidification when the liquid alloy is solidified between the liquidus and eutectic temperatures. Knowledge of how the alloying metals affect the impurity segregation ratio is necessary to have a better understanding of the impurity removal by the alloying−leaching

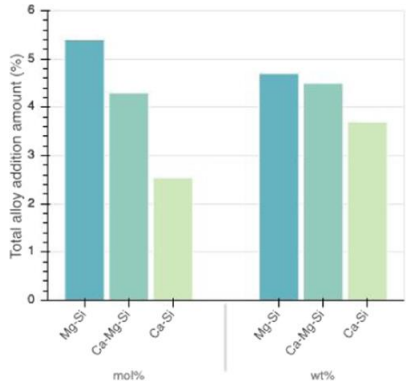

Figure 13. Comparison of required alloy addition amount for around 80% P removal.

approach. In the Ca−Mg−Si alloying system, the segregation coefficient of P between solidified Si grains and the remaining liquid can be expressed as

$$k_P^{\text{Ca-Mg-Si}} = \frac{X_{\text{P in Si(s)}}}{X_{\text{P in Ca-Mg-Si(l)}}} \tag{19}$$

where $X_{\text{P in Si(s)}}$ and $X_{\text{P in Ca-Mg-Si(l)}}$ are the P concentrations in solid primary Si and the remaining Ca−Mg−Si alloy melt, respectively, during the solidification. While the system is under an equilibrium state, the chemical potential of P in the coexisting solid and liquid phases is the same. Assuming that the dissolution energy difference of P in liquid Si and the liquid Si-rich alloy is insignificant due to the ultralow P concentration, and considering the negligible amount of metallic impurities in the solid Si, one obtains

$$\frac{X_{\text{P in Si(s)}}}{X_{\text{P in Ca-Mg-Si(l)}}} = \frac{\gamma_{\text{P in Ca-Mg-Si(l)}}}{\gamma^0_{\text{P in Si(s)}}} \tag{20}$$

https://dx.doi.org/10.1021/acssuschemeng.0c05564
ACS Sustainable Chem. Eng. 2020, 8, 15953−15966

where $\gamma_{P\ in\ Ca-Mg-Si(l)}$ and $\gamma^0_{P\ in\ Si(s)}$ are the activity coefficients of P in the Ca−Mg−Si melt and in primary Si, respectively. In addition, the activity coefficient of P in the Ca−Mg−Si melt can be further reasonably written in terms of the first-order interaction coefficient terms, as expressed by Bale and Pelton[72]

$$\ln \gamma_{P\ in\ Ca-Mg-Si(l)} = \ln \gamma^0_{P\ in\ Si(l)} + \ln \gamma_{Si(l)} + \varepsilon^P_{P\ in\ Si} X_{P\ in\ Si(l)} + \varepsilon^P_{Mg\ in\ Si} X_{Mg\ in\ Si(l)} + \varepsilon^P_{Ca\ in\ Si} X_{Ca\ in\ Si(l)} \quad (21)$$

Neglecting the self-interaction term of P due to its sufficiently low content, and also $\ln \gamma_{Si(l)} \approx 0$, eq 22 can be derived by combining eqs 19 and 21

$$k_P^{Ca-Mg-Si} = \exp(\varepsilon^P_{Mg\ in\ Si} X_{Mg\ in\ Si(l)} + \varepsilon^P_{Ca\ in\ Si} X_{Ca\ in\ Si(l)}) \quad (22)$$

It can be seen that the P segregation coefficient in its dilute solutions in Si is mainly influenced by the alloyed Mg and Ca concentrations and their interaction coefficient value with P. The averaged value of $\varepsilon^P_{Mg\ in\ Si}$ during the solidification of the Mg−Si system was estimated to be −10.8 in our previous work,[23] and the value of $\varepsilon^P_{Ca\ in\ Si}$ at 1450 °C was determined to be −14.6(±1.7) according to Shimpo et al.[15] Thus, if we assume that the averaged value of $\varepsilon^P_{Ca\ in\ Si}$ during the whole solidification range is equivalent to −14.6, reasonably, it can be expected that Ca leads to more reduction of the P segregation coefficient than that of Mg with the same amount.

Figure 14 is plotted to investigate further the effect of Ca and Mg alloying on the P segregation behavior, and the isocurve of

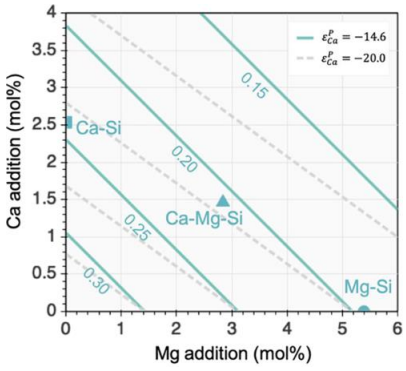

Figure 14. Calculated isocurves of the P segregation coefficient with varying Ca and Mg additions for different ε^P_{Ca} values; symbols show the experimental compositional locations of the studied alloys.

the P segregation coefficient with varying alloying concentrations is also shown as the solid lines. The P segregation coefficient is seen to decrease distinctly with increasing concentrations of Ca and Mg components. Meanwhile, it also follows the trend Ca−Si sample < Ca−Mg−Si sample < Mg−Si sample. However, since the leaching results suggest that the studied alloys show almost equivalent P removal, several reasons may be attributed to this inconsistency. First, the stronger cracking effect of the Ca−Si system may promote the P removal. Second, the averaged value of $\varepsilon^P_{Ca\ in\ Si}$ during the whole solidification range might be more negative than the measured value at 1450 °C. To investigate the effect of the interaction coefficient value, a tentative empirical value of $\varepsilon^P_{Ca\ in\ Si} = -20.0$ was also employed to calculate the isocurves as presented in Figure 13 by the dashed lines. It can be seen that a more negative interaction coefficient value fits better with the experimental results. Nevertheless, no matter which value is appropriate, it can be safely concluded that Ca exhibits stronger P affinity than Mg based on the above thermodynamic analysis.

CONCLUSIONS

In the present work, a comparative study of MG-Si leaching purification with Mg, Ca, and Mg−Ca additions to MG-Si was carried out. The following conclusions were drawn:

- The doping metal significantly affects the alloy microstructure, leaching behavior, and Si purification efficiency.
- In the Ca−Si alloy, the main precipitate was $CaSi_2$ and it led to the formation of a viscous byproduct siloxene during acid leaching along with a strong cracking effect. This causes the fastest leaching kinetics and the highest impurity removal efficiency. However, this cracking effect lowered the Si recovery compared to other samples.
- The Mg−Si alloy system achieved the highest Si recovery with the highest impurity removal efficiency, especially P removal. Nevertheless, the main precipitate Mg_2Si led to the slowest leaching kinetics.
- In the Ca−Mg−Si alloy system, the main phase was determined as $Ca_7Mg_{7.5\pm\delta}Si_{14}$ with a unique crystal structure that contains both a planar Si_{12} ring and isolated Si. As a result, the leaching of the Ca−Mg−Si alloy was found to be a cleaner process that avoids the disadvantages of both Ca−Si and Mg−Si systems. In addition, high Si recovery remained with fast leaching kinetics and high impurity removal, especially P removal.
- A cracking−shrinking principle-based kinetics model was developed for the leaching kinetics of Mg−Si and Ca−Mg−Si alloys. Thermodynamic analysis further revealed that the P removal ability is related to the doping metal concentration and its interaction coefficient with P, while Ca shows a stronger affinity to P than that of Mg.
- The novel Ca−Mg−Si ternary alloy system exhibited more sustainable performance as compared to the other two binary alloys.

AUTHOR INFORMATION

Corresponding Authors

Mengyi Zhu − *Department of Materials Science and Engineering, Norwegian University of Science and Technology (NTNU), N-7491 Trondheim, Norway;* orcid.org/0000-0002-5758-9747; Email: mengyi.zhu@ntnu.no

Sheng Ying Yue − *Department of Mechanical Engineering, University of California, Santa Barbara, California 93106, United States; Aachen Institute for Advanced Study in Computational Engineering Science (AICES), RWTH Aachen University, Aachen 52062, Germany;* orcid.org/0000-0003-2646-579X; Email: sheng.ying.yue@rwth-aachen.de

Authors

Kai Tang − *SINTEF Industry, N-7491 Trondheim, Norway*

Jafar Safarian − *Department of Materials Science and Engineering, Norwegian University of Science and Technology (NTNU), N-7491 Trondheim, Norway*

Complete contact information is available at: https://pubs.acs.org/10.1021/acssuschemeng.0c05564

Notes

The authors declare no competing financial interest.

■ ACKNOWLEDGMENTS

This work was performed at NTNU within the Research Center for Sustainable Solar Cell Technology (FME SuSolTech, project number 257639), co-sponsored by the Norwegian Research Council and industry partners.

■ REFERENCES

(1) Murgau, A.; Safarian, J. Solar Silicon Production through Metallurgical Route and REC Solar Advancements. *Silicon Chem. Sol. Ind. XIV* **2018**, 183−192.
(2) Safarian, J.; Tranell, G.; Tangstad, M. Processes for Upgrading Metallurgical Grade Silicon to Solar Grade Silicon. *Energy Procedia* **2012**, *20*, 88−97.
(3) Forniés, E.; Ceccaroli, B.; Méndez, L.; Souto, A.; Pérez Vázquez, A.; Vlasenko, T.; Dieguez, J. Mass Production Test of Solar Cells and Modules Made of 100% UMG Silicon. 20.76% Record Efficiency. *Energies* **2019**, *12*, 1495.
(4) Tucker, N. P. Preparation of High Purity Silicon. *J. Iron Steel Ind.* **1927**, *15*, 412−414.
(5) Dietl, J. Hydrometallurgical Purification of Metallurgical-Grade Silicon. *Sol. Cells* **1983**, *10*, 145−154.
(6) Chu, T. L.; Chu, S. S. Partial Purification of Metallurgical Silicon by Acid Extraction. *J. Electrochem. Soc.* **1983**, *130*, 455.
(7) Juneja, J. M.; Mukherjee, T. K. A Study of the Purification of Metallurgical Grade Silicon. *Hydrometallurgy* **1986**, *16*, 69−75.
(8) Santos, I. C.; Goncalves, A. P.; Santos, C. S.; Almeida, M.; Afonso, M. H.; Cruz, M. J. Purification of Metallurgical Grade Silicon by Acid Leaching. *Hydrometallurgy* **1990**, *23*, 237−246.
(9) Lu, H.; Wei, K.; Ma, W.; Xie, K.; Wu, J.; Lei, Y.; Dai, Y. Effect of Acetic Acid on the Leaching Behavior of Impurities in Metallurgical Grade Silicon. *Sep. Sci. Technol.* **2017**, *52*, 1257−1264.
(10) Guan, B.; Sun, Y.; Li, X.; Wang, J.; Chen, S.; Schweizer, S.; Wang, Y.; Wehrspohn, R. B. Conversion of Bulk Metallurgical Silicon into Photocatalytic Nanoparticles by Copper-Assisted Chemical Etching. *ACS Sustainable Chem. Eng.* **2016**, *4*, 6590−6599.
(11) Tian, C.; Lu, H.; Wei, K.; Ma, W.; Xie, K.; Wu, J.; Lei, Y.; Yang, B.; Morita, K. Effect of CH3COOH on Hydrometallurgical Purification of Metallurgical-Grade Silicon Using HCl-HF Leaching. *JOM* **2018**, *70*, 527−532.
(12) Liu, S.; Huang, K.; Zhu, H. Removal of Fe, B and P Impurities by Enhanced Separation Technique from Silicon-Rich Powder of the Multi-Wire Sawing Slurry. *Chem. Eng. J.* **2016**, *299*, 276−281.
(13) Zhao, D.; Li, Y. Revealing the Factors Influencing Grain Boundary Segregation of P, As in Si: Insights from First-Principles. *Acta Mater.* **2019**, *168*, 52−62.
(14) Anders, S.; Tuset, J. K.; Tveit, H. *Production of High Silicon Alloys*; Tapir Academic Press: Trondheim, Norway, 1998.
(15) Shimpo, T.; Yoshikawa, T.; Morita, K. Thermodynamic Study of the Effect of Calcium on Removal of Phosphorus from Silicon by Acid Leaching Treatment. *Metall. Mater. Trans. B* **2004**, *35*, 277−284.
(16) Lai, H.; Huang, L.; Lu, C.; Fang, M.; Ma, W.; Xing, P.; Li, J.; Luo, X. Leaching Behavior of Impurities in Ca-Alloyed Metallurgical Grade Silicon. *Hydrometallurgy* **2015**, *156*, 173−181.
(17) Johnston, M. D.; Barati, M. Calcium and Titanium as Impurity Getter Metals in Purification of Silicon. *Sep. Purif. Technol.* **2013**, *107*, 129−134.
(18) Meteleva-Fischer, Y. V.; Yang, Y.; Boom, R.; Kraaijveld, B.; Kuntzel, H. Microstructure of Metallurgical Grade Silicon and Its Acid Leaching Behaviour by Alloying with Calcium. *Miner. Process. Extr. Metall.* **2013**, *122*, 229−237.
(19) Espelien, S.; Safarian, J. Effect of Acid Leaching Conditions on Impurity Removal from Silicon Doped by Magnesium. *AIMS Energy* **2017**, *5*, 636−651.
(20) Safarian, J.; Espelien, S. In *Hydrometallurgical Purification of Maganesium-Doped Silicon by Difference Acids*, 33 European Photovoltaic Solar Energy Conference and Exhibition, 2017; pp 480−482.
(21) Zhu, M.; Murgau, A.; Safarian, J. In *Effects of Magnesium-Doping on Silicon Leaching for Solar Grade Feedstock Production*, 35 European Photovoltaic Solar Energy Conference and Exhibition, 2018; pp 465−468.
(22) Espelien, S.; Tranell, G.; Safarian, J. Effect of Magnesium Addition on Removal of Impurities from Silicon by Hydrometallurgical Treatment. In *Energy Technology 2017*; Springer, 2017; pp 355−366.
(23) Zhu, M.; Azarov, A.; Monakhov, E.; Tang, K.; Safarian, J. Phosphorus Separation from Metallurgical-Grade Silicon by Magnesium Alloying and Acid Leaching. *Sep. Purif. Technol.* **2020**, *240*, No. 116614.
(24) Yoshikawa, T.; Morita, K. Refining of Silicon during Its Solidification from a Si−Al Melt. *J. Cryst. Growth* **2009**, *311*, 776−779.
(25) Ban, B.; Bai, X.; Li, J.; Li, Y.; Chen, J.; Dai, S. The Mechanism of P Removal by Solvent Refining in Al-Si-P System. *Metall. Mater. Trans. B* **2015**, *46*, 2430−2437.
(26) Yoshikawa, T.; Morita, K. Removal of Phosphorus by the Solidification Refining with Si-Al Melts. *Sci. Technol. Adv. Mater.* **2003**, *4*, 531−537.
(27) Yu, W.; Ma, W.; Lv, G.; Ren, Y.; Dai, Y.; Morita, K. Low-Cost Process for Silicon Purification with Bubble Adsorption in Al-Si Melt. *Metall. Mater. Trans. B* **2014**, *45*, 1573−1578.
(28) Li, J.-W.; Zhan-Cheng, G.; Li, Li. J.-C.; Yu, Zhi. Super Gravity Separation of Purified Si from Solvent Refining with the Al-Si Alloy System for Solar Grade Silicon. *Silicon* **2015**, *7*, 239−246.
(29) Lei, Y.; Qiu, P.; Chen, K.; Chen, X.; Ma, W.; Wu, J.; Wei, K.; Li, S.; Lv, G.; Qiu, J. Mechanism of ZrB2 Formation in Al-Si Alloy and Application in Si Purification. *ACS Sustainable Chem. Eng.* **2019**, *7*, 12990−12996.
(30) Huang, L.; Lai, H.; Lu, C.; Fang, M.; Ma, W.; Xing, P.; Li, J.; Luo, X. Enhancement in Extraction of Boron and Phosphorus from Metallurgical Grade Silicon by Copper Alloying and Aqua Regia Leaching. *Hydrometallurgy* **2016**, *161*, 14−21.
(31) Ren, Y.; Ueda, S.; Morita, K. Formation Mechanism of ZrB2 in a Si-Cu Melt and Its Potential Application for Refining Si and Recycling Si Waste. *ACS Sustainable Chem. Eng.* **2019**, *7*, 20107−20113.
(32) Huang, L.; Danaei, A.; Thomas, S.; Xing, P.; Li, J.; Luo, X.; Barati, M. Solvent Extraction of Phosphorus from Si-Cu Refining System with Calcium Addition. *Sep. Purif. Technol.* **2018**, *204*, 205−212.
(33) Ren, Y.; Morita, K. Low-Temperature Process for the Fabrication of Low-Boron Content Bulk Si from Si−Cu Solution with Zr Addition. *ACS Sustainable Chem. Eng.* **2020**, *8*, 6853−6860.
(34) Li, Y.; Zhang, L. Application of Si-Based Solvents to the Purification of Metallurgical Grade-Silicon. *Sep. Purif. Rev.* **2019**, 1−24.
(35) Ma, X.; Lei, Y.; Yoshikawa, T.; Zhao, B.; Morita, K. Effect of Solidification Conditions on the Silicon Growth and Refining Using Si−Sn Melt. *J. Cryst. Growth* **2015**, *430*, 98−102.
(36) Khajavi, L. T.; Morita, K.; Yoshikawa, T.; Barati, M. Removal of Boron from Silicon by Solvent Refining Using Ferrosilicon Alloys. *Metall. Mater. Trans. B* **2015**, *46*, 615−620.
(37) Margarido, F.; Bastos, M. H.; Figureueiredo, M. O.; Martins, J. P. The Structural Effect on the Kinetics of Acid Leaching Refining of Fe-Si Alloys. *Mater. Chem. Phys.* **1994**, *38*, 342−347.
(38) Margarido, F.; Martins, J. P.; Figureueiredo, M. O.; Bastos, M. H. Kinetics of Acid Leaching Refining of an Industrial Fe-Si Alloy. *Hydrometallurgy* **1993**, *34*, 1−11.
(39) Yin, Z.; Oliazadeh, A.; Esfahani, S.; Johnston, M.; Barati, M. Solvent Refining of Silicon Using Nickel as Impurity Getter. *Can. Metall. Q.* **2011**, *50*, 166−172.
(40) Nesper, R. The Zintl-Klemm Concept - A Historical Survey. *Z. Anorg. Allg. Chem.* **2014**, *640*, 2639−2648.
(41) Kresse, G.; Furthmüller, J. Efficiency of Ab-Initio Total Energy Calculations for Metals and Semiconductors Using a Plane-Wave Basis Set. *Comput. Mater. Sci.* **1996**, *6*, 15−50.

(42) Kresse, G.; Furthmüller, J. Efficient Iterative Schemes for Ab Initio Total-Energy Calculations Using a Plane-Wave Basis Set. *Phys. Rev. B* **1996**, *54*, 11169−11186.
(43) Blöchl, P. E. Projector Augmented-Wave Method. *Phys. Rev. B* **1994**, *50*, 17953−17979.
(44) Kresse, G.; Joubert, D. From Ultrasoft Pseudopotentials to the Projector Augmented-Wave Method. *Phys. Rev. B* **1999**, *59*, 1758−1775.
(45) Perdew, J. P.; Burke, K.; Ernzerhof, M. Generalized Gradient Approximation Made Simple. *Phys. Rev. Lett.* **1996**, *77*, 3865−3868.
(46) Klimeš, J.; Bowler, D. R.; Michaelides, A. Chemical Accuracy for the van Der Waals Density Functional. *J. Phys.: Condens. Matter* **2010**, *22*, No. 022201.
(47) Klime, J.; Bowler, D. R.; Michaelides, A. Van Der Waals Density Functionals Applied to Solids. *Phys. Rev. B* **2011**, *83*, No. 195131.
(48) Bellaiche, L.; Vanderbilt, D. Virtual Crystal Approximation Revisited: Application to Dielectric and Piezoelectric Properties of Perovskites. *Phys. Rev. B* **2000**, *61*, 7877−7882.
(49) Miedema, A. R.; de Châtel, P. F.; de Boer, F. R. Cohesion in Alloys - Fundamentals of a Semi-Empirical Model. *Physica B+C* **1980**, *100*, 1−28.
(50) Takeuchi, A.; Inoue, A. Classification of Bulk Metallic Glasses By Atomic Size Difference, Heat of Mixing and Period of Constituent Elements and Its Application To Characterization of the Main Alloying Element. *Mater. Trans.* **2005**, *46*, 2817−2829.
(51) Gröbner, J.; Chumak, I.; Schmid-Fetzer, R. Experimental Study of Ternary Ca−Mg−Si Phase Equilibria and Thermodynamic Assessment of Ca−Si and Ca−Mg−Si Systems. *Intermetallics* **2003**, *11*, 1065−1074.
(52) Villars, P.; Cenzual, K.; Daams, J.; Gladyshevskii, R.; Shcherban, O.; Dubenskyy, V.; Melnichenko-Koblyuk, N.; Pavlyuk, O.; Stoiko, S.; Sysa, L. *Landolt-Börnstein New Series III/43A3*, 2006.
(53) Nesper, R.; Currao, A.; Wengert, S. Nonaromatic Planar Si12 Ring System of Approximate D(6h) Symmetry in Ca7Mg(7.5±δ)Si14. *Chem. - Eur. J.* **1998**, *4*, 2251−2257.
(54) Uehara, M.; Katagiri, A.; Kurokawa, M.; Akiyama, K.; Shimizu, T.; Matsushima, M.; Uchida, H.; Kimura, Y.; Funakubo, H. Preparation of CaMgSi and Ca7Mg7.25Si14 Single Phase Films and Their Thermoelectric Properties. *MRS Adv.* **2019**, *4*, 1503−1508.
(55) Cui, S.; Paliwal, M.; Jung, I.-H. Thermodynamic Optimization of Ca-Fe-Si System and Its Applications to Metallurgical Grade Si-Refining Process. *Metall. Mater. Trans. E* **2014**, *1*, 67−79.
(56) Margaria, T.; Anglezio, J.; Servant, C. In *Inlcrmetallic Compounds in Metallurgical Silicon*, Proceedings of the 6th International Ferroalloys Congress, Cape Town, 1992; pp 209−214.
(57) Vogg, G.; Brandt, M. S.; Stutzmann, M. Kinetics of the Topotactic Formation of Siloxene. *Chem. Mater.* **2003**, *15*, 910−915.
(58) Stutzmann, M.; Brandt, M. S.; Rosenbauer, M.; Fuchs, H. D.; Finkbeiner, S.; Weber, J.; Deak, P. Luminescence and Optical Properties of Siloxene. *J. Lumin.* **1993**, *57*, 321−330.
(59) Baranek, P.; Schamps, J.; Noiret, I. Ab Initio Studies of Electronic Structure, Phonon Modes, and Elastic Properties of Mg2Si. *J. Phys. Chem. B* **1997**, *101*, 9147−9152.
(60) Nandi, K. C.; Mukherjee, D.; Biswas, A. K.; Acharya, H. N. Optimization of acid concentration, temperature and particle size of magnesium silicide, obtained from rice husk, for the production of silanes. *J. Mater. Sci. Lett.* **1993**, *12*, 1248−1250.
(61) Vijh, A. K.; Bélanger, G. Some Trends in the Electrocatalytic Activities of Metal Silicides for the Hydrogen Evolution Reaction. *J. Mater. Sci. Lett.* **1995**, *14*, 982−984.
(62) Martins, J. P.; Margarido, F. The Cracking Shrinking Model for Solid-Fluid Reactions. *Mater. Chem. Phys.* **1996**, *44*, 156−169.
(63) Fang, M.; Lu, C.; Huang, L.; Lai, H.; Chen, J.; Li, J.; Ma, W.; Xing, P.; Luo, X. Effect of Calcium-Based Slag Treatment on Hydrometallurgical Purification of Metallurgical-Grade Silicon. *Ind. Eng. Chem. Res.* **2014**, *53*, 972−979.
(64) Martins, J. P.; Margarido, F. The Cracking Shrinking Model for Solid-Fluid Reactions. *Mater. Chem. Phys.* **1996**, *44*, 156−169.
(65) Dickinson, C. F.; Heal, G. R. A Review of the ICTAC Kinetics Project, 2000. Part 1. Isothermal Results. *Thermochim. Acta* **2009**, *494*, 1−14.
(66) Kröger, C.; Ziegler, G. Über Die Geschwindigkeiten Der Zur Glasschmelze Führenden Reaktionen. III. *Glas. Berichte* **1954**, *27*, 199−212.
(67) Kröger, C.; Ziegler, G. Über Die Geschwindigkeiten Der Zur Glasschmelze Führenden Reaktionen. II. *Glas. Berichte* **1953**, *26*, 346−353.
(68) Jander, W. Reaktionen Im Festen Zustande Bei Höheren Temperaturen. Säureplatzwechsel Bei Einigen Wolframaten Und Molybdaten. *Z. Anorg. Allg. Chem.* **1930**, *190*, 397−406.
(69) Provis, J. L. On the Use of the Jander Equation in Cement Hydration Modeling. *RILEM Tech. Lett.* **2016**, *1*, 62.
(70) Khawam, A.; Flanagan, D. R. Solid-State Kinetic Models: Basics and Mathematical Fundamentals. *J. Phys. Chem. B* **2006**, *110*, 17315−17328.
(71) Ginstling, A.; Brounshtein, B. I. Concerning the Diffusion Kinetics of Reactions in Spherical Particles. *J. Appl. Chem. USSR* **1950**, *23*, 1327−1338.
(72) Bale, C. W.; Pelton, A. D. The Unified Interaction Parameter Formalism: Thermodynamic Consistency and Applications. *Metall. Mater. Trans. A* **1990**, *21*, 1997−2002.

https://dx.doi.org/10.1021/acssuschemeng.0c05564
ACS Sustainable Chem. Eng. 2020, 8, 15953−15966

Paper 4

Materials and Design 198 (2021) 109348

Contents lists available at ScienceDirect

Materials and Design

journal homepage: www.elsevier.com/locate/matdes

Impurity removal from Si by Si-Ca-Mg ternary alloying-leaching system

Mengyi Zhu [a,*], Di Wan [b,*], Kai Tang [c], Jafar Safarian [a]

[a] Department of Materials Science and Engineering, Norwegian University of Science and Technology, Trondheim, Norway
[b] Department of Mechanical and Industrial Engineering, Norwegian University of Science and Technology, Trondheim, Norway
[c] SINTEF Industry, Trondheim, Norway

HIGHLIGHTS

- Parametric study on the Si-Ca-Mg alloying-leaching system was carried out.
- Ca/Mg ratio and solidification conditions significantly affect microstructure.
- Leaching kinetics of Si-Ca-Mg alloy follows a modified Kröger-Ziegler model.
- Increasing Ca/Mg ratio promotes impurity removal.
- A model for P removal prediction was obtained for ternary Si alloy system.

GRAPHICAL ABSTRACT

ARTICLE INFO

Article history:
Received 23 September 2020
Received in revised form 8 November 2020
Accepted 19 November 2020
Available online 21 November 2020

Keywords:
Silicon
Phosphorous
Impurity
Microstructure
Segregation
Thermodynamics

ABSTRACT

In this work, Si-Ca-Mg alloys were made with different compositions and solidification conditions to investigate the impurity segregation and separation performance from Si, especially for the crucial P impurity at several ppmw levels. Varying acid leaching parameters were also employed to investigate the optimized process window. Results indicate that the novel Si-Ca-Mg alloying-leaching system is valid for high P extraction. The ternary intermetallic phase $Ca_7Mg_{7.5\pm\delta}Si_{14}$ appears as the main precipitate in all alloys to gather other minor impurities. Rapid cooling significantly reduced the size of precipitates and Si grain, the impurity segregation was also limited. In the acid leaching experiments, HCl is found as the most economical leaching agents among the studied combinations. Smaller particle size promotes the leaching efficiency, but the increment narrows with increasing Ca/Mg ratio. Leaching kinetics of the studied alloys was found following the modified Kröger-Ziegler model based on a cracking-shrinking mechanism. The impurity purification efficiency increases with increasing Ca/Mg mixing ratio, but significantly reduced by rapid cooling. An analytical model was developed for ternary alloy system to predict the P segregation and its removal with varying alloy concentration through the thermodynamic approach, which shows good agreements of the experimental results.

1. Introduction

There is growing interest in developing a more environmentally friendly approach to produce solar-grade silicon (SoG-Si, purity 99.9999%) for the photovoltaic (PV) industry. The current SoG-Si production is dominated by the modified Siemens process and fluidized bed reactor process. As an emerging process with advantages of sustainability, the metallurgical route is known for lower energy consumption, lower carbon footprint, and less energy payback time [1–3]. Additionally, the increasing amount of the cutting kerf from Si ingot and the end-of-life Si solar panels has also made the metallurgical route become a potential candidate for the recycling of Si materials regarding a circular materials flow economy.

The main challenge for the metallurgical process is the removal of large amount of impurities from the metallurgical grade Si (MG-Si),

* Corresponding authors.
E-mail addresses: mengyi.zhu@ntnu.no (M. Zhu), di.wan@ntnu.no (D. Wan).

https://doi.org/10.1016/j.matdes.2020.109348

especially the problematic B and P impurities due to the restrict impurity concentration limits of SoG-Si. To date, a number of metallurgical processes have been studied for the purification of MG-Si to SoG-Si, including slag refining [4–10], solvent refining [11–15], acid leaching [16–18], vacuum refining [19–21], and gas refining [22–25]. Among the above purification techniques, acid leaching is known to play a crucial role in the removal of P impurity and other metallic impurities. The principle of acid leaching purification is to digest the impurity phase precipitated out of Si phase; however, in practice, the final purification efficiency is always affected by several processing factors. After the pioneering research performed by Tucker almost a century ago [26] for the MG-Si leaching, extensive interest in Si purification has been paid afterward to seek the optimal purification conditions [27–31]. Kim et al. [32] studied the dissolution window of Fe silicides and found the leaching efficiency is dependent on the acid combination and impurity phase composition. The reactivity of impurity precipitates was determined by Margarido et al. [33,34] and the leaching kinetics of ferrosilicon were found to follow a cracking-shrinking core model [35]. Recently, several alloying elements were introduced into MG-Si as impurity getter to modify the impurity precipitation and further enhance the leaching efficiency. One successful approach is known as the solvent refining, which aims at low-temperature operation by adding large amounts of alloying elements such as the well-studied Si-Al [36–41], Si-Cu [12,42], and Si-Fe [43–45] systems. Another alloying approach is adding only a limited amount of additives but with strong impurity affinity as an impurity getter. Ca [17,46–49] is the most often studied alloying impurity getter due to its strong affinity to P to form the stable compound Ca_3P_2. In the recent study from our group [16,50–52], Mg also exhibited high P affinity in Si and the effectiveness of large extent impurities extraction. The separation of the alloy phase by hydrometallurgical treatment was found affected by a variety of leaching parameters such as temperature, acid combination, particle size, and alloying concentration.

The ternary Si-Ca-Mg system is a novel alloying-leaching refining system with different alloying phases. Subsequently, the leaching behavior differs with the binary Si-Ca and Si-Mg system. However, there is still a lack of understanding and investment in the ternary system. Thus, in the present work, a parametric study is carried out to investigate the ternary Si-Ca-Mg system aiming to reveal the effect of a number of factors on the final impurity separation performance. Alloys with different compositions were prepared and refined under different conditions. The effect of Ca/Mg mixing ratio and cooling rate on the microstructural evolution, purification efficiency, and Si recovery were examined and compared as well as the impact of different leaching agents and particle sizes on the impurity removal efficiency. The leaching kinetics was also investigated based on a developed cracking-shrinking model. Finally, a purification model for P removal was established for the ternary alloy system through a thermodynamic approach and Gulliver-Scheil solidification principles.

2. Experimental

2.1. Sample preparation

Commercial MG-Si was used as the starting Si source and physically mixed with a specific amount of impurity-free fluidized bed Si (FBR-Si) to attain the P impurity (as the main element of interest) as low as several ppmw levels. High purity Mg (99.8% purity, Alfa Aesar) and granular Ca (99% purity, Sigma Aldrich) were selected as the doping metal materials. As shown in Fig. 1, the composition of selected alloys was initially designed to obtain different Ca/Mg mixing mole ratios as Ca/Mg = 0.5 (1.5 mol% Ca and 3.0 mol% Mg), 1 (2.25 mol% Ca and 2.25 mol% Mg), and 2 (3.0 mol% Ca and 1.5 mol% Mg), respectively, which are marked as CM0.5, CM1, and CM2 in this work. In addition, a casted alloy (marked as CM1-Casted) with the composition closes to sample CM1 was also made to study the cooling rate effect. It is also

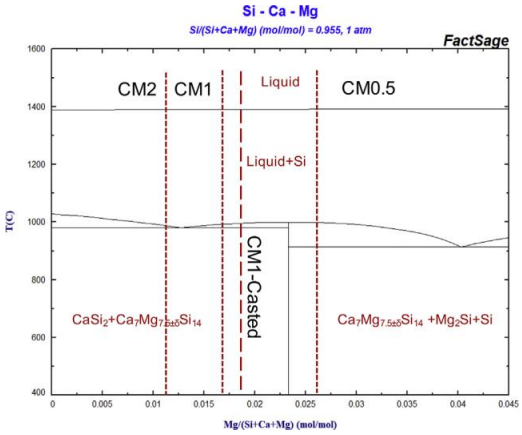

Fig. 1. Phase diagram of Si-Ca-Mg system with the designed sample composition, calculated by FactSage®. (digital version in color).

worth noting that as the alkaline-earth metals evaporate at the high-temperature, the final obtained alloy composition will be slightly different but close to the Ca/Mg ratio as designed. Prior to the alloy melting process, around 400 g Si mixtures (160 g MG-Si and 240 g FBR-Si) were put into a high-density graphite crucible with a specific amount of Ca addition, while Mg piece was doped later after melting, respectively, 9.2 g Ca and 11.5 g Mg for CM0.5, 13.8 g Ca and 8.3 g Mg for CM1, 18.4 g Ca and 5.6 g Mg for CM2, and 13.3 g Ca and 8.1 g Mg for CM1-Casted. The graphite crucible was then heated in an induction furnace under a pure Ar (99.9999% purity) flow atmosphere. The molten alloy was held at 1773 K for 10 min with intensive stirring flow induced by the induction heating and yielded proper melt homogenization. The melt was then slowly cool down in the furnace (cooling rate c.a. 10^{-1}-10^{1} K/s) or cast to a water-cooled copper mold (cooling rate 10^{2}–10^{3} K/s). The obtained Si-Ca-Mg bulk alloys were then crushed and milled in a ring mill to the target particle sizes (0.2–1 mm and < 0.2 mm) using Retsch Vibratory Disc Mill RS200 with the tungsten carbide sets. The final compositions of the alloys determined by a high resolution inductively coupled plasma mass spectroscopy (ICP-MS, Agilent 8800) after sizing are listed in Table 1.

Table 1
Measured compositions of MG-Si and obtained Si alloys (ppmw).

Sample	Particle size (mm)	P	Ca	Mg	Al	Fe	Ti	Zr
MG-Si	Lump	14.8	331.7	10.7	1859.7	2723.9	218.2	7.9
CM0.5	0.2–1	4.5	14,780.1	21,533.3	539.7	783.9	68.8	3.0
	<0.2	7.1	27,658.0	39,360.4	936.6	1397.2	122.0	4.7
	Master alloy	5.2	18,173.4	26,230.7	644.3	945.5	82.9	3.4
CM1	0.2–1	4.7	23,182.8	13,884.1	565.6	805.2	71.2	2.8
	<0.2	6.4	38,940.6	23,163.2	910.3	1277.2	116.7	5.9
	Master alloy	5.3	27,910.1	16,667.8	669.0	946.8	84.9	3.7
CM2	0.2–1	4.3	27,668.0	8981.9	510.9	746.8	66.9	5.1
	<0.2	5.9	51,559.8	15,961.7	881.1	1325.8	117.5	4.1
	Master alloy	4.7	34,092.5	10,858.8	610.4	902.5	80.5	4.8
CM1-Casted	0.2–1	4.8	22,040.0	15,696.6	635.6	917.8	90.6	3.2
	<0.2	6.1	26,938.6	19,629.6	781.8	1201.0	113.3	4.0
	Master alloy	5.1	23,416.5	16,801.8	676.7	997.4	97.0	3.4

2.2. Characterization

Metallographic samples were prepared for the microstructural characterization. Electron Probe Micro-Analyzer (EPMA, JXA-8500F) supported with wavelength-dispersive spectroscopy (WDS) was applied for the elemental mapping and phase composition determination. The crystallographic properties were also measured by electron backscattered diffraction (EBSD) using NORDIF system. The EBSD scan was conducted in a Quanta 650 scanning electron microscope (SEM, ThermoFisher Scientific Inc.) operated at an accelerating voltage of 20 kV, an aperture of 100 μm and a spot size of 4.0. The working distance was about 20 mm for the 70° pre-tilt specimen, and the dynamic focus in the SEM was adopted to improve the focal distance over a relatively large probe area of about 1.2×1.2 mm^2.

2.3. Leaching-refining trials

Acid leaching experiments for the impurity segregation and removal study were carried out by mixing 2 g samples and 10 mL 10% HCl solutions in perfluoroalkoxy alkane (PFA) bottles, which were in a bath with ultrasonic-assisted mixing. The leaching conditions are determined according to our previous investigations [53] that the leaching temperature was set at 60 °C with a leaching period of 0–3 h. Several leaching agent combinations were designed to compare the leaching efficiency using CM0.5 (particle size 0.2–1 mm) as a reference sample, including HCl, concentrated aqua regia, diluted aqua regia (50%), HCl + 10% $FeCl_3$ (volume ratio), HCl + 10% Glycerin, and HCl + 10% oxalic acid ($C_2H_2O_4$). The leached samples were then washed by deionized water and ethanol. The impurity concentrations in all samples were measured by high-resolution ICP-MS as the alloys.

3. Results and discussion

The obtained results are presented and discussed with supplementary theoretical calculations as follows.

3.1. Microstructure

3.1.1. Effect of Ca/Mg mixing ratio

The effect of the Ca/Mg mixing ratio on the alloy microstructure and the segregation of metallic impurities such as Ca, Mg, Al, Fe, and Ti, were characterized by EPMA elemental mapping. As the results presented in Fig. 2, impurities are found concentrated in the regions at the end stage of solidification. It is also seen that the alloy microstructure is significantly affected by the alloy composition as the large phases are marked in the backscattered electrons (BSE) image. The ternary intermetallic $Ca_7Mg_{7.5\pm6}Si_{14}$ phase is found as the common main precipitate that appears in all the Si-Ca-Mg alloys. The binary precipitate Mg_2Si and $CaSi_2$ are also found coexist with $Ca_7Mg_{7.5\pm6}Si_{14}$, respectively, in samples CM0.5 and CM2, as the phase diagram suggested in Fig. 1. However, it is worth noting that in sample CM1, the precipitates Mg_2Si, $Ca_7Mg_{7.5\pm6}Si_{14}$, and $CaSi_2$ are observed together, which is not thermodynamically preferred. This may be related to non-equilibrium solidification even when the samples are cooled down in the furnace. Unlike the microstructure observed in binary Si-Ca and Si-Mg alloys, in the Si-Ca-Mg alloying system, Al is found most likely to be dissolved in the ternary $Ca_7Mg_{7.5\pm6}Si_{14}$ phase as the form of the solid solution rather than to form specific compounds. Transition-metal silicide is an essential family of the intermetallic phases in MG-Si, also known with poor reactivities to acids. Iron is the most abundant impurity in MG-Si and distributed as single secondary precipitate phase in the Si matrix. However, in all of the obtained Si-Ca-Mg alloys, Fe impurity is found only located inside the $Ca_7Mg_{7.5\pm6}Si_{14}$ phase with fine Ti impurity particles being adjacent. The result of EPMA-WDS point analysis further indicates the Fe-bearing phase is with the stoichiometry Fe_3Si_7, which is in agreement with the high-temperature $FeSi_2$ phase (also known as $FeSi_{2.4}$ or α-leboite) that stabilized by Al impurity down to room temperature [54,55]. However, a certain extent ultrafine low-temperature $FeSi_2$ phase with Si could also possibly exist as the decompose products of the high-temperature stable Fe_3Si_7 phase but cannot be fully separated and detected due to the slow solid-solid decompose reaction. Thus, in the present work, the Fe-bearing phase is described as Fe_3Si_7($FeSi_2$ + Si). Since the transition metal impurity phases are gathered in the leachable ternary $Ca_7Mg_{7.5\pm6}Si_{14}$ phase, it may also imply the effectiveness of enhanced Fe and Ti removal with Ca and Mg alloying.

3.1.2. Effect of cooling rate

The microstructure of MG-Si and Si alloys is greatly affected by the solidification condition [47,56]. As presented in Fig. 3, the typical precipitates of the CM1-Casted sample were also characterized by EPMA elemental mapping, which is observed still as $Ca_7Mg_{7.5\pm6}$ Si_{14}, $CaSi_2$, and Fe_3Si_7($FeSi_2$ + Si), but all with a much less and fine structure. In addition, it is also seen that a large fraction of Si islands embedded inside the main precipitates.

The elemental composition of each precipitate is also imperative to compare since it may imply the segregation extent information of impurities. Thus, the detected atomic fraction of each phase in sample CM1 and CM1-Casted were analyzed by EPMA, as listed in Table 2. By comparing the purity of the Si matrix, it is found that the Si matrix in the sample CM1-Casted contains more impurities since the Si purity 99.60% is slightly lower than that of the sample CM1 with the Si purity 99.76%. Furthermore, the measured composition of all precipitates shows a higher Mg concentration in the sample CM1-Casted. Even though the considerably high Mg atomic fraction (7.01%) in the Fe_3Si_7($FeSi_2$ + Si) phase may be owing to the measuring error caused by the thin precipitate thickness, the higher Mg/Ca ratio also suggests the findings. Another evidence for the limited impurity segregation via fast cooling can be obtained from the measured composition of different particle sizes listed in Table 1. For instance, the composition differences of CM1-Casted with different particle sizes are narrower than that of the other three furnace cooled samples, demonstrating a more homogenized and less segregated impurity distribution. Thus, it is concluded that the fast cooling of the Si-Ca-Mg alloys leads to insufficient segregation of impurities and the non-equilibrium precipitation at the end of solidification.

The comparison of the microstructure between the furnace cooled sample CM1 and casted sample CM1-Casted can be seen in Fig. 4. By comparing the overview images shown in Fig. 4(a) and Fig. 4(c), apparently, it is found that the precipitates in the sample CM1 are much less and coarser than that of the sample CM1-Casted. Meanwhile, in the sample CM1-Casted, the size of the precipitates and Si both shrink dramatically.

Since the crystal structural parameters may directly reflect the properties of the material, EBSD measurement was applied to further investigate the effect of cooling rate on the Si grain structural properties. As presented by Fig. 4(b) and Fig. 4(d), it can be seen that the Si grains in the furnace cooled sample CM1 are much larger than that of the casted sample CM1-Casted, and most of the precipitated phases (the dark areas) are also found located along the Si grain boundary. Thus, most of the precipitates would be exposed after crushing, and the Si grains would remain after leaching. However, practically, the final Si recovery could be reduced by the fast cooling as the fine Si grains (especially the ultrafine Si grains shown in Fig. 4(b)) could increase Si loss during the leaching and the post Si-collecting process.

The corresponding crystallographic orientation (in terms of normal direction of the sample) is also captured by different colors. It is observed that CM1-Casted sample shows more random and messy crystal orientation distribution, which reflects the profoundly disturbed primary Si crystal growth condition by casting. Consequently, the impurity segregation is limited and more impurities could be trapped by the growing Si crystal so that further limits the final purification performance according to the mechanism proposed by Ban et al. [57]. Thus, even with similar alloy compositions, the Si purification efficiency could be significantly affected by the solidification conditions.

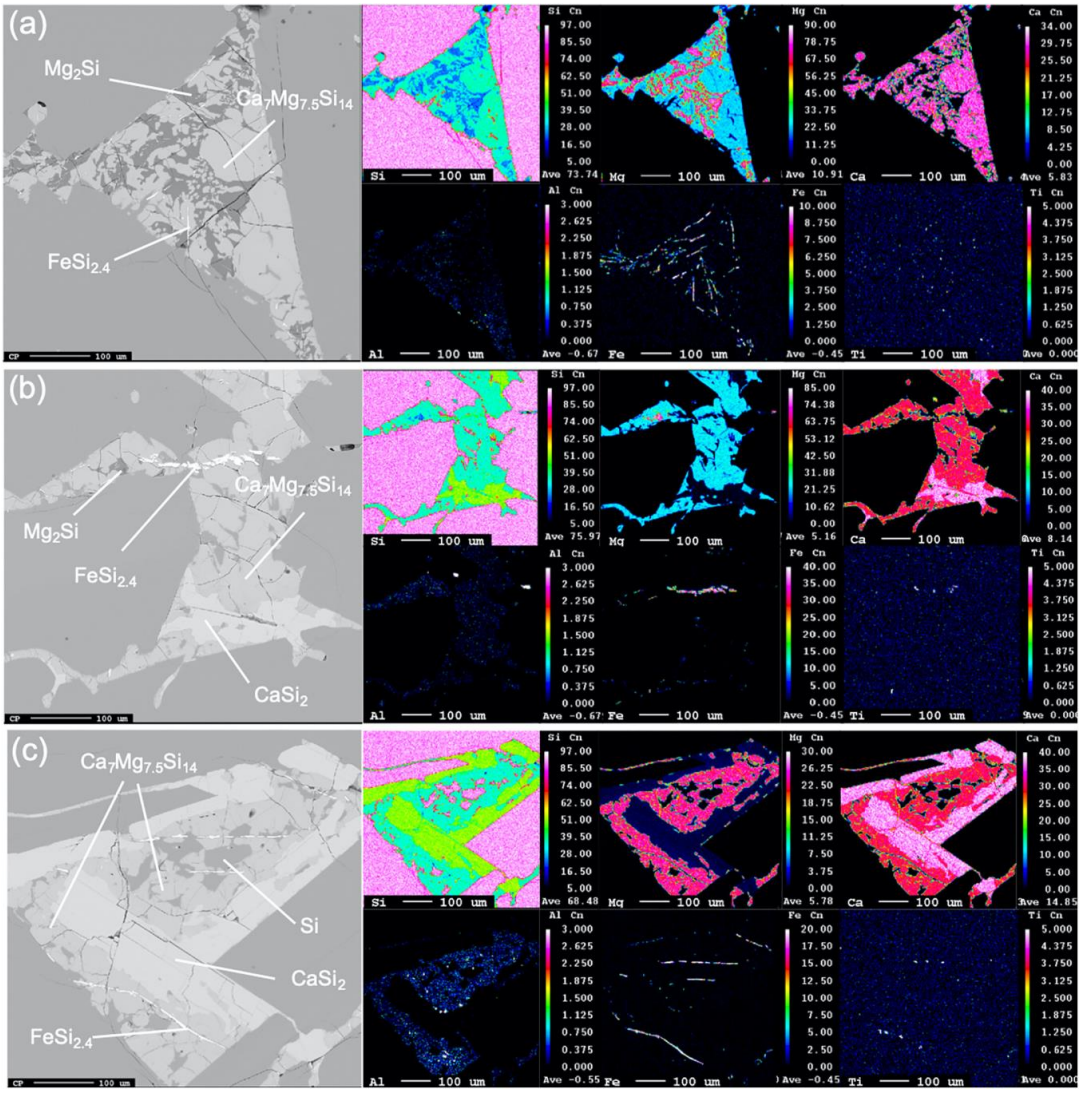

Fig. 2. Typical precipitates and EPMA elemental mapping results of studied alloys (a) sample CM0.5, (b) sample CM1, and (c) sample CM2. (digital version in color).

3.2. Leaching characteristics

In this section, a variety of leaching parameters and characteristics are discussed, including the effect of leaching agents, particle size, and leaching kinetics. It is worth noting that the leaching efficiency is defined here as the percentage of extracted impurity of the initially charged materials (coarse or fine particles) listed below:

$$\textit{Leaching efficiency} = \frac{C_{\textit{particles for leaching}} - C_{\textit{after leaching}}}{C_{\textit{particles for leaching}}} \times 100\% \quad (1)$$

where the $C_{\textit{particles for leaching}}$ and $C_{\textit{after leaching}}$ are initial impurity concentration of coarse or fine Si alloy particles and the final impurity concentration of leached Si in weight percent, respectively.

3.2.1. Effect of leaching agents

After obtaining knowledge of the microstructure of the Si-Ca-Mg alloys, it is then necessary to determine the suitable leaching agents. On the basis of our previous work [50], HCl (10%) aqueous solution was found the most effective compared to other commonly used acids. Accordingly, several HCl-based leaching combinations and aqua regia solutions were employed to study their effect on the leaching efficiency as the results shown in Fig. 5. It is also worth to noting that the comparison is only restricted to the acid solution with the selected concentration. It is seen that almost all of the doped Ca and Mg can be removed by the selected acid combinations, only the combination of HCl + 10% Glycerin shows a slightly lower efficiency as 93% removal and the highest efficiency 97% is achieved by the diluted aqua regia and HCl + 10% $FeCl_3$. Meanwhile, HCl + 10% $FeCl_3$ is also found the most

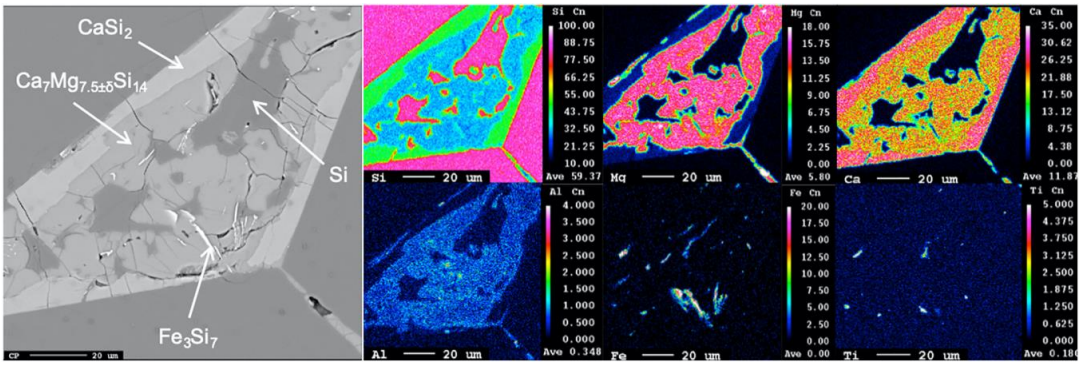

Fig. 3. EPMA elemental mapping results of sample CM1-Casted. (digital version in color).

Table 2
Detected composition (in at.%) of phases in sample CM1 and CM1-Casted by EPMA.

Sample	Phase	Si	Mg	Ca	Al	Fe
CM1	Si	99.76	0.10	0.11	0.03	0.01
	$CaSi_2$	66.59	1.59	31.71	0.11	0.01
	$Ca_7Mg_{7.5}Si_{14}$	48.77	25.94	24.42	0.85	0.01
	Fe_3Si_7($FeSi_2$ + Si)	68.89	0.81	0.82	0.53	28.95
CM1-Casted	Si	99.60	0.23	0.12	0.05	0.01
	$CaSi_2$	65.77	2.79	31.33	0.10	0.01
	$Ca_7Mg_{7.5}Si_{14}$	47.03	28.98	22.99	0.99	0.01
	Fe_3Si_7($FeSi_2$ + Si)	66.21	7.01	4.10	0.68	22.00

effective for the Al extraction that 79% removal is obtained. However, for the extraction of the transition metals impurities, concentrated aqua regia and its diluted solutions appear to be inefficient as leaching efficiency is only around 30–40%, while the addition of $FeCl_3$, Glycerin, and oxalic acid all reached the leaching efficiency around 50%. The reason may be owing to the strong oxidizing environment caused by the aqua regia so that the Si anion in the silicide phase is likely to be oxidized to SiO_2, subsequently, hinders the leaching kinetics, which is also suggested by Kim et al. [58] by the phase stability analysis. On the contrary, as the addition of $FeCl_3$ accelerates the particle disintegration [33], it then results in a faster kinetics. Thus, the combination of HCl + 10% $FeCl_3$ is seen with the highest leaching efficiency overall. Nevertheless, it is seen that HCl aqueous solution without additives also exhibits satisfying leaching results at a cheaper cost. In summary, the reactivity of acids for interacting with the studied Si-Ca-Mg alloy can be ordered as:

HCl + 10% $FeCl_3$ > HCl > HCl + 10% $C_2H_2O_4$ ≈ HCl + 10% Glycerin > Diluted aqua regia (50%) > Aqua regia.

3.2.2. Effect of particle size

Leaching efficiency is sensitive to the silicon particle size, and generally, higher efficiency is obtained by decreasing the particle size. The reason is attributed to the more exposed surface to acid solution by particle size reduction. In this work, two different particle sizes (coarse particle with range 0.2–1 mm and fine particle with diameter < 0.2 mm) were treated in HCl (10%) aqueous solution for 1 h at 60°C. As the results presented in Fig. 6, the leaching efficiency of most of the impurities is higher with fine particle size, especially for the sample CM0.5. For instance, the efficiency of Ca and Mg extraction increased from 95% to 99%, the Al extraction increased from 74% to 84%, and both of the Fe and Ti leaching efficiency improved from around 45% to 54% as well. However, it is seen that the increment of CM1 and CM2 turns into smaller by the fine particles leaching. Comparatively, the leaching efficiency of Ca, Mg, and Al of sample CM2 with different particle sizes are almost equivalent, and only the extraction of Fe and Ti have been increased from 62% to 70%, and from 65% to 71%, respectively. The increment of Ca, Mg, and Al of sample CM1 are seen in between sample CM0.5 and CM2, while the abnormal equivalent extraction of Fe and Ti impurities with different particle sizes is more likely deviations from slightly uneven sampling. The reason for the smaller leaching efficiency enhancement of increasing Ca/Mg ratio by the particle size reduction is considered owing to the strong cracking tendency of the $CaSi_2$ phase during leaching. As a result, the coarse particle disintegrates into the finer particle itself so that the leaching kinetics is being improved spontaneously. Thus, our result may also highlight the fact that the reduction of particle size could become unimportant for the leaching of the Si alloys contains the main phase with fast leaching kinetics. This is because, like dealing with Si-Ca-Mg alloys with high Ca content, the strong cracking effect could "auto-catalyze" the leaching process itself. In addition, in practice, the enhancement of leaching efficiency through particle size reduction might also be not significant enough to compensate for the cost of the extra process and more material losses.

3.2.3. Leaching kinetics

The leaching kinetics of Si-Ca-Mg alloys was investigated by performing a series of leaching trials of sample CM0.5 in different leaching periods of 5, 10, 20, 30, 45, 60 and 120 min by HCl (10%) at 60 °C under ultrasonic bath within the particle size range 0.2–1 mm. The results of the impurity extraction degree against leaching time are plotted in Fig. 7(a). It is seen that most of the impurity extraction took place in the first one hour, especially at the initial stage. After 20 min leaching, 88.2% of Ca and Mg, 67.2% of Al, 50.2% of P, and around 40% of Fe and Ti were extracted. In addition, it is also seen that impurities can be classified into three groups from the leaching time plot and follows kinetics trend: Ca, Mg > Al, P > Ti, Fe. Apparently, as the main phase and the impurity getter, Ca and Mg exhibit the fastest kinetics. The similar extraction trend of Al and P may suggest that P could also distribute in the ternary $Ca_7Mg_{7.5\pm6}Si_{14}$ phase, as the EPMA elemental mapping results of Al shown in Fig. 2. The impurity extraction curve also reveals that Ti impurity stays together with Fe as suggested by the EMPA mapping results shown in Fig. 2 as well.

Martins and Magarido [59] developed a cracking-shrinking core model for the leaching of Si-Fe alloy system since the acid leaching of Si-based alloys are often found with cracking effect [33]. However, for the leaching of Si-Ca-Mg alloys in this work, this model failed to fit out results linearly. Nevertheless, a novel cracking-shrinking based model is found valid for the Si-Ca-Mg alloy system by employing the cracking

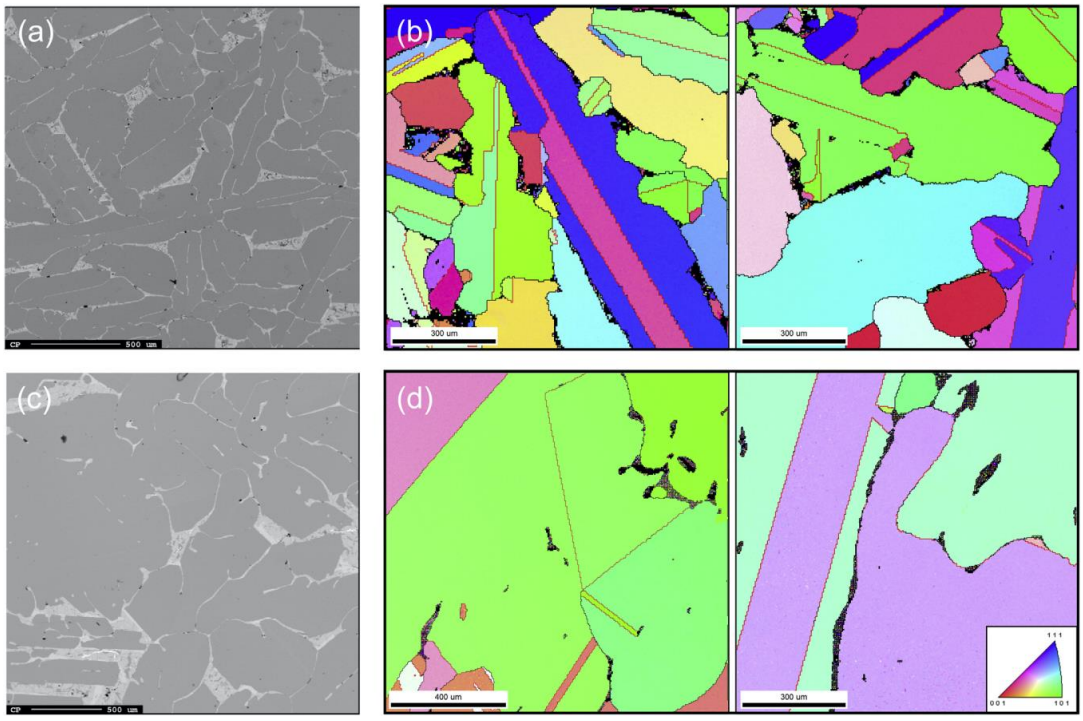

Fig. 4. Effect of cooling rate on Si-Ca-Mg alloy microstructure. (a) BSE image of sample CM1-Casted (b) EBSD crystallographic mapping of CM1-Casted (c) BSE image of sample CM1 (d) EBSD mapping of sample CM1. For EBSD maps: orientation with respect to the normal direction of the sample, color-coded according to the legend in the bottom-right corner. Black lines indicate high-angle grain boundaries (misorientation >15°) and red lines indicate twin boundaries. (digital version in color).

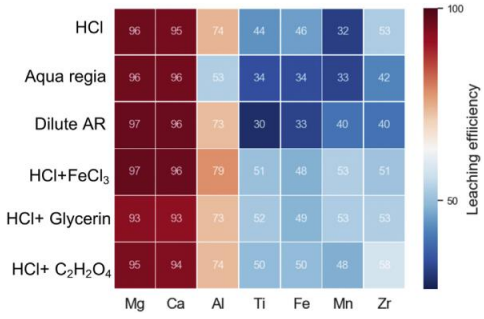

Fig. 5. The effect of leaching agents on the impurities removal (%) from sample CM0.5, leached at 60 °C with particle size of 0.2–1 mm. (digital version in color).

feature to a modified Kröger-Ziegler model with the consideration of spherical shrinking condition.[52] It is assumed that particle surface was first attacked by acids during the leaching. With the propagation of the surface micro-cracks, the whole particle eventually disintegrates at the time t_c with the impurity conversion X_c. For simplification, only one-time particle disintegration assumed to happen. Thus, a core shrinking stage is considered to start with $t \geq t_c$ and the impurity conversion is re-normalized as $\alpha = \frac{X-X_c}{1-X_c}$. Thus, the kinetic relationship is described as two stages, respectively:

Cracking stage:

$$X = k_C t \ (0 \leq t < t_c) \ (2)$$

Shrinking stage:

$$1-\frac{2}{3}\left(\frac{X-X_C}{1-X_C}\right)-\left(1-\left(\frac{X-X_C}{1-X_C}\right)\right)^{\frac{2}{3}} = K_S \ln\left(\frac{t}{t_c}\right) \ (t_c \leq t) \ (3)$$

where k_C and k_S are the rate constant of the cracking stage and the K-Z model. Additionally, since the conversion of Ca and Mg is always synchronous and the fastest in the leaching of Si-Ca-Mg alloy, the conversion of impurity i after cracking can be expressed as $X_{i,\,c} = \xi_i X_c^{Mg+Ca}$, where $\xi_i \in [0,1]$ and indicates the relative reaction rate of impurity i compared to Ca and Mg. Thus, the cracking-shrinking model is also written as:

$$Y(X_i) = 1-\frac{2}{3}\left(\frac{X_i-\xi_i X_c^{Mg+Ca}}{1-\xi_i X_c^{Mg+Ca}}\right)-\left(1-\left(\frac{X_i-\xi_i X_c^{Mg+Ca}}{1-\xi_i X_c^{Mg+Ca}}\right)\right)^{\frac{2}{3}} = K_S \ln\left(\frac{t}{t_c}\right) \ (t \geq t_c) \ (4)$$

It is also worth noting that special treatment needs to be paid to the P fitting because not all the P had chance to participate in the reaction as

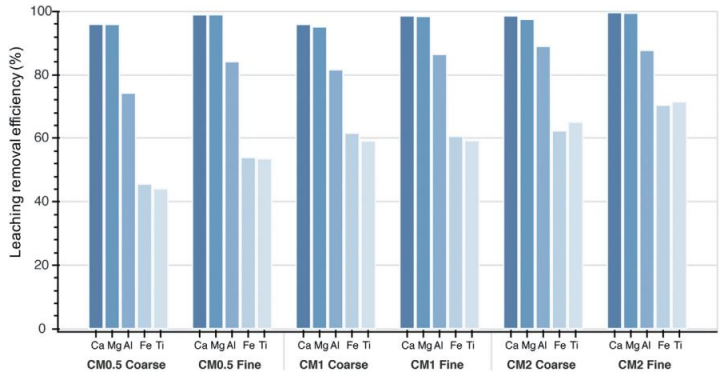

Fig. 6. Effect of particle size on the leaching efficiency by 10% HCl for "Coarse", and "Fine" alloy samples. (digital version in color).

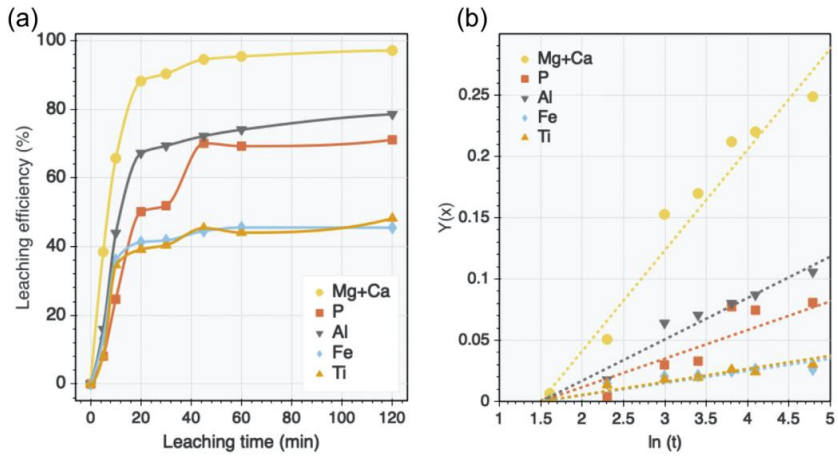

Fig. 7. Effect of leaching time on impurity removal of sample CM0.5 (0.2–1 mm particles by HCl at 60 °C) (b) Application of the cracking-shrinking model to studied impurities Mg + Ca, P, Al, Fe, and Ti. (digital version in color).

only the part of P segregated outside the Si primary grains is leachable, and the rest is dissolved in the structure of Si matrix. Consequently, the effective P conversion is introduced as:

$$X_{P,eff} = \frac{\eta N_{total} - N_t}{\eta N_{total}} \quad (5)$$

where N_{total} and N_t denote the overall P concentration and the P concentration with leaching time t. η is the percentage that P segregated into precipitates, which is estimated as 0.85 from the final leaching purification results.

By fitting the data of the leaching results, linear relationship was observed between $Y(X_i)$ and ln t as shown in Fig. 7(b). Meanwhile, one of the main features is seen is that all fitting lines origins from the starting point, which indicates the assumed cracking time. The relevant fitting parameters and obtained rate constants are listed in.

Table 3. The results demonstrate that the leaching cracking stage occurs in a short time which indicates the intensive reaction happened at the beginning of leaching. In addition, impurity extraction kinetics follows the order as discussed above that: Ca, Mg > Al > P > Ti ≈ Fe.

3.3. Purification efficiency

The purification efficiency of studied alloys (CM0.5, CM1, CM2, and CM1-Casted) and MG-Si after leaching under the same conditions that with HCl (10%) at 60 °C under ultrasonic bath for the particle size ranges from 0.2 to 1 mm. The purification efficiency is calculated as:

Table 3
The obtained kinetic parameters from cracking-shrinking model for the impurities extraction from sample CM0.5.

Impurity	$ln(t_c)$ (min)	Xc 1	ξ 1	K_C (min^{-1})	K_S 1
Mg + Ca	1.5	0.2	1.0	0.045	0.082
P			0.4	0.018	0.022
Al			0.6	0.027	0.034
Fe			0.2	0.009	0.011
Ti			0.2	0.009	0.011

$$Purificationefficiency = \frac{C_{bulkmaterial} - C_{afterleaching}}{C_{bulkmaterial}} \times 100\% \quad (6)$$

where $C_{bulk\ material}$ represents the initial impurity concentration of the bulk Si master alloy or MG-Si, and $C_{after\ leaching}$ is the final impurity concentration of leached Si in weight percent.

The compositions of purified Si are listed in Table 4 and the calculated purification efficiency results are compared in Fig. 8. A distinct trend can be seen that the purification efficiency for all impurities follows the order: MG-Si < CM1-Casted< CM0.5 < CM1 < CM2. Hence, it is concluded that the Ca—Mg alloying significantly improves the impurity removal and the purification efficiency increases with increasing Ca/Mg ratio and decreases with increasing cooling rate. Taking into account the P extraction, the purification efficiency is, respectively, 31.7% (MG-Si), 62.2% (CM1-Casted), 81.1% (CM0.5), 83.1% (CM1), and 87.0% (CM2).

The variation of the purification efficiency for each impurity is related to the impurity segregation behavior affected by the doping metals and the cooling conditions. Even though Ca and Mg are both alkaline-earth elements with similar chemical properties, Ca shows a higher affinity to the impurities. The reason is explained by the cation difference that Ca is larger, softer, and less polarizing compared to Mg, so that Ca exhibits a higher reactivity. It is also worth noting that the significant decline of purification efficiency by casting CM1-casted also highlights the critical role of cooling rate on impurity segregation that with a high cooling rate, impurities may undergo insufficient diffusion, finally, the segregation behavior is limited.

3.4. P removal modelling

The leaching results suggest that P segregation and its removal is strongly affected by Ca/Mg alloying ratio even though P is apt to segregate on Si grain boundary as well [60]. Thus, it is necessary to investigate the effect of Ca and Mg alloying on P segregation. In our previous work [16], a Gulliver-Scheil segregation based model for binary Si alloy system was developed to estimate the P removal degree after acid leaching combined with the thermodynamic properties of the doping metal. For an arbitrary Si-rich ternary alloying system Si-Me_1-Me_2, if the consideration is still limited to the dilute solution scheme, the model can be extended to the ternary system by ignoring the second-order interaction coefficient. Therefore, the P activity coefficient in the melt $\gamma_{P\ in\ Si-Me1-Me2(l)}$ can be written as the unified formalism proposed by Bale and Pelton [61]:

$$\ln \gamma_{P\ in\ Si-Me_1-Me_2(l)} = \ln\ \gamma_P^0 + \ln\ \gamma_{Si} + \varepsilon_P^P X_P + \varepsilon_{Me1}^P X_{Me1} + \varepsilon_{Me2}^P X_{Me2} \quad (7)$$

where γ_P^0 represents the activity coefficient of P in the solvent at infinite dilution, and γ_{Si} represents the activity coefficient of solvent Si, which is close to unity. ε_P^P, ε_{Me}^Prepresent the first order interaction coefficient of P itself and P with doping metal Me, and X_{Me} represents the concentration of doping metal Me in Si melt. However, the term ln γ_{Si} and $\varepsilon_P^P X_P$ can be ignored since they are close to zero. So that we have:

$$\frac{\gamma_{P\ in\ Si-Me_1-Me_2(l)}}{\gamma_{P\ in\ Si\ (l)}^0} = \exp\left(\varepsilon_{Me1}^P X_{Me1} + \varepsilon_{Me2}^P X_{Me2}\right) \quad (8)$$

Table 4
Impurity concentration of purified Si alloys and MG-Si.

Impurity	CM0.5	CM1	CM2	CM1-Casted	MG-Si
P	1.0	0.9	0.6	1.9	10.1
Ca	888.1	627.6	442.1	3865.7	59.1
Mg	1219.7	508.1	260.6	2781.4	2.3
Al	149.6	91.2	63.3	242.2	972.4
Fe	419.9	285.1	260.9	479.6	1470.9
Ti	37.7	26.4	24.4	46.9	129.8

It is known that at the equilibrium state, the chemical potential of P in the two phases are equal:

$$\mu_{in\ Si\ (s)} = \mu_{in\ Si-Me_1-Me_2\ (l)} \quad (9)$$

Subsequently, the following relationship is obtained in term of Gibbs energy and activities:

$$\Delta G^{\circ}_{P\ in\ Si\ (s)} + RTln\ a_{P\ in\ Si\ (s)} = \Delta G^{\circ}_{P\ in\ Si-Me_1-Me_2\ (l)} + \mathrm{RTln}a_{P\ in\ Si-Me_1-Me_2\ (l)} \quad (10)$$

After arrangement, and regarding the fact that Gibbs energy is a state function and there is only trace amount of P in the phases with insignificant Gibbs energies of dissolution (in solid and liquid phases), it yields:

$$\Delta G^{\circ fus}_{P\ in\ Si-Me_1-Me_2} = \Delta G^{\circ fus}_{P\ in\ Si} \quad (11)$$

$$\frac{a_{P\ in\ Si\ (s)}}{a_{P\ in\ Si-Me_1-Me_2(l)}} = \exp\left(\frac{\Delta G^{\circ fus}_{P\ in\ Si-Me_1-Me_2}}{RT}\right) \quad (12)$$

where $\Delta G^{\circ fus}_{P\ in\ Si}$and $\Delta G^{\circ fus}_{P\ in\ Si-Me1-Me2}$ indicate the Gibbs energy of fusion for P in Si and in the ternary system.

Moreover, the P segregation coefficient in the ternary system Si-Me_1-Me_2 can be expressed as:

$$k_P^{Si-Me1-Me2} = \frac{X_{P\ in\ Si(s)}}{X_{P\ in\ Si-Me_1-Me_2(l)}} = \exp\left(\frac{\Delta G^{\circ fus}_{P\ in\ Si-Me_1-Me_2}}{RT}\right)\frac{\gamma_{P\ in\ Si-Me_1-Me_2(l)}}{\gamma_{P\ in\ Si\ (s)}} \quad (13)$$

Similarly, for the binary Si-P system:

$$k_P^{Si} = \exp\left(\frac{\Delta G^{\circ fus}_{P\ in\ Si}}{RT}\right)\frac{\gamma^0_{P\ in\ Si\ (l)}}{\gamma^0_{P\ in\ Si\ (s)}} \quad (14)$$

Since the concentration of alloying elements in solid Si is neglectable, thus, $\gamma_{P\ in\ Si\ (s)} = \gamma^0_{P\ in\ Si\ (s)}$. Combining Eq. (8), Eq. (13), and Eq. (14):

$$k_P^{Si-Me1-Me2} = \exp\left(\frac{\Delta G^{\circ fus}_{P\ in\ Si}}{RT}\right)\frac{\gamma^0_{P\ in\ Si\ (l)}}{\gamma_{P\ in\ Si\ (s)}}\frac{\gamma_{P\ in\ Si-Me_1-Me_2(l)}}{\gamma^0_{P\ in\ Si\ (l)}} = k_P^{Si}\frac{\gamma_{P\ in\ Si-Me_1-Me_2(l)}}{\gamma^0_{P\ in\ Si\ (l)}} \quad (15)$$

By introducing Eq. (8), it then gives,

$$k_P^{Si-Me1-Me2} = k_P^{Si}\exp\left(\varepsilon_{Me1}^P X_{Me1} + \varepsilon_{Me2}^P X_{Me2}\right) \quad (16)$$

It is assumed that all doping metals will stay in the remaining liquid phase during solidification due to their very low segregation coefficients, thus, Eq.(17) can be obtained for when a fraction f_s is solidified:

$$X_{Me} = \frac{X_{Me}^{initial}}{(1-f_s)} \quad (17)$$

And,

$$k_P^{Si-Me1-Me2} = k_P^{Si}\exp\left(\frac{\varepsilon_{Me1}^P X_{Me1} + \varepsilon_{Me2}^P X_{Me2}}{1-f_s}\right) \quad (18)$$

The P removal degree is defined as the ratio of the removed P over the initial P in Si before doping, which is written as:

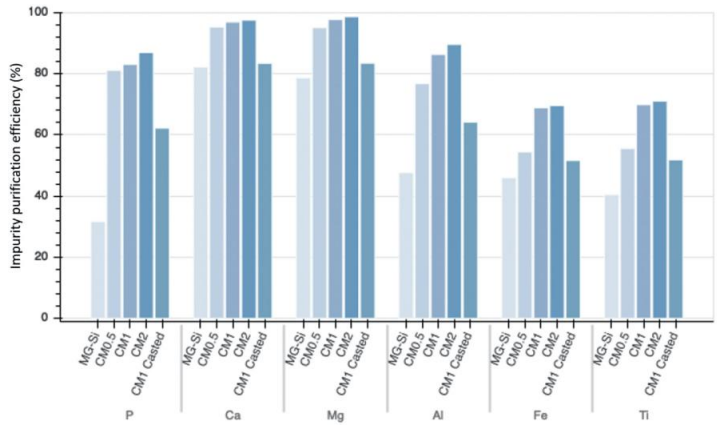

Fig. 8. Purification efficiency of studied Si-Ca-Mg alloys and MG-Si leached by HCl at 60 °C for 3 h, particle size: 0.2–1 mm. (digital version in color).

$$\eta = \left(\frac{X^{initial}_{\text{P in Si}(l)} - X_{\text{P in Si}(s)}}{X^{initial}_{\text{P in Si}(l)}}\right) \times 100\% \quad (19)$$

where $X^{initial}_{\text{P in Si}(l)}$ and $\overline{X}_{\text{P in Si}(s)}$ represent the initial P concentration in Si and the averaged P concentration in purified Si after leaching.

Herein, $\overline{X}_{\text{P in Si}(s)}$ can be obtained by integrating the Gulliver-Scheil equation from the starting point of solidification to the eutectic point:

$$X_{\text{P in Si}(s)} = \frac{X^{initial}_{\text{P in Si}(l)}}{f^{Eu}_s}\left(1-\left(1-f^{Eu}_s\right)^{k_P^{Si-Me1-Me2}}\right) \quad (20)$$

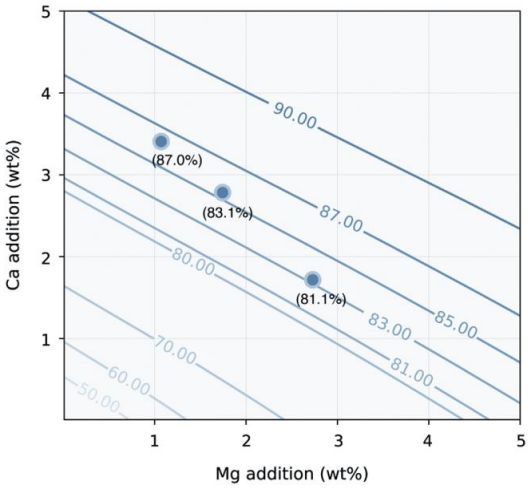

Fig. 9. Comparison between predicted (solid lines) and measured (scatters with numbers in parentheses) P removal degree of Si-Ca-Mg alloying-leaching system. (digital version in color).

With,

$$X^{Eu}_{\text{P in Si }(l)} = X^{initial}_{\text{P in Si}(l)}\left(f^{Eu}_s\right)^{k_P^{Si-Me1-Me2}-1} \quad (21)$$

Thus, after rearrangement, the P removal degree can be further re-written as:

$$\eta = \left(1-\frac{1-\frac{X_{\text{P in Si }(l)}}{X^{initial}_{\text{P in Si}(l)}}\left(1-f^{Eu}_s\right)}{f^{Eu}_s}\right) \times 100\% \quad (22)$$

To further cope with the expression of the $\frac{X^{Eu}_{\text{P in Si }(l)}}{X^{initial}_{\text{P in Si}(l)}}$, the definition of Gulliver-Scheil equation:

$$(1-f_s)\mathrm{d}X_{P(l)} = (X_{P(l)} - X_{P(s)})\mathrm{d}f_s \quad (23)$$

Considering the relationship $X_{P(s)} = k_P^{Si-Me1-Me2}X_{P(l)}$, it yields:

$$\frac{\mathrm{d}X_{P(l)}}{X_{P(l)}} = \frac{1-k_P^{Si-Me1-Me2}}{(1-f_s)}\mathrm{d}f_s \quad (24)$$

The term is thus obtained after integration:

$$\ln\frac{X^{Eu}_{\text{P in Si}(l)}}{X^{initial}_{\text{P in Si}(l)}} = \int_0^{f^{Eu}_s}\frac{1-k_P^{Si-Me1-Me2}}{1-f_s}\mathrm{d}f_s \quad (25)$$

Finally, the P removal degree model for ternary alloy system is obtained:

$$\eta = \left(1-\frac{1-\frac{\exp\left(k_P^{Si}E_i\left(\frac{\varepsilon^P_{Me1}X_{Me1}+\varepsilon^P_{Me2}X_{Me2}}{1-f^{Eu}_s}\right)\right)}{\exp\left(k_P^{Si}E_i(\varepsilon^P_{Me1}X_{Me1}+\varepsilon^P_{Me2}X_{Me2})\right)}}{f^{Eu}_s}\right) \quad (26)$$

where the $E_i(x)$ function represents the exponential integral $E_i(x) = \int_{-\infty}^{x}\frac{e^t dt}{t}$.

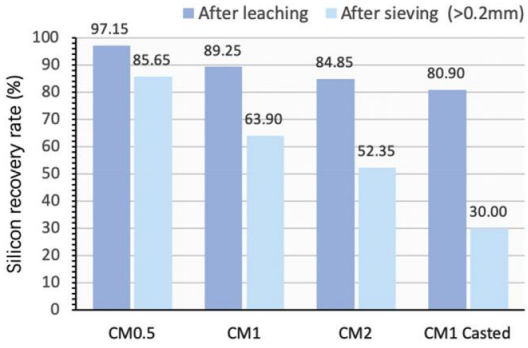

Fig. 10. Si recovery rates for particle size 0.2–1 mm. The dark blue column (left) indicates the Si recovery rate measured by the weight ratio of all obtained materials and charged materials; the light blue column (right) indicates the weight ratio of particle size bigger than 0.2 mm and charged materials. (digital version in color).

Subsequently, for the Si-Ca-Mg alloying system, we have:

$$\eta = \left(1 - \frac{1 - \frac{\exp\left(k_P^{Si} E_i \left(\frac{\varepsilon_{Ca}^{P} X_{Ca\ in\ Si(l)}^{initial} + \varepsilon_{Mg}^{P} X_{Mg\ in\ Si(l)}^{initial}}{1 - f_s^{Eu}}\right)\right)}{\exp\left(k_P^{Si} E_i \left(\varepsilon_{Ca}^{P} X_{Ca\ in\ Si(l)}^{initial} + \varepsilon_{Mg}^{P} X_{Mg\ in\ Si(l)}^{initial}\right)\right)}}{f_s^{Eu}}\right) \quad (27)$$

The results of measured and predicted P removal degree after acid leaching are presented in Fig. 9. Good agreement can be seen by using the previously obtained value $\varepsilon_{Mg}^{P} = -10.8$ for Mg-P interaction [16] and the estimated value $\varepsilon_{Ca}^{P} = -22.4$ is calculated from the Waseda model [62] at 1687 K. Since ε_{Ca}^{P} is more negative, it is seen that with fixed P removal degree, less metal doping amount is needed for Ca. Furthermore, the model also suggests an essential parameter for the alloying-leaching process that 80% P removal can be reached by alloying around 4.5 wt% Mg or 3 wt% Ca, while for the Si-Ca-Mg ternary alloying-leaching, between 3 and 4.5 wt% metal alloying is needed.

3.5. Si recovery

Si recovery rate is a critical index which directly determines the process profits and feasibility. However, the effect of alloying composition and solidification conditions on the Si recovery is still rarely reported. By measuring the weight of material before and after leaching, the results of Si recovery rate of the studied Si-Ca-Mg alloys are shown in Fig. 10. It is apparently seen that Si recovery follows the order: CM0.5 (97.15%) > CM1 (89.25%) > CM2 (84.85%) > CM1-Casted (80.90%). The reason is attributed to the increasing particle disintegration with increasing Ca/Mg ratio that enhanced the fine particle loss in the post-cleaning and washing process. A more distinct trend can be seen by sieving out fine particles with a diameter of less than 0.2 mm (the minimum charging particle size) that the Si recovery significantly decreases with increasing Ca/Mg ratio and by casting. For example, only 52.35% and 30.00% Si were recovered for sample CM2 and CM1-Casted. Thus, even though a high Ca/Mg mixing ratio brings a better leaching efficiency, but it is, however, detrimental to the Si recovery. This result suggests that an optimal alloy composition design should balance the impurity removal efficiency and the final Si yield. Additionally, by comparing CM1 and CM1-Casted, cooling rate also plays an important role on Si recovery as the finer Si grain resulted by fast cooling (as presented in Fig. 4) may lead to higher Si loss in the purification process.

4. Conclusions

In the present work, a parametric study was carried on studying the effect of Ca/Mg mixing ratio and solidification conditions on the Si alloying-leaching purification. The results can be summarized as follows:

(1) $Ca_7Mg_{7.5\pm\delta}Si_{14}$ was found as the main phase of all studied Si-Ca-Mg alloys that gathering impurities and affect leaching behavior, while Mg_2Si and $CaSi_2$ appear depends on the Ca/Mg mixing ratio. Compared to furnace cooling, rapid cooling reduces Si grain size distinctly and suppresses impurity segregation.
(2) HCl is found as the most economical leaching agents among the studied combinations. Finer particle size promotes higher leaching efficiency, but with increasing Ca/Mg ratio, the increment narrows.
(3) The leaching kinetics of Si-Ca-Mg alloys follows a cracking-shrinking model on the basis of the modification of Kröger-Ziegler model under spherical condition.
(4) Impurity purification efficiency increases with increasing Ca/Mg mixing ratio but considerably decreases with fast cooling.
(5) A model for P removal degree prediction was developed for ternary alloy system and in good agreement with the leaching results of the studied Si-Ca-Mg alloys.

Declaration of Competing Interest

The authors declare that they have no known competing financial interests or personal relationships that could have appeared to influence the work reported in this paper.

Acknowledgment

This work was performed at NTNU within the Research Centre for Sustainable Solar Cell Technology (FME SuSolTech, project number 257639), co-sponsored by the Norwegian Research Council and industry partners. The authors also appreciate the fruitful discussions with Arman Hoseinpur and the ICP-MS assistance by Gagan Paudel from NTNU.

References

[1] A. Murgau, J. Safarian, Solar silicon production through metallurgical route and REC solar advancements, Silicon Chem. Sol. Ind. XIV (2018) 183–192 Svolvær, Norway.
[2] J. Safarian, M. Tangstad, Processes for upgrading metallurgical grade silicon to solar grade silicon, Energy Procedia 20 (2012) 88–97, https://doi.org/10.1016/J.EGYPRO.2012.03.011.
[3] Z. Yu, W. Ma, K. Xie, G. Lv, Z. Chen, J. Wu, J. Yu, Life cycle assessment of grid-connected power generation from metallurgical route multi-crystalline silicon photovoltaic system in China, Appl. Energy 185 (2017) 68–81, https://doi.org/10.1016/j.apenergy.2016.10.051.
[4] J. Safarian, G. Tranell, M. Tangstad, Boron removal from silicon by CaO-Na2O-SiO2 ternary slag, Metall. Mater. Trans. E. 2 (2015) 109–118, https://doi.org/10.1007/s40553-015-0048-7.
[5] L.A.V. Teixeira, K. Morita, Removal of boron from molten silicon using CaO-SiO2 based slags, ISIJ Int. 49 (2009) 783–787, https://doi.org/10.2355/isijinternational.49.783.
[6] J. Wu, D. Yang, M. Xu, W. Ma, Q. Zhou, Z. Xia, Y. Lei, K. Wei, S. Li, Z. Chen, K. Xie, Boron removal from silicon using secondary refining techniques by metallurgical method, Sep. Purif. Rev. 49 (2020) 68–88, https://doi.org/10.1080/15422119.2018.1523191.
[7] Y. Wang, K. Morita, Evaporation removal of boron in molten silicon using reactive fluxes, Miner. Met. Mater. Ser. (2017) 367–375, https://doi.org/10.1007/978-3-319-52192-3_36.
[8] M. Fang, C. Lu, L. Huang, H. Lai, J. Chen, X. Yang, J. Li, W. Ma, P. Xing, X. Luo, Multiple slag operation on boron removal from metallurgical-grade silicon using Na2O-SiO2 slags, Ind. Eng. Chem. Res. 53 (2014) 12054–12062, https://doi.org/10.1021/ie404427c.

[9] J. Wu, F. Wang, W. Ma, Y. Lei, B. Yang, Thermodynamics and kinetics of boron removal from metallurgical grade silicon by addition of high basic potassium carbonate to calcium silicate slag, Metall. Mater. Trans. B Process Metall. Mater. Process. Sci. 47 (2016) 1796–1803, https://doi.org/10.1007/s11663-016-0615-z.

[10] H. Chen, K. Morita, X. Ma, Z. Chen, Y. Wang, Boron removal for solar-grade silicon production by metallurgical route:a review, Sol. Energy Mater. Sol. Cells 203 (2019) 110169, https://doi.org/10.1016/j.solmat.2019.110169.

[11] T. Yoshikawa, K. Morita, Refining of silicon during its solidification from a Si–Al melt, J. Cryst. Growth 311 (2009) 776–779, https://doi.org/10.1016/J.JCRYSGRO.2008.09.095.

[12] L. Huang, H. Lai, C. Lu, M. Fang, W. Ma, P. Xing, J. Li, X. Luo, Enhancement in extraction of boron and phosphorus from metallurgical grade silicon by copper alloying and aqua regia leaching, Hydrometallurgy. 161 (2016) 14–21, https://doi.org/10.1016/j.hydromet.2016.01.013.

[13] L.T. Khajavi, K. Morita, T. Yoshikawa, M. Barati, Removal of boron from silicon by solvent refining using ferrosilicon alloys, Metall. Mater. Trans. B Process Metall. Mater. Process. Sci. 46 (2014) 615–620, https://doi.org/10.1007/s11663-014-0236-3.

[14] X. Ma, T. Yoshikawa, K. Morita, Si growth by directional solidification of Si–Sn alloys to produce solar-grade Si, J. Cryst. Growth 377 (2013) 192–196, https://doi.org/10.1016/J.JCRYSGRO.2013.05.024.

[15] Y. Li, L. Zhang, Application of Si-based solvents to the purification of metallurgical grade-silicon, Sep. Purif. Rev. (2019) 1–24, https://doi.org/10.1080/15422119.2019.1623253.

[16] M. Zhu, A. Azarov, E. Monakhov, K. Tang, J. Safarian, Phosphorus separation from metallurgical-grade silicon by magnesium alloying and acid leaching, Sep. Purif. Technol. 240 (2020) 116614, https://doi.org/10.1016/j.seppur.2020.116614.

[17] A. Schei, Metallurgical production of high purity silicon, 4th Int.Ferro Alloys Cong. (1986) 389–398 Rio de Janeiro, Brazil.

[18] H. Lai, L. Huang, C. Lu, M. Fang, W. Ma, P. Xing, J. Li, X. Luo, Leaching behavior of impurities in Ca-alloyed metallurgical grade silicon, Hydrometallurgy. 156 (2015) 173–181, https://doi.org/10.1016/j.hydromet.2015.06.012.

[19] J. Safarian, M. Tangstad, Vacuum refining of molten silicon, Metall. Mater. Trans. B Process Metall. Mater. Process. Sci. 43 (2012) 1427–1445, https://doi.org/10.1007/s11663-012-9728-1.

[20] A. Hoseinpur, K. Tang, J. Safarian, Kinetic study of vacuum evaporation of elements from ternary melts; case of dilute solution of P in Si-Al melts, Sep. Purif. Technol. 235 (2020)https://doi.org/10.1016/j.seppur.2019.116284.

[21] S.-S. Zheng, T. Abel Engh, M. Tangstad, X.-T. Luo, Separation of phosphorus from silicon by induction vacuum refining, Sep. Purif. Technol. 82 (2011) 128–137, https://doi.org/10.1016/j.seppur.2011.09.001.

[22] J. Safarian, K. Tang, K. Hildal, G. Tranell, Boron removal from silicon by humidified gases, Metall. Mater. Trans. E. 1 (2014) 41–47, https://doi.org/10.1007/s40553-014-0007-8.

[23] Ø.S. Sortland, M. Tangstad, Boron removal from silicon melts by H2O/H2 gas blowing: mass transfer in gas and melt, Metall. Mater. Trans. E. 1 (2014) 211–225, https://doi.org/10.1007/s40553-014-0021-x.

[24] Z. Xia, J. Wu, W. Ma, Y. Lei, K. Wei, Y. Dai, Separation of boron from metallurgical grade silicon by a synthetic CaO-CaCl2 slag treatment and Ar-H2O-O2 gas blowing refining technique, Sep. Purif. Technol. 187 (2017) 25–33, https://doi.org/10.1016/j.seppur.2017.06.037.

[25] J. Wu, Y. Zhou, W. Ma, M. Xu, B. Yang, Synergistic separation behavior of boron in metallurgical grade silicon using a combined slagging and gas blowing refining technique, Metall. Mater. Trans. B Process Metall. Mater. Process. Sci. 48 (2017) 22–26, https://doi.org/10.1007/s11663-016-0860-1.

[26] N.P. Tucker, Preparation of high purity silicon, J. Iron Steel Ind. 15 (1927) 412–414.

[27] L.P. Hunt, V.D. Dosaj, J.R. McCormick, L.D. Crossman, Production of solar-grade silicon from purified metallurgical silicon, 12th IEEE Photovolt. Spec. Conf. (1976) 125–129.

[28] J. Dietl, Hydrometallurgical purification of metallurgical-grade silicon, Sol. Cells. 10 (1983) 145–154, https://doi.org/10.1016/0379-6787(83)90015-7.

[29] I.C. Santos, A.P. Goncalves, C.S. Santos, M. Almeida, M.H. Afonso, M.J. Cruz, Purification of metallurgical grade silicon by acid leaching, Hydrometallurgy. 23 (1990) 237–246, https://doi.org/10.4028/www.scientific.net/AMR.418-420.1590.

[30] T.L. Chu, S.S. Chu, Partial purification of metallurgical silicon by acid extraction, J. Electrochem. Soc. 130 (1983) 455, https://doi.org/10.1149/1.2119730.

[31] H. Lu, K. Wei, W. Ma, K. Xie, J. Wu, Y. Lei, The effect of secondary refining on the removal of phosphorus from metallurgical-grade silicon by acid leaching, Metall. Mater. Trans. B Process Metall. Mater. Process. Sci. 48 (2017) 2768–2780, https://doi.org/10.1007/s11663-017-1042-5.

[32] E. Kim, K. Osseo-Asare, Dissolution windows for hydrometallurgical purification of metallurgical-grade silicon to solar-grade silicon: eh–pH diagrams for Fe silicides, Hydrometallurgy. 127–128 (2012) 178–186, https://doi.org/10.1016/J.HYDROMET.2012.05.013.

[33] F. Margarido, J.P. Martins, M.O. Figueiredo, M.H. Bastos, Kinetics of acid leaching refining of an industrial Fe-Si alloy, Hydrometallurgy. 34 (1993) 1–11, https://doi.org/10.1016/0304-386X(93)90077-Q.

[34] F. Margarido, M.H. Bastos, M.O. Figueiredo, J.P. Martins, The structural effect on the kinetics of acid leaching refining of Fe-Si alloys, Mater. Chem. Phys. 38 (1994) 342–347, https://doi.org/10.1016/0254-0584(94)90211-9.

[35] J.P. Martins, F. Margarido, The cracking shrinking model for solid-fluid reactions, Mater. Chem. Phys. 44 (1996) 156–169, https://doi.org/10.1016/0254-0584(95)01670-P.

[36] T. Yoshikawa, K. Morita, An evolving method for solar-grade silicon production: solvent refining, Jom. 64 (2012) 946–951, https://doi.org/10.1007/s11837-012-0371-8.

[37] B. Ban, X. Bai, J. Li, J. Chen, S. Dai, Effect of kinetics on P removal by Al-Si solvent refining at low solidification temperature, J. Alloys Compd. 685 (2016) 604–609, https://doi.org/10.1016/j.jallcom.2016.05.312.

[38] J. Li, Y. Liu, Y. Tan, Y. Li, L. Zhang, S. Wu, P. Jia, Effect of tin addition on primary silicon recovery in Si–Al melt during solidification refining of silicon, J. Cryst. Growth 371 (2013) 1–6, https://doi.org/10.1016/J.JCRYSGRO.2012.12.098.

[39] G. Qian, L. Sun, H. Chen, Z. Wang, K. Wei, W. Ma, Enhancing impurities removal from Si by controlling crystal growth in directional solidification refining with Al–Si alloy, J. Alloys Compd. 820 (2020) 153300, https://doi.org/10.1016/j.jallcom.2019.153300.

[40] Y. Li, Y. Tan, J. Li, K. Morita, Si purity control and separation from Si–Al alloy melt with Zn addition, J. Alloys Compd. 611 (2014) 267–272, https://doi.org/10.1016/J.JALLCOM.2014.05.138.

[41] Y. Lei, P. Qiu, K. Chen, X. Chen, W. Ma, J. Wu, K. Wei, S. Li, G. Lv, J. Qiu, Mechanism of ZrB2 formation in Al-Si alloy and application in Si purification, ACS Sustain. Chem. Eng. 7 (2019) 12990–12996, https://doi.org/10.1021/acssuschemeng.9b02065.

[42] L. Huang, J. Chen, A. Danaei, S. Thomas, L. Huang, X. Luo, M. Barati, Effect of Ti addition to cu-Si alloy on the boron distribution in various phases, J. Alloys Compd. 734 (2018) 235–242, https://doi.org/10.1016/j.jallcom.2017.10.279.

[43] L. Tafaghodi Khajavi, M. Barati, Thermodynamics of phosphorus in solvent refining of silicon using ferrosilicon alloys, Metall. Mater. Trans. B Process Metall. Mater. Process. Sci. 48 (2017) 268–275, https://doi.org/10.1007/s11663-016-0804-9.

[44] L.T. Khajavi, K. Morita, T. Yoshikawa, M. Barati, Thermodynamics of boron distribution in solvent refining of silicon using ferrosilicon alloys, J. Alloys Compd. 619 (2015) 634–638, https://doi.org/10.1016/j.jallcom.2014.09.062.

[45] F. Yang, J. Wu, W. Ma, Thermodynamic modeling and experimental study on interaction of Fe to P in silicon solution, Metall. Mater. Trans. B Process Metall. Mater. Process. Sci. 51 (2020) 2381–2390, https://doi.org/10.1007/s11663-020-01895-9.

[46] T. Shimpo, T. Yoshikawa, K. Morita, Thermodynamic study of the effect of calcium on removal of phosphorus from silicon by acid leaching treatment, Metall. Mater. Trans. B Process Metall. Mater. Process. Sci. 35 (2004) 277–284, https://doi.org/10.1007/s11663-004-0029-1.

[47] Y.V. Meteleva-Fischer, Y. Yang, R. Boom, B. Kraaijveld, H. Kuntzel, Microstructure of metallurgical grade silicon and its acid leaching behaviour by alloying with calcium, Trans. Institutions Min. Metall. Sect. C Miner. Process. Extr. Metall. 122 (2013) 229–237, https://doi.org/10.1179/0371955313Z.00000000068.

[48] M.D. Johnston, M. Barati, Calcium and titanium as impurity getter metals in purification of silicon, Sep. Purif. Technol. 107 (2013) 129–134, https://doi.org/10.1016/j.seppur.2013.01.028.

[49] H. Sakiani, S.H. Tabaian, J. Chen, Effect of calcium addition on the silicon purification in the presence of low concentration of iron, J. Alloys Compd. 830 (2020) 154112, https://doi.org/10.1016/j.jallcom.2020.154112.

[50] J. Safarian, S. Espelien, Hydrometallurgical purification of Maganesium-doped silicon by difference acids, 33 Eur. Photovolt. Sol. Energy Conf. Exhib. (2017) 480–482.

[51] M. Zhu, A. Murgau, J. Safarian, Effects of magnesium-doping on silicon leaching for solar grade feedstock production, 35 Eur. Photovolt. Sol. Energy Conf. Exhib. (2018) 465–468, https://doi.org/10.4229/35thEUPVSEC20182018-2AV.1.3.

[52] M. Zhu, S.Y. Yue, K. Tang, J. Safarian, New insights into silicon purification by alloying—leaching refining: a comparative study of Mg—Si, Ca—Si, and Ca—Mg—Si systems, ACS Sustain. Chem. Eng. 8 (42) (2020) 15953–15966, https://doi.org/10.1021/acssuschemeng.0c05564.

[53] S. Espelien, G. Tranell, J. Safarian, Effect of magnesium addition on removal of impurities from silicon by hydrometallurgical treatment, in: Energy Technol. 2017, Springer, 2017: pp. 355–366. doi: https://doi.org/10.1007/978-3-319-52192-3_35.

[54] S. Cui, M. Paliwal, I.-H. Jung, Thermodynamic Optimization of Ca-Fe-Si System and Its Applications to Metallurgical Grade Si-Refining Process, 2020https://doi.org/10.1007/s40553-014-0010-0.

[55] M.C.J. Marker, B. Skolyszewska-Kühberger, H.S. Effenberger, C. Schmetterer, K.W. Richter, Phase equilibria and structural investigations in the system Al-Fe-Si, Intermetallics. 19 (2011) 1919–1929, https://doi.org/10.1016/j.intermet.2011.05.003.

[56] Y.V. Meteleva-Fischer, Y. Yang, R. Boom, B. Kraaijveld, H. Kuntzel, Microstructure of metallurgical grade silicon during alloying refining with calcium, Intermetallics. 25 (2012) 9–17, https://doi.org/10.1016/j.intermet.2012.02.009.

[57] B. Ban, X. Bai, J. Li, Y. Li, J. Chen, S. Dai, The mechanism of P removal by solvent refining in Al-Si-P system, Metall. Mater. Trans. B Process Metall. Mater. Process. Sci. 46 (2015) 2430–2437, https://doi.org/10.1007/s11663-015-0449-0.

[58] E. Kim, K. Osseo-Asare, Dissolution windows for hydrometallurgical purification of metallurgical-grade silicon to solar-grade silicon: eh-pH diagrams for Fe silicides, Hydrometallurgy. 127–128 (2012) 178–186, https://doi.org/10.1016/j.hydromet.2012.05.013.

[59] J.P. Martins, F. Margarido, The cracking shrinking model for solid-fluid reactions, Mater. Chem. Phys. 44 (1996) 156–169, https://doi.org/10.1016/0254-0584(95)01670-P.

[60] D. Zhao, Y. Li, Revealing the factors influencing grain boundary segregation of P, as in Si: insights from first-principles, Acta Mater. 168 (2019) 52–62, https://doi.org/10.1016/J.ACTAMAT.2019.02.014.

[61] C.W. Bale, A.D. Pelton, The unified interaction parameter formalism: thermodynamic consistency and applications, Metall. Mater. Trans. A 21A (1989).

[62] S. Ueno, Y. Waseda, K.T. Jacob, S. Tamaki, Theoretical treatment of interaction parameters in multicomponent metallic solutions, Steel Res. 59 (1988).

Paper 5

Silicon for the Chemical and Solar Industry XV
Trondheim, Norway, June 15 – 18, 2020

The effect of Ti and Y addition on the microstructure and leaching purification of Ca-alloyed metallurgical silicon

Mengyi Zhu[1)], Kai Tang[2)], Jafar Safarian[1)]

1) *Department of Materials Science and Engineering, Norwegian University of Science and Technology (NTNU), No-7491 Trondheim, Norway*
2) *SINTEF Materials and Chemistry, No-7491 Trondheim, Norway*

Abstract

Metallurgical-grade silicon (MG-Si) purification through metal alloying combined with acid leaching is a feasible technique with low-cost and low energy consumption features. To improve the impurities removal efficiency, especially for the removal of B and P, the present work was carried out to study the effects of Ti and Y addition on the impurities removal in acid leaching of Ca-doped silicon. Commercial MG-Si was mixed with 4 wt% reagent grade Ca and specific amounts of Ti or Y, the mixture was then melted, and then was slowly solidified and cooled down. Obtained alloys were further crushed to specific particle size (0.1-0.6 mm). Acid leaching trials were performed with 10%HCl at 60 °C under ultrasonic mixing. The concentrations of the impurities of the obtained ternary Si alloys and the leaching products were characterized by inductively coupled plasma mass spectrometry (ICP-MS). Electron microscopy examination indicates that the main precipitates in Si-Ca-Y alloys are silicides such as $CaSi_2$, YSi_2, $CaAl_2Si_2$, and Al-Fe-Y-Si phase, and they are distributed between the primary silicon grains. In the Si-Ca-Ti alloys, however, the main silicide precipitates are $CaSi_2$, $TiSi_2$, $CaAl_2Si_2$, and $FeTiSi_2$. In both cases, the main impurities, such as P and Fe, are concentrated in specific silicides. After leaching, it was found that Ti and Y exhibit relatively equivalent P removal ability with both around 75% removal, but the Si-Ca-Y alloys show 20% B removal, which is higher than that of the Si-Ca-Ti alloy with 10% B removal.

Introduction

There have been significant efforts devoted to the reduction of energy consumption and the carbon footprint of the solar-grade silicon (SoG-Si) production in the photovoltaic

industry. In recent years, transformational technology for the alternate Siemens SoG-Si production has been developed in Norway, known as the ELKEM Solar process, which has been operated by REC Solar Norway in recent years, that can significantly improve process sustainability. According to the investigation from Murgau and Safarian [1], the energy consumption of the ELKEM process is significantly reduced from ~170kWh/kg Si to 30-60 kWh/kg Si with also 10.8 kg CO_2/kg SoG-Si carbon footprint compared to the traditional Siemens process. In the ELKEM Solar process [1], [2], the metallurgical-grade silicon (MG-Si) produced from submerge arc furnace is further refined through a combination of a series metallurgical refining techniques; slag refining, acid leaching, and directional solidification. As one of the most crucial purification targets, phosphorus impurity is largely removed in the acid leaching procedure in order to fit the strict requirements of SoG-Si. The main principle of the leaching technique is based on the digestion of segregated impurities along Si grain boundaries and thus to obtain the pure primary Si grains. The optimum leaching conditions and leaching efficiency of direct Si leaching have been studied by many researchers [3]–[7], and it has been found out that predominant metallic impurities can be removed by this approach, but the efficiency of B and P removal is still limited, in particular B removal.

To date, considerable work had been done on the improvement of the acid leaching technique by alloying Si with other metal refiners to modify the impurity segregation behaviour. As one successful strategy, solvent refining is known to achieve high P removal degree and also a certain amount of B removal by alloying Si with a large amount of metal refiner, such as Al[8]–[12], Fe[13], Sn[14]–[16], and Cu[17], [18]. It has to be emphasized that solvent refining is a high-temperature process, which is different from the alloying-leaching process. However, the addition of a small amount of refiner metal with high impurity affinity exhibits more benefits for the industry for the alloying-leaching process. In this way, alkaline earth elements (Ca[19]–[22] and Mg[23]–[25]) are of the most often studied metal refiners due to their high P affinity and good leaching kinetics. Schei et al.[20] reported Ca addition can significantly enhance the precipitation of impurities in the leachable $CaSi_2$ phase upon solidification and reach high purification efficiency, a great number of attention has been paid to the Si-Ca related alloying systems. Shimpo et al.[21] also studied the P removal of Ca-alloyed Si by acid leaching, and measured the interaction coefficient $\varepsilon^{P}_{Ca\ in\ Si}$ to be 14.6±1.7 at 1723K, which indicates a great P activity reduction after Ca alloying into the Si melt. Meteleva-Fisher et al.[26] also confirmed the decisive role of Ca on impurity gathering and studied the effect of cooling rate on microstructure of Ca-alloyed Si. Apart from the alkaline earth elements, the Group IV elements (Ti[22], Zr[27], Hf[28]) and rare earth elements (REE)[29], [30] also attract great attention for researchers recently due to their high affinity to B and P. According to Johnston et al. [22], as much as ~50% B can be removed with 5wt% Ti addition into MG-Si, and ~80% P removal with 1wt% rare earth elements addition [29].

In the present work, novel ternary alloying refining systems of Si-Ca-Ti and Si-Ca-Y were designed to explore their purification efficiency. Since there is very rare information about these alloying systems, the effect of Ti and Y addition on the microstructure of Ca-alloyed MG-Si was also studied.

140

Materials and methods

Commercial MG-Si was used in the present study for the alloying-leaching purification. The MG-Si was first mixed with reagent grade Ca and Ti (Y) in an alumina crucible. Materials were then heated up to 1500 °C to form a Si-Ca-Ti (Y) melt in an induction furnace. After the mixture was fully melted, the melt was slowly cooled down to the room temperature inside the furnace chamber. The obtained alloys were then crushed and milled in a ring mill, and finally sieved to the particle size range 0.1-0.6 mm for the acid leaching. The average compositions of two analysed samples for each material are listed in Table 1.

Table 1: Composition (in ppmw) of MG-Si and obtained Si-Ca-Ti and Si-Ca-Y alloys.

Impurity	Si-Ca-Ti	Si-Ca-Y
B	42.22±3.79	41.50±0.83
P	12.09±0.16	12.84±0.19
Ca	26974.58±499.13	30386.76±1554.91
Mg	16.74±0.02	20.30±2.67
Al	5781.09±275.84	8064.72±559.58
Fe	2749.14±8.42	2435.62±105.27
Ti	20821.95±187.18	217.99±2.93
Y	0.65±0.05	15693.55±1122.24

Alloy samples were leached by hydrochloric acid (HCl) with a concentration of 10% at a temperature of 60°C for 2 hours. All the leaching trials were performed in an ultrasonic bath. The samples after leaching were washed by distilled water and ethanol, and were then dried at 80°C for 1h.

The microstructure and impurity distribution of the obtained alloys were analysed by Electron Probe Micro-Analyzer (EPMA). In addition, the samples before and after leaching were analyzed by the high-resolution Inductively Coupled Plasma-Mass Spectroscopy (ICP-MS) technique for the impurities determination.

Results and discussion

Effect of Ti and Y-doping on Si microstructure

The microstructure of the obtained Si-Ca-Ti and Si-Ca-Y alloys can be seen in Figure 1. To further study the impurity segregation behaviour affected by the Ti and Y addition, EPMA analysis was performed, as typical results are shown in Figure 2. It is worth noting that the concentration of B, P, and Mg is much lower than the EPMA detection sensitivity. Thus, the mapping results of B, P, and Mg should be not reliable, while they are good for comparing the phases qualitatively. Subsequently, only the main impurity phases were discussed. The detailed compositions of detected impurity phases measured by WDS in EPMA are presented in Table 2 and Table 3 for Si-Ca-Ti and Si-Ca-Y alloys, respectively.

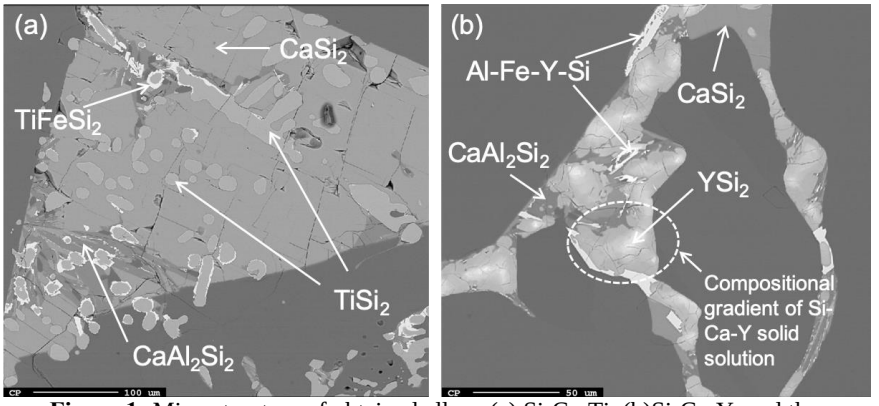

Figure 1: Microstructure of obtained alloys (a) Si-Ca-Ti, (b)Si-Ca-Y, and the characterized secondary precipitates between primary silicon grains.

It can be seen that the main abundant precipitated secondary phase in the Si-Ca-Ti alloy is $CaSi_2$. No ternary Ca-Ti-Si intermetallic phase is observed, and a number of $TiSi_2$ islands (more globular) were found embedded inside and out of the $CaSi_2$ precipitates. Compared to the morphology of the $TiSi_2$ phase observed in the binary Ti-Si system obtained by Johnston et al.[22], the $TiSi_2$ phase is more spherical rather than the irregular shape reported [22]. Additionally, the Ti-Fe-Si phase was found to surround the $TiSi_2$ phase to form either $TiFeSi_2$ compound or a $(Ti,Fe)Si_2$ solid solution. This also indicates a strong affinity between Ti and Fe in the Si melt. It is worth noting that a large amount of $CaAl_2Si_2$ phase with needle shape was found to be distributed in the $CaSi_2$ phase, which is attributed to small corrosion of the alumina crucible surface, in addition to small Al in the original MG-Si. This is found by comparing the compositions of materials in Table 1.

To the best knowledge of the authors, there have been no studies about the microstructure of the Si-Ca-Y alloy system. In the present work, it can be seen that the distribution of Ca and Y in the secondary precipitated phases has a conjugated composition gradient. The center part of the Si-Ca-Y phase is more bright, indicating more Y, and YSi_2 phase enriched with around 5at% Ca, and this area is surrounded by a $(Ca,Y)Si_2$ solid solution with less Y, i.e., 5-10at% Y. The reason for this unique microstructure may be the known Hume-Rothery rules that Ca and Y to form interstitial solid solution since they sit near with each other in the periodic table, and consequently, show similar atomic radius and electronegativity. The slow cooling during the alloy making may also have a positive effect on this phenomenon. The $CaAl_2Si_2$ phase was observed in between the Si-Ca-Y precipitates, indicating the deposition of these phases most likely upon eutectic reaction. The segregation behaviour of Fe impurity is significantly affected by the Y addition, and an Al-Fe-Y-Si intermetallic phase was observed, while neither $FeSi_{2.4}$ nor the $FeTiSi_2$ phase was formed, which usually exist along the grain boundaries of the MG-Si.

142

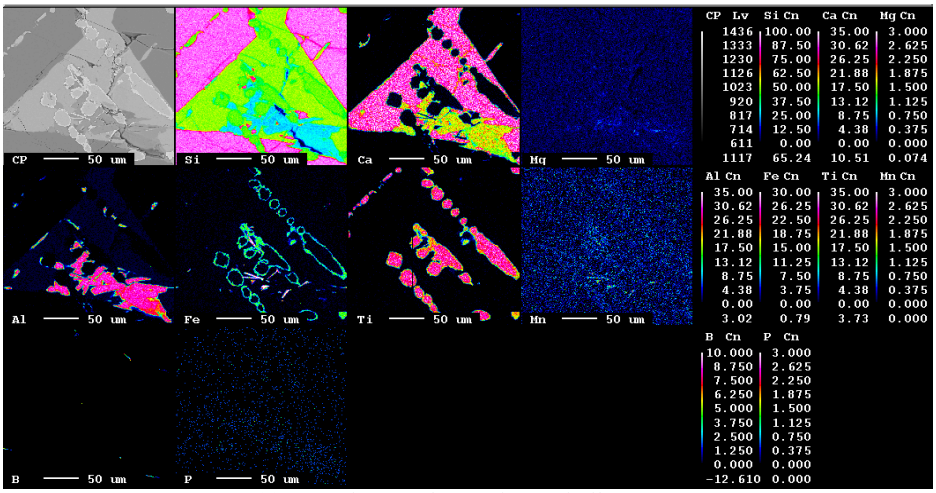

(a) Mapping results of Si-Ca-Ti alloy

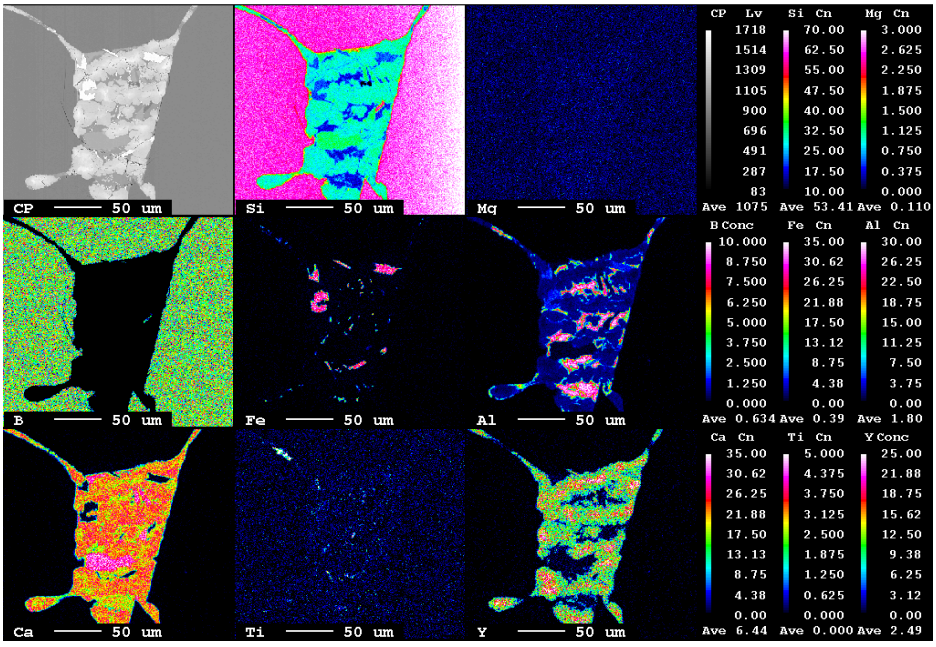

(b) Mapping results of Si-Ca-Y alloy

Figure 2: X-Ray elemental mapping of the obtained Si-Ca-Ti and Si-Ca-Y alloying system measured by EPMA.

Table 1: Measured composition of major impurity in Si-Ca-Ti alloy by WDS.

Phase	Composition (at%)				
	Si	**Ca**	**Al**	**Fe**	**Ti**
$CaSi_2$	66.20±0.12	32.87±0.12	0.78±0.04	0.04±0.01	0.09±0.05
$CaAl_2Si_2$	40.78±0.25	19.24±0.04	39.61±0.26	0.07±0.02	0.14±0.07
$TiSi_2$	66.03±0.19	0.32±0.07	0.21±0.11	0.10±0.06	33.31±0.16
$TiFeSi_2$	48.80±0.36	0.64±0.05	2.10±0.21	24.92±0.23	24.92±1.74
$(Ti,Fe)Si_2$	63.18±0.27	0.45±0.05	0.45±0.27	8.22±0.16	27.28±0.66

Table 3: Measured composition of major impurity in Si-Ca-Y alloy by WDS.

Phase	Composition (at%)					
	Si	**Ca**	**Al**	**Fe**	**Ti**	**Y**
$CaSi_2$	65.73±0.07	33.20±0.07	0.76±0.09	0.02±0.02	0.01±0.01	0.25±0.03
$CaAl_2Si_2$	40.50±0.12	19.06±0.09	38.96±0.10	0.04±0.00	0.00±0.01	0.32±0.07
YSi_2	64.90±0.36	5.36±0.84	0.49±0.10	0.06±0.08	0.00±0.01	29.10±1.08
$(Ca,Y)Si_2$	63.00±0.96	27.35±1.73	2.34±0.64	0.06±0.05	0.00±0.01	7.19±1.85
Al-Fe-Y-Si	59.09±0.31	0.66±0.02	8.84±0.07	23.97±0.10	0.13±0.04	7.30±0.21

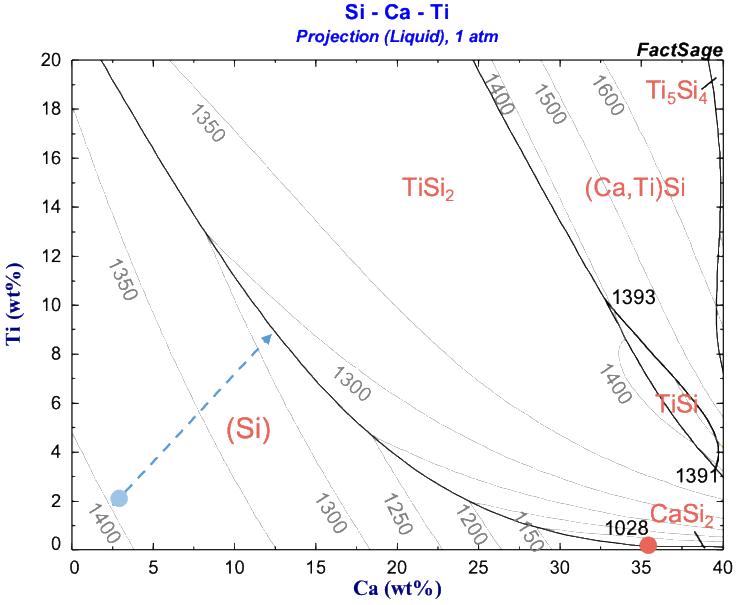

(a) Calculated liquidus surface and solidification path of Si-Ca-Ti alloy

144

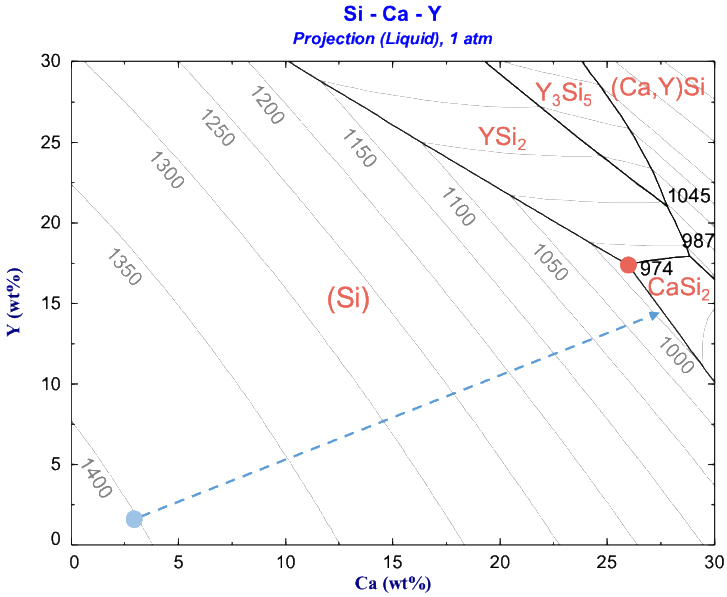

(b) Calculated liquidus surface and solidification path Si-Ca-Y alloy

Figure 3: Calculated liquidus surface and solidification path of (a) Si-Ca-Ti and (b) Si-Ca-Y alloy system where the blue circle indicates the starting alloy composition and the red circle indicates the ternary eutectic point. Isothermal lines are presented in degrees Celsius.

The phase diagram of the Si-Ca-Ti and Si-Ca-Y system was determined by thermodynamic software Factsage, and the results are shown in Figure 3. It can be seen that Si is the primary precipitate for both alloys, and no ternary intermetallic compounds were found as well. For the Si-Ca-Ti system shown in Figure 3(a), the secondary precipitating phase suggested as $TiSi_2$, which coincides with the study of Morita and Miki [31] and the finding of the separated $TiSi_2$ islands outside of the $CaSi_2$ phase. However, for the Si-Ca-Y system shown in Figure 3(b), the secondary precipitate becomes $CaSi_2$ rather than YSi_2. Compared with the microstructure presented in Figure 1 and Figure 2, it would be better for the leaching process to have the $CaSi_2$ phase as the secondary phase because other impurity phases can be well-embedded inside the leachable $CaSi_2$ phase.

In order to study further for the reason of different microstructure and impurity distribution, the values of the heat of mixing between atomic pairs $\Delta^*_{+,-}$ were obtained from Miedema's model for the binary system with equal-atomic composition [32], as shown in Figure 4. It can be seen that silicides show all negative values, which suggests the possibility to form the binary silicides with Ca, Ti, Fe, and Y, for instance, $CaSi_2$, $TiSi_2$, $FeSi_{2.4}$, and YSi_2. Furthermore, in the Ca column, all values are positive. This could explain the reason why there is no Si-Ca-Ti and Si-Ca-Y ternary intermetallics that were not found in microanalysis. Additionally, the mixing enthalpy values reveal why the $TiSi_2$

islands solely distributed in the $CaSi_2$ phase in the Ti-doped sample, since the Ca-Ti pair exhibits the most positive value. Meanwhile, the much less positive Ca-Y pair value indicates only a much weaker repulsive interaction between Ca and Y, and therefore it may explain the compositional gradients in Ca-Y-Si precipitates in the Si-Ca-Y alloy.

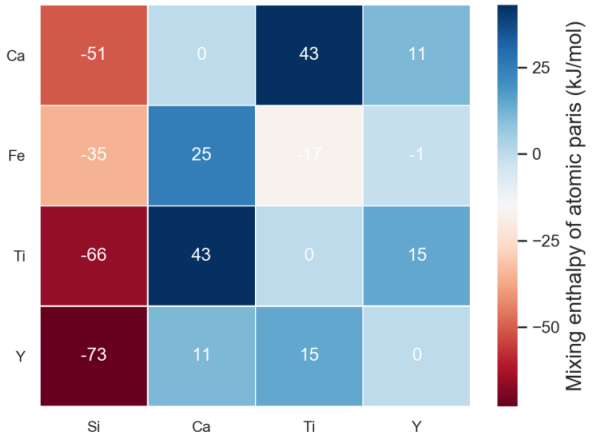

Figure 4: The values of $\boldsymbol{\Delta H_{AB}^{mix}}$ (kJ/mol) obtained by Miedema's model for atomic pairs in a Si-Ca-Ti-Y system.

Leaching performance

To further study the segregation behaviour affected by the Ti and Y addition in Ca-alloyed MG-Si, acid leaching experiments were performed, and the removal of impurities was measured by chemical composition changes. The impurities removal degree is calculated as:

$$Removal\ degree = \frac{C_i - C_f}{C_i} \times 100\% \quad (1)$$

where the C_i and C_f are initial impurity concentration (before leaching) and final concentration (after leaching) in weight percent, respectively.
The results of the leaching refining on elements removal are presented in Figure 5.

146

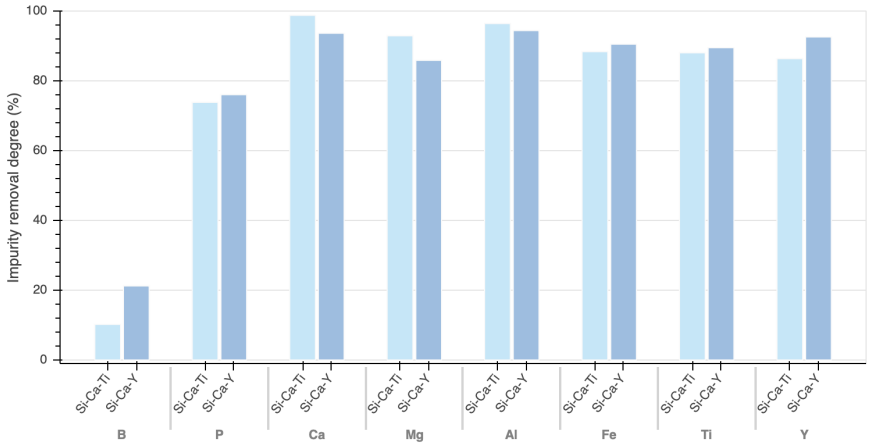

Figure 5: Comparison of impurities removal degree of the Si-Ca-Ti, and Si-Ca-Y alloying systems.

It can be seen that both of the alloys showed high purification efficiency for the metallic impurities. Since it is known that the $TiSi_2$ phase is usually considered with a low leachability in HCl aqueous solution [33], the high Ti removal from the Si-Ca-Ti sample with the existing of a large amount of the $TiSi_2$ phase may be owing to the high reactivity of $CaSi_2$ and its cracking effect that makes the insoluble impurity phase becomes easier to be carried away through washing. A nearly equivalent ability for the P removal was found for the studied Si-Ca-Ti and Si-Ca-Y alloys. The ~75% P removal is also close to the performance of the well-studied binary Si-Ca alloy[22], [29]. It may draw a conclusion that Ti and Y could have similar P affinity as Ca does. However, another factor should also be considered that the adoption of alumina crucible may also affect the P impurity segregation, which seems to be a negative effect compared to the main doping metals. It is also seen that ~10% B removal is achieved by the Si-Ca-Ti sample, and ~20% B removal by the Si-Ca-Y sample. This result suggests that B segregation behaviour could be more affected by Y than Ti in the Si-Ca system. This result also indicates that the doping of rare earth elements may have the potential for the co-removal of conventionally problematic impurities B and P.

Compared to conventional alkaline earth elements doping, the major challenge of the rare earth elements doping is from the economic concern. However, the low vapor pressure of the rare earth elements makes it possible to directly dope $ReCl_3$ into Si, where the $ReCl_3$ can be directly recycled from the leaching solution. In addition, the generated $SiCl_4$ vapor can be also easily recycled by reacting with water to obtain the HCl aqueous solution. In this way, a closed-loop material flow may significantly reduce the cost. Thus, the door for the design of a potential novel Si purification process keeps open.

Conclusions

In this work, the effect of doping Ti and Y on the impurity segregation and the leaching purification performance of Ca-alloyed MG-Si has been investigated. The main results are summarized as follows:

- It was found that the doping of Si-Ca by Ti and Y significantly affects the microstructure about the precipitated phases.
- In Si-Ca-Ti alloy, the main silicide precipitates are $CaSi_2$, $TiSi_2$, $CaAl_2Si_2$, $FeTiSi_2$, and solid solution $(Ti,Fe)Si_2$.
- In the Si-Ca-Y alloy, the main precipitates are $CaSi_2$, YSi_2, $CaAl_2Si_2$, and Al-Fe-Y-Si phase. A compositional gradient in a Si-Ca-Y solid solution phase was found due to the weak repulsive interaction between Ca and Y.
- In the leaching experiments, Ti and Y exhibited relatively equivalent ability for the removal of all elements except phosphorus.
- Higher B removal (~20%) was found in the Si-Ca-Y system than Si-Ca-Ti, which shows the co-removal of B and P by rare earth elements doping.

Acknowledgement

This work was performed at NTNU within the Research Centre for Sustainable Solar Cell Technology (FME SuSolTech, project number 257639), co-sponsored by the Norwegian Research Council and industry partners.

References

1. A. Murgau and J. Safarian, *Solar silicon production through metallurgical route and REC solar advancements*, Silicon for the Chemical and Solar Industry XIV, 2018, pp. 183–192.
2. J. Safarian, G. Tranell, and M. Tangstad, *Processes for upgrading metallurgical grade silicon to solar grade silicon*, Energy Procedia. vol. 20, pp. 88–97, 2012.
3. N. P. Tucker, *Preparation of high purity silicon*, J. Iron Steel Ind., vol. 15, pp. 412–414, 1927.
4. J. Dietl, Hydrometallurgical purification of metallurgical-grade silicon, Sol. Cells, vol. 10, no. 2, pp. 145–154, 1983.
5. J. M. Juneja and T. K. Mukherjee, *A study of the purification of metallurgical grade silicon*, Hydrometallurgy, vol. 16, no. 1, pp. 69–75, 1986.
6. I. C. Santos, A. P. Goncalves, C. S. Santos, M. Almeida, M. H. Afonso, and M. J. Cruz, *Purification of Metallurgical Grade Silicon by Acid Leaching*, Hydrometallurgy, vol. 23, pp. 237–246, 1990.
7. T. L. Chu, *Partial Purification of Metallurgical Silicon by Acid Extraction*, J. Electrochem. Soc., vol. 130, no. 2, p. 455, 1983.
8. T. Yoshikawa and K. Morita, *Removal of phosphorus by the solidification refining with Si-Al melts*, Sci. Technol. Adv. Mater., vol. 4, no. 6, pp. 531–537, 2003.

9. T. Yoshikawa and K. Morita, *Refining of silicon during its solidification from a Si–Al melt, J. Cryst. Growth*, vol. 311, no. 3, pp. 776–779, Jan. 2009.
10. T. Yoshikawa and K. Morita, *An Evolving Method for Solar-Grade Silicon Production: Solvent Refining*, JOM, vol. 64, no. 8, pp. 946–951, Aug. 2012.
11. Y. Li et al., *Effect of Cooling Rate on Phosphorus Removal During Al-Si Solvent Refining*, Metall. Mater. Trans. B, vol. 46, no. 2, pp. 542–544, Apr. 2015.
12. B. Ban, X. Bai, J. Li, Y. Li, J. Chen, and S. Dai, *The Mechanism of P Removal by Solvent Refining in Al-Si-P System*, Metall. Mater. Trans. B Process Metall. Mater. Process. Sci., vol. 46, no. 6, pp. 2430–2437, Sep. 2015.
13. L. T. Khajavi, K. Morita, T. Yoshikawa, and M. Barati, *Removal of Boron from Silicon by Solvent Refining Using Ferrosilicon Alloys*, Metall. Mater. Trans. B, vol. 46, no. 2, pp. 615–620, Apr. 2015.
14. X. Ma, Y. Lei, T. Yoshikawa, B. Zhao, and K. Morita, *Effect of solidification conditions on the silicon growth and refining using Si–Sn melt*, J. Cryst. Growth, vol. 430, pp. 98–102, Nov. 2015.
15. L. Hu, Z. Wang, X. Gong, Z. Guo, and H. Zhang, *Purification of metallurgical-grade silicon by Sn – Si refining system with calcium addition*, Sep. Purif. Technol., vol. 118, pp. 699–703, 2013.
16. J. Li et al., *Effect of tin addition on primary silicon recovery in Si–Al melt during solidification refining of silicon*, J. Cryst. Growth, vol. 371, pp. 1–6, May 2013.
17. L. Huang et al., *Enhancement in extraction of boron and phosphorus from metallurgical grade silicon by copper alloying and aqua regia leaching*, Hydrometallurgy, vol. 161, pp. 14–21, 2016.
18. L. Huang et al., *Solvent extraction of phosphorus from Si-Cu refining system with calcium addition*, Sep. Purif. Technol., vol. 204, pp. 205–212, Oct. 2018.
19. Y. V. Meteleva-Fischer, Y. Yang, R. Boom, B. Kraaijveld, and H. Kuntzel, *Microstructure of metallurgical grade silicon during alloying refining with calcium*, Intermetallics, vol. 25, pp. 9–17, 2012.
20. A. Schei, *High Purity Silicon Production*, in International seminar on refining and alloying of liquid aluminium and Ferro-alloys, 1985.
21. T. Shimpo, T. Yoshikawa, and K. Morita, *Thermodynamic study of the effect of calcium on removal of phosphorus from silicon by acid leaching treatment*, Metall. Mater. Trans. B, vol. 35, no. April, pp. 277–284, 2004.
22. M. D. Johnston and M. Barati, *Calcium and titanium as impurity getter metals in purification of silicon*, Sep. Purif. Technol., vol. 107, pp. 129–134, 2013.
23. M. Zhu, A. Murgau, and J. Safarian, *Effects of Magnesium-Doping on Silicon Leaching for Solar Grade Feedstock Production*, in 35 Eur. Photovolt. Sol. Energy Conf. Exhib., 2018, pp. 465–468.
24. M. Zhu, A. Azarov, E. Monakhov, K. Tang, and J. Safarian, *Phosphorus separation from metallurgical-grade silicon by magnesium alloying and acid leaching*, Sep. Purif. Technol., vol. 240, no. January, p. 116614, 2020.

25. S. Espelien, G. Tranell, and J. Safarian, *Effect of magnesium addition on removal of impurities from silicon by hydrometallurgical treatment*, in Energy Technology 2017, Springer, 2017, pp. 355–366.
26. Y. V. Meteleva-Fischer, Y. Yang, R. Boom, B. Kraaijveld, and H. Kuntzel, *Microstructure of metallurgical grade silicon during alloying refining with calcium*, Intermetallics, vol. 25, pp. 9–17, 2012.
27. Y. Lei, W. Ma, G. Lv, K. Wei, S. Li, and K. Morita, *Purification of metallurgical-grade silicon using zirconium as an impurity getter*, Sep. Purif. Technol., vol. 173, pp. 364–371, 2017.
28. Y. Lei et al., *Leaching behaviors of impurities in metallurgical-grade silicon with hafnium addition*, Hydrometallurgy, vol. 169, pp. 433–439, 2017.
29. Y. Meteleva-Fischer, Y. Yang, R. Boom, B. Kraaijveld, and H. Kuntzel, *Alloying Refining of Metallurgical Grade Silicon with Rare Earth Elements*, in EPD Congress 2013, Hoboken, NJ, USA: John Wiley & Sons, Inc., 2013, pp. 201–209.
30. K. Tang, O. M. Løvvik, J. Safarian, X. Ma, and M. Tangstad, *Removal of Phosphorus in Metallurgical Silicon by Rare Earth Elements*, Metall. Mater. Trans. E, vol. 1, no. 3, pp. 257–262, Sep. 2014.
31. K. Morita and T. Miki, *Thermodynamics of solar-grade-silicon refining*, Intermetallics, vol. 11, pp. 1111-1117, 2003.
32. A. Takeuchi and A. Inoue, *Metallic Glasses By Atomic Size Difference, Heat of Mixing and Period of Constituent Elements and Its Application To Characterization of the Main Alloying Element*, Mater. Trans., vol. 46, no. 12, pp. 2817–2829, 2005.
33. E.G. Rochow. *The Chemistry of Silicon: Pergamon International Library of Science, Technology, Engineering and Social Studies*. vol. 9. Elsevier, 2013.

Paper 6

This paper is awaiting publication and is not included in NTNU Open

Paper 7

This paper is awaiting publication and is not included in NTNU Open

ISBN 978-82-326-6057-5 (printed ver.)
ISBN 978-82-326-5949-4 (electronic ver.)
ISSN 1503-8181 (printed ver.)
ISSN 2703-8084 (online ver.)

NTNU

Norwegian University of
Science and Technology